3 July 2009 | $10

Science

AAAS

Epigenetics sample and assay technologies by QIAGEN

Trust in methylation analysis

Rely on QIAGEN epigenetics sample and assay technologies for:

- **DNA purification**
- **Bisulfite conversion**
- **Whole bisulfitome amplification**
- **Methylation-specific PCR**
- **Methylation detection and quantification with Pyrosequencing**

Making improvements in life possible — www.qiagen.com

QIAGEN®

Sample & Assay Technologies

ADNAEpigenetics0309S1WW

Submission deadline August 1

Rewarding brilliance since 1995.

The GE & Science Prize for Young Life Scientists. Because brilliant ideas build better realities.

Imagine standing on the podium at the Grand Hotel in Stockholm, making your acceptance speech. Imagine joining the ranks of those published in Science magazine and having your essay on your work in molecular biology read by your peers around the world. Imagine taking part in a seminar with the other Prize winners and Nobel Prize laureates and discussing your work with leaders in the field. Imagine what you could do with the $25,000 prize money. Imagine what a brilliant start to your career, and where it could lead. Now stop imagining. If you were awarded your Ph.D in 2008, submit your 1000-word essay by August 1 and make it reality.

Want to build a better reality? Go to www.gelifesciences.com/science

GE & Science Prize for Young Life Scientists

imagination at work

Science AAAS

* For the purpose of this prize, molecular biology is defined as "that part of biology which attempts to interpret biological events in terms of the physico-chemical properties of molecules in a cell".

(McGraw-Hill Dictionary of Scientific and Technical Terms, 4th Edition).

Biacore systems

from inspiration ...to publication

Highest quality, information-rich interaction data from Biacore™ systems deepen your understanding of molecular mechanisms and interaction pathways and enable you to add function to structure.

Select the perfect solution for your application and draw conclusions with confidence – from the company that continues to set the standard for label-free protein interaction analysis.

For further information or register to have one of our scientific experts contact you, please visit **www.gelifesciences.com/biacore-science**

Biacore T100
unmatched performance

Biacore X100
ready to run research system

Biacore Flexchip
array-based comparative profiling

imagination at work

EDITORIAL

NEWS OF THE WEEK

NEWS FOCUS

LETTERS

BOOKS *ET AL.*

POLICY FORUM

PERSPECTIVES

CONTENTS continued >>

page 24

page 48

COVER

The Phoenix spacecraft on the martian polar plains (68°N latitude). The footpad at the bottom is about 1 meter below the spacecraft deck seen at the lower left. Overlaid images are trenches dug to either nearly pure water ice or ice-cemented soil. Analyses of samples taken from these trenches give clues to the history of the region. Results from the Phoenix mission are discussed in four Reports beginning on page 58.

Image: NASA/JPL-Caltech/University of Arizona/Texas A&M/ M. T. Lemmon

DEPARTMENTS

Published by AAAS

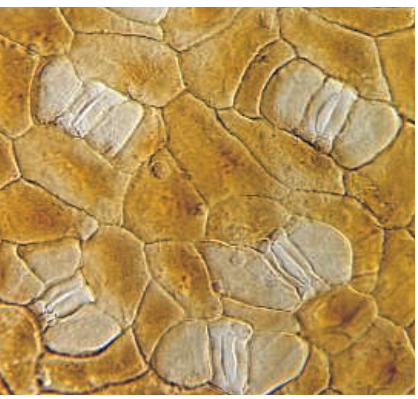

page 36

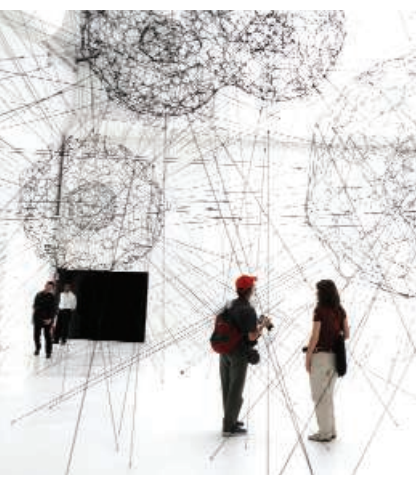

page 37

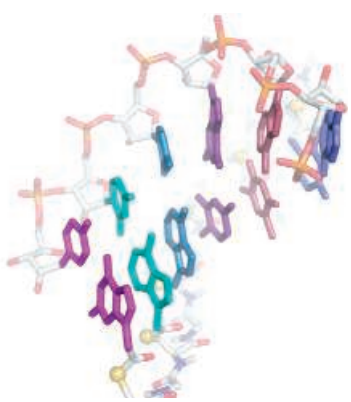

page 73

REVIEW

BREVIA

RESEARCH ARTICLE

REPORTS

Published by AAAS

SCIENCEONLINE

SCIENCEXPRESS
www.sciencexpress.org

Transmission and Pathogenesis of Swine-Origin 2009 A(H1N1) Influenza Viruses in Ferrets and Mice
T. R. Maines et al.
10.1126/science.1177238

Pathogenesis and Transmission of Swine-Origin 2009 A(H1N1) Influenza Virus in Ferrets
V. J. Munster et al.
Animal experiments compare the dynamics and effects of the virus causing the 2009 flu outbreak to those of seasonal H1N1 flu.
10.1126/science.1177127
>> News story p. 17

The Dynamics of Phenotypic Change and the Shrinking Sheep of St. Kilda
A. Ozgul et al.
Environmental change has led to decreasing body size in a sheep population over 20 years, despite selection for increased size.
10.1126/science.1173668

Radio Imaging of the Very-High-Energy γ-Ray Emission Region in the Central Engine of a Radio Galaxy
The VERITAS Collaboration et al.
Particles are accelerated to very high energies in close proximity to a super-massive black hole.
10.1126/science.1175406

Detection of 16 Gamma-Ray Pulsars Through Blind Frequency Searches Using the Fermi LAT
A. A. Abdo et al.
Most of these identifications correspond to gamma-ray sources long suspected to be pulsars.
10.1126/science.1175558

A Population of Gamma-Ray Millisecond Pulsars Seen with the Fermi Large Area Telescope
A. A. Abdo et al.
These objects appear to share a common emission mechanism with standard gamma-ray pulsars.
10.1126/science.1176113

SCIENCENOW
www.sciencenow.org
Highlights From Our Daily News Coverage

Brain Recordings Take Flight
A new lightweight device measures brain activity in homing pigeons in midflight.

Evolution Heats Up in the Tropics
Warmer climates accelerate evolution rate in mammals, a new study says.

Ancient Flutes Suggest Rich Life in Stone-Age Europe
New discoveries indicate that cave-dwellers played music 35,000 years ago.

SCIENCESIGNALING
www.sciencesignaling.org
The Signal Transduction Knowledge Environment

EDITORIAL GUIDE: Challenging Times
M. B. Yaffe
The deluge of NIH "challenge grants" promises to strain the reviewer pool.

RESEARCH ARTICLE: Therapeutically Targeting ErbB3—A Key Node in Ligand-Induced Activation of the ErbB Receptor–PI3K Axis
B. Schoeberl et al.
Computational modeling of the ErbB signaling network affirms ErbB3 as a therapeutic target.

RESEARCH ARTICLE: PKCε Regulation of an α_5 Integrin–ZO-1 Complex Controls Lamellae Formation in Migrating Cancer Cells
S. Tuomi et al.
Phosphorylated ZO-1 relocalizes from tight junctions to lamellae to associate with α_5 integrin and control migration.

PERSPECTIVE: AIMing 2 Detect Foreign DNA
A. M. Krieg
AIM2 is a receptor for cytoplasmic double-stranded DNA and induces the formation of an IL-1β–secreting inflammasome.

PODCAST
U. B. Nielsen and A. M. VanHook
Mathematical modeling of signaling pathways can be used to identify candidate targets for cancer therapies.

GLOSSARY
Find out what ERM, FMN, and LH mean in the world of cell signaling.

SCIENCECAREERS
www.sciencecareers.org/career_magazine
Free Career Resources for Scientists

Taken for Granted: An Alternative to the Ph.D. Track
B. L. Benderly
Employment prospects for professional science master's degree program graduates seem strong.

Fun with Fungi: Mycology Careers
S. Coelho
Mycologists can find career opportunities in areas from academic research to applied agriculture.

Funding News
GrantsNet Staff
The Funding News, now published weekly, provides the latest index of research funding and student support.

SCIENCENOW
Homing phone.

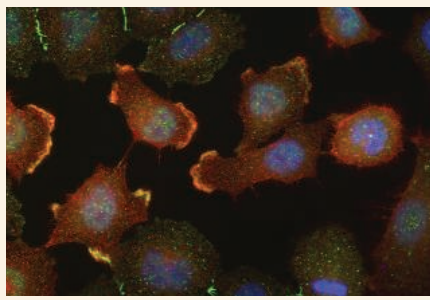

SCIENCESIGNALING
Adhesion proteins in lamellae.

SCIENCEPODCAST
www.sciencemag.org/multimedia/podcast
Free Weekly Show
Download the 3 July *Science* Podcast to hear about evidence of water at the Mars Phoenix landing site, how Serengeti birds maintain forests, the origins of nervous systems, and more.

ORIGINSBLOG
blogs.sciencemag.org/origins
A History of Beginnings

SCIENCEINSIDER
blogs.sciencemag.org/scienceinsider
Science Policy News and Analysis

SCIENCE (ISSN 0036-8075) is published weekly on Friday, except the last week in December, by the American Association for the Advancement of Science, 1200 New York Avenue, NW, Washington, DC 20005. Periodicals Mail postage (publication No. 484460) paid at Washington, DC, and additional mailing offices. The title SCIENCE is a registered trademark of the AAAS. Domestic individual membership and subscription (51 issues): $146 ($74 allocated to subscription). Domestic institutional subscription (51 issues): $835; Foreign postage extra: Mexico, Caribbean (surface mail) $55; other countries (air assist delivery) $85. First class, airmail, student, and emeritus rates on request. Canadian rates with GST available upon request, GST #1254 88122. Publications Mail Agreement Number 1069624. **Printed in the U.S.A.**

Change of address: Allow 4 weeks, giving old and new addresses and 8-digit account number. **Postmaster:** Send change of address to AAAS, P.O. Box 96178, Washington, DC 20090–6178. **Single-copy sales:** $10.00 current issue, $15.00 back issue prepaid includes surface postage; bulk rates on request. **Authorization to photocopy** material for internal or personal use under circumstances not falling within the fair use provisions of the Copyright Act is granted by AAAS to libraries and other users registered with the Copyright Clearance Center (CCC) Transactional Reporting Service, provided that $20.00 per article is paid directly to CCC, 222 Rosewood Drive, Danvers, MA 01923. The identification code for *Science* is 0036-8075. *Science* is indexed in the *Reader's Guide to Periodical Literature* and in several specialized indexes.

AAAS
ADVANCING SCIENCE, SERVING SOCIETY

EDITED BY STELLA HURTLEY

Bringing Back the Large Blue >>

Flagship endangered species, such as the Large Blue butterfly have driven conservation programs worldwide. However, the Large Blue butterfly (*Maculinea arion*) became extinct in the United Kingdom. The apparent driver of this extinction was a complex set of events documented by **Thomas *et al.*** (p. 80, published online 18 June; see the Perspective by **Settele and Kühn**). Life-tables and modeling demonstrate how ecological changes, affecting multiple species, cascaded to negatively impact Large Blue populations. When the changes that cause these extinctions were addressed, reintroduction efforts proved successful. Other insects have experienced similar declines and, hopefully, on sites where their known resources remain abundant, a similar approach may be applied.

Did I Really Do That?

Most of us believe that our daily actions occur because we exert conscious effort to make them happen; nevertheless, we sometimes seem to end up doing the precise thing we had hoped to avoid. **Wegner** (p. 48) reviews the recent psychological research on ironic processes. The findings support the view that the unwanted outcomes are held in working memory and that the monitoring centers that usually ensure correct behavior can be distracted or exhausted, allowing the taboo idea to escape.

El Niño's Cousin

The most energetic and well-known quasi-periodic, air-sea temperature disturbance is ENSO, the mother of the warming of equatorial eastern Pacific surface waters known as El Niño. El Niño, and its cold sister La Niña, can produce dramatic effects on weather across the globe and so it is of great interest and importance to understand it better. Warming in the eastern tropical Pacific is not the only recurring pattern of sea-surface temperature variability in the Pacific, however. **Kim *et al.*** (p. 77; see the Perspective by **Holland**) report that a pattern of extensive warming in the central Pacific also occurs on a quasi-periodic basis, that it has a large effect on atmospheric circulation, and that it is more predictable than El Niño. These central Pacific warming events have become increasingly more frequent in the last few decades, making it even more vital that we understand them.

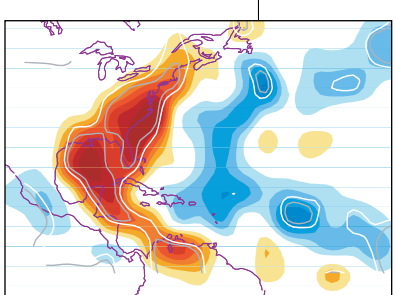

Card Sorting Monkeys

Single-neuron studies in primates help to establish a detailed understanding of cognitive processing and to provide an experimental base for understanding the cognitive deficits incurred by patients who have suffered damage to areas of the brain. **Buckley *et al.*** (p. 52) present the results of an intensive behavioral analysis of a group of monkeys bearing lesions to distinct areas of the prefrontal lobe. The Wisconsin Card Sorting Task is widely used in the clinic to assess the flexible learning of abstract rules. In the primates, a functional dissociation was observed across three regions: the principal sulcus, the orbitofrontal cortex, and the anterior cingulate cortex. This set of results contributes to the ongoing discussion of goal-directed behavior and serves to bridge neuropsychological studies in human patients and neurophysiological studies in primates.

Phoenix Ascending

The Phoenix mission landed on Mars in March 2008 with the goal of studying the ice-rich soil of the planet's northern arctic region. Phoenix included a robotic arm, with a camera attached to it, with the capacity to excavate through the soil to the ice layer beneath it, scoop up soil and water ice samples, and deliver them to a combination of other instruments—including a wet chemistry lab and a high-temperature oven combined with a mass spectrometer—for chemical and geological analysis. Using this setup, **Smith *et al.*** (p. 58) found a layer of ice at depths of 5 to 15 centimeters, **Boynton *et al.*** (p. 61) found evidence for the presence of calcium carbonate in the soil, and **Hecht *et al.*** (p. 64) found that most of the soluble chlorine at the surface is in the form of perchlorate. Together these results suggest that the soil at the Phoenix landing site must have suffered alteration through the action of liquid water in geologically the recent past. The analysis revealed an alkaline environment, in contrast to that found by the Mars Exploration Rovers, indicating that many different environments have existed on Mars. Phoenix also carried a lidar, an instrument that sends laser light upward into the atmosphere and detects the light scattered back by clouds and dust. An analysis of the data by **Whiteway *et al.*** (p. 68) showed that clouds of ice crystals that precipitated back to the surface formed on a daily basis, providing a mechanism to place ice at the surface.

A Hole New Approach

Quantum dots can behave as artificial atoms, exhibiting a ladder of quantized energy levels with the number of electrons added to the dot being controllable. They are thus being extensively studied for application in the likes of quantum information processing strategies. However, the electrons interact with their environment and quickly lose their coherence properties. **Brunner *et al.*** (p. 70; see the Perspective by **Kolodrubetz and Petta**) now show that if the charge of the dot is manipulated so that it is positive; that is, populated with a single hole,

CREDITS (TOP TO BOTTOM): DAVID SIMCOX; KIM *ET AL.*

Published by AAAS

then the coherence properties of the dot can be extended. The strategy of using holes instead of electrons may provide a solution to the decoherence problem.

Adaptable DNA Analogs

The defining feature of DNA as a genetic blueprint is its capacity for self-replication. In the cell, however, the replication process requires the assistance of multiple elaborate enzymes. How then at the origin of life could DNA or its precursor replicate before enzymes were present? **Ura *et al.*** (p. 73, published online 11 June) have achieved the long-sought goal of preparing a synthetic DNA analog that can dynamically adapt its sequence in free solution. Their analog (as yet only studied in relatively short, 20-unit oligomers) replaces DNA's sugar and phosphate backbone by a peptide strand in which cysteines reversibly bind the conventional DNA bases through thioester tethers. These strands can pair with complementary sequences of true DNA and furthermore swap one tethered base for another if different DNA templating strands are added to the solution in succession.

Breaking the Barrier

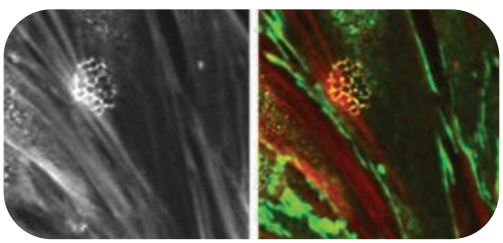

Being able to deliver drugs into the brain to treat degenerative diseases such as Alzheimer's or Parkinson's requires the ability to traverse the blood-brain barrier (BBB). Understanding the formation of the very specific adherent junctions (AJ) and tight junctions present at the BBB cell junctions is a prerequisite to the design of such therapeutics. However, diminishing the expression of any one component involved in the formation of these intercellular junctions destroys them. **Coureuil *et al.*** (p. 83, published online 11 June) exploited the specific recruitment of AJ proteins by *Neisseria meningitidis* to dissect this process. Adhesion of the bacteria to human brain endothelial cells recruited the polarity complex Par3/Par6/PKCζ required for the establishment of eukaryotic cell polarity and the formation of intercellular junctions. The bacterial recruitment of the polarity complex depleted junctional proteins at the cell-cell interface opening the intercellular junctions at the brain-endothelial interface.

Biogenic Amine Receptors

Biogenic amines have important effects on behavior in humans and other animals. These agents can act by binding to heterotrimeric guanine nucleotide–binding protein (G protein)–coupled receptors, but can also activate ligand-gated ion channels. **Ringstad *et al.*** (p. 96) explored the family of ion channels that respond to biogenic amines in the worm *Caenorhabditis elegans* and characterized two family members that appear to function as chloride channels. One was a receptor activated by dopamine that could bind drugs used in humans as antipsychotics. The other was activated by tyramine and was shown in genetic studies to modulate behavior. Thus, the worm family of biogenic amine–activated channels is larger than previously recognized. If the same is true in humans, related channels may account, in part, for effects of currently used drugs or could be beneficial targets for development of therapeutics.

Idolizing Cholesterol Control

The low-density lipoprotein receptor (LDLR) removes LDL, the so-called "bad" cholesterol particles, from the blood through a mechanism that involves LDL binding and internalization into liver cells. Because the LDLR plays a pivotal role in heart disease risk, there is substantial interest in understanding how its expression is regulated, and a large body of previous work has established the importance of transcriptional control. A new study identifies a signaling pathway that appears to regulate the LDLR at the level of protein degradation. **Zelcer *et al.*** (p. 100, published online 11 June) show that a sterol-responsive transcription factor called LXR induces the expression of Idol (for inducible degrader of the LDLR), a protein that triggers ubiquitination of the receptor and targets it for degradation. Activation of this pathway suppresses cellular uptake of LDL and, in a mouse model, leads to higher plasma LDL levels, raising the possibility that the pathway could be targeted pharmacologically to control plasma cholesterol levels.

CREDIT: COUREUIL *ET AL.*

Published by AAAS

Eppendorf Consumables – it's your sample

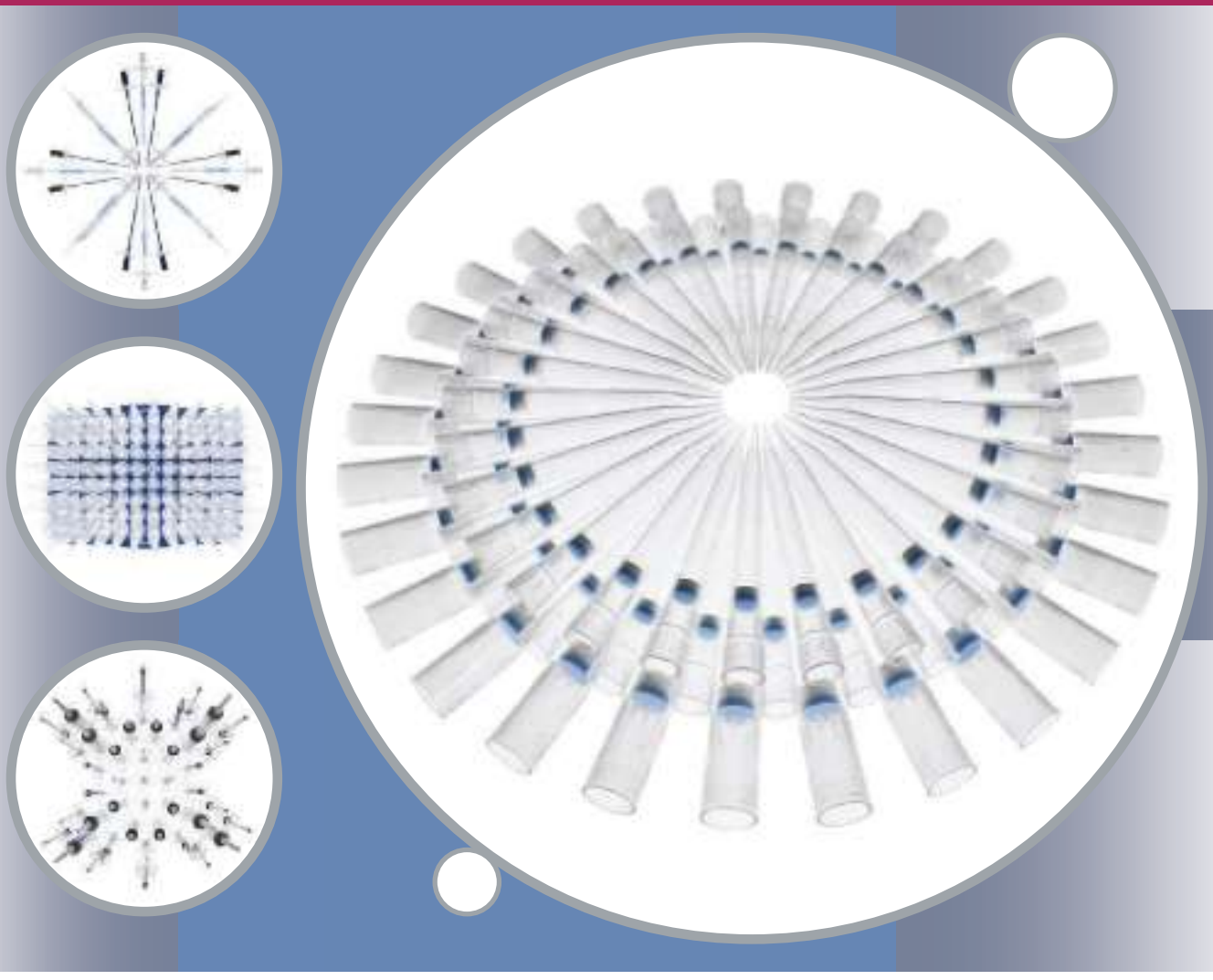

Make the best of it!

Top quality for your sample

Each of your valuable samples deserves the best treatment. See for yourself how the Eppendorf tips will save time and reduce costs.

With respect to material, fit, design and operating forces our tips set new standards. The close environment of each sample should be adapted to its specific quality and purity needs. This can involve a specific purity level or the absence of certain substances, but also stability, reliability, or geometry. The Eppendorf tips are designed to cover all of the specific needs of your samples!

Stop Aerosols! Eppendorf ep Dualfilter T.I.P.S.®

- Maximum protection of pipette and sample by our unique two phase filter technology
- Ultimate absorption of aerosols and biomolecules
- Free from PCR inhibiting additives and particles from the filter material itself

Learn more about Eppendorf ep Dualfilter T.I.P.S.®:
www.eppendorf.com/dualfilter
Learn more about Eppendorf consumables:
www.eppendorf.com/consumables

eppendorf

In touch with life

Your local distributor www.eppendorf.com/worldwide · **Application Support** E-Mail: support@eppendorf.com
Eppendorf AG · Hamburg · Germany · Tel: +49 40 538 01-0 · Eppendorf North America, Inc. · USA · Tel.: +1 800 645 3050

Thomas R. Pickering served as U.S. ambassador to the United Nations and Russia and to countries in Asia, Africa, Central America, and the Middle East, and was U.S. Undersecretary of State for Political Affairs from 1997 to 2001.

An Opportunity We Cannot Waste

THE STRUGGLES AGAINST WORLD POVERTY ARE MORE CHALLENGING THAN EVER, GIVEN THE GLOBAL financial crisis. At the London G-20 summit in April, leaders of the world's largest economies acknowledged that financial recovery could be sustained only if progress is made in alleviating world poverty. Thus, the path to stable worldwide recovery requires that the issues of economic growth, development, and poverty be seen as linked with the key drivers of food, water, and health, just as climate change is now linked to the key drivers of energy and environment.

I co-chaired a 2008 study by the U.S. National Academies that recommended that the president call attention to the needs of global health.* But health is intimately connected to nutrition, and thus to agriculture; and both are affected by shortages of potable and irrigation water. It is hard to imagine successful agriculture without adequate water or healthy farmers, or that good health can be achieved without clean water and nutritional food. And water availability cannot be ensured without careful soil management and healthy individuals to develop and properly use water resources. Thus, health, food, and water are all central to dealing with poverty and the challenge of growth. We can begin to think now on a larger scale—an opportunity not to be wasted. Because improvements in any one area depend on the other two, why not devote a summit at the United Nations (UN) General Assembly to the interlinked broad questions of food, water, and health?

The world still looks to the United States for leadership in such work because of our scientific capabilities and our wealth. We are already demonstrating commitment in a few of these areas, notably in the last administration's multibillion dollar program to relieve the impact of HIV/AIDS, principally in Africa. But overall, U.S. foreign assistance programs have been lagging in the food, water, and health areas, with funding for the U.S. Agency for International Development (USAID) declining from $8 billion to $6 billion per year over recent decades. Moreover, the numerous federal agencies that provide science and technology–based international aid suffer from lack of coordination in their efforts. Another National Academies study that I co-chaired concluded that USAID, bolstered by new senior administrators with science and technology expertise, should play a major part in overseeing this much-needed coordination.† The Academies' studies also indicate that an extra $10 billion per year will be needed to set the nation on a productive course in our international aid efforts.

A pledge now by the United States to an expanded program that focuses on strengthening health systems in general, while simultaneously increasing local capacities in food production and water stewardship, would inspire other nations to support such a synergistic program. A UN summit could then be designed to obtain the full commitment of the world community to these interlinked approaches for reaching the UN Millennium Goals. Hopefully, this meeting could take place before the next G-20 summit in September.

It may not be easy to find new resources at a time of world financial crisis. But the poverty-stricken will be the first to be hit by this crisis and suffer the greatest setbacks, adversely affecting industrialized and developing countries alike. An additional $10 billion per year from the United States seems small in light of the trillion dollars that the government has put forward to address the economic crisis, and paltry compared to the sums pledged by the G-20. The United States has terrific research capacity and wide experience in dealing with food, health, and water. The challenge lies in the nation's continued willingness to put our expertise at the service of humankind. The recent increase in the U.S. assistance budget from $36 billion to over $51 billion by the Obama administration in its 2010 budget is encouraging in this regard. **– Thomas R. Pickering**

**The U.S. Commitment to Global Health: Recommendations for the New Administration* (National Academies Press, Washington, DC, 2009).

†The Fundamental Role of Science and Technology in International Development: An Imperative for the U.S. Agency for International Development (National Academies Press, Washington, DC, 2006).

10.1126/science.1175089

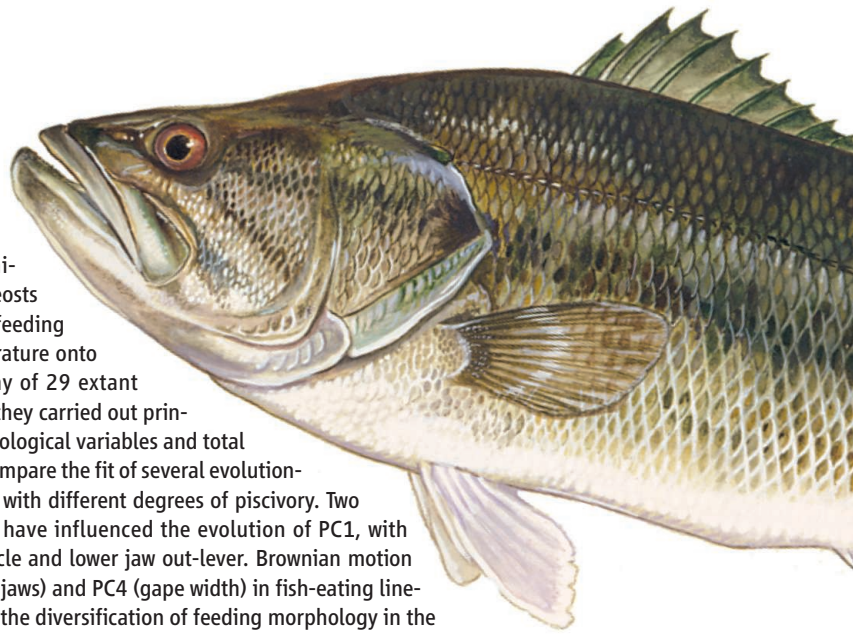

EVOLUTION

Unable to Diversify

The decline in fitness with increasing distance from an adaptive peak can constrain morphological divergence between sister lineages. Collar *et al.* examine whether the functional demands of feeding on fish have limited morphological diversification in the Centrarchidae, an endemic clade of North American freshwater teleosts that includes sunfish and bass. To reconstruct ancestral feeding strategies, they map diet data synthesized from the literature onto a well-resolved, time-calibrated, multilocus phylogeny of 29 extant species. After measuring functional aspects of the skull, they carried out principal-components analysis of seven size-corrected morphological variables and total length. For each principal component (PC), the authors compare the fit of several evolutionary models, allowing parameters to vary across lineages with different degrees of piscivory. Two adaptive peaks (piscivory and nonpiscivory) appear to have influenced the evolution of PC1, with strongest loadings on the pharyngeal jaw adductor muscle and lower jaw out-lever. Brownian motion models reveal slow evolution of PC2 (muscle closing oral jaws) and PC4 (gape width) in fish-eating lineages. These findings indicate that piscivory has curtailed the diversification of feeding morphology in the centrarchids and that the effects have been strongest in highly piscivorous lineages. — SJS

Evolution **63**, 1557 (2009).

GEOCHEMISTRY

Guiding Mercury's Meandering

Mercury's toxicity impels wide-ranging study of the binding and redox behavior of the element under varying environmental conditions. Sulfate-reducing bacteria in soils and sediments are known to enhance mercury accumulation in higher species such as fish and humans by methylating oxidized Hg(II) ions. To what extent do geochemical reactions at mineral surfaces play a role in controlling the fate of Hg? Lee *et al.* uncover sharp variations in Hg(II) adsorption behavior on muscovite as they shift the local concentration of naturally abundant organic acids; complexation by the organics in free solution appeared to enhance adsorption more effectively than did a preformed film on the surface. In a related study, Wiatrowski *et al.* show that when Hg(II) adsorbs onto redox-active mineral surfaces such as magnetite, soluble Hg(II) is quickly reduced to highly mobile gaseous Hg(0). It remains unclear how organic layers on redox-active mineral surfaces specifically influence these and similar electron transfer reactions. Taken together, the two studies suggest that mineral-associated processes such as adsorption and phase transformation may provide stiff competition for the bacteria that catalyze Hg methylation reactions in mediating Hg fate and mobility. — NW

Environ. Sci. Technol. **43**, 10.1021/es900214e; 10.1021/es9003608 (2009).

MOLECULAR BIOLOGY

Liverish Days and Nights

Biological processes with circadian rhythms show periodicity that correlates with the day/night cycle, and many metabolic pathways display such a regulatory mechanism. Prior work has suggested that between 2 and 10% of the liver transcriptome is under circadian control. Gatfield *et al.* show that miR-122, an abundant hepatocyte microRNA, is under circadian control. The abundance of the miR-122 precursor varies 4- to 10-fold during the day. However, accumulation is constant in the liver of mice lacking the orphan nuclear receptor REV-ERBα. When miR-122 is knocked down, hundreds of mRNAs are expressed. Peroxisome proliferation–activated receptor (PPAR) β/δ and the coactivator SMARCD1/BAF60a, two known metabolism regulators, are specific miR-122 targets, linking circadian rhythms with the PPAR family of nuclear receptors and liver metabolism. — BAP

Genes Dev. **23**, 1313 (2009).

IMMUNOLOGY

Maintaining Diversity

Exposure to infectious agents has exerted selective pressure on the evolution of one group of immune system genes. The hygiene hypothesis, proposed two decades ago, posits that the reduced exposure of inhabitants of modern industrialized societies to microbes and macropathogens (such as parasitic worms) has increased susceptibility to inflammatory conditions such as allergies and autoimmune disease. Taking a population genetics approach, Fumagalli *et al.* investigated how infectious agents have affected the genetic variability of interleukins, which are critical signaling molecules of the immune system, and their associated receptors. They found that pathogen richness, a measure of pathogen diversity in a specific geographic area, has driven the selection of several

CREDITS (TOP TO BOTTOM): U.S. BUREAU OF RECLAMATION; ISTOCK.COM

Published by AAAS

interleukin family genes; in particular, balanced selection, a type of selection that maintains genetic variation within populations and is unusual in humans, has contributed to the evolution of five interleukin genes. Finally, the authors demonstrated that six of the nine known risk alleles associated with inflammatory conditions such as celiac disease and Crohn's disease correlated with pathogen richness, but in contrast to the hygiene hypothesis, more so with bacteria, viruses, and fungi rather than worms. Hence, pathogen-influenced evolution is a double-edged sword: The same bugs that helped us to develop an immune response to a wide array of pathogens also may have contributed to the appearance of debilitating inflammatory diseases. — KLM

J. Exp. Med. **206**, 1395 (2009).

APPLIED PHYSICS

Half Metal, Full Spin

For optimal efficiency in spintronic applications (which replace ordinary charge flow with spin current), host materials should ideally be completely spin-polarized. Unfortunately, not many materials have this property. Heusler alloys constitute an emerging prospect. These are metals, or rather half-metals, in which the conduction band is split into two polarizations—one half occupied, the other empty—thus providing 100% spin polarized current transport. However, the materials studied so far have shown strongly temperature-dependent behavior due to the band structure, making them unsuitable for practical device applications. Shan *et al.* now show that Fermi-level tuning by the introduction of appropriate dopant atoms, a technique similar to electron or hole enrichment in semiconductors, can be applied to the Heusler alloy $Co_2FeAl_{0.5}Si_{0.5}$. With a spin-polarization exceeding 90% and a weak temperature dependence up to room temperature, the resulting material highlights the potential of Fermi-level tuning for attaining high performance in spintronic applications. — ISO

Phys. Rev. Lett. **102**, 246601 (2009).

GEOCHEMISTRY

Well-Aged Granite

Granite is not unique to our planet. Granite-like rocks have been found, albeit comparatively rarely, on Mars, Venus, and the Moon and within meteorites. Terada and Bischoff report the age of a granite-like fragment found in a stony meteorite (Adzhi-Bogdo) that fell in Mongolia in 1949. Their analysis of the fragment using a high-resolution ion microprobe implies that its parental granite-like magma crystallized 4.53 billion years ago. Granites on Earth and the Moon crystallized at a later stage, making this fragment the earliest example of granite-like material in the solar system. Its age reveals that such material must have formed very early in the solar system's history. On Earth, granite formation is thought to require the presence of water and plate tectonics. This fragment, however, must have formed under dry conditions and without plate tectonics, calling for a different formation mechanism. — MJC

Astrophys. J. **699**, L68 (2009).

BIOPHYSICS

Tissue-Engineering Principals

If Robert Moses, the driving force behind the construction of the congested artery known as the Brooklyn-Queens Expressway, were alive today, he would marvel at the cellular engineers who relocate still-functioning blood vessels from nearby healthy tissue into healing wounds. After an injury, force-generating cells have previously been shown to reinforce the initial fibrin-based

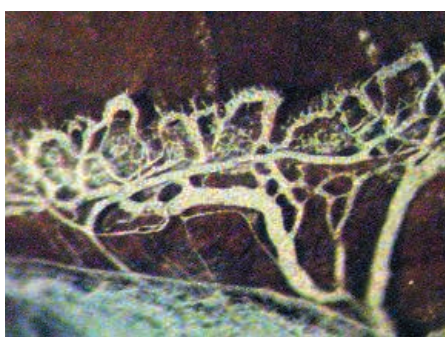

matrix and to latch onto and contract subsequently deposited extracellular matrix (ECM) components. Kilarski *et al.* show that myofibroblasts, in response to tensile stress and soluble growth factors, pull intact blood vessels with them as highly perfused granulation tissue (the reddish patch in a healing wound) migrates into the injured area [represented by a fibrin-collagen gel in an in vitro system or by a sutured cornea in an in vivo preparation (above)]. The mediating mechanisms are not yet precisely defined, but Legant *et al.* describe their microfabricated tissue gauge (or μTUG) and use it to quantitate the interplay between matrix mechanics and fibroblasts during remodeling of collagen mesh. Increasing matrix stiffness, both in vitro and in a computational model, elicited higher cellular contractility (which is roughly 20 nN per cell), whereas increasing mechanical stress evoked higher levels of expression of cytoskeletal and ECM proteins. — GJC

Nat. Med. **15**, 657 (2009); *Proc. Natl. Acad. Sci. U.S.A.* **106**, 10097 (2009).

CREDIT: KILARSKI *ET AL.*, *NAT. MED.* **15**, 657 (2009)

www.sciencemag.org

Science

1200 New York Avenue, NW
Washington, DC 20005
Editorial: 202-326-6550, FAX 202-289-7562
News: 202-326-6581, FAX 202-371-9227
Bateman House, 82-88 Hills Road
Cambridge, UK CB2 1LQ
+44 (0) 1223 326500, FAX +44 (0) 1223 326501

Subscription Services For change of address, missing issues, new orders and renewals, and payment questions: 866-434-AAAS (2227) or 202-326-6417, FAX 202-842-1065. Mailing addresses: AAAS, P.O. Box 96178, Washington, DC 20090-6178 or AAAS Member Services, 1200 New York Avenue, NW, Washington, DC 20005

Institutional Site Licenses please call 202-326-6755 for any questions or information

Reprints: Author Inquiries 800-635-7181
Commercial Inquiries 803-359-4578

Permissions 202-326-7074, FAX 202-682-0816

Member Benefits AAAS/Barnes&Noble.com bookstore www.aaas.org/bn; AAAS Online Store www.apisource.com/aaas/ code MKB6; AAAS Travels: Betchart Expeditions 800-252-4910; Apple Store www.wapple/eppstore/aaas; Bank of America MasterCard 1-800-833-6262 priority code FAA3YU; Cold Spring Harbor Laboratory Press Publications www.cshlpress.com/affiliates/aaas.htm; GEICO Auto Insurance www.geico.com/landingpage/go51.htm?logo=17624; Hertz 800-654-2200 CDP#343457; Office Depot https://bsd.officedepot.com/portalLogin.do; Seabury & Smith Life Insurance 800-424-9883; Subaru VIP Program 202-326-6417; VIP Moving Services www.vipmayflower.com/domestic/index.html; Other Benefits: AAAS Member Services 202-326-6417 or www.aaasmember.org.

science_editors@aaas.org	(for general editorial queries)
science_letters@aaas.org	(for queries about letters)
science_reviews@aaas.org	(for returning manuscript reviews)
science_bookrevs@aaas.org	(for book review queries)

Published by the American Association for the Advancement of Science (AAAS), *Science* serves its readers as a forum for the presentation and discussion of important issues related to the advancement of science, including the presentation of minority or conflicting points of view, rather than by publishing only material on which a consensus has been reached. Accordingly, all articles published in *Science*—including editorials, news and comment, and book reviews—are signed and reflect the individual views of the authors and not official points of view adopted by AAAS or the institutions with which the authors are affiliated.

AAAS was founded in 1848 and incorporated in 1874. Its mission is to advance science, engineering, and innovation throughout the world for the benefit of all people. The goals of the association are to: enhance communication among scientists, engineers, and the public; promote and defend the integrity of science and its use; strengthen support for the science and technology enterprise; provide a voice for science on societal issues; promote the responsible use of science in public policy; strengthen and diversify the science and technology workforce; foster education in science and technology for everyone; increase public engagement with science and technology; and advance international cooperation in science.

Information for Authors
See pages 807 and 808 of the 6 February 2009 issue or access www.sciencemag.org/about/authors

EDITOR-IN-CHIEF **Bruce Alberts**
EXECUTIVE EDITOR **Monica M. Bradford** NEWS EDITOR **Colin Norman**
MANAGING EDITOR, RESEARCH JOURNALS **Katrina L. Kelner**
DEPUTY EDITORS **R. Brooks Hanson, Barbara R. Jasny, Andrew M. Sugden**

Editorial senior editor/commentary Lisa D. Chong, Brad Wible; **senior editors** Gilbert J. Chin, Pamela J. Hines, Paula A. Kiberstis (Boston), Marc S. Lavine (Toronto), Beverly A. Purnell, L. Bryan Ray, Guy Riddihough, H. Jesse Smith, Phillip D. Szuromi (Tennessee), Valda Vinson, Jake S. Yeston; **associate editors** Kristen L. Mueller, Nicholas S. Wigginton, Laura M. Zahn; **online editor** Stewart Wills; **associate online editors** Robert Frederick, Tara S. Marathe; **web content developer** Martyn Green; **book review editor** Sherman J. Suter; **associate letters editor** Jennifer Sills; **editorial manager** Cara Tate; **senior copy editors** Jeffrey E. Cook, Cynthia Howe, Harry Jach, Barbara P. Ordway, Trista Wagoner; **copyeditors** Chris Filiatreau, Lauren Kmec; **editorial coordinators** Carolyn Kyle, Beverly Shields; **publications assistants** Ramatoulaye Diop, Carlos L. Durham, Joi S. Granger, Jeffrey Hearn, Lisa Johnson, Scott Miller, Jerry Richardson, Jennifer A. Seibert, Brian White, Anita Wynn; **editorial assistants** Emily Guise, Michael Hicks, Patricia M. Moore; **executive assistant** Sylvia S. Kihara; **administrative support** Maryrose Madrid

News deputy news editors Robert Coontz, Eliot Marshall, Jeffrey Mervis, Leslie Roberts; Contributing Editors Elizabeth Culotta, Polly Shulman; **news writers** Yudhijit Bhattacharjee, Adrian Cho, Jennifer Couzin, David Grimm, Constance Holden, Jocelyn Kaiser, Richard A. Kerr, Eli Kintisch, Andrew Lawler (New England), Greg Miller, Elizabeth Pennisi, Robert F. Service (Pacific NW), Erik Stokstad; **interns** Michael Torrice, Brittany Johnson, Preyanka Makadia; **contributing correspondents** Dan Charles, Jon Cohen (San Diego, CA), Daniel Ferber, Ann Gibbons, Robert Koenig, Mitch Leslie, Charles C. Mann, Virginia Morell, Evelyn Strauss, Gary Taubes; **copy editors** Linda B. Felaco, Melvin Gatling, Melissa Raimondi; **administrative support** Scherraine Mack, Fannie Groom; **bureaus** New England: 207-549-7755, San Diego, CA: 760-942-3252, FAX 760-942-4979, Pacific Northwest: 503-963-1940

Production director James Landry; **senior manager** Wendy K. Shank; **assistant manager** Rebecca Doshi; **senior specialists** Steve Forrester, Chris Redwood; **specialist** Anthony Rosen; **Preflight director** David M. Tompkins; **manager** Marcus Spiegler; **specialist** Jason Hillman

Art director Yael Kats; **associate art director** Laura Creveling; **senior illustrators** Chris Bickel, Katharine Sutliff; **illustrator** Yana Greenman; **senior art associates** Holly Bishop, Preston Huey, Nayomi Kevitiyagala; **art associates** Jessica Newfield, Matthew Twombly; **photo editor** Leslie Blizard

***Science* International**

Europe (science@science-int.co.uk) **editorial: international managing editor** Andrew M. Sugden; **senior editor/commentary** Julia Fahrenkamp-Uppenbrink; **senior editors** Caroline Ash, Stella M. Hurtley, Ian S. Osborne, Peter Stern; **associate editor** Maria Cruz; **locum editor** Helen Pickersgill; **editorial support** Deborah Dennison, Rachel Roberts, Alice Whaley; **administrative support** John Cannell, Janet Clements, Louise Moore; **news: Europe news editor** John Travis; **deputy news editor** Daniel Clery; **contributing correspondents** Michael Balter (Paris), John Bohannon (Vienna), Martin Enserink (Amsterdam and Paris), Gretchen Vogel (Berlin); **intern** Claire Thomas

Asia Japan Office: Asca Corporation, Eiko Ishioka, Fusako Tamura, 77 Tenjin-cho, Shinjuku, Tokyo 162-0808, Japan; +81 3 6802 4616, FAX +81 3 6802 4615, inquiry@sciencemag.jp; **asia news editor** Richard Stone (Beijing: rstone@aaas.org); **contributing correspondents** Dennis Normile (Japan: +81 (0) 3 3391 0630, FAX +81 (0) 3 5936 3531; dnormile@gol.com); Hao Xin (China: +86 (0) 10 6307 4439 or 6307 3676, FAX +86 (0) 10 6307 4358; cindyhao@gmail.com); Pallava Bagla (South Asia: +91 (0) 11 2271 2896; pbagla@vsnl.com)

EXECUTIVE PUBLISHER **Alan I. Leshner**
PUBLISHER **Beth Rosner**

Fulfillment Systems and Operations (membership@aaas.org); **director** Waylon Butler; **senior systems analyst** Nomuna Nyamaa; **customer service supervisor** Pat Butler; **specialists** Latoya Casteel, LaVonda Crawford, Vicki Linton, April Marshall; **data entry supervisor** Cynthia Johnson; **specialists** Shirlene Hall, Tarrika Hill, William Jones

Business Operations and Administration director Deborah Rivera-Wienhold; **assistant director, business operations** Randy Yi; **manager, business analysis** Michael LoBue; **manager, business operations** Jessica Tierney; **financial analysts** Priti Pamnani, Celeste Troxler; **rights and permissions: administrator** Emilie David; **associate** Elizabeth Sandler; **marketing director** Ian King; **marketing managers** Allison Pritchard, Alison Chandler, Julianne Wielga; **marketing associates** Aimee Aponte, Mary Ellen Crowley, Adrian Parham, Wendy Wise; **marketing executive** Jennifer Reeves; **director, site licensing** Tom Ryan; **director, corporate relations** Eileen Bernadette Moran; **publisher relations, eresources specialist** Kiki Forsythe; **senior publisher relations specialist** Catherine Holland; **publisher relations, east coast** Phillip Smith; **publisher relations, west coast** Philip Tsolakidis; **fulfillment supervisor** Iquo Edim; **fulfillment coordinator** Carrie MacDonald; **marketing associate** Mary Lagnaoui; **electronic media: manager** Lizabeth Harman; **project manager** Trista Snyder; **assistant manager** Lisa Stanford; **senior production specialists** Christopher Coleman, Walter Jones; **production specialists** Nichele Johnston, Kimberly Oster

Advertising director, worldwide ad sales Bill Moran

Product (science_advertising@aaas.org); **midwest/west coast/w. canada** Rick Bongiovanni: 330-405-7080, FAX 330-405-7081; **east coast/e. canada** Laurie Faraday: 508-747-9395, FAX 617-507-8189; **uk/europe/asia** Roger Goncalves: TEL/FAX +41 43 243 1358; **japan** Mashy Yoshikawa: +81 (0) 3 3235 5961, FAX +81 (0) 3 3235 5852; **senior traffic associate** Deiandra Simms

Commercial Editor Sean Sanders: 202-326-6430

Project Director, Outreach Brianna Blaser

Classified (advertise@sciencecareers.org); **u.s.: sales manager** Daryl Anderson: 202-326-6543; **midwest** Tina Burks: 202-326-6577; **east coast** Alexis Fleming: 202-326-6578; **west/south central** Nicholas Hintibidze: 202-326-6533; **sales coordinators** Rohan Edmonson, Shirley Young; **international: sales manager** Tracy Holmes: +44 (0) 1223 326525, FAX +44 (0) 1223 326532; **sales** Susanne Kharraz, Dan Pennington, Alex Palmer; **sales assistant** Lisa Patterson; **japan** Mashy Yoshikawa: +81 (0) 3 3235 5961, FAX +81 (0) 3 3235 5852; **advertising support manager** Karen Foote: 202-326-6740; **advertising production operations manager** Deborah Tompkins; **senior production specialist/graphic designer** Amy Hardcastle; **senior production specialist** Robert Buck; **senior traffic associate** Christine Hall;

AAAS Board of Directors retiring president, chair James J. McCarthy; **president** Peter C. Agre; **president-elect** Alice Huang; **treasurer** David E. Shaw; **chief executive officer** Alan I. Leshner; **board** Alice Gast, Linda P. B. Katehi, Nancy Knowlton, Cherry A. Murray, Julia M. Phillips, Thomas D. Pollard, David S. Sabatini, Thomas A. Woolsey

AAAS
ADVANCING SCIENCE, SERVING SOCIETY

Ancient Granaries

Before the agricultural revolution some 10,000 years ago could really take off, people had to find a way to store their produce. Archaeologists working in Jordan now say they have found the remains of several granaries built nearly 1000 years before cereals were first domesticated.

A team led by archaeologists Ian Kuijt of the University of Notre Dame in Indiana and Bill Finlayson of the Council for British Research in the Levant in Amman, Jordan, has uncovered at least 10 stone and mud-brick structures that were probably used both as houses and as food-processing centers at the site of Dhra` just east of the Dead Sea, which was occupied about 11,300 years ago. Interspersed among these buildings were at least four circular structures, about 3 meters in diameter, which were probably granaries. Inside the best-preserved one are notched stones, which the archaeologists hypothesize supported wooden beams forming a raised floor to protect the grains. The granaries apparently stored wild barley, the team reported last week in the *Proceedings of the National Academy of Sciences*.

The team argues that storing wild grains was an essential precursor to key features of the farming revolution: domestication of cereals and the growth of large communities. Dorian Fuller, an archaeologist at University College London, agrees with the authors, adding that because farmers were already cultivating wild plants when these granaries were built, hunter-gatherers were probably not engaging in large-scale storage, as some archaeologists assume.

Excavation reveals notched stones from granary (*inset*).

CREDITS (TOP TO BOTTOM): STEVE IRVINE; BILL FINLAYSON; (INSET) NATIONAL ACADEMY OF SCIENCES; MIT

Master of Nanotechnology

Chad Mirkin, a chemist and director of the International Institute for Nanotechnology at Northwestern University in Evanston, Illinois, has won this year's $500,000 Lemelson-MIT Prize, known as the "Oscar for Inventors."

Mirkin, 45, has created a host of nano-diagnostic devices, including the Verigene ID System, which combines nanoparticles and DNA to detect proteins marking a range of illnesses including infectious diseases, cancer, heart disease, and genetic disorders. He's also developed a high-resolution printing mechanism called Dip-Pen Nanolithography that replicates molecules from cells and viruses so their functions can be examined.

Mirkin says he plans to invest part of his winnings in his new company, AuraSense, which will seek new ways to apply nanotechnology to therapeutics—in particular, raising levels of HDL, the "good" cholesterol, to prevent heart disease. He has already founded two other companies, Nanosphere and NanoInk.

Look Out for Flashers

"The fireflies, twinkling among leaves, make the stars wonder."

—Rabindranath Tagore

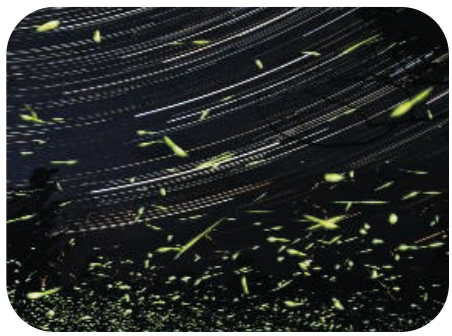

Consider the firefly. That's what Boston's Museum of Science wants everyone to do. "People are always asking 'Is the firefly population declining?'" says Sara Lewis, an evolutionary ecologist at Tufts University in Medford, Massachusetts. So the museum set up a Firefly Watch, now beginning its second summer, which invites people to report firefly sightings in their backyards (www.mos.org/fireflywatch). So far, there are reports from about 1300 locations, most in the United States but some from as far afield as India.

Fireflies don't provide any noteworthy ecosystem services, but they may be sensors for environmental degradation by light and toxins because they attract mates by flashing and spend most of their lives as larvae in the ground living off earthworms and the like.

Fireflies are hard to count, Lewis admits. But other data are easier to gather: Different species light up in several colors and in a variety of different patterns, from single signals to clumps of multiple ones to continuous flashing.

Plum Internship

Get in on the ground floor in the hunt for the Higgs boson! CERN is looking for a young media whiz to make the Large Hadron Collider (LHC) look great in the fall when it finally starts up "the most complex scientific project ever conceived by mankind." The European physics lab is inviting applicants to submit a video or multimedia project, lasting up to 5 minutes, about ATLAS, one of LHC's four big particle detectors. It can be "fiction or documentary," and applicants are free to pluck material from videos and photographs supplied on the CERN Web site. The deadline is 31 July.

The winner will spend 3 months on a multimedia project documenting the first collisions in the 25-meter-tall, 45-meter-long ATLAS device.

Published by AAAS

Competing for an Antarctic contract
20

Excavating China's terra-cotta figures
22

CARBON TRADING

House Vote Seen as Big Step Toward Cooling the Greenhouse

Its praises have been sung as an energy security bill and a jobs bill. But the American Clean Energy and Security Act passed last Friday by the U.S. House of Representatives is in fact milestone greenhouse legislation.

At the heart of the bill, cobbled together over several weeks by representatives Henry Waxman (D–CA) and Edward Markey (D–MA), is a so-called cap-and-trade system that assigns permits to pollute to those sectors of the economy that generate the bulk of the country's greenhouse gas emissions. The bill faces serious political challenges: After squeaking through the House on a vote of 219 to 212, with 44 Democrats opposing it and only eight Republicans supporting it, its future in the Senate is uncertain. If it becomes law, however, economists are optimistic that it will achieve significant reductions in carbon emissions.

"I'd give it a B," says economist Dallas Burtraw of Resources for the Future in Washington, D.C. "We know how cap-and-trade works. We can count on it to deliver" the promised emission reductions: 17% below 2005 levels in 2020, rising to 83% by 2050. Economists worry about the cost of those reductions in the wake of compromises struck to gain passage in the House. Still, assuming those add-ons are rigorously administered, "cap-and-trade will limit emissions as claimed," says economist Richard Schmalensee of the Massachusetts Institute of Technology (MIT) in Cambridge.

Tell that to the Europeans. Many opponents of cap-and-trade say that the European Union's experience with its Emissions Trading System, launched in 2005 under the Kyoto Protocol, should be enough to kill the idea in the United States.

As in all cap-and-trade systems, the E.U. issued a set number of permits, or allowances, that let big polluters emit a specified amount of carbon dioxide per allowance. That's the cap, which would decrease over time. Over the first 3 years, companies that had paid to reduce their own emissions sold their spare allowances to companies emitting more than their initial allowances.

That market trading set a price on carbon emissions. Coal consumers, for example, could choose to switch to natural gas—which yields less CO_2 per unit of energy—or to remove CO_2 from their stacks and bury it. "May the cheapest option win," as Burtraw puts it.

However, the first 3 years of the E.U.'s trading did not go smoothly. "If you look at the performance of the market, it was a fiasco," says Burtraw. But he and others blame flaws in the E.U.'s trading system rather than the cap-and-trade concept itself. "It proved that stupid design features will get you stupid results," says Schmalensee.

Targets. The cap-and-trade provision in the House bill is aimed at reducing emissions from factories and agriculture and includes offsets to buffer the cost of such reductions.

One of the E.U.'s missteps, say economists, was to issue more allowances than actual emissions. It also gave away most allowances rather than selling them at auction, and it did not let polluters carry over allowances from the initial 3-year trading period to the next 5-year period. As a result, some companies made "windfall profits" off their allowances, and the market price of carbon swung wildly before ending up at zero at the end of 2007. Participating countries hope to meet their promised Kyoto emission reductions by 2012.

Despite those start-up problems, "I judge it as a success," says economist A. Denny Ellerman of MIT, who has analyzed the European experience with colleagues. Cap-and-trade neither destroyed the economy, as some had feared, he notes, nor did it drastically reduce emissions, as some had hoped. But it did manage to set a price on carbon, he says, which in the end reduced emissions by the small amount intended.

Supporters of the House bill say they have learned some do's and don'ts of cap-and-trade from what happened in Europe. The House version lets emitters carry allowances over long periods, for example. And the number of U.S. allowances issued should be close to what is needed, says Ellerman.

The most debated aspect of the Waxman-Markey bill has been its provision for auctioning only 20% of allowances, a share that grows to 70% by 2030. The rest are distributed free. Some Republican opponents see that as a massive corporate giveaway. But economists disagree. "Does the economics literature support auctioning 100% of allowances?" asks emeritus professor Thomas Tietenberg of Colby College in Waterville, Maine. "Yes. Does it destroy the system if allowances are given away? No. Does it make it a bit more expensive and less efficient? Yes."

Economist Robert Stavins of Harvard University sees the Waxman-Markey distribution of allowances as even more benign. The political wheeling and dealing that led to the allocation of free allowances to particular public activities built support for the legislation, Stavins says, without increasing costs or emissions.

For example, he calculates that whereas 20% of the value of allocations in Waxman-Markey would go to private industry, 80% would end up benefiting consumers or society in general. The list includes a variety of public endeavors, from job training and cost protection for lower-income households to encouraging the preservation of overseas forests. The last, he notes, would lead to an overall reduction of CO_2 emissions.

Perhaps of greatest concern to economists and many environmentalists is the bill's use of

CREDITS: JUPITERIMAGES

Published by AAAS

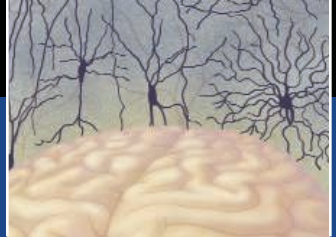

Nervous origins 24

On the trail of conflict of interest 28

so-called offsets to reduce the cost of cutting emissions. The concept of offsets—a polluter's payment to have someone else reduce emissions—is uncontroversial. A power plant operator might find it cheaper to pay another party who does not fall under cap-and-trade—say, a lumberer—to cut emissions by not clearing a forest. "It can be a win-win in terms of reducing costs," says Nigel Purvis, president of Climate Advisers in Washington, D.C., and a former U.S. climate negotiator, who calls this offset approach "exactly right."

But offsets also entail risks, say Purvis and others, notably how to verify that a claimed emission would otherwise really have happened without the intervention. "We really don't know what the rules will be" governing the validation of offsets, notes Burtraw, "and therefore how rigorous the administration of offsets will be." Doubts were heightened just days before passage when Waxman, at the insistence of Representative Collin Peterson (D–MN) and other farm-state advocates, agreed to shift responsibility for overseeing domestic offsets from the Environmental Protection Agency to the Department of Agriculture.

"You have to worry about that," says climate policy specialist Michael Oppenheimer of Princeton University. The agriculture department doesn't have EPA's monitoring experience, he notes, and it has a history of protecting the interests of farmers. Offsets are "the one place the bill could go south," Oppenheimer cautions.

Although the Obama Administration campaigned hard for passage of Waxman-Markey, it's been careful not to dictate the terms. That's just as well. Most observers expect the Senate to put its own stamp on the cap-and-trade provisions. Supporters can only hope that senators heed the words of House Speaker Nancy Pelosi (D–CA) when she urged her colleagues "not only to pass the bill but [to make sure] it does the job that it sets out to do." **–RICHARD A. KERR**

PANDEMIC INFLUENZA

Ferrets Shed Light on New Virus's Severity and Spread

When scientists want to know how a new flu strain behaves, one of the first things they do is squirt it up the noses of ferrets. The small carnivores' responses often closely resemble those of humans, assuring them the unenviable status of flu virologists' favorite model animal.

Now, two groups have infected ferrets with the new pandemic A(H1N1) influenza strain, and their papers, published online by *Science* this week, confirm what doctors around the world appear to be seeing: The new virus is a bit more pathogenic than seasonal influenza but nowhere near as dangerous as the 1918 pandemic virus or H5N1 avian influenza. The studies disagree, however, on how easily the virus spreads: One team concludes that it does so very well, but the other believes that it's only moderately adept at jumping from one animal to the next, or, for that matter, between humans.

For the studies, Terrence Tumpey of the U.S. Centers for Disease Control and Prevention (CDC) in Atlanta, Georgia, inoculated 18 ferrets, six each with H1N1 viruses isolated from patients in California, Texas, and Mexico (www.sciencemag.org/cgi/content/abstract/1177238). A team led by Ron Fouchier of Erasmus Medical Center in Rotterdam, the Netherlands, infected six ferrets with a virus isolated from the first Dutch patient (www.sciencemag.org/cgi/content/abstract/1177127). Both used a seasonal H1N1 strain as a control and both found that the pandemic virus caused more severe disease.

Fouchier found that the pandemic virus descends deeper into the lungs, infecting not just the nasal cavity but also the trachea and the bronchi. Tumpey's team also found it in the intestinal tract, which is interesting, says swine flu expert Christopher Olsen of the University of Wisconsin, Madison, because vomiting and gastrointestinal disease are common in pandemic flu victims.

By putting infected and healthy ferrets in cages next to one another, the teams discovered that the virus can be transmitted through the air, but whereas Fouchier's team found that the new virus spreads as well as the seasonal strain, Tumpey found that it's a less efficient transmitter: For all three of the pandemic strains tested, only two out of three animals in adjoining cages became infected.

"I wouldn't make too much of that difference," says flu expert Peter Palese of Mount Sinai School of Medicine in New York City, who believes that the numbers are too small to be significant. Fouchier adds that data from other researchers, presented at a meeting in Minneapolis, Minnesota, last week, also suggest that the new virus is highly transmissible. But Tumpey believes that it's genuinely handicapped compared with seasonal flu. "We have a lot of experience with this model," he says. His team's findings jibe with unpublished epidemiological data from CDC suggesting that only 10% of patients' household contacts become infected, Tumpey adds, which is low for a pandemic virus.

Both teams agree on one thing: The ferret is a good model to test vaccines or drugs against the new strain, and, as the pandemic unfolds, to test viral mutants suspected of higher virulence or easier transmission. "The whole world is coughing up new sequences and making them public in real time," Fouchier says. "When we see something that's unusual, we can put it into ferrets immediately."

–MARTIN ENSERINK

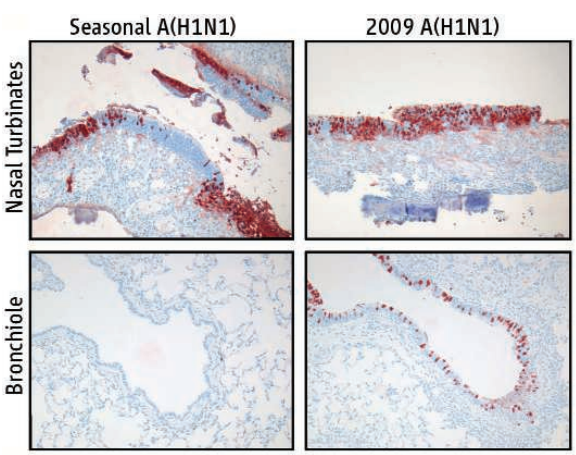

Going deeper. Both seasonal and pandemic H1H1 infect ferrets' nasal cavities (*top*), but only the pandemic virus penetrates into the lungs (*bottom right*).

CREDIT: VINCENT J. MUNSTER *ET AL.*, *SCIENCE*

Published by AAAS

SBIR PROGRAM

Researchers Fight Against Bigger Slice to Small Business

A coalition of U.S. scientific societies and university organizations is urging Congress not to expand a $2.3 billion research program for small businesses. To succeed, however, the coalition must overcome one of the most influential interest groups in Washington, D.C., and mend fences with legislators still smarting from a recent tweak to the program.

The campaign involves changes to the Small Business Innovation Research (SBIR) program. Begun in 1983 and funded by taxing the research budgets of 11 federal agencies, the SBIR set-aside is meant to help a sector that many people agree will be key in pulling the country out of its economic doldrums.

Last month, the Senate small business panel passed a bill (S.1233) that would increase the set-aside by 40%, from 2.5% to 3.5%, over 11 years. Under the same legislation, a smaller, younger effort to aid university start-ups, the Small Business Technology Transfer (STTR) program, would grow from 0.3% to 0.6%. "This is an important program that is working, and we believe that an increase is essential," says Senator Mary Landrieu (D–LA), chair of the Senate panel and one of SBIR's biggest fans. Last year, the panel approved a doubling of the SBIR set-aside over 5 years, but the bill died.

Science lobbyists, however, argue that even the smaller, more gradual rise in play this year would take too big a bite out of the government's overall research budget. They are especially concerned about its impact on the National Institutes of Health (NIH), which runs the second-largest SBIR program after the Department of Defense. NIH has seen a sharp drop in the number of SBIR applications (see graph), and its officials are worried that expanding the program could force it to fund low-quality projects.

The science community much prefers a proposal (H.R.2965) to maintain the current set-aside, passed separately last week by the science and small business committees in the House of Representatives. So does the president's science adviser, John Holdren, who on 2 June wrote Landrieu to say that "the current budget set-asides provide a sufficient floor for agencies to invest in innovation from small businesses."

The lobbying to contain the program is led by the Federation of American Societies for Experimental Biology (FASEB), reflecting a heightened concern among life scientists that expanding the SBIR program will reduce federal funding for academic biomedical research. "Rather than increasing support for one area at the expense of all others, we urge you to increase funding for all research agencies," says Richard Marchase, president of FASEB. On 23 June, the coalition sent letters to Landrieu and Senator Olympia Snowe (R–ME), the committee's ranking member, urging them to scrap the increase.

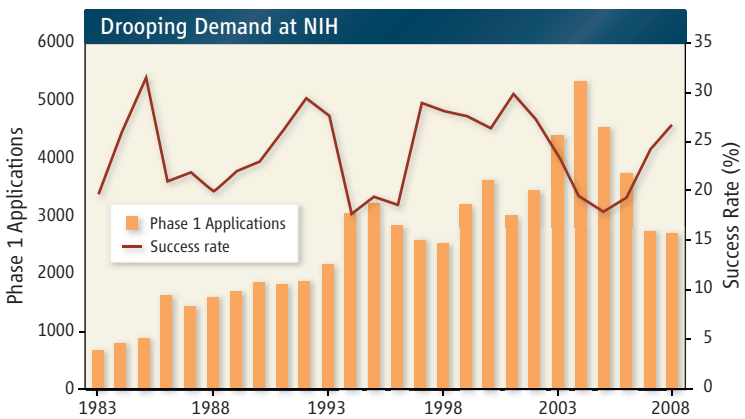

Nothing ventured. The number of SBIR applications dropped sharply following new rules on participation by venture capital firms, but the connection is not clear.

But FASEB faces an uphill battle. The small business sector lost out when Congress added a last-minute provision to the $787 billion American Recovery and Reinvestment Act (ARRA)—known familiarly as the stimulus package—that excluded NIH's SBIR program from its share of the additional $8.2 billion that the agency will receive. That move could come back to haunt the research community.

None of the key committees was consulted about the provision, says Representative David Wu (D–OR), chair of the technology panel for the House science committee and a co-sponsor of the House bill. "I feel strongly that ARRA funds should have been part of the set-aside," he says. "Exempting them sets a bad precedent and is not a positive thing." Adds a Senate aide, "We think small business should get its fair share, and, frankly, this seemed like dirty pool."

The exclusion has become a political hot potato. Wu says that "no one has claimed credit, but NIH has confessed to asking for it." At a 23 April hearing on the program, Wu asked an NIH official about the apparent contradiction between the exclusion and a letter from acting NIH Director Raynard Kington to Landrieu and Snowe that Wu said "commits" NIH to preserving the set-aside in all appropriations. Sally Rockey, head of NIH's Office of Extramural Programs, acknowledged that NIH was concerned about a dearth of "scientifically meritorious projects" if the SBIR set-aside was applied to the stimulus funds. But in response to a follow-up question from Wu, Rockey wrote the committee that "I have no specific details of how this exemption was put into ARRA."

Science asked Kington to clarify his position. In response, an NIH spokesperson noted that NIH is not required to devote stimulus funds to the SBIR program but that "small businesses are able to, already have, and will receive NIH ARRA funds … through various [other] funding opportunity announcements" that are not reserved for small businesses. "NIH remains committed to the SBIR and STTR programs," the spokesperson added.

While science lobbyists are focused on the size of the set-aside, other groups are embroiled in a battle over a provision that affects venture capital firms. The Senate and House bills differ in how best to modify a restriction, in place since 2002, on the eligibility of companies in which venture capitalists hold a controlling interest (see *Science*Insider.org, 22 June). In addition, although both bodies want to boost the size of the awards, now $750,000 for Phase II, the House would go up to $2 million, which is twice the Senate level. The House bill would continue the program for two more years, whereas the Senate bill would let it run until 2023.

The clock is ticking on a compromise. The program expires on 31 July, and although all sides say they want to finish work by then, it's more likely that a short-term extension will be needed so legislators can keep plugging away.

–JEFFREY MERVIS

SOURCE: NIH SBIR PROGRAM

Published by AAAS

BUDGET CUTS

Proposal to Slash Salaries Riles California Researchers

Proposed salary cuts and/or furloughs for all faculty and staff members are causing consternation at the University of California (UC), one of the nation's largest public universities, with approximately 170,000 employees. The proposed cuts, outlined in a letter to all employees by UC President Mark Yudof on 17 June, would help reduce a projected $800 million shortfall in state funding for UC over the next 2 years, a result of the state's economic meltdown. "The University has never faced a funding deficit of this magnitude, and responding to it will require sacrifice from every member of the University community," Yudof wrote.

Nobody likes a pay cut, but many science faculty and staff members are particularly peeved because their salaries are at least partly paid by grants from the National Institutes of Health, the National Science Foundation, and other agencies. Cutting pay from these nonstate sources won't save UC any money, they argue, and could make matters worse.

Yudof's letter outlines three proposals that combine salary cuts and furloughs to different extents. All amount to a roughly 8% reduction in pay (4% for those making less than $46,000 a year) for 1 year and would save UC roughly $195 million. Graduate student stipends would not be cut. The reductions would apply to all employees, regardless of where their salaries come from. "That's the approach he thinks is the fairest and makes the most sense," says Paul Schwartz, a spokesperson for the UC office of the president.

Bearer of bad news. UC President Mark Yudof has proposed pay cuts to help address the university's budget woes.

CREDITS (TOP TO BOTTOM): NASA/JPL/SPACE SCIENCE INSTITUTE; JEFF CHIU/AP PHOTO

But equity is in the eye of the beholder. "The fairness argument just doesn't hold water with people," says Daniel Donoghue, a biochemist and chair of the academic senate at UC San Diego (UCSD). At UCSD, for example, only 25% of salary expenditures come from state funds; the rest come from federal grants, medical center income, and other sources, says Donoghue, citing UC's 2007–08 financial report. He and others question why people paid with nonstate funds should have to suffer, especially when it won't help UC's bottom line. "If I'm bringing in this research money from Washington … and I lose my grant, the rest of the university doesn't have to feel my pain, and I wouldn't expect them to," says Andrea Bertozzi, director of applied mathematics at UC Los Angeles (UCLA).

Across-the-board pay cuts may even deprive UC of income. "There's a net loss of income to the UC system that accompanies cutting [the salaries of] people who are not state-funded," says Quentin Williams, a professor of earth sciences and chair of the academic senate at UC Santa Cruz. That's because the amount of money a university can charge grant-giving agencies for the indirect costs of research, such as building maintenance and utilities, is a fixed percentage of the direct costs of a grantee's research, including salaries and equipment purchases.

If the university decides to dock salaries derived from outside grants—many of which have already been awarded—it's not clear what would happen with the leftover money. Many grants allow for enough flexibility in budgeting that the money could probably still be used to purchase equipment or to cover other expenses.

UC scientists also worry about recruiting and retention. Despite having many distinguished departments, UC faculty members already earn 20% to 25% less on average than faculty at top private schools like Harvard and Stanford universities, according to the university's annual accountability report. "It presents an opportunity for private universities to raid the University of California," says UCLA neuroscientist Arthur Toga.

Yudof is taking these concerns into consideration, says Schwartz. But time is short. The UC Regents begin meeting in San Francisco on 14 July, and Yudof is expected to winnow down his three original proposals to one—including any modifications based on feedback from the faculty and staff—after the long 4 July weekend. **–GREG MILLER**

ScienceNOW.org

From *Science*'s Online Daily News Site

Brain Recordings Take Flight

Homing pigeons use landmarks to guide them safely home. But how do the birds track these familiar sites hundreds of meters below as they zip by at 65 km/h? Scientists are trying to answer that question with a new device that lets them record brain activity while pigeons fly. http://tinyurl.com/kjnms6

Icy Enceladus Getting Wetter

The hottest topic in the frigid outer solar system is the water of Saturn's moon Enceladus. Is it all lifeless, deep-chilled ice, or is some of it liquid and thus capable of sustaining life? Two sets of observations reported in *Nature*—one made by touching ice spewing from the moon and the other made from Earth—again suggest that there could be liquid water beneath the surface of 500-km-diameter Enceladus. Even so, it's not gushing like a geyser directly from a deep ocean. http://tinyurl.com/mb4va8

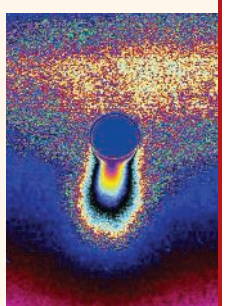

Evolution Heats Up in the Tropics

Time for a pop quiz. Which mammal evolves more rapidly? Is it the ringtail, a raccoonlike animal common in the southwestern United States, or the closely related cacomistle, which lives in tropical forests in southern Mexico and Central America? A surprising new study indicates that lower elevations and lower latitudes seem to speed up microevolution in mammals, giving the nod to the cacomistle. http://tinyurl.com/nc9gga

Stone-Age Europeans Led Rich Life

Archaeologists have discovered what may be the oldest musical instruments ever found. They are bird-bone and ivory flutes that appear to be at least 35,000 years old. The flutes' design and studies of other artifacts from the site suggest that music was an integral part of human life far earlier than first thought. http://tinyurl.com/mht7k7

Read the full postings, comments, and more on **sciencenow.sciencemag.org**.

Published by AAAS

NSF ANTARCTIC LOGISTICS

A Hot Competition for a Cold Contract

The five billboards lining the tracks inside the Ballston Metro station outside Washington, D.C., aren't selling anything that the 25,000 daily commuters could ever buy. But that's okay with the company that purchased the advertisements. Their message—"The toughest team for the toughest environment"—is aimed at the National Science Foundation, the federal agency located directly above the station.

This fall, the National Science Foundation (NSF) will award a contract worth nearly $2 billion to provide logistical support for its $300-million-a-year Antarctic research program. And officials from Antarctic Research Support (ARS), a joint venture formed 4 months ago by two large systems-engineering companies for the express purpose of winning that contract, hope that the billboards demonstrate that they can be good stewards of science on the frozen continent.

ARS is one of a half-dozen companies bidding for the 12-year contract, the biggest award made by the $6.5-billion-a-year federal agency. Such competitions are typically very low-key, partly because the work isn't sexy and partly because the rules governing such competitions don't allow for much boasting. But ARS's high-profile approach—it's also running ads in Metro cars and on this magazine's Web site—is part of a broader strategy to raise the visibility of its parent companies, CSC and EG&G, and tout the scientific expertise of its team, led by two scientists who held major science posts in the last Administration. And ARS isn't the only bidder trying to grab the public spotlight. Lockheed Martin has also taken out a billboard at the Ballston station, although its message is even more cryptic: "Between supporting science everywhere and anywhere, there is one important word: How."

"When I tell people what I'm doing, they ask me if Antarctica is an ocean or a continent," says retired Vice Admiral Conrad Lautenbacher, the former head of the National Oceanic and Atmospheric Administration who's leading the ARS team. "So I think people need to learn more about what's going on there. In addition, CSC is a $17 billion company, but it doesn't have a signature product. So the idea [behind the advertisements] is to gain some recognition of the fact that we have the necessary skills and should be given the chance to perform them."

Frozen treat. Several bidders for the logistics contract have also decided to tout the science being done in Antarctica.

Kenneth Asbury, president of the civil division within the integrated systems and solutions program at Lockheed Martin, says that the aerospace giant was attracted by NSF's desire "to extract the most science possible from the facilities down there. It requires getting the right thing to the right place at the right time in what's probably the most hostile environment imaginable." Asbury said the billboard is meant to publicize "the extent of the government's commitment to Antarctica." A third bidder, Houston, Texas–based KBR, has also taken out a Metro ad promoting polar science. Its spokesperson, Heather Browne, says the company, if it wins the contract, hopes to make changes in the program that would "significantly increase the efficiency of science support."

Some companies in the hunt, including the incumbent, Raytheon Polar Services Co., were reticent to discuss their bids. "We have a policy not to discuss open procurements," explains Jennifer Thompson, a communications manager for the Antarctic team at CH2MHill, a Fortune 500 company based in Englewood, Colorado, citing the need to adhere to government rules. "But I can say that I've gotten more questions about it from folks in the halls than on any other project. It's an exciting opportunity."

NSF is expected to choose a winner this fall. The contract would begin in April 2010 and, with extensions, could run until 2023.

–JEFFREY MERVIS

2010 BUDGET

House Panel Cuts DOE Education Program

A House spending panel has rejected a comprehensive $115 million science education initiative from the Department of Energy (DOE) to train a new cadre of scientists pursuing basic and applied research on clean energy.

President Barack Obama unveiled the effort, dubbed RE-ENERGYSE, in a 27 April speech to the National Academy of Sciences, and it is part of the department's 2010 budget request now before Congress. The program spans the education spectrum, from elementary and high schools through postdoctoral study, and includes technical training at community colleges as well as public outreach. DOE officials say that they are still working out the details and hope to involve the National Science Foundation and other federal agencies.

But legislators feel that the idea is still half-baked. "Everybody is for more science and math education. And a lot of other agencies are already very active," says Representative Ed Pastor (D–AZ), acting chair of the energy and water appropriations subcommittee, speaking last week after the panel marked up DOE's overall budget request. "We don't want to curb their enthusiasm. But we want to make sure that DOE integrates its plans with other, ongoing programs within the department and across the rest of the government." Pastor said the subcommittee has included $7 million for RE-ENERGYSE (REgaining our ENERGY Science and Engineering Edge) in the bill as a way to "get things moving."

The panel provided DOE's Office of Science with its full request of $4.9 billion as part of a $26.9 billion budget that includes the department's responsibilities for nuclear weapons and environmental cleanup. The panel cut the entire $1.5 billion request for a loan-guarantee program to support innovative energy technologies, noting that the program has sufficient money from this year's stimulus package to operate for 2 years. The bill now goes to the full committee before heading to the House floor later this month.

–JEFFREY MERVIS

CREDIT: PHOTO COURTESY OF CSC

Published by AAAS

PHARMACEUTICALS

Betting on Biotech to Transform Guangdong, China's Export Hub

GUANGZHOU, CHINA—The timing could not have been worse, or so it seemed: Last November, as the global financial crisis was deepening, Yan Guangmei opened a $100 million drug R&D center here in the capital of Guangdong, the southern province that churns out the lion's share of goods bearing the "Made in China" label. Since then, tens of thousands of Guangdong companies have gone bankrupt. But Yan, a neuropharmacologist and vice president of Sun Yat-sen University in Guangzhou, is still smiling. He has already hired 50 staff members, half from overseas, for his Southern China Center for Innovative Pharmaceuticals (SCCIP). The center will team up with companies to move drug candidates into clinical trials and will conduct its own exploratory research.

Yan has good reason to be upbeat. Local officials are betting that biotech will help wean the province off its heavy dependence on cheap exports. "Companies that don't have core technology are the ones who are now suffering," says Li Xinghua, director general of the Guangdong Science and Technology Department. Last year, he says, Guangdong spent more than $1 billion, mostly on infrastructure, to induce high-tech companies to set up shop in the province; the pace of such spending has increased by 5% or so this year.

Officials acknowledge that Guangdong is slow off the blocks. Shanghai is the undisputed center of gravity for biopharma in China, and ambitious high-tech parks have taken root in Suzhou, Tianjin, and elsewhere. "Guangdong has shown that it is great at doing business," says Larry Zhang, a medicinal chemist at the Guangzhou Institutes of Biomedicine and Health. "But in science, we have a lot of catching up to do."

Among the new initiatives, Guangdong is developing a "Biotech Island" off Guangzhou and is about to launch a program to reel in at least 100 overseas scientists to commercial labs, universities, and state research institutes. Benefits will include free housing and $1.3 million lab start-up packages. "We see the financial crisis as an unprecedented opportunity to attract top scientists," Guangdong's vice governor, Wan Qingliang, told *Science*. Such an infusion of talent is "desperately needed," says Zhai Yifan, president of the Chinese Biopharmaceutical Association, which brokered connections between U.S.-based Chinese scientists and Guangdong enterprises at its annual meeting in Guangzhou last week. "It is urgent for Guangdong to move away from its labor-based economy," says Zhai.

According to Yan, a recent returnee, Guangdong offers advantages over other regions. Drug R&D costs are a fraction of those in the West, says Yan, who says SCCIP will team up with a private primate center in nearby Zhaoqing and will create its own dog facility for preclinical testing. And for scientists seeking a Western lifestyle, Hong Kong is a 1-hour commute.

Come hither. Guangdong vice governor Wang Qingliang hopes SSCIP (*inset*) and other investments will lure scientific talent to his province.

Guangdong officials have bought into that vision. The province has plunked down half of SCCIP's start-up funds, with the other half coming from Guangzhou municipality, a special economic zone, the central government, and Chinese pharmaceutical companies. In about 5 years, SCCIP will relocate from temporary digs to Biotech Island. Guangzhou has already resettled thousands of people from the 1.8-square-kilometer island in the Pearl River, near Sun Yat-sen University, to convert the island into an R&D center.

As high-tech moves in, low-cost production will shift to "the hinterlands"—China's western and central provinces—predicts Ivan Tselichtchev, an expert on Asian economies at the Japan Center for Economic Research in Tokyo. "Yes, many companies collapsed," he says. "But the economy is still growing. It's an amazing phenomenon." **–RICHARD STONE**

CREDITS: R. STONE/*SCIENCE*; (INSET) COURTESY OF SCCIP

ScienceInsider

From the *Science* Policy Blog

Congress picked up the pace last week in meeting its obligation to pass annual spending bills. Senate appropriators approved a 5% boost in 2010 for both **NASA and NOAA** as part of a bill that's more generous than what the U.S. House of Representatives has adopted.

The U.S. Centers for Disease Control and Prevention (CDC) is urging cities and states to start planning a **massive vaccination campaign** against swine flu. Citing modeling, CDC estimated last week that more than 1 million people in the United States are already infected.

When French President Nicolas Sarkozy reshuffled his Cabinet, the new deck did not include geochemist **Claude Allègre**, a global warming skeptic and former science minister. Rumor had it that Allègre, 72, might head a new superministry of innovation and international trade.

Also in flux is the $3 billion **California Institute for Regenerative Medicine**. Marie Csete, the operation's chief scientific officer, resigned without explanation after a little more than a year on the job. Board Chair Robert Klein recently announced that he plans to leave next year.

Four members of Congress have asked the U.S. National Academies for advice on **keeping U.S. academic research strong**. The letter asks for a thorough review of current federal policies affecting higher education, including an assessment of "the relationship, or lack of relationship," between universities and national laboratories.

A study last week in the *Proceedings of the National Academy of Sciences* makes a case for the **impact of federal funding of biomedical research**. The analysis correlates declining U.S. death rates over the past half-century with funding for the National Institutes of Health. The authors argue that more money is needed so the longer-lived elderly can help meet demand for U.S. workers.

You can keep up with the latest news at **blogs.sciencemag.org/scienceinsider**.

Published by AAAS

CHINA

Archaeologists Seek New Clues to the Riddle of Emperor Qin's Terra-Cotta Army

XI'AN, CHINA—In life, he subdued China's warring states and became the country's first emperor. In death, he brought an army to heaven to perpetuate his rule. Since the stunning discovery of Emperor Qin Shihuang's tombs 35 years ago, archaeologists have unearthed about 1300 life-size terra-cotta soldiers and horses and a wealth of other artifacts that illuminate the brief but world-changing Qin Dynasty 2200 years ago. Last month at the renowned site, archaeologists began the latest round of excavation in a pit untouched for 2 decades. They hope to penetrate lingering puzzles about the Qin Dynasty, and they will test a new method of preserving the terra-cotta warriors' exquisitely perishable hues.

Perhaps the biggest mystery is why Qin led an army into the afterlife. "We've never found anything like it in the tombs of earlier kings," says the excavation's executive director, archaeologist Xu Weihong of the Museum of the Terracotta Warriors and Horses of Emperor Qin Shihuang here. There are several theories, including a popular one that Qin believed his army would awaken and empower him in the spirit world. Supporting that idea, archaeologists have uncovered only real weapons—no facsimiles—interred with the soldiers. But the evidence is not decisive. "The larger question of the significance and purpose of burying life-size replicas of Qin soldiers remains, in my opinion, largely unanswered," says Jeffrey Riegel, an East Asia scholar at the University of Sydney in Australia.

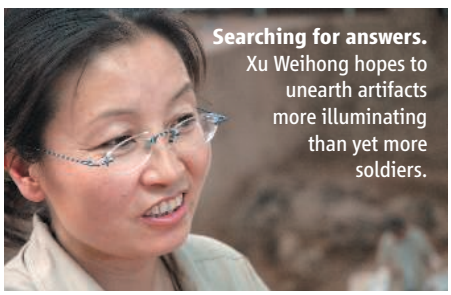

Searching for answers. Xu Weihong hopes to unearth artifacts more illuminating than yet more soldiers.

Contemporary accounts paint a broad-brush view of Qin Shihuang's life. Born in 259 B.C.E., the future emperor, Ying Zheng, ascended to the throne of Qin State when he was 13. Nine years later a regent ceded him power, and the young monarch was soon tested by internal revolt. Ying pacified Qin and then proceeded to conquer China's other six states. He proclaimed himself emperor and took the name Qin Shihuang in 221 B.C.E.

After unifying China, Qin Shihuang set out to modernize it. Annals recount how he abolished the feudal system, built roads to China's far corners, and standardized weights, measures, and handwriting. During his reign, hundreds of thousands of laborers erected much of the Great Wall and scores of palaces. Legend has it that in his 40s, the emperor grew obsessed with death and searched for an elixir of immortality. But he failed to even attain old age: Qin died when he was 50. In the power vacuum that followed, rival armies vied for control of the empire. The victor was Liu Bang, founder of the Han Dynasty.

Soon after Qin took power, he began preparing for the afterlife. Construction of his mausoleum at Mount Li, 35 kilometers east of Xi'an, took 38 years. The mausoleum, once crowned with pavilions, was never a secret, and even today it is visible as a kilometer-long wooded mound that rises a gentle 75 meters above the surrounding land.

Nearby, one of archaeology's greatest surprises lay hidden for centuries. In March 1974, farmers digging a well discovered pottery fragments about 1.5 kilometers east of the mausoleum. Excavations revealed the smashed-up remains of Qin's terra-cotta army—8000 clay soldiers and horses, researchers estimate—arrayed in three vast pits.

Over the centuries, fire and floods bled many warriors of their original colors. Past excavations unearthed some figures with intact paint, but within minutes after exposure to air, the paint would peel off and reveal the dull-gray

PALEOANTHROPOLOGY

Still Seeking Peking Man

ZHOUKOUDIAN, CHINA—On a sweltering late June day, Zhang Xiaoling hunches under a makeshift canvas roof over one of Asia's most famous Stone Age sites. It's roasting in the shelter, but Zhang, a stone-tools specialist at the Institute of Vertebrate Paleontology and Paleoanthropology (IVPP) in Beijing who just earned her Ph.D., is grinning from ear to ear. "I think we'll find something soon," she says. "I'm so excited."

Last week, work commenced on a new excavation here in the cave-riddled hills of Zhoukoudian, 50 kilometers southwest of Beijing, where early last century scientists discovered Peking Man: a trove of *Homo erectus* fossils as well as rudimentary tools and the bones of woolly rhinos and other Ice Age fauna. The new dig aims to both stabilize the iconic site and unearth evidence that could influence simmering debates, such as whether Peking Man was a hunter or a scavenger and whether the hominin tamed fire.

Perilous perch. The excavation will take place at the edge of an unstable 40-meter-high cliff.

"I strongly support new excavations," says paleoanthropologist Russell L. Ciochon of the University of Iowa in Iowa City. "For too many years, Zhoukoudian has been treated more as a shrine rather than a valuable paleoanthropological site."

Peking Man (now called Beijing Man in Chinese) has a storied history. European scientists discovered a few ancient teeth here at Dragon Bone Hill in the 1920s before archaeologist Pei Wenzhong made a stunning find in 1929: a nearly complete skull. Up until the Japanese invasion in 1937, Pei and others unearthed some 200 bones, including five more partial skulls—all of which vanished during World War II—and thousands of pieces of worked stone. In a paper last March in *Nature*, IVPP Vice-Director Gao Xing and colleagues used the ratio of aluminum-26 and beryllium-10 in quartz crystals to date the Peking Man strata to 680,000 to 780,000 years old, about 200,000 years older than previously thought.

The new excavation is in a 20-square-

CREDITS: R. STONE/*SCIENCE*

Published by AAAS

Everlasting army. Pieced-together terra-cotta warriors on display at Pit 1.

fired clay. The loss was more than aesthetic. For example, one warrior's face was different from the rest: Instead of the usual cream-colored pigments, it was painted a garish green. "We think he was a kind of wizard meant to terrify the enemy," says Rong Bo, an analytical chemist and conservation scientist at the museum. Because such tantalizing clues flaked off before their eyes, archaeologists sharply limited further excavations.

In the meantime, Rong and others set out to crack the riddle of the brittle pigments. Working with experts from the Bavarian State Conservation Office in Germany, the museum researchers determined that Qin artisans ground up semiprecious stones, such as azurite and malachite, for the pigments. The much-admired "Han purple," they found, is a mixture of barium copper silicate and a dash of cinnabar. Pigments were applied after fired figures were glazed with two layers of *qi* lacquer. The collaborators also figured out why the warriors have a bad case of peeling: Xi'an's bone-dry air shrinks the lacquer.

Hoping to prevent shrinkage, scientists tried every off-the-shelf adhesive they could lay their hands on. Nothing worked. "It was so frustrating," says Rong. Finally, they hit upon two solutions. One employs polyethylene glycol (PEG), used in everything from laxatives to skin creams. Short-chain PEGs penetrate the lacquer's tiny pores, replacing water that would have evaporated out, and a polymethacrylate dispersion helps keep the lacquer adhered to the clay. In a second technique, a compound called Plex 6801-3, a sealant for sewage pipes containing 2-hydroxy ethyl methacrylate, works its way into the lacquer and is hardened by electron beam irradiation. But preventing the terra-cotta warriors' colors from fading remains a major challenge, independent experts say.

After reviewing the new methodology, the State Administration of Cultural Heritage certified the museum to resume excavations. The museum is going it alone, having ditched its earlier partner, the Shaanxi Institute of Archaeology. (A Qin expert formerly with the institute declined to speak with *Science*.) The new dig at the UNESCO World Heritage site is attracting intense scrutiny from authorities and the public. "We feel a heavy responsibility on our shoulders," says Xu.

Work is now under way at Pit 1, the biggest of the three and until last month undisturbed (apart from hosting millions of tourists) since 1986. By the end of the year, 200 square meters will be excavated; the plan is to complete 2000 square meters in 5 years. Workers frequently sprinkle water on the soil to protect relics. Xu's aim is not to raise the tally of disinterred warriors but to find artifacts that could help researchers understand Qin funerary practices. "Digging up more soldiers is not in the least bit interesting," she insists. "They really provide little information about that time."

Soon after the Qin Dynasty fell, annals say, the king of Chu State raided the tombs and torched their wooden rafters. His forces also razed the palaces and pavilions around the mausoleum but evidently failed to penetrate the mausoleum's inner sanctums. Annals tell of treasures there that would make King Tutankhamen look like a pauper, including a ceiling studded with jewels representing celestial bodies and flowing "rivers of mercury" representing China's great rivers. Archaeologists have peered inside with equipment such as ground-penetrating radar and have measured intriguingly high mercury levels in the soil. But the heritage administration forbids any digging at the mausoleum, and Xu insists she's not curious. "Not in 100 years will it be opened," she says. Rong, looking on, smiles. "*I'm* curious," he says. "But we have to leave something for future generations." **–RICHARD STONE**

meter section of the western end of Site 1, where remains of some 40 *H. erectus* individuals have been unearthed. One objective is to stabilize the site, perched on the edge of a cliff and at risk of collapse, says Gao, the project leader. The first 2 months will be spent removing a hazardous outcropping. Team members will be roped like mountain climbers. "It's very dangerous to work here," Gao says.

Gao is downplaying expectations of what he describes as a salvage archaeology operation. The biggest prize, he says, would be a skull: It would be "sheer luck" to find one, he says. Only casts remain of the missing skulls. Gao says he would be happy with a jawbone, which could clarify evolutionary relationships with other hominin subspecies, or finger bones, which could shed light on Peking Man's dexterity for fashioning tools. Researchers also hope to examine stone tools in situ. A better understanding of the timeline of hominin occupation "may be more important than the discovery of isolated fossils," Gao says.

Under no illusions. Finding a skull would be sheer luck, says Gao Xing.

Excavations will continue through October. Outside the glare of that spotlight, Gao and others are planning field surveys and excavations at localities across China under a 5-year, $2 million project funded by the science ministry. Gao is eyeing one site in particular: a cave in Jianshi in central China's Hubei Province, dating to more 1 million years ago. "It has great potential" to yield *H. erectus* fossils, he says. Of course, they would have to be especially dazzling to nudge Zhoukoudian and Peking Man off center stage. **–RICHARD STONE**

CREDITS: R. STONE/*SCIENCE*

Published by AAAS

On the Origin of
The Nervous System

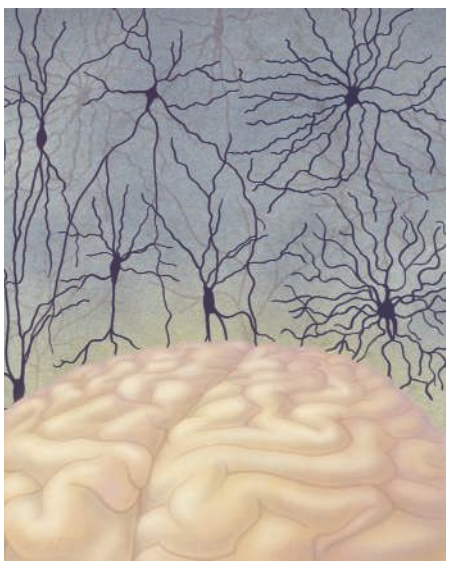

The nervous systems of modern animals are amazingly diverse. A few hundred nerve cells are all a lowly nematode needs to find food and a mate. With about 100,000 neurons, a fruit fly can perform aerial acrobatics, dance to woo a mate, and throw kicks and punches to repel a rival. The sperm whale's 8-kilogram brain, the largest on the planet, is the navigation system for cross-ocean travel and 1000-meter dives and enables these highly social creatures to communicate. The human brain—one-sixth that size—is the wellspring of art, literature, and scientific inquiry.

But how did they all get started? What did the first neurons and nervous systems look like, and what advantages did they confer on the animals that possessed them? These were questions the father of evolution, Charles Darwin, was ill-equipped to address. Although comparative neuroanatomy dates back to ancient Greece, the tools of the trade had not been refined much by the mid-19th century. In Darwin's day, anatomists were limited to gross observations of brains; they knew relatively little about the workings of nerves themselves. Only around the time Darwin died in 1882 were scientists beginning to develop stains to label individual cells for more detailed postmortem neuroanatomical studies. Methods for investigating the electrical properties of individual neurons in living brain tissue were still decades away, to say nothing of techniques for investigating genes and genomes.

Using such modern tools, scientists have recently begun to gain some tantalizing clues about the evolutionary origins of nervous systems. They've found that some of the key molecular building blocks of neurons predate even the first multicellular organisms. By looking down the tree of life, they are concluding that assembling these components into a cell a modern neuroscientist would recognize as a neuron probably happened very early in animal evolution, more than 600 million years ago. Most scientists agree that circuits of interconnected neurons probably arose soon thereafter, first as diffuse webs and later as a centralized brain and nerves.

But the resolution of this picture is fuzzy. The order in which early branches split off the animal tree of life is controversial, and different arrangements imply different story lines for the origins and early evolution of nervous systems. The phylogeny is "a bit of a rat's nest right now," says Sally Leys of the University of Alberta in Edmonton, Canada. Scientists also disagree on which animals were the first to have a centralized nervous system and how many times neurons and nervous systems evolved independently. Peering back through the ages for a glimpse of the first nervous systems is no easy trick.

In addition, there is some intellectual inertia that may need to be overcome, some researchers say. "If you look at any other organ or structure, people easily assume it could evolve multiple times, … but for some reason, people are stuck on [a single origin] of neurons," says Leonid Moroz, an evolutionary neurobiologist at the Whitney Laboratory in St. Augustine, Florida.

How to build a neuron

Like nervous systems, nerve cells come in many varieties. Neurons are easy to recognize but somewhat slippery to define. They all share directionality—i.e., the ability to receive information at one end and transmit information at the other. Electrical excitability is another defining feature; a neuron can regulate the flow of ions across its outer membrane to conduct electrical impulses. Nearly all neurons form synapses, points of contact where chemical neurotransmitters convey messages between cells, and many neurons possess branches called dendrites for receiving synaptic inputs and long axons for conducting outgoing signals.

Arranged in circuits, neurons open up new behavioral possibilities for an animal. Electrical conduction via axons is faster and more precise than the diffusion of chemical signals, enabling quick detection and a coordinated response to threats and opportunities. With a few upgrades, a nervous system can remember past experiences and anticipate the future.

Although the advantages of going neural are clear, how it first happened is anything but. One hypothesis that still resonates today dates back to 1970. George Mackie of the University of Victoria in Canada envisioned something like the sheet of tissue that makes up the bell of a jellyfish as starting material. Cells in the sheet can both detect physical contact and contract in response. Mackie proposed that these multifunctional cells may have given rise to two new cell types: specialized sensory cells on the sheet's surface and muscle cells underneath. Initially, cells in the two layers touched, with ions passing through pores in the cells' membranes to conduct electrical impulses between them. With further specialization, the distance between the sensory and muscle cells grew and axons arose to bridge the gap. Eventually, "interneurons" appeared, forming synapses with sensory neurons at one end and with muscle cells at the other end.

It's a plausible scenario, says Detlev Arendt, a developmental biologist at the European Molecular Biology Laboratory in Heidelberg, Germany. But there are other possibilities, and they're not mutually exclusive, Arendt says. Moroz agrees: "Neurons may have appeared in multiple lineages in a relatively short time."

Consistent with this idea, some crucial components of neurons exist in many cell types that predate the first neurons. Voltage-gated ion channels, tiny pores that control the flow of ions across a neuron's outer membrane to create electrical signals, can be found in bacteria and archaebacteria, notes Robert Meech, a neurophysiologist at the University of Bristol in the United Kingdom. And in the 1960s, researchers found that when the single-celled *Paramecium caudatum* bumps

THE YEAR OF DARWIN

This essay is the seventh in a monthly series. For more on evolutionary topics online, see the Origins blog at **blogs.sciencemag.org/origins.** For more on the nervous system, listen to a podcast by author Greg Miller at **www.sciencemag.org/multimedia/podcast.**

CREDITS (TOP TO BOTTOM): KATHARINE SUTLIFF/*SCIENCE*; WIKIPEDIA/GEORGE RICHMOND, FROM ORIGINS, RICHARD LEAKEY AND ROBERT LEWIN

Published by AAAS

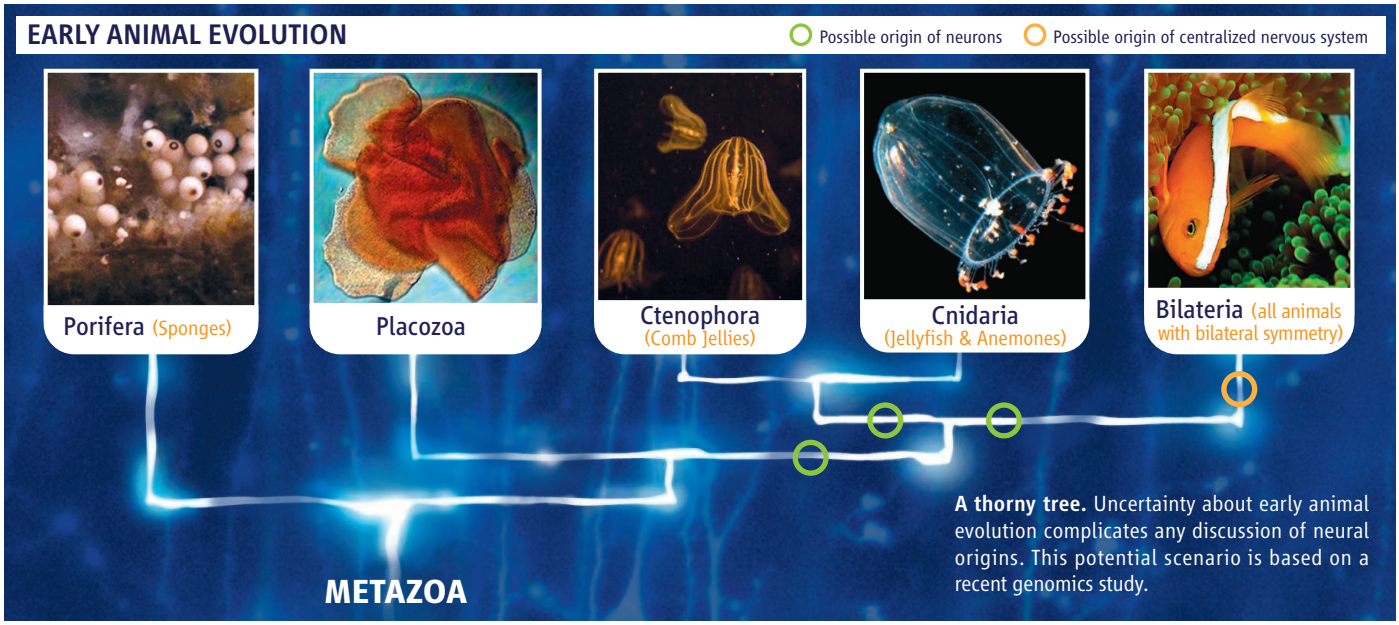

A thorny tree. Uncertainty about early animal evolution complicates any discussion of neural origins. This potential scenario is based on a recent genomics study.

CREDITS (FROM LEFT TO RIGHT): (BACKGROUND) DR JONATHAN CLARKE, WELLCOME IMAGES; BRYONY FAHEY; ANA SIGNOROVITCH/YALE; STEVEN G. JOHNSON/WIKIPEDIA; KEVIN RASKOFF, 2005; JENNY HUANG/WIKIPEDIA

into an obstacle, a voltage change sweeps from one end to the other, much like the "action potentials" that convey a signal down the length of a neuron. In *Paramecium*, this electrical blip reverses the beat of its cilia, temporarily altering its course. Electrical excitability, it seems, evolved long before neurons made it their specialty.

On the brink

To hunt for additional clues about neuron evolution, researchers have turned to some of the most primitive animals alive on Earth today: sponges. Many scientists think these marine and freshwater filter feeders are the living creatures most similar to the common ancestor of all animals. And to many researchers, sponges look like animals on the verge of a nervous breakthrough. Sponges don't have a nervous system, or even neurons, but they do have a surprising number of the building blocks that would be needed to put a nervous system together.

Researchers working to unravel the genome of the marine sponge *Amphimedon queenslandica* reported in *PLoS ONE* in 2007 that these animals contain the genetic blueprints for a set of proteins typically found on the receiving side of a synapse. In neurons, these proteins provide a scaffold that anchors neurotransmitter receptors into the cells' outer membrane. Yet electron microscope studies have failed to find synapses in sponges. And although their genomes contain genes for some neurotransmitter receptors, sponges appear to lack the type of receptors used for most excitatory neural communication in other animals. Thus, the function of these synaptic scaffolding proteins in a sponge is a mystery, says Kenneth Kosik, a neuroscientist at the University of California, Santa Barbara, who led the study.

Last year, the *Amphimedon* genome yielded another surprising find. A team led by Bernard Degnan of the University of Queensland in Brisbane, Australia, reported in *Current Biology* that cells in the sponge's larvae express a handful of genes that spur neural precursor cells to develop into full-fledged neurons in more complex animals.

> "I think everybody agrees that nervous systems were at first diffuse and then evolved to be centralized. … But there's no consensus yet on exactly when this happened."
>
> —Detlev Arendt, European Molecular Biology Laboratory

Inserting the sponge version of one of these genes into frog embryos and fruit fly larvae led to the birth of extra neurons. Degnan suspects that the cells that express them might be a type of protoneuron. These cells sit on the outer surface of the sponge larvae, and Degnan speculates that they may somehow help the free-floating larvae sense their environment and find a suitable place to settle down and metamorphose into their adult form.

Physiological experiments with sponges have also turned up signs of neural foreshadowing. Some sponges, for example, generate action potentials. In a 1997 *Nature* paper, Leys and Mackie reported that when the glass sponge *Rhabdocalyptus dawsoni* gets bumped or detects sediment in the water it filters for food, a voltage change sweeps across its body, and the cilia that pump water through the sponge's body shut down. (The glass sponge is essentially one giant cell with a continuous, weblike intracellular space.) This electrical blip lasts about 5 seconds, compared with a millisecond or so for most action potentials in neurons, but it seems to accomplish the same basic goal as a reflex mediated by neurons: generating a coordinated response to an external stimulus.

All in all, says Leys, sponges provide a tantalizing picture of what an animal on the brink of evolving a nervous system might look like. Their cells have many of the right components, but some assembly is still required. And although they have a wider behavioral repertoire than most people realize, Leys says, their "reflexes" are far slower than those of animals with a nervous system.

But some researchers argue that sponges aren't the most primitive living animals. In one controversial study, published in the 10 April 2008 issue of *Nature*, a team of European and North American researchers

Published by AAAS

reported that their analysis of 150 gene fragments from each of 77 animal taxa suggested that ctenophores, not sponges, are the lowest branch on the animal tree of life. Ctenophores, or comb jellies, are translucent, bloblike marine organisms that bear a passing resemblance to some jellyfish. Like true jellies, ctenophores have bona fide neurons and a simple netlike nervous system. Their position at the base of the animal family tree—if it stands up—would shake up many researchers' views on nervous system evolution.

Among the unpalatable implications, in the eyes of some researchers, is that if ctenophores came before sponges, the assorted nervous system components that have turned up in sponges may not be foreshadowing after all but rather the remnants of a nervous system that was lost after the sponge lineage split off from that of ctenophores.

What's new, jellyfish?

Another contender for most primitive animals with a proper nervous system are cnidarians, a group that includes the true jellyfish, corals, and sea anemones. As in ctenophores, the nervous system of cnidarians is often described as a "nerve net." This description is apt for anemones, which have a diffuse web of neurons with no discernible concentration of neurons in any one place. But some jellyfish, such as the bell-shaped *Aglantha digitale*, are more organized, with clearly defined bundles of nerves running around the base of the bell.

Cnidarian neurons generate action potentials and release neurotransmitters to communicate across synapses. The genome of the starlet sea anemone, *Nematostella vectensis*, reveals a surprisingly large array of genes encoding enzymes that synthesize or break down neurotransmitters, as well as receptors for these signaling molecules (*Science*, 6 July 2007, p. 86). The genome hints at a complexity of neural signaling similar to that seen in more complex animals, says Michel Anctil, a comparative neurobiologist at the University of Montreal in Canada: "The potential is there. How much they use it is what we have to figure out."

Getting a head

Just as sponges, comb jellies, and sea anemones may hold clues to how the first nerves and nerve nets arose, other creatures may shed light on the evolution of more complex neural circuitry. "I think everybody agrees that nervous systems were at first diffuse and then evolved to be centralized," with a concentration of neurons in the front end of the animal—that is, a brain—and a nerve cord connecting it to the rest of the body, says Arendt. "But there's no consensus yet on exactly when this happened." Arendt and others have argued that a centralized nervous system existed in the ancestor of all bilaterally symmetrical animals, or bilaterians.

Studies dating back to the early 1990s have found that several genes involved in shaping the central nervous system as it develops in fruit flies are expressed in a similar pattern and play a similar role in nervous system development in vertebrates and in distantly related invertebrates such as annelid worms. That implies that these genes were already present in the last common ancestor of all these creatures—the ancestor of all bilaterians—and suggests to Arendt and others that this ancestor had a centralized nervous system.

But not everyone is so sure. Christopher Lowe of the University of Chicago in Illinois and colleagues have found that *Saccoglossus kowalevskii*, a wormlike creature that belongs to the group of invertebrates most closely related to vertebrates, the hemichordates, has many of the same neural development genes expressed in a similar pattern. Yet *Saccoglossus* has a mostly diffuse nervous system. If having the genes and expressing them in a given pattern isn't sufficient to establish a centralized nervous system, that leaves open the possibility that the bilaterian ancestor had a diffuse nervous system, Lowe says. "I would argue that we have a range of possibilities," he says. Because most but not all modern bilaterians have a centralized nervous system, there will be awkward implications no matter what. If the bilaterian ancestor had a diffuse nervous system, centralized nervous systems must have originated multiple times in multiple bilaterian lineages—a far less parsimonious scenario than a single origin. On the other hand, if the ancestor had a centralized nervous system, several lineages, including that of *Saccoglossus*, must have later reverted to a diffuse nervous system—an apparent downgrade that's hard to explain.

The puzzles don't end there. Fast-forwarding a bit in evolutionary time raises a new set of questions. What is the origin of the myelin insulation that speeds conduction down axons and ensures the fidelity of neural signals? Or of the glial cells that are proving to have important roles in brain function and appear to be more numerous in complex nervous systems?

For that matter, how many ways are there to build a complex brain? Aristotle's notion of a *scala naturae*, or natural ladder, influenced the thinking of researchers well into the 20th century, says R. Glenn Northcutt, an expert on vertebrate brain evolution at the University of California, San Diego. "It was assumed that all vertebrates and invertebrates could be arranged in a linear series, with man and the angels at the top," Northcutt says, but "we now know that's just nonsense." Most researchers now agree that equally complex—but anatomically different—brains have evolved in birds, mammals, and other animal lineages, Northcutt says: "At least four or five times independently, … major radiations of vertebrates have evolved complex brain structure." But whether brains that are put together differently operate on similar principles is still an open question. And then there is the enduring question of what, if anything, is special about the human brain. Perhaps the emerging clues about the long evolutionary path we've taken will one day help us decide where we are.

–GREG MILLER

ORIGINS OF NEURONS

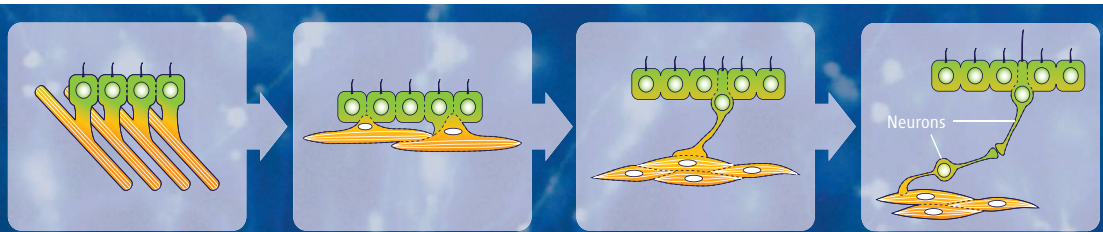

One way to build a neuron. Neurons may have arisen from multifunctional cells—like those in a jellyfish's bell (*far left*)—that gradually became more specialized.

SOURCE: ADAPTED FROM G. O. MACKIE, "NEUROID CONDUCTION AND THE EVOLUTION OF CONDUCTING TISSUES", *THE QUARTERLY REVIEW OF BIOLOGY* **45**, 319 (1970)

NEWSMAKER INTERVIEW

Behavioral Geneticist Celebrates Twins, Scorns PC Science

Last month, the Behavior Genetics Association held its annual meeting in Minneapolis, home of the world-famous Minnesota Study of Twins Reared Apart. Attendees took the occasion to honor psychologist Thomas Bouchard, the man who started it all. Bouchard, 71, is retiring after 40 years at the University of Minnesota, Twin Cities, and has moved to Steamboat Springs, Colorado.

Bouchard spoke with *Science* at the meeting; his comments have been edited for clarity and brevity. **–CONSTANCE HOLDEN**

Q: What got you into twin studies?

T.B.: I was teaching the psychology of individual differences, and in 1979, two different people put a copy in my mailbox of a story about twins reared apart and their similarities when they met. [These were the "Jim twins," Jim Springer and Jim Lewis, who had been separated at birth and reunited at age 39. Both married women named Linda, divorced, and remarried women named Betty. They named their sons James Allan and James Alan, respectively, and both had dogs named Toy.] They sounded interesting, so I asked a few of my colleagues to help me study them. We ended up studying twins reared apart—126 pairs including 74 pairs of identical twins—for 20 years. [The twin study wound down in 2000.] I found that I loved working with twins. They're still amazing and a major mystery to me.

Q: What were attitudes toward behavioral genetics in the early years of your career?

T.B.: In graduate school at UC [the University of California] Berkeley, I was reading a book edited by psychiatrist D. D. Jackson on the etiology of schizophrenia. The first chapter, by a geneticist, was on twin studies. Then Jackson refuted it all with just the kind of crap you hear now against twin studies. He said families are the cause of schizophrenia. I remember saying in a graduate seminar, "Most of this stuff [in Jackson's argument] is junk"—I crawled out of the seminar room a bloody pulp. The reaction [from seminar members] was my first absolutely clear-cut demonstration that psychologists believed correlation is causation, … and many still do.

In the '70s, when I was teaching research by [IQ researcher Arthur] Jensen and [twin researcher Francis] Galton, people picketed me, called me a racist, tried to get me fired. The progressive student association sent members in to ask hostile questions. … So I put a tape recorder on the podium and said: "I'm going to tape my lectures." I never heard from them again. They knew what they were saying was nonsense and I would be able to prove it.

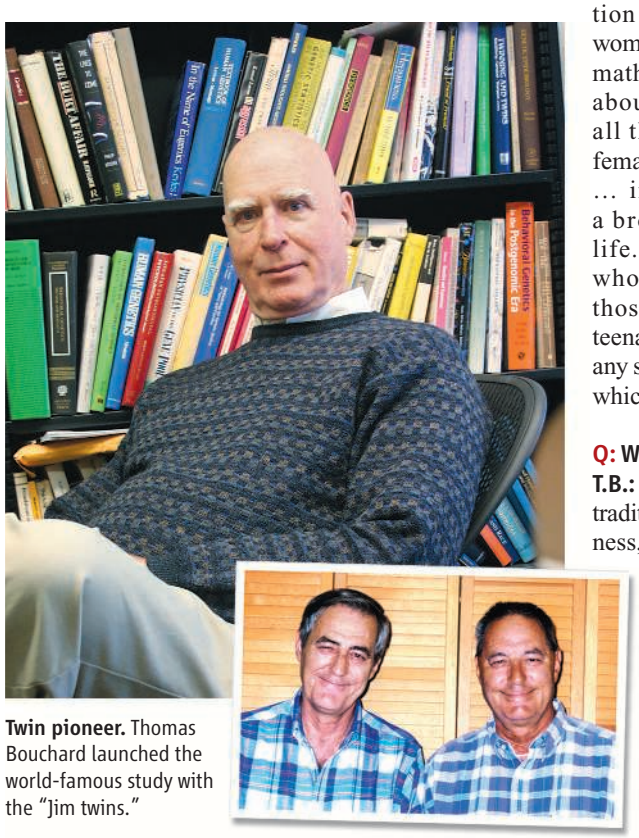

Twin pioneer. Thomas Bouchard launched the world-famous study with the "Jim twins."

Q: Do you think perceptions have changed dramatically since the '70s now that twin research has revealed genetic bases for many disorders, such as autism (which had been blamed on cold mothers) and ADHD (for which many blamed food dyes)?

T.B.: Within the university—at least at U. Minnesota—the cumulative impact of behavioral genetics findings has had a lot of effect. There's a lot more tolerance for the idea of genetic influences in individual differences.

But we still have whole domains we can't talk about. One of the great dangers in the psychology of individual differences is self-censorship. For example, when I was a student, it was widely accepted that black self-esteem was much lower than white self-esteem, and that was a cause of differences in achievement between the two groups. Now that's been completely overturned—there is virtually no racial difference in self-esteem. But people had enormous amounts of data [showing this] that they didn't publish because it did not fit the prevailing belief system. How much wasted effort was generated by the flawed self-esteem work as an explanation of the black-white IQ difference? Nowadays, I'm sure there are people who are not publishing stuff on sex differences. Look what happened to Larry Summers [who resigned as president of Harvard University after suggesting that discrimination alone doesn't account for women's lower representation in math-based disciplines]. I talk about those things in my class all the time—that males and females have different interests; … in a sense, females have a broader and richer view of life. There are a lot of people who simply won't talk about those things. Academics, like teenagers, sometimes don't have any sense regarding the degree to which they are conformists.

Q: What are you working on now?

T.B.: I'm studying what I call the traditional-values triad: religiousness, conservatism, and authoritarianism. They correlate with each other. In our most recent paper [based on Minnesota twin data], we showed that the same genes affect all three traits. The superfactor [the underlying trait they share] is traditionalism; I think the underlying psychological process is the notion of obedience. It's exactly the same trait that Stanley Milgram studied in the '60s [when students willingly administered electric shocks to unseen victims]. Most researchers talk about obedience as being a bad thing. But it's also the glue that holds societies together.

Q: Anything you would have done differently?

T.B.: Bouchard has gotten everything he wanted from day one. … I've led a charmed life. … If I had it to do all over again, I would do almost exactly what I've done. I know there are people who really dislike what I do. … But look, I'm retired—they're not going to take my skis away.

CREDITS: KELLY MACWILLIAMS; (INSET) COURTESY OF JIM LEWIS AND JIM SPRINGER

Published by AAAS

Sunshine man. Senator Grassley says company payments to doctors should be made public.

ETHICS

Private Money, Public Disclosure

A Senate investigation is forcing federally funded medical institutions to reveal exactly how much money their researchers receive from industry

In the mid-1990s, psychiatrist Alan Schatzberg and colleagues wanted to test a new way of treating psychotic depression. Their aim was to suppress the brain's receptors for the hormone cortisol, which is elevated in patients with this disease. They decided to try a cortisol blocker called mifepristone, also known as RU-486, the abortion drug. Schatzberg, then at Stanford University in Palo Alto, California, won funding from the National Institutes of Health (NIH) for a small clinical study that showed that mifepristone appeared to help some patients overcome psychotic depression.

Stanford then applied for a patent to use mifepristone for treating psychotic depression. When the pharmaceutical industry showed no interest in developing the drug, Schatzberg co-founded a company in 1998, Corcept Therapeutics, to license the technology and test it in larger clinical studies. For nearly 3 decades, federal law has encouraged such interactions so that taxpayer-funded discoveries can make their way into products.

Last summer, the Stanford-Corcept arrangement came under fire. Senator Charles Grassley (R–IA) accused Schatzberg of concealing from his university that he held stock in Corcept worth $6 million. When Stanford informed Grassley it knew the stock's value and argued that Schatzberg was not directly involved with the clinical trial, the senator came back with new questions: Why did Schatzberg head a grant to study mifepristone? And why had he co-authored papers on the clinical results? At that point, Stanford removed Schatzberg from the NIH grant but said no rules were broken.

Schatzberg and Stanford argue that, although their reading of U.S. regulations may surprise the public, it's for a good cause: developing a new drug for severely depressed patients. Grassley is skeptical: He has suggested that medical entrepreneurs at research universities who fail to properly disclose outside income are violating the law and may bias their work in a way that distorts medical care. Grassley's efforts to clean up what he sees as a corrupt enterprise have targeted about a dozen researchers like Schatzberg to date.

As part of his probe, Grassley has homed in on an overlooked trouble spot: federal rules requiring that institutions track and "manage" faculty members' industry ties. NIH is now contemplating the first major overhaul of these rules in nearly 15 years. It has solicited public comments on a variety of issues—the deadline for responses is next week—as a prelude to proposing tighter regulations. The end result is expected to vastly expand the information that faculty—both basic and clinical—must report to their institutions and to NIH. And it will likely ask for more details on how institutions follow up on conflicts. In a related effort, Grassley has introduced a bill that would require drug and device companies to disclose their payments to doctors in an online database. It would inform the public about conflicts and help ensure that researchers report honestly.

Grassley has blamed NIH for not keeping a close enough watch over conflicts; some academic observers agree that the government needs to take a stronger hand. But NIH leaders, echoing the views of the research community, say the primary burden of overseeing conflicts should remain with institutions because rigid rules would stifle innovation. The system has worked well, although it may have been tainted by some bad apples, they say. "A few cases are getting heavily covered in the press. And the implication is that the entire system is corrupt. That is not true. … That's why it's so important for the scientific community to own this, to see what's at stake here," acting NIH Director Raynard Kington said in an interview earlier this year.

When the final rules have been agreed upon, universities will need to show that they can follow through, says Eric Campbell

THE EVOLUTION OF CONFLICTS-OF-INTEREST POLICIES

1980
Bayh-Dole Act encourages public-private research deals

1995
Public Health Service issues regulation on grantee conflicts of interests

1999
Patient Jesse Gelsinger dies in public-private gene therapy trial

CREDIT: RYAN KELLY/*CONGRESSIONAL QUARTERLY*/GETTY IMAGES; ILLUSTRATION: J. NEWFIELD/*SCIENCE*

Published by AAAS

of Harvard Medical School in Boston, an expert on industry-academic relations. University leaders have "staved off federal intervention for a long time" with the argument that only they can manage the problem, he says. "Over time, public scrutiny wears that argument away"—and right now it seems to have worn thin.

Conflicting signals

Relatively few academic researchers had ties to companies before 1980, when Congress passed the Bayh-Dole Act. That change in the law encouraged universities to patent and commercialize discoveries made by faculty members who received federal funds. It also led universities to create technology transfer offices and spurred hundreds of start-up companies, industry-endowed chairs, private funding for clinical studies, and consulting deals.

These changes also raised the potential for industry money to bias studies. To deal with that risk, the Public Health Service (which includes NIH), issued its first conflicts-of-interest regulation for PHS-funded investigators in 1995, after 6 years of debate. It requires grantees to report to their institution financial conflicts "related to the research" that are "significant"—defined as more than $10,000 per year from a given company, or 5% equity in a company. These cutoff points, says Susan Ehringhaus, an attorney at the Association of American Medical Colleges (AAMC), were arbitrary. Institutions must review the information, reduce or manage any conflicts, and tell NIH if a grant involves a significant conflict.

Concerns about gaps in this oversight system have been mounting ever since. After a volunteer died in 1999 in a gene therapy trial in which the lead investigator and university had a financial interest, two strong research lobbies—AAMC and the Association of American Universities (AAU)—came forward with plans for reform. Among other recommendations, in 2001 they urged members to adopt a policy barring clinical researchers from having significant conflicts except in compelling circumstances. But when AAMC surveyed members 2 years later, it found many were still lagging behind on the recommendations.

In 2004, a congressional investigation of conflicts within NIH set off alarm bells again. It led NIH to ban industry consulting by in-house scientists, making the rules for NIH researchers far more draconian than those covering their colleagues in academia. The spotlight, university officials realized, could soon swing back to extramural researchers and their industry ties. Last year, it did: The Inspector General of the Department of Health and Human Services slammed NIH for lax oversight of conflicts at grantee institutions.

The issue exploded in the media a year ago thanks to Grassley, the ranking member of the Senate Finance Committee. The 75-year-old Midwesterner, a longtime fraud buster, started out investigating defense contracts. In recent years, Grassley, citing his committee's oversight of Medicare and Medicaid, began probing conflicts of interest involving the approval of drugs such as Paxil and Vioxx.

In 2007, these probes led Grassley's investigators to conflicts of interest at biomedical research institutions. Using a strategy that had worked well in an inquiry by the House of Representatives, they asked both companies and institutions about payments to a faculty member and looked for discrepancies. Grassley says they got leads from media reports and "whistleblowers" such as critical faculty members.

Grassley's team made its first big splash with a front-page story in *The New York Times* last June. They alleged that three Harvard child psychiatrists had failed to report hundreds of thousands of dollars in income they received over several years from drug companies. Other psychiatrists and surgeons have since been accused of hiding similar payments, and some have been disciplined (see table, p. 30).

Risky business

Several of the universities targeted by Grassley's investigation are now tightening their conflicts policies, and several broad reform efforts are under way. Even before Grassley's campaign, some major medical schools had begun to restrict faculty participation in industry-funded medical education courses and promotional talks arranged by speakers' bureaus. An Institute of Medicine (IOM) panel this spring urged all schools to curb these activities, which some of Grassley's quarry said they didn't think they needed to report (*Science*, 1 May, p. 579).

NIH also says it is taking action. It has suspended a $9 million grant to one university for failing to handle conflicts properly. This spring, the agency announced that it may strengthen the PHS conflict rule and asked for comment on questions such as whether researchers should be required to provide much more specific financial information. Many universities ask researchers to check a box if outside payments are above a certain threshold. If that threshold is, say, "above $50,000," that means a payment of $57,000 or $2 million would look the same. "That's a huge problem," because it doesn't distinguish between minor and major conflicts, says conflicts researcher Lisa Bero of the University of California, San Francisco, a member of the IOM panel.

That could change if NIH follows the advice of the academic community. Three heavyweight organizations—IOM and, in comments to NIH, AAMC and AAU—all say that investigators should disclose to their institutions specific payments, no matter how small, that are directly or indirectly related to their research. The Federation of American Societies for Experimental Biology (FASEB) recommends reporting income of $200 or more. AAMC and AAU say they'd like to see the "significant" threshold for reporting to NIH lowered to $5000 from the current $10,000, and 0.1% equity rather than 5%.

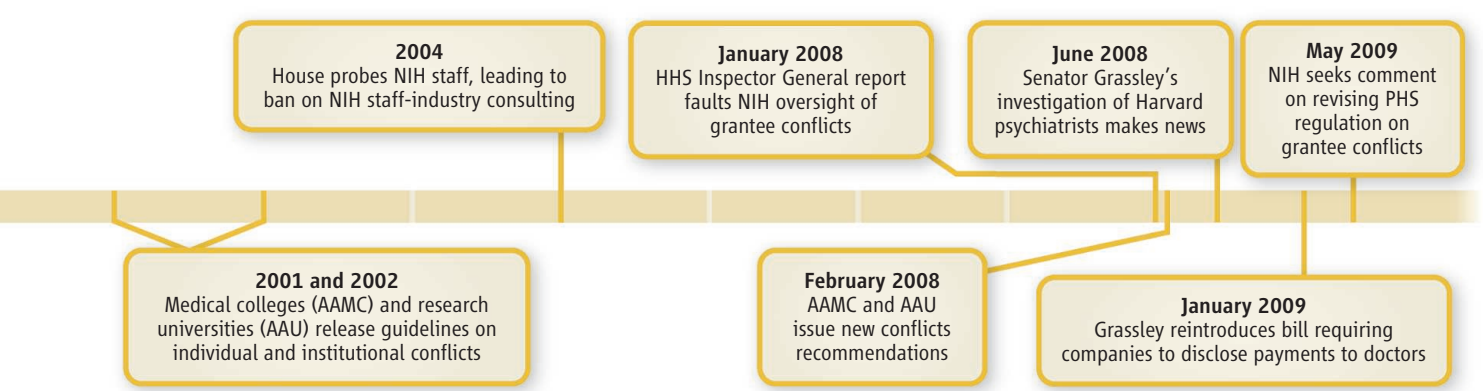

SENATE PROBE OF RESEARCH PSYCHIATRISTS

Senator Charles Grassley (R–IA) has cast a wide net in search of physicians who failed to fully disclose payments they received from drug and device companies. One of his concerns, he said, is that biased research could be influencing treatment decisions. Starting with psychiatrists in 2007, Grassley's investigators moved on to orthopedic surgeons this year; he has also looked into fees paid to academic cardiologists, professional associations, and a radio show host.

About 30 universities have now received queries from Grassley. This table includes cases made public by Grassley involving NIH-funded researchers—all psychiatrists, many of whom allegedly received consulting income from companies whose drugs they were studying. (Some researchers have said they didn't realize that certain types of payments had to be disclosed.) Dollar amounts are based on letters and statements from Grassley. **–J.K.**

Researcher	Industry Income Disclosed	Total Received	Status
Melissa DelBello, University of Cincinnati	about $100,000 over 2 years	more than $238,000 from AstraZeneca	UC has increased monitoring of DelBello's industry activities.
Joseph Biederman, Harvard/Mass General Hospital	about $200,000 over 7 years	about $1.6 million	MGH and Harvard are still reviewing, but Biederman agreed to suspend his industry-related activities in December 2008. Harvard is reviewing its conflicts policy.
Thomas Spencer, Harvard/Mass General Hospital	about $200,000 over 7 years	about $1 million	MGH and Harvard are reviewing.
Timothy Wilens, Harvard/Mass General Hospital	about $200,000 over 7 years	about $1.6 million	MGH and Harvard are reviewing.
Alan Schatzberg, Stanford	more than $100,000	$6 million in stock	Stanford says it knew the stock's value. Stanford's medical school soon plans to publicly disclose faculty members' industry ties but not dollar amounts.
Charles Nemeroff, Emory	$1.2 million over 7 years	more than $2.4 million	NIH suspended a $9 million grant to Emory. The HHS Inspector General is investigating the case. Last December, Nemeroff stepped down from research and as department chair.
Zachary Stowe, Emory	not available	$253,700 over 2 years from GSK for about 95 lectures	Emory told Stowe to eliminate his conflicts in April. The school recently banned promotional speaking.
Karen Wagner, University of Texas, Austin	about $100,000 over 7 years	more than $236,000	UT is reviewing.
Augustus John Rush, University of Texas, Southwestern	about $600,000 over 7 years	more than $600,000	Rush left UT for Singapore last August and is no longer being investigated, according to Grassley's staff.

SOURCES: SENATE FINANCE COMMITTEE (MINORITY); UNIVERSITY OF CINCINNATI; HARVARD/MASS GENERAL HOSPITAL; STANFORD UNIVERSITY; EMORY UNIVERSITY; UT SYSTEM

AAMC and AAU also agree that NIH should collect more details from institutions on the conflicts they're managing. Under the current rules, institutions only have to tell NIH whether a conflict was managed, reduced, or eliminated. That's partly where the current problems stem from, suggests Julie Gottlieb, assistant dean for policy coordination at Johns Hopkins University School of Medicine in Baltimore, Maryland. If NIH officials are serious, says Gottlieb, "they need to do more than they've been doing."

However, a prohibition on financial conflicts above a specific level remains unpopular, even for studies involving human subjects. Although AAMC and AAU have recommended to their members that significant conflicts should be prohibited in clinical research, they say institutions need flexibility, and in comments to NIH they oppose an "a priori prohibition." One reason to avoid broad caps, notes Gottlieb, is that a great deal of human subjects research is low-risk—on human tissue samples, for example. AAU and AAMC also argue that it's premature to require policies for institutional-level conflicts. They warn that "imposing overzealous regulations could disrupt productive partnerships to the detriment of science and the public."

Grassley has applauded the AAMC and AAU statements, saying NIH "should consider everything" in the comment letter. At least one expert on academic-industry ties, however, thinks the regulation should prohibit any conflicts in clinical research. "I think there should be a zero threshold, or very small," says Sheldon Krimsky of Tufts University in Medford, Massachusetts, because even a $100 payment could influence a researcher's objectivity.

No rule is universally obeyed, of course, and scientists could still hide their income. Many of those Grassley has probed allegedly were not following existing rules. The remedy for that, many observers say, is a public database of payments reported by companies—such as one that would be created by the bill introduced by Grassley and Senator Herbert Kohl (D–WI), potentially by October 2011. University officials could use the database to audit their faculty members, say AAMC and AAU, which support the bill.

The disclosure system would work much better, the IOM report says, if the research community developed a standard reporting format. Some major medical centers have begun discussing this with companies so that items they consider irrelevant—such as a research grant or reimbursement for travel expenses—don't get counted as income. AAMC's Ehringhaus says standardization is "a terrific idea," but "I don't know yet" if her organization will move it forward. FASEB has suggested that PHS develop a "universal" form.

Harvard's Campbell thinks institutions are making progress. "It's gone from the Wild West 15 years ago to a system that seems to be much more regulated. Over time, people will pay greater and greater attention," says Campbell, who was also on the IOM panel.

Even with stricter rules and full public disclosure, none of these steps will change the fundamental contradiction spurred by Bayh-Dole, says C. K. Gunsalus, special counsel at the University of Illinois, Urbana-Champaign, a longtime follower of integrity in science: "We tell people with one side of the mouth to be pure as the driven snow and with the other side say, 'Take this money,' " says Gunsalus. Stanford's Schatzberg, for example, was following both commands when he came under fire for receiving compensation related to his NIH-funded research. But with the new reforms at least one thing will be clear: Right from the start, everyone will know about that private money.

–JOCELYN KAISER

TAXONOMY

China Searches for an 11th-Hour Lifesaver for a Dying Discipline

With hundreds of thousands of collected specimens unidentified and many more undiscovered, China hopes to prop up its taxonomists before vital skills slip away

BEIJING—Every week, Liu Quanru gives 18 lectures on taxonomy, the science of classifying life. It's not because he loves taxonomy—which he does. Rather, he is the only professor at Beijing Normal University qualified to teach the subject. "It's really very tiring," Liu says, and ultimately deflating: Only a few of his students end up majoring in taxonomy.

Such apathy could have grave consequences for the preservation of China's biological resources, Liu and others say. "If people don't know what they're dealing with, how can you identify anything," says Lu Zhi, executive director of the Center for Nature and Society at Beijing University. "It is still not clear how many species of plants are in China," or how many are endangered, explains Hong Deyuan, a former official at the National Natural Science Foundation of China (NSFC). Of more than 2 million herbarium specimens at the Institute of Botany of the Chinese Academy of Sciences (CAS) in Beijing, at least 20% have not been identified. A similar lacuna exists for fauna. "After we retire, nobody in our museum will be able to do research on special animal species that have important economic significance," such as termites or earwigs, says Qiao Gexia, curator of the National Animal Museum in Beijing.

Taxonomy is in decline around the world. But although the situation is just as grim in China, the country's dwindling band of taxonomists has one of their own in a powerful position: NSFC President Chen Yiyu, a taxonomist who majored in systematics and biogeography. In 2002, NSFC, the country's basic research grants agency, set up a classic taxonomy fund, which has thrown a $500,000-a-year lifeline to established taxonomists. But that's not enough, Chen acknowledges. "If there are fewer and fewer young persons doing taxonomy, there will be a huge negative impact," he says. To prevent Chinese taxonomy from slipping into oblivion, NSFC has invited applications for a pair of 4-year initiatives, to be launched in 2010, that aim to better integrate the field with molecular biology.

Taxonomy in China wasn't always in such a parlous state. Until the late 1980s, it was the primary focus of many of the country's botanists. Some 312 plant taxonomists together edited the first edition of *Flora of China*, launched in 1959, says Hong, a vice chief editor of recent editions. But the field has been hemorrhaging talent for years. "Many of our generation have already transferred their main research fields away from taxonomy," says Sun Hang, vice director of Kunming Institute of Botany, who studies plant taxonomy and geography.

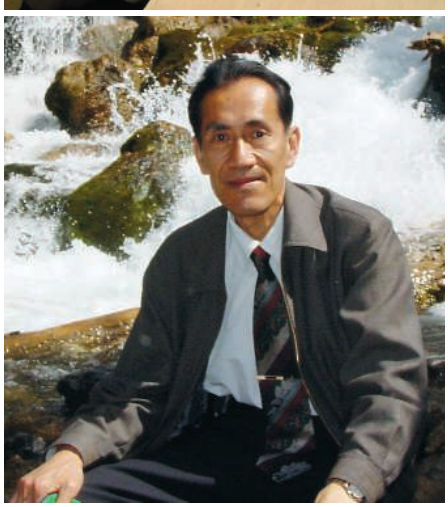

Endangered species? Liu Quanru, examining a bromegrass (*top*), is one of the few classical taxonomists left in China. NSFC President Chen Yiyu has urged the field to modernize.

Sun and others blame the field's woes on China's evaluation system, which awards promotions and allots funds mainly according to a scientist's publication record: the number of papers they land in Science Citation Index journals and the number of citations the articles receive. Chen agrees that the evaluation system is unfair. "It is almost impossible for taxonomical articles to be published in high-impact-factor journals," he says. Taxonomists, he argues, should be judged by a different standard.

A few have managed to pull this off. For example, the National Animal Museum evaluates its taxonomists according to their expertise in identifying and handling specimens, says Qiao. And at the Institute of Botany, Hong founded a classical taxonomy research group whose members are evaluated according to the quality of articles and monographs they publish, not impact factors. But in Sun's view, the special evaluation systems allow the field to survive, not thrive; they cannot help taxonomists advance in rank or win grants in national competitions. NSFC's classical taxonomy fund has alleviated the problem and will continue for the foreseeable future, says Chen, who also hopes that universities will expand taxonomy curricula.

For taxonomists to flourish, Chen argues, they must spread their scientific wings into molecular biology. He holds up as an example a former student, He Shunping, a taxonomist at CAS's Institute of Hydrobiology in Wuhan and curator of its Aquatic Organisms Museum. He uses DNA bar coding—a species-specific mitochondrial DNA sequence—to identify fish species. Unlike many of his peers, He doesn't complain about funding: His DNA-based taxonomy has earned him a wide network of foreign collaborators and steady grants.

He's success rankles some classical taxonomists. "There are many problems to judge species by DNA," says Liu, who says that classical taxonomical analysis is much more reliable for species identification. Chen, however, says it's time for classical taxonomy in China to move on: "The period of taxonomists simply identifying species is already past."

What's needed, says Sun, is a kind of Manhattan Project for taxonomy: a mega-project that would force taxonomists to work together and train the next generation. One possibility that the central government is contemplating, says Beijing University's Lu, is a comprehensive survey of China's biodiversity. Such a years-long project would require an army of taxonomists, perhaps working in tandem with molecular biologists. That would rejuvenate the field, says Sun. "Taxonomy," he says, "would play an important role in China once again." **–LI JIAO**

Li Jiao is a writer in Beijing.

CREDITS (TOP TO BOTTOM): LIU QUANRU; CHEN YIYU

Published by AAAS

LETTERS

edited by Jennifer Sills

Standing the Test of Time Variations

IN HIS NEWS FOCUS STORY "RENEWABLES TEST IQ OF THE GRID" (10 APRIL, P. 172), D. Charles describes the widely held belief that large-scale use of renewables will become viable with a smart electric grid and short-term energy storage devices (such as pumped storage and batteries). However, the problems of integrating renewables with the electricity grid in a low-carbon world are much larger. Renewables are a time-varying source of energy that does not automatically match the demand-side time variations. Electricity demand varies daily, over a 3-day weather-related cycle, weekly, and seasonally. The seasonal variation in electric demand in much of the country is greater than a factor of 2, with seasonal mismatches between renewable production and demand.

In a low-carbon world, the major energy options (nuclear, fossil fuels with carbon-dioxide sequestration, and renewables) have high capital costs and low operating costs. These high–capital-cost systems for electricity generation operate most economically when they are at full load all the time. For renewables, this is the maximum output given solar or wind conditions. To optimize their operation and to meet the storage needs of renewables requires systems that can store large amounts of energy and can do so on a daily to seasonal basis. The only existing such technologies are large hydroelectric dams—but there is not enough water storage capacity to meet the need.

Hydroelectric dam. Dams such as this one can store large amounts of energy on a flexible schedule, but they have insufficient water storage capacity globally to be our sole renewable energy source.

There is limited ongoing work on several new technologies. For example, in nuclear-hydrogen peak electricity systems, the nuclear reactor operates at steady state on a continuous basis (*1*). At times of low electricity demand, steam and electricity from the reactor are converted to hydrogen and oxygen by a solid-oxide high-temperature electrolyzer. At times of peak electricity demand, the reactor sends electricity to the grid and the electrolyzer is operated in reverse on hydrogen and oxygen from storage as a high-temperature fuel cell to produce electricity. Large-scale seasonal hydrogen storage is economical with use of current underground natural gas storage technologies. Eliminating greenhouse gas emissions from electricity production and large-scale use of renewables is not possible until we develop multiple, seasonal, energy storage systems with fast response capability to address mismatches between electricity production and demand.

CHARLES FORSBERG* AND MUJID KAZIMI

Department of Nuclear Science and Technology, Massachusetts Institute of Technology, Cambridge, MA 02139, USA.

*To whom correspondence should be addressed. E-mail: cforsber@mit.edu

Reference

1. C. W. Forsberg, M. S. Kazimi, 4th OECD-NEA Information Exchange Meeting on the Nuclear Production of Hydrogen, 14 to 16 April 2009, Oakbrook, IL; http://mit.edu/canes/pdfs/nes-10.pdf.

Heliophysics Missions Show Promise

A RECENT NEWS OF THE WEEK STORY ("Report puts NASA's solar program under a cloud," A. Lawler, 13 March, p. 1415) noted that a report from the National Research Council (NRC) ("A performance assessment of NASA's heliophysics program") was critical of the performance of NASA's Heliophysics Division with respect to the 2003 Decadal Survey for Solar and Space Physics. NASA's heliophysics program has a record of remarkable success with its recent space flight programs. These have, in general, been well-managed, cost-effective, and scientifically exciting efforts. They have returned far more than the minimum science goals, and they continue to constitute a "Great Observatory" of the Sun-Earth system.

It is unfortunate that the mainstays of heliophysics space mission funding lines (the Solar Terrestrial Probe and Explorer lines) were hugely reduced in the Fiscal Year (FY) 2005 budgets of NASA (*1*). More than half the budgetary authority for the Solar Terrestrial Probe and Explorer mission lines was removed. With such evisceration and consequent programmatic uncertainty, it is not surprising that it is difficult for the Heliophysics Division to maintain and manage its space flight program.

The NRC review gave a low grade to the "Geospace Network" program. However, the Radiation Belt Storm Probes part of Geospace Network is already approaching its critical design review and is well on its way to a 2012 launch. Also, the mentioned Magnetospheric Multiscale program was subjected to an extended (nearly 5-year) initial study phase before beginning in earnest. It was reassigned to three different NASA administrators and five different associate administrators before being allowed to hit its stride. This is the "disastrous" result to which one of us (D.N.B.) was referring in his quote to Lawler.

Similarly, a very creative part of the heliophysics program, a modified Solar Probe mission, has been included in NASA's budget. NASA should be commended for accelerating scientifically rewarding programs,

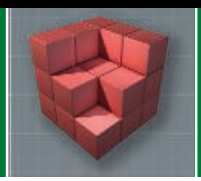

Organization of memory

40

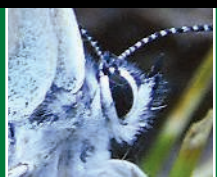

A conservation success story

41

and not punished—as the NRC performance review seems to do—for advancing one of the most important missions in solar and heliospheric physics.

It is clear that all of NASA (and other components of the U.S. space program as well) is witnessing large cost growths in flight missions. As Lawler points out, this has specifically been true of several recent solar and space physics missions. NASA must bring the best management techniques to bear (*2*) to help rein in mission cost growth. Heliophysics is clearly not alone in seeing cost overruns in its programs. However, based on its history and track record, heliophysics may have the best chance of turning this trend around to the great benefit of all.

DANIEL N. BAKER[1]* AND THOMAS H. ZURBUCHEN[2]

[1]Laboratory for Atmospheric and Space Physics, University of Colorado, Boulder, CO 80303, USA. [2]College of Engineering Entrepreneurial Program, University of Michigan, Ann Arbor, MI 48109–2143, USA.

*To whom correspondence should be addressed. E-mail: daniel.baker@lasp.colorado.edu

References and Notes

1. D. N. Baker, "Exploration Without Explorers?", *Space News*, 24 April 2006, p. 19.
2. National Research Council, *Assessment of Mission Size Trade-Offs for NASA's Earth and Space Science Missions* (National Academy Press, Washington, DC, 2000).
3. The authors are chair and vice-chair, respectively, of the NRC Committee on Solar and Space Physics, but they make their comments here as individuals.

How the Gray Wolf Got Its Color

THE REPORT "MOLECULAR AND EVOLUTIONary history of melanism in North American gray wolves" (T. M. Anderson *et al.*, 6 March, p. 1339) suggests that the K^B gene for black coat color was introgressed from dogs (*Canis lupus familiaris*) into North American gray wolves (*C. lupus*). However, the authors fail to consider an alternative hypothesis: The K^B gene may have originated in the historic black wolves of eastern North America (*C. niger*, *C. rufus*, and *C. lycaon*).

The potential for gray wolf and eastern wolf introgressive hybridization (*1*) provides a mechanism to move an eastern wolf–derived variant into *C. lupus* during the Wisconsin glaciation (11,000 to 18,000 years ago). The only evidence for the K^B gene in coyotes is in the range of the eastern wolf where hybridization between the two species (*C. lycaon* x *latrans*) has occurred (*2*) and not in more western geographies where gray wolves, dogs, and coyotes overlap. These coyote samples, however, were excluded from the analysis of the most recent common ancestor. If the selection hypothesis for black coat color in forested habitats is true, the prevalence of black pelage in the original timber wolves of the eastern temperate forests of Canada and the United States makes the inclusion of eastern wolf specimens critical for assessing the three

possible evolutionary histories proposed by Anderson *et al*. We suggest that a more complete examination of black canids from eastern North America be conducted before conclusions of introgressive hybridization from dogs to gray wolves are drawn.

LINDA Y. RUTLEDGE,[1]* PAUL J. WILSON,[2,3] CHRISTOPHER J. KYLE,[3] TYLER J. WHEELDON,[4] BRENT R. PATTERSON,[4] BRADLEY N. WHITE[5]

[1]Department of Environmental and Life Sciences, Trent University, Peterborough, ON K9J 7B8, Canada. [2]Department of Biology, Trent University, Peterborough, ON K9J 7B8, Canada. [3]Department of Forensic Science, Trent University, Peterborough, ON K9J 7B8, Canada. [4]Ontario Ministry of Natural Resources, Wildlife Research and Development Section, c/o Trent University, Peterborough, ON K9J 7B8, Canada. [5]Department of Biology, Natural Resources DNA Profiling and Forensic Centre, Trent University, Peterborough, ON K9J 7B8, Canada.

*To whom correspondence should be addressed. E-mail: lrutledge@nrdpfc.ca

References

1. T. Wheeldon, B. N. White, *Biol. Lett.* **5**, 101 (2009).
2. C. J. Kyle *et al.*, *Conserv. Genet.* **7**, 273 (2006).

Response

WE APPRECIATE AND ENDORSE THE IDEA THAT additional molecular and phenotypic information on natural canid populations will add to our understanding of gene flow and evolutionary histories of domestic dogs and their wild relatives. However, this information could only expand upon, rather than revise, our primary conclusion that the K^B allele has been introduced into wolves from dogs.

Several lines of independent evidence indicate that K^B is "older" in dogs than in Arctic wolves and their descendants in Yellowstone National Park. Extended haplotypes associated with K^B are much shorter in dogs than in wolves, more point mutations have accumulated in dog K^B than in wolf K^B chromosomes, and the worldwide distribution patterns for K^B are much broader in dogs than in wolves. Had the k^y to K^B mutation originated in North American eastern wolves, as Rutledge and colleagues speculate, it is difficult to envision how it could have spread so widely among dog breeds around the world. Thus, even if K^B was introduced from eastern to western wolves during the Wisconsin glaciation, K^B in eastern wolves would still have been acquired originally from American (in this case, Native American) dogs.

GREGORY S. BARSH,[1]* TOVI M. ANDERSON,[1] BRIDGETT M. VONHOLDT,[2] SOPHIE I. CANDILLE,[1] MARCO MUSIANI,[3] DANIEL R. STAHLER,[2] JENNIFER A. LEONARD,[4] BADRI PADHUKASAHASRAM,[5] ETTORE RANDI,[6] CARLOS D. BUSTAMANTE,[5] ELAINE A. OSTRANDER,[7] HUA TANG,[1] ROBERT K. WAYNE[2]

[1]Department of Genetics, Stanford University, Stanford, CA 94305, USA. [2]Department of Ecology and Evolutionary Biology, University of California, Los Angeles, CA 91302, USA. [3]Faculty of Environmental Design, University of Calgary, Calgary, AB T2N 1N4, Canada. [4]Department of Evolutionary Biology, Uppsala University, 75236 Uppsala, Sweden. [5]Department of Biological Statistics and Computational Biology, Cornell University, Ithaca, NY 14853, USA. [6]Instituto Nazionale per la Fauna Selvatica (INFS), 40064 Ozzano Emilia (BO), Italy. [7]National Human Genome Research Institute, Bethesda, MD 20892, USA.

*To whom correspondence should be addressed. E-mail: gbarsh@stanford.edu

Letters to the Editor

Letters (~300 words) discuss material published in *Science* in the previous 3 months or issues of general interest. They can be submitted through the Web (www.submit2science.org) or by regular mail (1200 New York Ave., NW, Washington, DC 20005, USA). Letters are not acknowledged upon receipt, nor are authors generally consulted before publication. Whether published in full or in part, letters are subject to editing for clarity and space.

Published by AAAS

EVOLUTION

The Ecological Theater

Anne E. Magurran

Speciation and Patterns of Diversity

Roger K. Butlin, Jon R. Bridle, and Dolph Schluter, Eds.

Cambridge University Press, Cambridge, 2009. 345 pp. $140, £75. ISBN 9780521883184. Paper, $63, £35. ISBN 9780521709637. Ecological Reviews.

> Throw up a handful of feathers, and all must fall to the ground according to definite laws; but how simple is this problem compared to the action and reaction of the innumerable plants and animals which have determined, in the course of centuries, the proportional numbers and kinds of trees now growing on the old Indian ruins!
>
> –Charles Darwin, *Origin of Species* (*1*)

This bicentenary of Charles Darwin's birth has been marked by such a flood of books, exhibitions, t-shirts, mugs, podcasts, and television programs that few people can be unaware of his ground-breaking ideas about natural selection. His elegant explanation for the evolution of life on Earth has been extensively tested and comprehensively vindicated. However, Darwin's insights into ecology—in particular how the interactions among species mediate speciation and extinction and how evolution shapes the distribution and abundance of species—have received much less attention. These too have the potential to substantially enhance our understanding of the natural world. It is therefore fitting that a new volume explicitly linking ecology and evolution has been published this year. *Speciation and Patterns of Diversity*, edited by Roger Butlin, Jon Bridle, and Dolph Schluter, grew out of a meeting of the British Ecological Society, itself the progeny of an earlier symposium on macroecology. The book poses questions that Darwin, and indeed many early ecologists, mulled over and asks whether recent research on mechanisms of speciation [e.g., (*2*)] has shed light on these long-standing problems. Issues tackled include the uneven distribution of species abundances in ecological communities, the preponderance of rare species, the latitudinal gradient of diversity, and the disproportionate diversity of small-bodied taxa relative to large ones. These are challenging and intractable questions, so it is not surprising that the book fails to deliver comprehensive answers. It does nonetheless make an important contribution by explicitly linking ecology with evolution. It also reminds us that taking a broad view of biology (as Darwin himself did) exposes connections and mechanisms that can be obscured when scientists become highly specialized.

Speciation and Patterns of Diversity covers a lot of ground and, reviewers apart, is not a book to be read cover to cover. It extends from theory (such as genetic models of adaptive radiation) to a speciation transect among Lake Victoria cichlids, covers a diverse range of animal and plant communities (including fossil assemblages), embraces the rapidly emerging field of microbial ecology, draws on powerful phylogenetic analyses, and grapples with difficulties of identifying species (particularly in the context of asexual organisms). As often happens in multi-authored volumes, the focus of different chapters varies considerably, from thoughtful overviews of the field to detailed expositions of a single topic. Not everyone will agree with every idea presented, but I would be surprised if there are any evolutionary ecologists who do not come away better informed or at least able to examine an old problem from a new perspective.

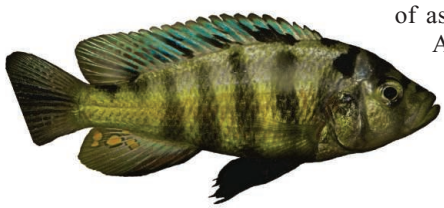

Intermediate cichlid. At Luanso Island, *Pundamilia pundamilia* and *P. nyererei* are merely extremes along a continuum of phenotypic variation.

CREDIT: OLE SEEHAUSEN/UNIVERSITY OF BERN & EAWAG

Among the conclusions that I found intriguing are Douglas Schemske's suggestion that the existence of greater opportunities for coevolution in the tropics contributes to increased species richness there, Albert Phillimore and Trevor Price's claim of ecological controls on the rate at which new species are formed, and Robert Ricklefs's idea that minimum viable population sizes constrain diversification. A general theme—explicit in some chapters and implicit in others—is that we might use the distinction between "ecological speciation" (due to divergent natural selection across environments) and "nonecological speciation" (attributed to factors such as drift) to tease out the imprint of ecology on evolution and vice versa. These and other overviews will translate into interesting research projects.

However, as Roger Butlin and others make clear, large gaps in knowledge remain, and there are serious methodological hurdles to be cleared. With the exception of polyploidy, the speciation mechanisms that have produced most taxa remain uncertain. It is even difficult to obtain accurate estimates of speciation rates because extant diversity patterns reflect the interplay between speciation and extinction. Indeed, the necessity of working with taxonomic groups that are diverse enough to be useful inevitably biases researchers toward organisms in which speciation outpaces extinction and may give a misleading impression that diversity has increased through time. Likewise, declines in diversity are invisible in phylogenetic trees.

One message that emerges is that although diversity is a potential driver of evolution, the relationship can operate in either direction. Low diversity can mean that there may be empty niches to be filled, whereas high diversity provides opportunities for coevolutionary interactions. In itself, none of this satisfactorily accounts for the universal patterns of commonness and rarity that Frank Preston (*3*) quantified and that Butlin and his colleagues, in their introduction, set out as one of the challenges both evolutionary biologists and ecologists must address. Yet, as is clear from the quote above, Darwin recognized not only that species vary in their abundance but also that this pattern of evenness is a product of the continuing interactions among species through time. At least some of these interactions will occur on tractable time scales. I hope that *Speciation and Patterns of Diversity* will encourage evolutionary biologists to look again at what Darwin had to say about ecology and ecologists to follow his lead in taking the long view and asking how the processes they study translate into rates of speciation and extinction.

The reviewer is at the Scottish Oceans Institute, School of Biology, University of St. Andrews, St. Andrews, Fife KY16 8LB, Scotland, UK. E-mail: aem1@st-andrews.ac.uk

References

1. C. Darwin, *On the Origin of Species by Natural Selection, or the Preservation of Favoured Races in the Struggle for Life* (John Murray, London, 1859).
2. J. A. Coyne, H. A. Orr, *Speciation* (Sinauer, Sunderland, MA, 2004); reviewed in (*4*).
3. F. W. Preston, *Ecology* **29**, 254 (1948).
4. B. K. Blackman, L. H. Rieseberg, *Science* **305**, 612 (2004).

10.1126/science.1175596

EVOLUTION

Green Life Through Time

Jonathan P. Wilson

Preserved since the Permian. Stomatal complexes in the cuticle of the seed fern *Dicroidium irnensis* (bar = 50 μm).

One may be forgiven for thinking that the field of paleobotany, with its focus on nonmotile, largely extinct organisms, should never be described as "fast-moving" except with tongue firmly in cheek. However, the molecular phylogenetics revolution, new fossil discoveries, and reinterpretations of existing material have catapulted our understanding of plant evolution ahead, leaving behind hypotheses and interpretations that were as good as fact a mere ten years ago. Thankfully, *Paleobotany: The Biology and Evolution of Fossil Plants* captures the current state of fossil plant anatomy and morphology. For this second edition, Michael Krings (Ludwig Maximilians University, Munich) has joined the earlier work's authorial duo of Thomas and Edith Taylor (University of Kansas). With the field's major texts long out of print and commanding three (or even four) figures online, and molecular, developmental, and paleontological studies locked in various stalemates (*1*–*4*), this up-to-date, encyclopedic treatment of fossil plants is a splendid gift for anyone interested in the evolution of terrestrial life.

Any book that includes two major thematic axes—increasing evolutionary diversity and complexity on one hand, and time on the other—faces a formidable organizational challenge. Many environmental events simultaneously affect disparate taxonomic groups, whereas evolutionary innovations may lead to within-group specializations that deserve to be discussed separately. Simply treating events stratigraphically risks giving short shrift to evolutionary trends, such as the increasingly rococo reproductive structures of the arborescent lycopods through the Carboniferous. However, a temporal framework makes it easier to portray the effects of large changes in climate and patterns of major adaptive radiations, such as the explosive diversifications of polypodiaceous ferns in tandem with angiosperm trees during the Late Cretaceous and Early Paleogene. Taylor, Taylor, and Krings split the difference by beginning with the enigmatic fossils of the Archean Eon and proceeding along each lineage from its appearance: fungi, nonvascular plants, lycopods, ferns, seed plants, and angiosperms. The encyclopedic coverage is weighted toward the last five groups. The authors describe in detail vegetative and reproductive structures, where known; summarize variation; and offer comparisons. They give orphaned organ taxa (particularly foliage and seeds) individual chapters, in which they note tentative or speculative associations with other fossil groups.

Paleobotany
The Biology and Evolution of Fossil Plants. 2nd ed.
by Thomas N. Taylor, Edith L. Taylor, and Michael Krings
Academic (Elsevier), Burlington, MA, 2009. 1252 pp. $125, £62.99, €91.95. ISBN 9780123739728.

The authors synthesize the recent discoveries that have made paleobotany crucial to the understanding of plant relationships and diversity. The most welcome additions come from descriptions of early angiosperm fossils (*5*, *6*), Mesozoic seed ferns that almost certainly (albeit cryptically) represent the lineage that led to the origin of flowering plants (*7*), and Paleozoic plants that demonstrate novel variations on reproductive and vegetative biology absent in living plants (*8*). Organisms that the previous edition limited to a few pages now occupy complete chapters. Furthermore, the demise of the anthophyte hypothesis (which linked angiosperms to the living seed plants *Gnetum*, *Ephedra*, and *Welwitschia*) has left a vacuum that could be crippling to a book focused on the evolution of plants. However, the authors took this development as an opportunity to recapitulate many of the hypotheses that have circulated in the literature over the past hundred years (some fanciful, others quite interesting) along with the available evidence for and against each. By opening the door to a diversity of ideas, the authors turned what could have been a gaping void into an agenda for many a lab meeting or conference session.

On opening the cover, two features jump out. The pages are dominated by large color photographs—a first for any textbook on the evolution of plants. And, to preserve the field's roots, many of these images are photographs (both candid and posed) or paintings of paleobotanical researchers, going back to the early 19th century. (It appears that paleobotanical ideas and facial topiary evolved in parallel.) The color photographs are important because they present morphological details that are crucial to the use of plant fossils in stratigraphy, systematics, and—especially—understanding physiology and function. For example, a comparison of the fascinating wood anatomy of the arborescent lycopods, the Paleozoic sphenophyte *Sphenophyllum*, and the early fern *Zygopteris illinoiensis* yields a powerful illustration of the effects of convergent evolution on plant form.

For anyone interested in the development, evolution, or impact of plants, this volume deserves to be within arm's length. It reveals the fossil record of terrestrial plants from the humblest fungal hyphae to the loftiest rainforest trees. Nevertheless, readers, especially those unfamiliar with botany or geology, may find the book daunting. The authors have smoothed the road with chapters on plant morphology, anatomy, and preservation and a useful glossary of terms. The vast amount of anatomical and descriptive detail, however, is staggering. The relative scarcity of cladograms throughout the text may disappoint those having an eye toward the evolutionary relationships of fossil plants. I would urge a closer look: numerous species of virtually every fossil plant genus are fully described and, in most cases, illustrated. A more beneficial and durable data set would be difficult to imagine.

Taylor, Taylor, and Krings provide the most accurate, useful, and well-illustrated comprehensive account of fossil plants now in print. Their new edition has caught up with recent discoveries and the progress of thoughts about plant evolution. It points the way toward the most promising avenues for future research.

The reviewer is at the Division of Geological and Planetary Sciences, California Institute of Technology, 1200 East California Boulevard, Pasadena, CA 91125, USA. E-mail: jpwilson@post.harvard.edu

References
1. M. W. Frohlich, M. W. Chase, *Nature* **450**, 1184 (2007).
2. E. M. Friis, K. R. Pedersen, P. R. Crane, *Am. J. Bot.* **96**, 252 (2009).
3. S. Mathews, *Am. J. Bot.* **96**, 228 (2009).

4. G. W. Rothwell, W. L. Crepet, R. A. Stockey, *Am. J. Bot.* **96**, 296 (2009).
5. E. M. Friis, J. A. Doyle, P. K. Endress, Q. Leng, *Trends Plant Sci.* **8**, 369 (2003).
6. G. Sun *et al.*, *Science* **296**, 899 (2002).
7. E. L. Taylor, T. N. Taylor, H. Kerp, E. I. Hermsen, *J. Torrey Bot. Soc.* **133**, 62 (2006).
8. W. E. Stein, F. Mannolini, L. V. Hernick, E. Landing, C. M. Berry, *Nature* **446**, 904 (2007).

10.1126/science.1174659

EXHIBITIONS: ART

An Unsung Refrain of Science

Harriet Coles

A lifelike model of an art collector floats face down, dead in a pool while his naked lover (a live model) lounges indoors listening to music. Elsewhere, an artist swings a mallet at huge gilt-framed mirrors, sending shards of glass flying. These elaborate installations (Michael Elmgreen and Ingar Dragset's *The Collectors* and Michelangelo Pistoletto's *Twenty-Two Less Two*, respectively) on show at this year's Venice Biennale either parody or epitomize contemporary art as an exercise in navel-gazing—it's your choice. Amid the buzz of the art world, however, there is another theme: the clear if unsung refrain of the influence of science and technology on contemporary art. It is there in the use of scientific imagery, methods, and technology and in an engagement with cutting-edge science.

Since its inception in 1895, Venice's Biennale has emerged as the world's biggest and most celebrated art fair. And the 2009 exhibition is the largest yet. Seventy-seven countries show works by their chosen representatives, there are 44 "collateral events" around the city, and there is much more. Venice and its islands are laden with thousands of pieces on display until mid-November.

Anatomical images abound. These no longer represent the Renaissance struggle to define and celebrate humanist values but are employed to shock or to explore the darker side of being human. Bruce Nauman's exhibit in the U.S. Pavilion (winner of the Golden Lion for the best national participation) has a discrete measure of flayed body parts. Jan Fabre, however, is less restrained in his *From the Feet to the Brain*, which includes corpses, bottled brain, flayed heads, and a resin fountain of ejaculate.

The exception to the rule is Bill Viola's masterly use of contemporary clinical imaging for aesthetic ends. His video diptych *Bodies of Light* gently scans an Adam and Eve pair of figures. Over 21 minutes, a light intermittently sweeps them; four cycles reveal them naked, then their vasculature, their musculature, and finally their bones. Here, state-of-the-art medical scanning is employed for art's sake. Whereas a doctor would employ the technology for clinical enlightenment, Viola uses it to dimly visualize the "tree of vessels" (da Vinci's description of vasculature). The darkened figures are mesmerizing and bring an aesthetic to images we take for granted in a scientific context. *Bodies of Light* is on show at *In-finitum*, a superb exhibition at the equally wonderful Palazzo Fortuny.

Fare Mondi / Making Worlds
53rd International Art Exhibition
Daniel Birnbaum, Director
Venice Biennale, the Giardini, the Arsenale, and various other venues, Venice, Italy. To 22 November 2009. www.labiennale.org/en/art/

Numerous artists use other scientific imagery either consciously or unwittingly. One of the most striking results is by Argentinian Tomas Saraceno. He explores how complex geometry enables black widow spiders' silk to suspend considerable weight. Two huge polyhedra of elastic rope are anchored to the walls, floor, and ceiling of a large room. But would this engineered piece be most at home in a science museum, with the art of the piece taking a back seat?

Fewer artists set out to explicitly explore scientific themes. Portugal's representatives do so in their show named after Joseph Priestley's *Experiments and Observations on Different Kinds of Air*—a brave venture worth viewing if only to see how science is seen from the outside. Historic preservationist Jorge Otero-Pailos brings experimental method to his *Ethics of Dust*, which shares its title with a peculiar series of lectures John Ruskin published in 1865. Otero-Pailos has conserved pollution from a wall at the Doge's Palace on a huge latex sheet. The dust alone creates a spectacular sight and becomes a valued cultural product in its own right.

My favorite among several works that play with the psychology of perception was the Lithuanian Pavilion housed in the Scuola Grande della Misericordia, where Žilvinas Kempinas uses video tape to create a 20-or-so-meter-long louvered tunnel. Visitors can walk through *Tube* to great effect: their movements are revealed to them by the apparent motion of the tunnel walls. It is a three-dimensional extension of Bridget Riley's Op Art of the 1960s.

The 2009 Venice Biennale offers rich pickings and much entertainment. Although many of these works are one-trick ponies, all are part of a great spectacle.

10.1126/science.1177564

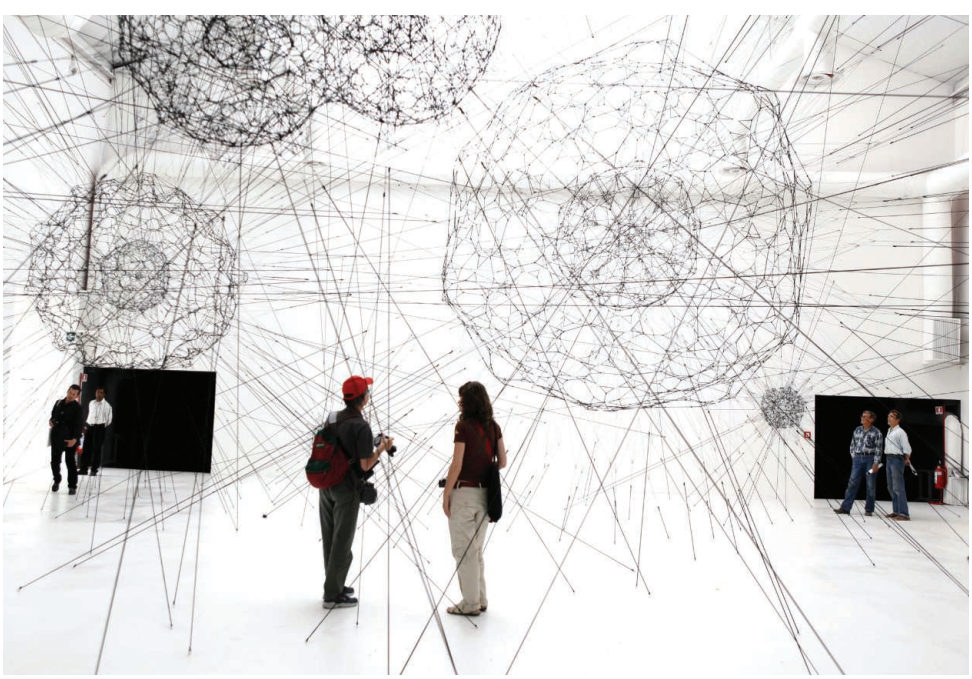

CREDIT: SICHOV/SIPA/ASSOCIATED PRESS

At the International Pavilion. Saraceno's *Galaxies Forming Along Filaments, Like Droplets Along the Strands of a Spider's Web*.

The reviewer is a freelance science writer in London. E-mail: harrietcoles2@aol.com

GENETICS

The Illusive Gold Standard in Genetic Ancestry Testing

New regulations on disclosure, authority, and responsibility would shape how genetic ancestry tests are used.

Sandra Soo-Jin Lee,[1]* Deborah A. Bolnick,[2] Troy Duster,[3,4] Pilar Ossorio,[5] Kimberly TallBear[6]

Genetic ancestry testing is being applied in areas as diverse as forensics, genealogical research, immigration control, and biomedical research (*1*–*3*). Use of ancestry as a potential risk factor for disease is entrenched in clinical decision-making (*4*), so it is not surprising that techniques to determine genetic ancestry are increasingly deployed to identify genetic variants associated with disease and drug response (*5*). Recently, direct-to-consumer (DTC) personal genomics companies have used ancestry information to calculate individual risk profiles for a range of diseases and traits.

Despite the proliferation of companies providing genetic ancestry information, DTC genetic ancestry tests fall into an unregulated no-man's land, with little oversight and few industry guidelines to ensure the quality, validity, and interpretation of information sold. Scholars and scientists have therefore urged the genetics community to take a leadership role in offering guidance to the DTC genetic ancestry market (*6*, *7*).

In November 2008, the American Society of Human Genetics (ASHG) issued recommendations on ancestry testing that emphasized the need for greater responsibility, research, explanatory clarity, collaboration, and accountability by DTC companies, academia, and potential consumers (*8*). While highlighting the clinical implications of ancestry testing, the statement also discussed limitations to the scientific approaches used to infer genetic ancestry, including the incomplete representation of human genetic diversity in existing databases, the false assumption that contemporary groups are reliable substitutes for ancestral populations, and the lack of transparency regarding the statistical methods that companies use to determine test results.

[1]Stanford Center for Biomedical Ethics, Stanford University Medical School, Palo Alto, CA 94304, USA. [2]Department of Anthropology, University of Texas, Austin, TX 78712, USA. [3]Department of Sociology, New York University, New York, NY 10012, USA. [4]Department of Sociology, University of California, Berkeley, CA 94720, USA. [5]University of Wisconsin Law School, Madison, WI 53706, USA. [6]Department of Environmental Science, Policy and Management, University of California, Berkeley, CA 94720, USA.

*Author for correspondence. E-mail: sandra.lee@stanford.edu

The ASHG statement identifies key issues surrounding the science of ancestry estimation and represents an important first step. However, an effective public policy for the growing market of genetic ancestry tests must build on the ASHG's recommendations and must generate specific mechanisms and approaches. Questions that remain include these: (i) In practice, what do responsibility and accountability mean for academia, industry, and consumers? (ii) How can diverse stakeholders reach a common understanding of the limitations of genetic ancestry tests and their broader implications for human identity? (iii) What role should governmental agencies play in creating infrastructure that effectively addresses the most challenging issues related to DTC genetic ancestry tests?

Mutual Responsibility and Accountability

The ASHG sees academia, industry, and potential consumers as sharing responsibility for conveying and understanding the limitations of genetic ancestry testing. But what do responsibility and accountability mean in human population genetics? This question is critical because the limitations of ancestry testing are entrenched in a broader set of issues that emerge well before these tests reach market. In particular, ethical questions about the collection and use of DNA samples must be resolved before researchers are permitted to sample many of the populations needed to approximate the full range of human genetic diversity. Historically, relations between researchers and study populations have ranged from open negotiations to opportunism, misunderstandings, and even duplicity (*9*).

The importance of this issue is illustrated by the recent decision of the Arizona Court of Appeals to reinstate the 2004 lawsuit of the Havasupai Tribe against the Arizona Board of Regents (*10*). The Havasupai originally consented to have Arizona State University researchers collect DNA samples for diabetes research, but the samples were used without permission to study schizophrenia, inbreeding, and prehistoric human migration from Asia (*11*). One Havasupai allegation is that ASU's ethics oversight was negligent. However, in many instances, research can be compliant with existing human subjects protections yet fail to recognize long-standing differences in access to institutional and legal power, as well as questions about who holds authority to determine future uses of samples (*12*). The Havasupai case is not the only instance of Native American samples collected with consent only for health research, but then used to pursue other areas of inquiry that were not originally identified. Samples taken and traded under less stringent ethical regimes still remain in scientists' collections and may be used for purposes beyond the original research questions (*13*, *14*). It is a scientific imperative that we enact enforceable policies that determine what constitutes responsible and accountable collection and secondary use of DNA samples.

Current guidelines issued by the Office for Human Research Protections (OHRP),

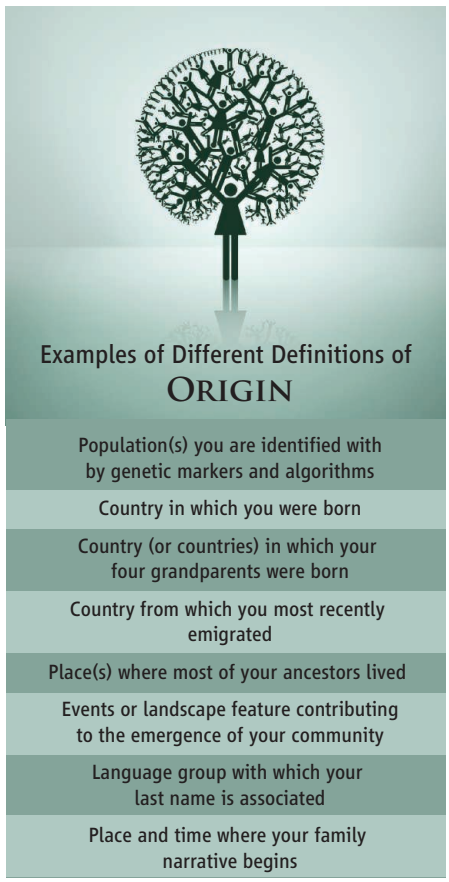

IMAGE CREDIT: ISTOCK

Published by AAAS

U.S. Department of Health anhd Human Services (DHHS), do not classify research involving previously collected samples that have been delinked from individually identifiable private information as "human subjects research" and, thus, do not specify requirements for informed consent in such research (*15*). With application of ancestry informative markers (AIMs), though, population-specific labels may be ascribed to anonymized DNA samples. Such samples, now identifiable to a politically and socially salient group, may be used to answer questions that were never approved when the group initially donated samples. Such practices fall outside current ethical oversight. The National Bioethics Advisory Commission has urged consideration of whether research on stored tissue would examine traits with political, economic, or cultural significance and could affect subjects' communities, but this recommendation has not been taken up by the OHRP (*16*). ASHG and other governing bodies should formulate policies to guide ethical collection, use, and repatriation (where appropriate) of biological samples.

Finding Common Language

The high stakes of genetic ancestry research require innovative approaches to dialogue, collaboration, and power-sharing between academia, industry, consumers, and community groups (especially those that have been disenfranchised from the research process) (*9*, *17*, *18*). A first step may be joint creation of a vernacular that characterizes key concepts like probability, association, origin, and ancestry to help minimize variability that exists in how such concepts are understood across fields, communities, and governmental and commercial entities with different vantage points.

For example, the term "origin" is not transparently or consistently defined. To a geneticist, origin might refer to ancestral populations inferred for an individual on the basis of specific genetic markers, specific algorithms for assessing genetic similarity, and specific reference populations. To a casual consumer, origin might mean "the country where I was born," "the country (or countries) where my grandparents were born," "the place or language group where my last name originated," or "the place and/or time where my family narrative begins" (see table, page 38). To a Native American, origin might also signify the landscape feature or event where his or her people emerged or acquired their identity.

Even accepting a genetic or genealogical conception of origin, should each identifiable ancestor or genealogical line be considered an origin? Population origins are rarely defined with that kind of multiplicity in mind. Given that each person may have many ancestors from the same place, does one have more ancestors than origins? Which biogeographical point in the genealogical line of an individual or population do we pinpoint as the origin? What is the rationale for naming ancient genetic lineages according to more recent and shifting ethnic, national, racial, or tribal categories? What are the implications of considering one contemporary population to be the ancestral origin of another?

There are no clear answers to these questions. However, recognizing that key terms can have disparate meanings for different groups will be a critical step toward effective dialogue. Refining a genetic vernacular requires educating both scientists and nonscientists and will depend on incorporating the multiple spheres of expert knowledge of human relatedness. Efforts by genetic researchers and other scholars, community groups, regulators, and industry partners to share their varied understandings may help stem miscommunication and increase rigor.

A Role for Leadership

Human genetic variation research is a continuously shifting landscape. This dynamic marketplace puts in stark relief the limitations of categorical thinking about how genetic information is produced and applied. Genetic ancestry information can rarely be compartmentalized as either clinically relevant or merely historical. Nor is there a bright line between academia and industry because genetic researchers in universities increasingly collaborate with and move into industry. Even notions of the greater "public" are blurred as consumers of genetic products start their own companies (*19*).

Given the very different interests of the various stakeholders, resolution of differences will not be an easy, much less voluntary, process. For instance, the ASHG statement calls for greater transparency, but private sector providers of ancestry testing have proprietary reasons for keeping secret their own particular combinations of key technology, software, and population sampling procedures, and many are unwilling to disclose the size and composition of their reference populations. Without mechanisms to enforce transparency, it is difficult to assess the scientific basis for specific assertions of biogeographical ancestry.

Federal agencies such as the Federal Trade Commission, the Food and Drug Administration, and the Centers for Disease Control and Prevention could play pivotal roles in setting industry standards for what constitutes responsible and accountable practices. These agencies can promote the dialogue and research necessary to discover common language and to identify best practices for presenting the limitations of current genomic technologies and the risks associated with over-extrapolating or misinterpreting genetic ancestry results. New regulations on such matters will help shape how practitioners are able to communicate genetic ancestry testing results to consumers. How these regulations will be put in place is going to be a struggle between various parties that have shown little indication that there will be a compromise that will be acceptable to all. Political will and leadership toward addressing fundamental differences in perspectives may ultimately determine whether a gold standard for genetic ancestry testing can be achieved.

References and Notes

1. B. Budowle, A. van Daal, *Biotechniques* **44**, 603 (2008).
2. M. D. Shriver, R. A. Kittles, *Nat. Rev. Genet.* **5**, 611 (2004).
3. S. Choudhry *et al.*, *Hum. Genet.* **123**, 455 (2008).
4. J. M. Flack, M. J. Hamaty, *J. Hypertens.* **17**(suppl.), S19 (1999).
5. W. H. Kao *et al.*, *Nat. Genet.* **40**, 1185 (2008).
6. D. A. Bolnick *et al.*, *Science* **318**, 399 (2007).
7. W. Burke, P. Kuszler, H. Starks, S. Holland, N. Press, *Am. J. Bioeth.* **8**, 54 (2008).
8. ASHG, *Ancestry Testing Statement*, 13 November 2008 (ASHG, Bethesda, MD, 2008); www.ashg.org/pdf/ASHGAncestryTestingStatement_FINAL.pdf.
9. L. Arbour, D. Cook, *Community Genet.* **9**, 153 (2006).
10. *Havasupai Tribe of the Havasupai Reservation* v. *Arizona Board of Regents and Therese Ann Markow*, Arizona Court of Appeals, No. 1 CA-CV 07-0454 and 1 CA-CV 07-0801.
11. S. Hart, K. Sobraske, *Investigative Report Concerning the Medical Genetics Project at Havasupai*, 23 December 2003; available at the Arizona State University Law Library and www.geneticpiracy.com/Documents/HartReport.pdf.
12. DHHS, Protection of Human Subjects, 45 *Code of Federal Regulations* (C.F.R.), 46 § 101 (2005).
13. R. Dalton, *Nature* **420**, 111 (2002).
14. D. Wiwchar, "Nuu-chah-nulth blood returns to West Coast," *Ha-Shilth-Sa* (tribal newspaper) **31**(25), 1 (16 December 2004).
15. 45 C.F.R. 46 § 102(f), (2004).
16. National Bioethics Advisory Commission, *Research Involving Human Biological Materials: Ethical Issues and Policy Guidance* (NBAC, Rockville, MD, vol. 1, 1999).
17. S. Goering *et al.*, *Hastings Cent. Rep.* **38**, 43 (2008).
18. D. Winickoff, "From benefit sharing to power sharing: Partnership governance in population genomics research" (Faculty Working Paper 68, Jurisprudence and Social Policy Program, Center for the Study of Law and Society, Berkeley, CA, 2008).
19. K. TallBear, *Native American DNA: Origins, Ethics, and Governance* (Univ. of Minnesota Press, Minneapolis, in press).

20. S.S.-J.L was supported by the Ethical, Legal, and Social Implications Research Program, National Human Genome Research Institute, NIH, grants K01 HL72465 and P50 HG003389. K.T. was supported by the University of California, Berkeley, and the Program in Science, Technology and Society, Division of Social and Economic Sciences, NSF, award 0724855.

10.1126/science.1173038

NEUROSCIENCE

Remembering Outside the Box

The mammalian brain may be organized in terms of multipurpose representations rather than psychologically defined modules.

Lisa M. Saksida

The prevailing view in memory research is that the mammalian brain is composed of a number of heterogeneous modules, each responsible for a different cognitive function, including different types of memory. An emerging alternative view, however, suggests that instead of such modules, the brain is organized in terms of the multipurpose representations that different regions support. As such, a given representation—and thus a given brain region—could be useful for many different functions. Evidence for this latter view has focused largely on demonstrating that regions within the putative memory system of the mammalian brain also play a role in another high-level function: perception (*1*–*4*). On page 87 of this issue, López-Aranda *et al*. (*5*) show that regions within the brain's putative perceptual system also play a role in memory, further solidifying evidence for a representational view of brain organization.

The dominant textbook paradigm of human memory is the multiple memory systems view, according to which different kinds of memory, such as declarative memory (memory for facts and events) and nondeclarative memory (memory for skills and procedures), are subserved by different modules in the brain (*6*, *7*). Declarative memory is the domain of the medial temporal lobe memory system, which includes structures such as the hippocampus and perirhinal cortex. This system can be contrasted with a separate perceptual representation system (*8*), which includes the extrastriate visual cortex (comprising roughly 30 regions including, V2, V3, V4, and IT in the primate brain). This perceptual system is, according to the standard view, critical both for representing the structure of visual stimuli and for nondeclarative memory functions such as priming (an increase in sensitivity to a stimulus due to prior experience).

However, it may be more useful to think about brain regions, not in terms of psychologically defined modules, but in terms of the representations that they contain (*9*–*12*) (see the figure). For example, in visual memory, structures within the medial temporal lobe (such as the perirhinal cortex) may be understood as an extension of the ventral visual object processing system—or the "what" pathway—which flows from the visual cortex to the medial temporal lobe (*13*, *14*). This view suggests that structures in the "what" pathway and the medial temporal lobe should not be segregated according to their putative roles in perceptual versus mnemonic function. Instead, the entire stream is important for multiple functions including both memory and perception.

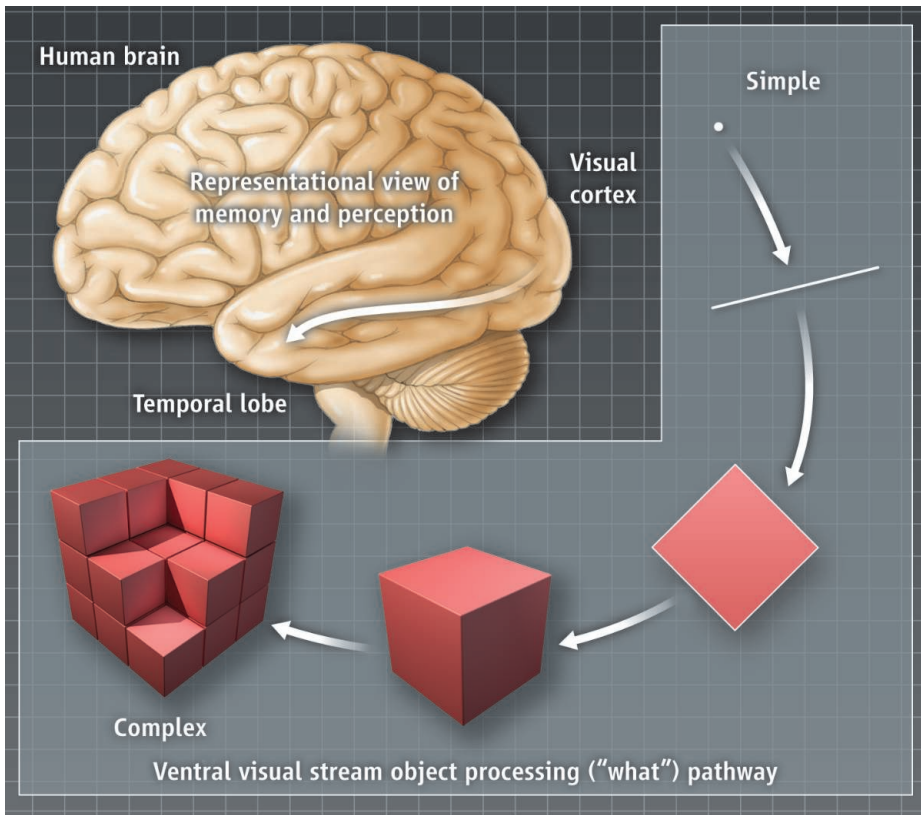

Brain organization. The standard view in memory research suggests that distinct brain regions support different cognitive functions. The representational view of the human brain, by contrast, suggests that a given brain region could be useful for multiple high-level functions. For example, information represented in the "what" pathway flowing through the visual cortex to the medial temporal lobe may be important for both memory and perception.

A behavioral paradigm that has been critical in establishing the multiple memory systems view is object recognition memory. In this model, a subject is presented with an object to study. After a delay, the study object and a novel object are presented. A typical subject will preferentially select or spend more time investigating the novel object, and this is taken to be an index of memory for the study object. Object recognition memory is considered to be a canonical example of declarative memory and is therefore thought to depend exclusively on the medial temporal lobe memory system (*15*). However, López-Aranda *et al*. demonstrate the involvement of an area outside this system—specifically, cells that comprise layer 6 of the extrastriate visual cortical area V2. In their study, lesions of cells in layer 6 of the V2 region in the rat brain impaired object recognition memory, which suggests that V2 is critical to this function. This is not consistent with the prevailing multiple memory systems view, which would predict that damage to regions outside the medial temporal lobe should have little effect on object recognition memory. This finding is consistent, however, with the representa-

CREDIT: C. BICKEL/*SCIENCE*

Department of Experimental Psychology, University of Cambridge, Cambridge CB2 3EB, UK. E-mail: lms42@cam.ac.uk

Published by AAAS

tional view, which would predict that damage to any region within the ventral visual cortex–to–hippocampal stream could affect object recognition memory.

It might be argued that damage to the V2 region may have cut off visual information to the medial temporal lobe. Such a disruption would render the medial temporal lobe memory system unable to function properly, thereby making the findings of López-Aranda *et al*. consistent with the modular view of memory. However, lesions made in the V2 region were highly selective in that an excitotoxin was used to damage only cell bodies in V2. Thus, neuronal extensions (fibers) would have been left intact, passing from V1 through V2, to downstream areas. Thus, visual information could still pass through V2. There were also plenty of "jumping projections" from neurons in information processing regions upstream of V2 to regions downstream from V2, including the medial temporal lobe.

More interestingly, López-Aranda *et al*. have provided further evidence to suggest that the involvement of V2 in object recognition memory cannot be interpreted simply in terms of a lack of information flowing from the visual cortex to the medial temporal lobe (due to V2 cell damage). When the protein RGS-14, which is involved in signaling pathways implicated in memory, was overexpressed in cells of layer 6 in V2, rats could remember more objects, and for much longer, relative to controls. The same manipulation within the medial temporal lobe (specifically, within the dentate gyrus and CA1 region of the hippocampus) had no effect on object recognition memory. Thus, López-Aranda *et al*. show that manipulations outside of the putative medial temporal lobe memory system can both impair and facilitate object recognition memory. This result is also consistent with previous studies reporting no effect of hippocampal manipulations on object recognition memory and is consistent with the view that the medial temporal lobe memory system is not a homogeneous system but contains distinct, dissociable components (*16*, *17*).

An outstanding question is how molecules such as RGS-14 facilitate memory and what function they have in the mechanisms of cognition in the normally functioning brain. These are critical questions for future research.

References

1. M. D. Barense *et al*., *J. Neurosci.* **25**, 10239 (2005).
2. J. T. Devlin, C. J. Price, *Curr. Biol.* **17**, 1484 (2007).
3. S. J. Bartko, B. D. Winters, R. A. Cowell, L. M. Saksida, T. J. Bussey, *J. Neurosci.* **27**, 2548 (2007).
4. T. J. Bussey, L. M. Saksida, E. A. Murray, *Eur. J. Neurosci.* **15**, 365 (2002).
5. M. F. López-Aranda *et al*., *Science* **325**, 87 (2009).
6. L. R. Squire, C. E. Stark, R. E. Clark, *Annu. Rev. Neurosci.* **27**, 279 (2004).
7. S. Zola-Morgan, L. R. Squire, *Annu. Rev. Neurosci.* **16**, 547 (1993).
8. E. Tulving, D. L. Schacter, *Science* **247**, 301 (1990).
9. T. J. Bussey, L. M. Saksida, *Curr. Opin. Neurobiol.* **15**, 730 (2005).
10. T. J. Bussey, L. M. Saksida, *Hippocampus* **17**, 898 (2007).
11. E. A. Murray, T. J. Bussey, L. M. Saksida, *Annu. Rev. Neurosci.* **30**, 99 (2007).
12. D. Gaffan, *Philos. Trans. R. Soc. London Ser. B* **357**, 1111 (2002).
13. R. Desimone, L. G. Ungerleider, in *Handbook of Neuropsychology,* F. Boller, J. Grafman, Eds. (Elsevier Science, New York, 1989), vol. 2, pp. 267–299.
14. M. Riesenhuber, T. Poggio, *Nat. Neurosci.* **2**, 1019 (1999).
15. J. R. Manns, C. E. Stark, L. R. Squire, *Proc. Natl. Acad. Sci. U.S.A.* **97**, 12375 (2000).
16. B. D. Winters, S. E. Forwood, R. A. Cowell, L. M. Saksida, T. J. Bussey, *J. Neurosci.* **24**, 5901 (2004).
17. M. W. Brown, J. P. Aggleton, *Nat. Rev. Neurosci.* **2**, 51 (2001).

10.1126/science.1177156

ECOLOGY

Insect Conservation

Understanding of ecosystem interactions and management has led to a major advance in the conservation of specialized insects.

Josef Settele and Elisabeth Kühn

Conservation efforts in Europe mainly aim to preserve and manage ecosystems that contain putatively endangered biotic communities. However, as Thomas *et al*. show on page 80 of this issue (*1*), this approach may not yield the desired results—particularly in the case of comparatively specialized taxa such as butterflies and other insect groups.

Many insects react rapidly to environmental change. For example, regional extinction rates of European butterflies have exceeded those of birds and higher plants by an order of magnitude in recent decades (*2*). Ensembles of closely interacting species are most vulnerable to change, because survival depends on the persistence of multiple group members. Thus, the greatest declines among butterflies were recorded in the many species that also depend on ants (myrmecophiles) (*3*). The best-documented example is the decline in the second half of the last century and eventual extinction in the UK in 1979 of the Large Blue *Maculinea arion* (*1*), a butterfly that during the first three larval stages depends on specific food plants (*Origanum* or *Thymus*) and later on the brood of specific *Myrmica* ants.

To improve the prospects for at least some insect groups, the 1992 European Habitats Directive listed examples of myrmecophiles (*4*), including three of the five European *Maculinea* species. All listed species must be kept in a favorable conservation status through appropriate management in the European-wide network of conservation areas called Natura 2000. However, because little was known about the biology of these species, conservation success was limited—and still would be, had it not been for groundbreaking research on *Maculinea* ecology started in the UK by Jeremy A. Thomas in the 1970s and joined from 1983 onward by Graham Elmes. Particularly in the 1990s through research by several labs, *Maculinea* became a key taxon in evolutionary and conservation biology.

Conservation under climate change. Through landscape management, it may be possible to mitigate climate change effects on species such as the Large Blue *M. arion* (**top**) and the Dusky Large Blue *M. nausithous* (**bottom**).

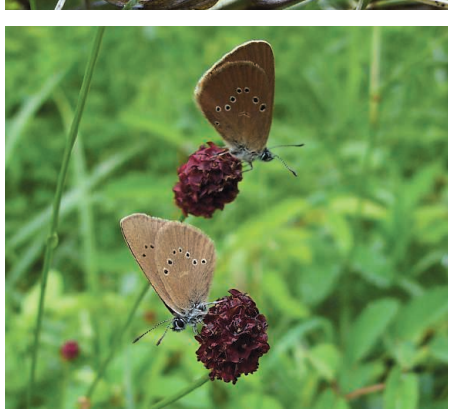

PHOTO CREDITS: (TOP) M. ARION, CHRIS VAN SWAAY/DEVLINDERSTICHTING; (BOTTOM) M. NAUSITHOUS, JOSEF SETTELE/UFZ

UFZ-Helmholtz Centre for Environmental Research, Department of Community Ecology, Theodor-Lieser-Strasse 4, 06120 Halle, Germany. E-mail: Josef.Settele@ufz.de; Elisabeth.Kuehn@ufz.de

In 2002, the European Union–funded *Maculinea* management research project "MacMan" started and grew quickly into a multinational endeavor. Its aims were to elucidate the functional ecology and genetic structure of *Maculinea* systems across Europe, assess the suitability of *Maculinea* butterflies as indicators of biodiversity along a European transect, and develop standards for monitoring *Maculinea* butterflies as indicators and tools for grasslands and their management (*5*).

This collaboration saw major scientific breakthroughs in evolutionary and conservation biology (*1*, *2*, *6*–*10*). In particular, grazing prescriptions developed for *M. arion* habitats—where maintenance of short turf height is a key factor (*1*)—served as a blueprint for the development of mowing regimes for two wet grassland species within MacMan. However, because mowing creates less small-scale heterogeneity in vegetation than grazing does, the right conditions for these wetland *Maculinea* can only be achieved on the landscape scale (*11*). Survival chances are increased through the recently discovered biannual cycle of many *Maculinea* species; larvae stay in the ants' nests for nearly 2 years (*12*).

The application of ecological knowledge to practical conservation requires a high level of local acceptance. Socioeconomic studies have revealed a high willingness to pay by local inhabitants (*13*). This acceptance emanated from the fascinating ecology of these butterflies, in particular their ability to mimic ants (*8*) and their parasitic and carnivorous larval life in the nests of ants (*7*).

Population and niche models have now been made available and validated by 25 years of successful restoration of *M. arion* in the UK (*1*). This enables us to use *Maculinea* systems to explore future challenges, particularly to investigate and model the combined impacts of human-induced changes in climate (*14*) and habitat (*15*, *16*) on these species. The next studies should focus on their local adaptations, changing niches, and different needs across a gradient of local climates. These results should then feed into models to assess the impacts of land use, climate, and socioeconomic change under a range of future scenarios (*17*, *18*) in different European regions. The ultimate goal should be new predictions on the mitigation of harmful impacts of multiple drivers.

As Thomas *et al*. show, ideal microclimatic conditions for the host ants of the Large Blue are achieved through different vegetation heights under different macroclimates. These insights should be transferred into recommendations for habitat management. Higher vegetation under warmer climates might extend the survival chances of local populations, leaving more time for the insects to adapt to their local environment than is recognized in current paradigms (*15*). Furthermore, management may allow modest temperature change to be counteracted by either creating cooler niches or making them accessible through connectivity, thereby buffering expected impacts on the distribution of the butterflies under certain scenarios of future development. The effect might well be that the realized changes in distribution resemble those originally expected under a less severe scenario (*14*). All such models and derived conservation recommendations will, however, have to be tested against large-scale habitat manipulations.

The study by Thomas *et al*. shows that precise knowledge of an endangered species' ecological requirements under a given climate can enable conservationists to reverse current declines by restoring or creating optimum conditions. In insects, this alone may increase by two to three orders of magnitude the size and stability of current populations, as well as creating new ones in landscapes and generating more emigrants to migrate in the future to climatically suitable habitat patches.

Management that creates cooler microtopographies and later (cooler) successional stages in current grasslands should mitigate the impacts of climate warming in the short to medium term. Such mitigation may not provide long-term (>100 year) solutions. Nevertheless, the findings of Thomas *et al*. suggest that the period during which local genotypes may persist on their current sites can be doubled, increasing the chances that individuals will adapt to changed conditions or migrate to cooler regions.

References and Notes

1. J. A. Thomas, D. J. Simcox, R. T. Clarke, *Science* **325**, 80 (2009).
2. J. A. Thomas *et al*., *Science* **303**, 1879 (2004).
3. J. A. Thomas *et al*., in *Studies in the Ecology and Conservation of Butterflies in Europe 2*, J. Settele, E. Kühn, J. A. Thomas, Eds. (Pensoft, Sofia, 2005), pp. 28–31.
4. European Commission Official Journal L 206, 22/07/1992, 7-50 (Council Directive 92/43/EEC; 1992; see http://ec.europa.eu/environment/nature/legislation/habitatsdirective/index_en.htm.
5. J. Settele, E. Kühn, J. A. Thomas, Eds., *Studies in the Ecology and Conservation of Butterflies in Europe 2* (Pensoft, Sofia, 2005).
6. J. A. Thomas *et al*., *Nature* **417**, 505 (2002).
7. T. D. Als *et al*., *Nature* **432**, 386 (2004).
8. J. A. Thomas, J. Settele, *Nature* **432**, 283 (2004).
9. D. R. Nash, T. D. Als, R. Maile, G. R. Jones, J. J. Boomsma, *Science* **319**, 88 (2008).
10. F. Barbero *et al*., *Science* **323**, 782 (2009).
11. K. Johst, M. Drechsler, J. A. Thomas, *J. Settele, J. Appl. Ecol.* **43**, 333 (2006).
12. M. Witek *et al*., *Oecologia* **148**, 729 (2006).
13. F. Wätzold, N. Lienhoop, M. Drechsler, J. Settele, *Ecol. Econ.* **68**, 295 (2008).
14. J. Settele *et al*., *BioRisk* **1**, 1-710 (2008); www.ufz.de/index.php?de=17472.
15. P. Nowicki *et al*., *Biol. Conserv.* **140**, 119 (2007).
16. C. Anton *et al*., *Mol. Ecol.* **16**, 3828 (2007).
17. O. Schweiger *et al*., *Ecology* **89**, 3472 (2008).
18. J. H. Spangenberg, *Sustainable Dev.* **15**, 343 (2007).

19. The authors were supported through the following EU-funded projects: MacMan (12; FP 5: EVK2-CT-2001-00126), ALARM (23; FP 6: GOCE-CT-2003-506675), SCALES (FP7 grant agreement no. 226852) and CLIMIT (Biodiversa funding scheme).

10.1126/science.1176892

APPLIED PHYSICS

Coherent Holes in a Semiconductor Quantum Dot

Michael H. Kolodrubetz and Jason R. Petta

Quantum states of positive charge carriers may be more stable to information loss than those of electron-based systems.

Building a quantum computer requires finding a system with long-lived coherence—one in which the wave function of a quantum state maintains its phase over time. In solid-state implementations of quantum information processing, coherent states can be generated with electron spins, and semiconductor quantum dots are powerful platforms for preparing, controlling, and measuring electron spin coherence (*1*). However, interactions between the electron spin and its environment destroy the fragile coherence (*2*) and lead to a loss of information. On page 70 of this issue, Brunner *et al*. (*3*) address this problem by using "holes"—positive charge carriers that result from unfilled states in an electronic band. They demonstrate that one measure of coherence, the inhomogeneous dephasing time of the hole spin, is at least an order of magnitude longer than that for electron spins.

Two main decoherence mechanisms operate in semiconductor quantum dots: The

Department of Physics, Princeton University, Princeton, NJ 08544, USA. E-mail: mkolodru@princeton.edu; petta@princeton.edu

spin-orbit interaction couples the spin to its motion in the crystal, and the hyperfine interaction couples the electron spin to the spins of nuclei of the host material. Practical manipulations of electron spins are feasible on a subnanosecond time scale, and spin-orbit interactions are weak enough in semiconductor quantum dots to allow long spin relaxation times that exceed 1 s (*1*, *4*). However, the hyperfine interaction is a different matter. In a typical quantum dot, the electron spin interacts with roughly 1 million nuclei and experiences an effective fluctuating magnetic field on the order of 2 mT (*5*). This field limits the time-ensemble averaged coherence time, T_2^*, to roughly 10 ns (*2*). Spin echo and nuclear polarization methods that suppress the effects of the nuclei can extend the coherence time to greater than 1 μs, but correcting for the deleterious effects of the nuclear spins adds an additional layer of complexity to already challenging experiments (*2*, *6*).

The hyperfine interaction has three contributions. One term couples the electron's orbital angular momentum to the nuclear spin, and a second dipole-dipole term couples the electron and nuclear spins at a distance. Typically, the largest interaction is the contact term, in which the classically forbidden overlap of the electronic wave function with the atomic nucleus leads to a large scalar interaction. Several alternative solutions to hyperfine-induced decoherence have been proposed. Among the most promising are to use host materials with spin-0 nuclei, or to work with p-type semiconductors in which holes are the charge and spin carriers. A dramatic reduction in the contact term is expected because the hole's wave function vanishes at the nucleus (see the figure, panel A).

Brunner *et al*. measured the coherence of a single hole spin confined in ~10-nm-diameter InGaAs quantum dots grown on a GaAs substrate. They control the number of holes trapped in one quantum dot by tuning a gate voltage such that charge carriers tunnel out of the dot and into the substrate until only one hole remains (*7*). A static magnetic field causes the hole states to undergo Zeeman splitting into a lower-energy spin-down level $|1\rangle$ and a higher-energy spin-up level $|2\rangle$. Lasers linearly polarized in the plane of the substrate (the *x* and *y* directions) can excite transitions from the hole spin states to the positively charged exciton level $|3\rangle$, which consists of two holes in a singlet state and a spin-up electron (see the figure, panel B).

Electron-spin coherence times are typically determined by measuring the time decay of Rabi oscillations (periodic cycling between two Zeeman-split spin states) or by performing spin echo measurements that refocus the spin back to its original state. Brunner *et al*. instead use coherent population trapping (CPT), which has been widely studied in three-level atomic systems (*8*, *9*), in part because this method does not require high-speed control of optical pulse amplitudes. Recently, CPT has been applied to solid-state systems, including electrons confined in quantum dots (*10*, *11*).

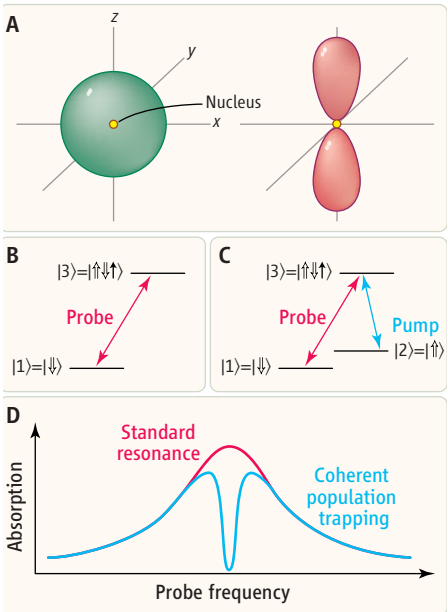

Measuring hole-spin coherence. (**A**) Electrons in a quantum dot occupy s-orbitals (left) and interact strongly with the nuclei. Holes form p-orbitals (right) that vanish at the positions of the nuclei and reduce the contact hyperfine interaction that causes decoherence. (**B** to **D**) Adding a second laser to an absorption spectroscopy experiment allows measurement of hole-spin coherence times. (B) In a two-level system, the spin-down ground state $|1\rangle$ is excited by a probe laser to state $|3\rangle$. (C) A second pump laser adds excitations from spin-up state $|2\rangle$ and creates a three-level system. (D) The two-level system results in an absorption peak at resonance (red). The three-level system is quickly trapped in a coherent dark state that is a superposition of states $|1\rangle$ and $|2\rangle$. The dark state does not interact with the lasers and results in a dip in absorption (blue) whose depth is determined by the hole-spin coherence time T_2^*.

In standard laser spectroscopy, two-energy-level systems are probed by measuring the laser absorption or transmission as a function of laser frequency. In the Brunner *et al*. experiment, temporarily ignoring state $|2\rangle$, the absorption of a *y*-polarized probe laser would peak around energies corresponding to the $|1\rangle$ to $|3\rangle$ transition (see the figure, panels B and D). The peak width is then set by the radiative lifetime of state $|3\rangle$.

In the CPT experiments, a pump laser is added to excite the $|2\rangle$ to $|3\rangle$ transition (see the figure, panel C). When the pump and probe lasers are tuned to energies that match their respective transitions, a coherent superposition of states $|1\rangle$ and $|2\rangle$ called the "dark state" is created rapidly once state $|3\rangle$ decays. The destructive interference of the two laser beams used for excitation prevents excitation of the dark state. Pumping of the bright superposition states into $|3\rangle$ followed by incoherent decay eventually drives the system into the dark state. As the probe laser is tuned through resonance, a dip in absorption profile results because the holes are quickly trapped in the dark state and cannot absorb light (see the figure, panel D).

The depth of the absorption dip is a sensitive measure of coherence (*12*); decoherence converts the dark state back to a bright emissive state and provides an observable limit of CPT. Because of the long measurement times, the measured hole spin coherence time is an ensemble-averaged or T_2^* value; averaging over many measurements limits the visibility of the destructive interference in the decay curves. Through rate equation modeling of the absorption dip, Brunner *et al*. find that T_2^* is almost certainly greater than 100 ns and has a 40% likelihood of exceeding 1 μs.

More investigation is required to determine what mechanism limits T_2^* and to determine the inherent coherence time T_2. Recent theoretical results suggest that dipole-dipole hyperfine interactions may still lead to appreciable decoherence (*13*). Even so, with $T_2^* \geq 100$ ns, hole spins remain coherent an order of magnitude longer than electron spins, indicating that nuclear interactions might indeed have a weaker effect on holes. The next step for quantum information processing will be to demonstrate time-resolved coherent control of an initially prepared hole spin state. Recent experiments demonstrating picosecond optical control of electron spin suggest that similar experiments on hole spins may be just around the corner (*14*).

References

1. R. Hanson *et al*., *Rev. Mod. Phys.* **79**, 1217 (2009).
2. J. R. Petta *et al*., *Science* **309**, 2180 (2005); published online 1 September 2005 (10.1126/science.1116955).
3. D. Brunner *et al*., *Science* **325**, 70 (2009).
4. S. Amasha *et al*., *Phys. Rev. Lett.* **100**, 046803 (2008).
5. A. V. Khaetskii *et al*., *Phys. Rev. Lett.* **88**, 186802 (2002).
6. D. J. Reilly *et al*., *Science* **321**, 817 (2008); published online 10 July 2008 (10.1126/science.1159221) .
7. B. D. Gerardot *et al*., *Nature* **451**, 441 (2008).
8. M. Fleischhauer *et al*., *Rev. Mod. Phys.* **77**, 633 (2005).
9. K. Bergmann *et al*., *Rev. Mod. Phys.* **70**, 1003 (1998).
10. K.-M. C. Fu *et al*., *Phys. Rev. Lett.* **95**, 187405 (2005).
11. X. Xu *et al*., *Nat. Phys.* **4**, 692 (2008).
12. A. Imamoglu, *Phys. Stat. Sol. B* **243**, 3725 (2006).
13. J. Fischer *et al*., *Phys. Rev. B* **78**, 155329 (2008).
14. D. Press *et al*., *Nature* **456**, 218 (2008).

10.1126/science.1176296

GEOCHEMISTRY

How Did Earth Accrete?

Isotope studies are providing clues to how Earth assembled and how its core formed.

Alex N. Halliday and Bernard J. Wood

How did Earth form, and what were the conditions on the early Earth? With the aid of mass spectrometry, high-pressure experiments, and computer modeling, researchers are beginning to decipher the signs left behind by our planet's early and violent beginning. Recent studies of the nature of core formation and the age of the Moon provide evidence that the first half of Earth's growth took less than 10 million years and was associated with reducing conditions. The final stages were more energetic and oxidizing and were probably not completed until ~100 million years, possibly after a substantial hiatus, in contrast to the continuous exponentially decreasing accretion that has long been assumed (see the figure).

Information on the very earliest times on our planet mainly comes from two sources. The first is Earth's division into silicate mantle and metal core, which is believed to have accompanied Earth accretion over the first ~100 million years. The concentrations and isotopic compositions of core-forming elements left behind in the silicate mantle provide a fingerprint of the conditions under which this separation occurred. The second source is the Moon, believed to have formed ~100 million years after the start of the solar system in a massive collision between Earth and another planetary precursor (*1*). This last episode of Earth's growth would have been accompanied by widespread melting and the final stage of core formation. The angular momentum and tidal effects generated by this "giant impact" must have played a key role in Earth's development.

Current thinking on Earth's early evolution is largely based on radiogenic isotope analyses, which—assuming simple mixing and metal segregation processes—provide key information on the rate at which Earth and its core formed. The validity of these assumptions has now been questioned. Dating the Moon provides an independent constraint on how quickly Earth formed, allowing the proposed core-formation mechanisms to be tested. The key issue is whether accretion was accompanied by (i) direct merging of incoming metal from preexisting planetary cores (see the figure, panel A) or (ii) continuous metal segregation from a hot magma ocean (*2*) (see the figure, panel B).

Radiogenic isotope variations are produced when metal-loving elements are redistributed within the Earth by core formation, changing the parent/daughter ratios. Carbonaceous chondrite meteorites have a composition similar to that of the Sun and hence to the solar system average. They are thus taken as representative of Earth's total composition. Comparison of the silicate Earth (total Earth minus core) to chondrites shows strong similarities in the relative abundances of refractory rock-loving elements. However, the mantle is depleted relative to chondrites in metal-loving elements (such as Ni, Co, W, and Pt), which entered the core.

Some of these metal-loving elements include daughters or parents of radioactive decay systems. Short-lived nuclides present at the start of the solar system produced changes in the atomic abundances of their daughter elements that are a function of time and of the parent-to-daughter element ratio. If this ratio is changed by core formation, the isotopic composition of the daughter element also changes over time. The ^{107}Pd-^{107}Ag system (half-life 6.5 million years) first showed that iron meteorites formed early (*3*). The ^{182}Hf-^{182}W system (half-life 9 million years), for which the parent Hf enters silicate and the daughter W enters metal, constrained these time scales for small asteroidal objects to within a million years of the start of the solar system (*4*).

Thus, accretion and core formation started within a million years. This insight provides support for continuous core formation. In this model, which was first proposed to quantify accretion time scales using W isotopes (*5*) (see the figure), the core grows in proportion to the growth of the planet. As more material is added to Earth, it mixes with the mantle and then segregates further core-forming metal. Assuming exponentially decreasing growth and equilibrium core formation, the ^{182}Hf-^{182}W chronometer indicates that Earth accretion was completed within 30 million years, culminating in the Moon-forming giant impact (*6*).

The dynamics of material addition to Earth is poorly understood, however. Simulations suggest that some incoming metal mixed directly with the core (see the figure, panel A) instead of first mixing with the silicate Earth mantle. However, such computer simulations (*1*) do not have the resolution needed to evaluate the detailed fluid dynamics of Earth accretion, and the energetics of the impact would be expected to provide at least localized Rayleigh-Taylor instabilities and dispersed droplets of metallic liquid in silicate liquid, leading to equilibrium

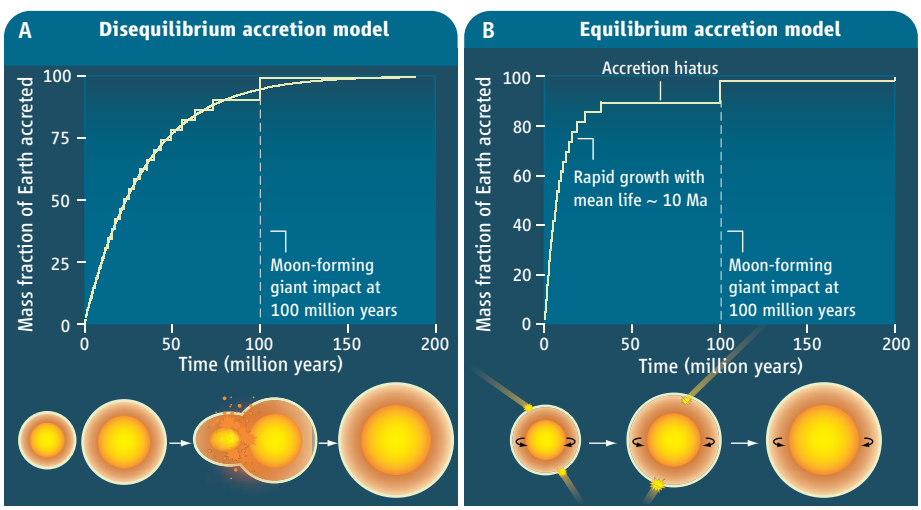

Earth's first 100 million years. Earth grew mainly from a series of accretion events (*15*) broadly comparable in scale to the giant impact, which formed the Moon ~100 million years after the start of the solar system (*8*, *10*). In disequilibrium accretion (**A**), the giant impact added metal directly to the core. In equilibrium accretion (**B**), metal segregated from silicate in a magma ocean. The concentrations of metal-loving elements left in the silicate Earth after core formation are better explained by scenario (B) (*12*). However, W isotope data then imply that accretion and core formation were mainly rapid, possibly with a substantial hiatus before the giant impact.

CREDIT: P. HUEY/*SCIENCE*

Department of Earth Sciences, University of Oxford, Parks Road Oxford, OX1 3PR, UK. E-mail: alex.halliday@earth.ox.ac.uk

Published by AAAS

accretion (see the figure, panel B) (*7*).

The age of the Moon provides an additional constraint that can be brought to bear on this issue. The W isotopic composition of the Moon (*8*) provides evidence that it formed more than 45 million years after the start of the solar system in an event that appears to have isotopically equilibrated the protolunar disk with the silicate Earth, as predicted for the giant impact (*9*). The best current estimate for the age of this event is 70 to 110 million years after the origin of the solar system (*10*). Knowing this age, we can use Earth's W isotopic composition (*6*) to simulate how it accreted before the giant impact (*10*) (see the figure). The two models in the figure both generate the correct W isotopic composition for the silicate Earth, with a giant impact at about 100 million years. The differences are in the degree of equilibration between incoming metal with the silicate Earth prior to further core growth. In panel A, 60% of the incoming metal is added directly to the core. In panel B, all incoming metal first equilibrates with the mantle, with no direct mixing. The implications for the rates of accretion before the giant impact are severe.

Of course, these are simple models, and the truth may lie somewhere in between. Fortunately, experiments provide additional constraints. As Earth grew, internal pressures and temperatures rose, affecting the degree to which key trace elements are partitioned into the core. If newly accreted material did not reequilibrate under the higher pressures of the growing Earth prior to segregating further metal, then the concentrations of these trace elements would reflect low-pressure core formation. It has long been known (*11*) that the mantle depletions in Ni and Co cannot be explained by core-mantle equilibrium experiments at low pressures. High pressure–high temperature data show (*12*) that the Ni and Co contents of the mantle can be reproduced if the core was separated at pressures of more than 30 GPa, whereas the mantle depletions of weakly metal-loving elements such as V and Cr require temperatures of more than 3000 K. The composition of the mantle thus largely results from protracted metal-silicate reequilibration deep within a large, hot, growing planet.

The appropriate accretion scenario should then involve little or no direct mixing of metallic core material during growth (see the figure, panel B). If this scenario was maintained throughout Earth's growth, most accretion would have occurred in the first 10 million years, with little further growth until the giant impact (*10*). These experimental partitioning data do not fit with the traditional view that Earth accreted at an exponentially decreasing rate (*5*, *10*, *13*).

The degree to which one can apply reasoning based on high-pressure partitioning data to the first half of Earth's accretion and equilibration history is limited, because the mantle composition is dominated by the effects of more recent growth and core segregation. Nevertheless, some trace elements, particularly V, provide evidence that early Earth accretion must have proceeded during far more reducing conditions than exist today. Models of continuous equilibrium core formation (*2*) reproduce the mantle concentrations of several refractory iron-loving elements (Ni, Co, W, V, Cr, Nb), provided that the pressure and temperature of metal segregation reached 40 GPa and 3150 K, but only if Earth started as a small reduced body that became oxidized during accretion.

Recently, a new approach has been proposed for determining which elements are present in the core and what this means for Earth's early evolution. Theory, experiments, and meteorite measurements suggest that isotopes can be fractionated even at high temperatures as a result of bonding differences between silicate and metallic liquids (*14*). Therefore, comparisons of the silicate Earth and meteorites from smaller solar system objects that did not form cores may resolve isotopic differences. Suitably calibrated, these data could provide powerful constraints on the temperature, pressure, and conditions of core formation.

References

1. R. M. Canup, *Philos. Trans. R. Soc. London Ser. A* **366**, 4061 (2008).
2. B. J. Wood, *Philos. Trans. R. Soc. A* **366**, 4339 (2008).
3. J. H. Chen, G. J. Wasserburg, *Geochim. Cosmochim. Acta* **54**, 1729 (1990).
4. A. Markowski *et al.*, *Earth Planet. Sci. Lett.* **242**, 1 (2006).
5. C. L. Harper, S. B. Jacobsen, *Geochim. Cosmochim. Acta* **60**, 1131 (1996).
6. Q. Yin *et al.*, *Nature* **418**, 949 (2002).
7. D. C. Rubie *et al.*, *Earth Planet. Sci. Lett.* **205**, 239 (2003).
8. M. Touboul *et al.*, *Nature* **450**, 1206 (2007).
9. K. Pahlevan, D. J. Stevenson, *Earth Planet. Sci. Lett.* **262**, 438 (2007).
10. A. N. Halliday, *Philos. Trans. R. Soc. London Ser. A* **366**, 4163 (2008).
11. A. E. Ringwood, *Geochim. Cosmochim. Acta* **30**, 41 (1966).
12. Ph. Kegler *et al.*, *Earth Planet. Sci. Lett.* **268**, 28 (2008).
13. G. W. Wetherill, in *Origin of the Moon*, W. K. Hartmann, R. J. Phillips, G. J. Taylor, Eds. (Lunar Planetary Institute, Houston, 1986), pp. 519–550.
14. V. B. Polyakov, *Science* **323**, 912 (2009).
15. M. Ogihara, S. Ida, A. Morbidelli, *Icarus* **188**, 522 (2007).

10.1126/science.1172587

TRANSCRIPTION

Sweet Silencing

A sugar molecule plays an unexpected role in controlling gene silencing by modifying repressor proteins.

Jeffrey A. Simon

Knowledge about protein modifications in gene regulation is rapidly expanding. The various modifications of histones (proteins associated with DNA) alone, including myriad phosphorylations, acetylations, methylations, and ubiquitylations, occur at more than 25 different locations on a nucleosome (the compact structure of histones and DNA that comprise chromatin). That doesn't include the many covalent modifications on nonhistone transcription factors, which can also be phosphorylated, acetylated, or methylated. By contrast, modification by sugar molecules might appear less relevant to regulating chromatin. Most sugar-conjugated proteins accumulate in domains at the cell surface or intracellular membrane compartments, far from the hub of gene transcription activity in the nucleus. A notable exception is modification by O-linked *N*-acetylglucosamine (O-GlcNAc) on serine and threonine residues of cytoplasmic and nuclear proteins (*1*). On page 93 in this issue, Gambetta *et al.* (*2*) reveal a key role for O-GlcNAc glycosylation in gene silencing by Polycomb group (PcG) proteins.

PcG proteins are highly conserved chromatin regulators with central roles in multicellular development and stem cell biology (*3*, *4*). They provide a key model for deciphering mechanisms that silence gene expression in organisms from flies to humans. There are about 15 PcG proteins that sort into several complexes that repress target genes. Three main PcG complexes, called Polycomb repressive complex 1 (PRC1), Polycomb repressive complex 2 (PRC2), and PHO repressive complex (PHO-RC), are well characterized. PHO-RC has DNA binding activity that helps select genomic targets for silencing, and PRC2 methylates histone H3 on lysine-27 (K27), a hallmark of PcG-silenced loci. Several functions have been attributed to PRC1 complexes, including ubiquitylation of

Department of Genetics, Cell Biology and Development, University of Minnesota, Minneapolis, MN 55455, USA. E-mail: simon004@umn.edu

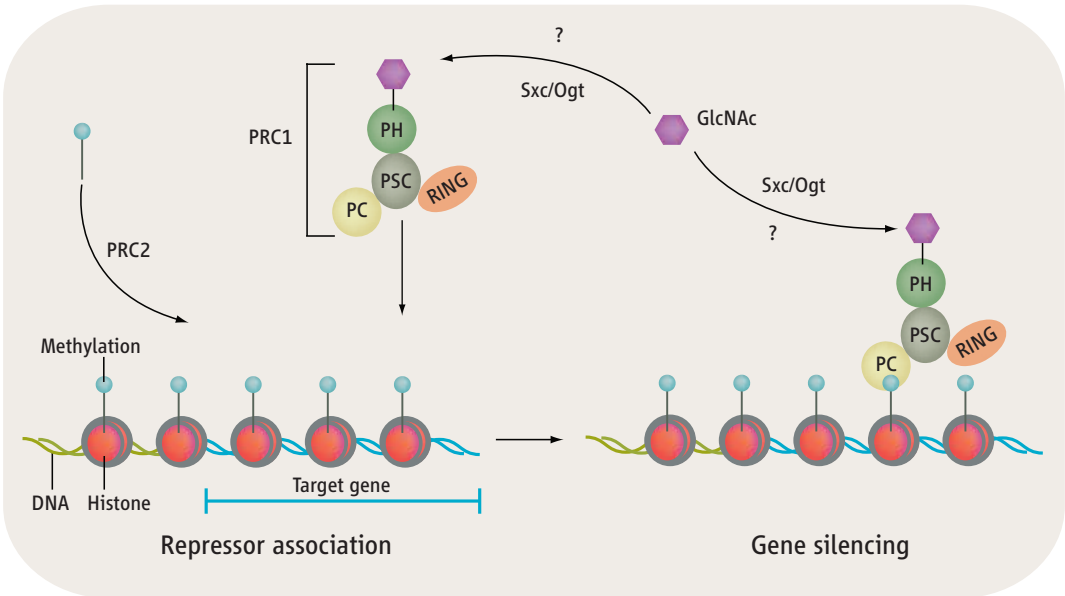

Adding sugar. The model depicts PRC1 associating with a chromatin target and bearing the molecule GlcNAc on the PH subunit. PRC1 interaction with nucleosomes is aided by binding of the PC subunit to methylated histones (trimethyl-H3-K27). Glycosylation of PH is required to silence gene expression, but it is not clear when this modification occurs.

histone H2A (*5*) and compaction of polynucleosomes (*6*). How these and other discrete functions integrate into stepwise mechanisms that ultimately impede gene transcription remains to be determined.

Some 25 years ago, the *super sex combs* (*sxc*) gene in the fly *Drosophila melanogaster* was identified as a PcG repressor (*7*). Specifically, *sxc* mutations impaired the silencing of *Hox* genes, leading to defects in anterior-posterior patterning. However, the molecular identity of *sxc* has remained a mystery. Gambetta *et al*. reveal that *sxc* encodes O-linked *N*-acetylglucosamine transferase (Ogt), the single fly enzyme that catalyzes attachment of the sugar molecule GlcNAc to proteins. Several *sxc* mutations encode proteins with disrupted catalytic domains; although these were produced in normal amounts, they were not functional, thereby implying that glycosyltransferase activity functions in PcG silencing. Furthermore, Gambetta *et al*. show that GlcNAc distribution in chromatin is highly coincident with PcG complexes at target genes.

GlcNAc could help recruit or bind PcG complexes to target loci. Alternatively, it could affect silencing by PcG complexes after their arrival at genomic targets (see the figure). Evidence supports the latter: Chromatin immunoprecipitation analyses of *sxc* mutant tissue show that all three PcG complexes remain attached at targets despite loss of GlcNAc. Only a slight (1.5- to 2-fold) reduction in PRC1 association with chromatin is detected, and nuclear localization of PRC1 appears unaffected. Thus, there is little evidence that GlcNAc affects PcG complex association with chromatin. Instead, a potentially more direct GlcNAc role in gene silencing is favored. Moreover, Gambetta *et al*. determined that of the PcG proteins tested, only PH is modified by GlcNAc.

PH is a core subunit of PRC1, along with PC, PSC, and RING subunits. The precise mechanism of PRC1 gene silencing is not understood: RING and PSC are implicated in histone H2A ubiquitylation (*8*, *9*), which may impact transcription elongation (*10*); PSC is most central to polynucleosome compaction (*6*); and PC binds methylated H3-K27 (*11*), which likely affects PRC1 association with chromatin. By contrast, PH has the least defined role. Thus, determining the effect of GlcNAc modification on PRC1 may first require deciphering the role of PH in PRC1 function. Notably, PH retains partial transcriptional repressor function even in the absence of GlcNAc modification. This is implied by the phenotype of fly embryos lacking *sxc*, which is milder than that seen with mutations in *ph*.

Because modification by GlcNAc involves a dynamic process of enzymatic attachment and removal, potential roles for regulating chromatin by an enzyme that removes O-GlcNAc should also be assessed. Also, there may be additional Ogt substrates, besides PH, that function in PcG silencing. It also is unclear whether GlcNAc modification has major roles in *Drosophila* other than PcG-mediated gene silencing, as flies lacking *sxc* do not show defects beyond those attributable to PcG loss.

Substrate specificity presents an intriguing evolutionary issue, with distinct pathways affected by GlcNAc loss in different organisms. For example, worms lacking GlcNAc develop normally but show altered formation of the hibernation-like dauer state (*12*); plants lacking GlcNAc display defects in response to the hormone gibberellin (*13*); and mouse embryonic stem cells are inviable without GlcNAc (*14*). Another potential divergence is that mammalian cells accumulate GlcNAc on the critical carboxyl-terminal domain of RNA polymerase II (*15*), whereas attachment of GlcNAc to polymerase II was not observed by Gambetta *et al*. in *Drosophila*. Conversely, GlcNAc function may be conserved in PcG silencing; mass spectrometric analysis of mouse brain tissue identified a PH homolog (Polyhomeotic-like protein 3) among the GlcNAc-modified proteins (*16*). Thus, certain key GlcNAc targets may well be conserved from flies to mammals. And in an era where discovery is increasingly driven by high-throughput approaches, the lesson remains that careful attention to old fly mutants continues to pay dividends.

References

1. G. W. Hart, M. P. Housley, C. Slawson, *Nature* **446**, 1017 (2007).
2. M. C. Gambetta, K. Oktaba, J. Müller, *Science*, **325**, 93 (2009); published online 28 May 2009 (10.1126/science.1169727).
3. Y. B. Schwartz, V. Pirrotta, *Nat. Rev. Genet.* **8**, 9 (2007).
4. J. Muller, P. Verrijzer, *Curr. Opin. Genet. Dev.* **19**, 150 (2009).
5. H. Wang *et al*., *Nature* **431**, 873 (2004).
6. N. J. Francis, R. E. Kingston, C. L. Woodcock, *Science* **306**, 1574 (2004).
7. P. W. Ingham, *Cell* **37**, 815 (1984).
8. R. Cao, Y. Tsukada, Y. Zhang, *Mol. Cell* **20**, 845 (2005).
9. A. Lagarou *et al*., *Genes Dev.* **22**, 2799 (2008).
10. J. K. Stock *et al*., *Nat. Cell Biol.* **9**, 1428 (2007).
11. W. Fischle *et al*., *Genes Dev.* **17**, 1870 (2003).
12. J. A. Hanover *et al*., *Proc. Natl. Acad. Sci. U.S.A.* **102**, 11266 (2005).
13. L. M. Hartweck, R. K. Genger, W. M. Grey, N. E. Olszewski, *J. Exp. Bot.* **57**, 865 (2006).
14. R. Shafi *et al*., *Proc. Natl. Acad. Sci. U.S.A.* **97**, 5735 (2000).
15. W. G. Kelly, M. E. Dahmus, G. W. Hart, *J. Biol. Chem.* **268**, 10416 (1993).
16. R. J. Chalkley, A. Thalhammer, R. Schoepfer, A. L. Burlingame, *Proc. Natl. Acad. Sci. U.S.A.* **106**, 8894 (2009).

10.1126/science.1177264

OCEANS

Predicting El Niño's Impacts

Insights into El Niño's spatial structure may help to predict its effect on Atlantic tropical cyclones.

Greg J. Holland

The quasi-periodic cycle of warming and cooling in the eastern, near-equatorial Pacific Ocean known as the El Niño Southern Oscillation (ENSO) is associated with marked ocean temperature changes in the tropics and with long-range weather connections across the globe. In western South America, the cool phase (La Niña) brings dry conditions and excellent fishing in the nutrient-rich upwelling water, whereas the warm phase (El Niño) leads to floods and cutbacks in the fishing industry (*1*). But the notoriety of ENSO lies in its impact on seasonal weather around the globe, from droughts in Australia, to changes in the Indian summer monsoon and global tropical cyclone activity. In a landmark report on page 77 of this issue (*2*), Kim *et al*. revisit the structure of ENSO. The study has important consequences for the predictability of global weather patterns.

The global impact of ENSO was first documented in the early 20th century by Sir Gilbert Walker, the director general of the Government Observatories in India, who noted a strong relationship between the surface air pressure gradient across the Pacific Ocean and Indian summer monsoon activity. He coined the term "Southern Oscillation" to describe the reversals in pressure gradient between Tahiti and Darwin. In a seminal paper, Bjerknes showed in 1969 that ENSO changes are communicated via long-range weather connections (teleconnections) to substantially affect regional climate around the globe (*3*). Widespread impacts of the particularly severe 1982/1983 El Niño focused attention on ENSO and led to the Tropical Ocean Global Atmosphere (TOGA) program, which helped to elucidate the physical mechanism that underlies ENSO and to develop ways of predicting its evolution.

ENSO teleconnections are now known to have substantial societal impacts, including food shortages and changes in insect-borne diseases (*4*). One of the stronger ENSO teleconnections is with global tropical cyclone activity in the North Atlantic Ocean (*5*). Here, ENSO drives large-scale atmospheric circulation changes that dominate the interannual variations in local tropical cyclone activity; activity is enhanced during cold La Niña events and reduced during warm El Niño events. This strong signal has led to extensive efforts to predict seasonal tropical cyclone activity in the North Atlantic and North Pacific, first with purely statistical methods (*6*) and more recently with coupled general circulation models (*7*).

Unfortunately, all such seasonal predictions are limited by a fundamental "predictability barrier" (*8*). ENSO resembles a nonlinear oscillator with two relatively stable attractors. In its cold and its warm phase, ENSO is highly predictable for several months ahead. However, as the ENSO moves closer to the transition zone between the phases, it may move in either direction, leading to considerable loss of predictive skill. Because the ENSO transition period is approximately phase-locked to the annual cycle, this predictability barrier typically occurs in the April-May period. Thus, tropical cyclone forecasts made before June have essentially no predictive skill when compared to a trivial ("no-skill") benchmark, such as using the mean activity of the previous 5 years. This barrier affects the usefulness of ENSO predictions; for example, the insurance-reinsurance industry has already locked in annual rates before April-May.

Kim *et al*. now show that seasonal predictability of Atlantic tropical cyclones may be improved by breaking the warm El Niño phase into two independent modes: an eastern Pacific warming (EPW) and a central Pacific warming (CPW). The EPW is indistinguishable from the classical El Niño, but the CPW is quite different, with warming concentrated in the central Pacific and essentially no warming found farther east. (The CPW is not really an El Niño, but has most likely been mistaken for El Niño in the past.) Of considerable interest is the finding that North Atlantic tropical cyclone activity rises during CPW to a level similar to that seen during La Niña—quite the opposite of the conventional understanding of El Niño. The CPW also appears to have a high level of predictability well before the April-May barrier.

Separating these two warm modes may thus lead to a useful improvement in seasonal Atlantic tropical cyclone prediction of Atlantic tropical cyclones (see the figure). The study by Kim *et al*. also raises wider issues. Can the development of a CPW preempt development of a full El Niño? Is the recent increase in frequency of CPW events—with 80% of those since 1950 occurring since 1990—associated with natural variability or with the appearance of a global warming signal? As global climate models improve to the point that they can simulate realistic ENSO variations, understanding the interactions between CPW and EPW and their relative importance to global weather teleconnections will help to further refine our capacity to predict the consequences of this critical coupled atmosphere-ocean phenomenon.

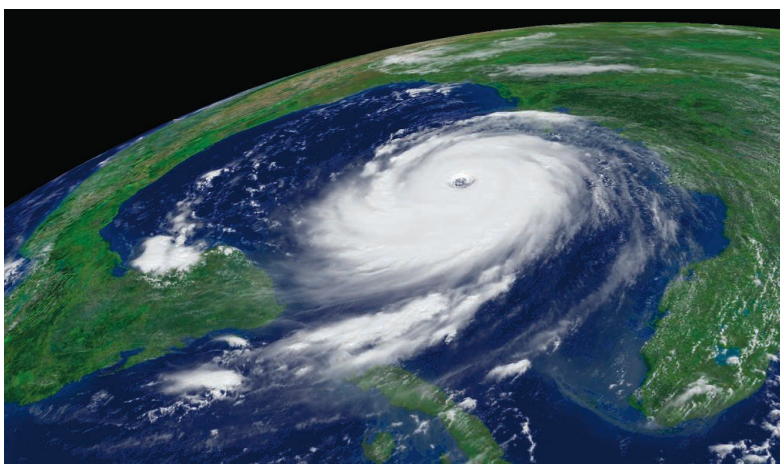

CREDIT: NOAA

Heading for destruction. This GOES-12 satellite image shows Hurricane Katrina on 28 August 2005, when the storm was at Category 5 strength and projected to impact New Orleans. Although 2005 was not an El Niño year, better understanding of ENSO will help to predict the frequency of such cyclones.

National Center for Atmospheric Research (NCAR), 1850 Table Mesa Drive, Boulder, CO 80305, USA. E-mail: gholland@ucar.edu

References and Notes

1. J. Tarazona, W. Arntz, E. Castillo, Eds., *El Niño in Latin America: Biological and Social Impacts* (Alfred Wegener Institute, Kiel, Germany, 2001).
2. H.-M. Kim, P. J. Webster, J. A. Curry, *Science* **325**, 77 (2009).
3. J. Bjerknes, *Mon. Weather Rev.* **97**, 163 (1969).
4. www.who.int/mediacentre/factsheets/fs192/en/index.html
5. W. M. Gray, *Mon. Weather Rev.* **112**, 1649 (1984).
6. W. M. Gray, *Mon. Weather Rev.* **112**, 1669 (1984).
7. F. Vitart *et al*., *Geophys. Res. Lett.* **34**, L16815 (2007).
8. P. J. Webster, S. Yang, *Q. J. R. Meteorol. Soc.* **118**, 877 (1992).
9. NCAR is funded by the NSF.

10.1126/science.1176515

How to Think, Say, or Do Precisely the Worst Thing for Any Occasion

Daniel M. Wegner

In slapstick comedy, the worst thing that could happen usually does: The person with a sore toe manages to stub it, sometimes twice. Such errors also arise in daily life, and research traces the tendency to do precisely the worst thing to ironic processes of mental control. These monitoring processes keep us watchful for errors of thought, speech, and action and enable us to avoid the worst thing in most situations, but they also increase the likelihood of such errors when we attempt to exert control under mental load (stress, time pressure, or distraction). Ironic errors in attention and memory occur with identifiable brain activity and prompt recurrent unwanted thoughts; attraction to forbidden desires; expression of objectionable social prejudices; production of movement errors; and rebounds of negative experiences such as anxiety, pain, and depression. Such ironies can be overcome when effective control strategies are deployed and mental load is minimized.

There are many kinds of errors. We can fall short, overreach, or skitter off the edge, of course, but we can also miss by a mile, take our eyes off the prize, throw the baby out with the bath water—and otherwise foul up in a disturbingly wide variety of ways. Standing out in this assortment of would-be wreckage, though, is one kind of error that is special: the precisely counterintentional error. This is when we manage to do the worst possible thing, the blunder so outrageous that we think about it in advance and resolve not to let that happen.

And then it does. We see a rut coming up in the road ahead and proceed to steer our bike right into it. We make a mental note not to mention a sore point in conversation and then cringe in horror as we blurt out exactly that thing. We carefully cradle the glass of red wine as we cross the room, all the while thinking "don't spill," and then juggle it onto the carpet under the gaze of our host. Normally, our vigilance for such pitfalls helps us avoid them. We steer away from ruts, squelch improper comments, and protect carpets from spills by virtue of our sensitivity to error. Knowing the worst that could happen is essential for control. But sometimes this sensitivity backfires, becoming part of a perverse psychological process that makes the worst occur.

Observers of human psychology have suggested that the mind can indeed generate just such ironic errors. Edgar Allan Poe called this unfortunate feature of mind the "imp of the perverse" (*1*). Sigmund Freud dubbed it the "counter will" (*2*). William James said too that "automatic activity in the nerves often runs most counter to the selective pressure of consciousness" (*3*). Charles Baudouin pronounced it the "law of reversed effort" (*4*), and Charles Darwin joined in to proclaim "How unconsciously many habitual actions are performed, indeed not rarely in direct opposition to our conscious will!" (*5*). Hieronymus Bosch illustrated this human preoccupation with the worst, depicting a world in which error, sin, and ruin are the usual consequence of human endeavor (Fig. 1).

Fig. 1. This detail from *The Last Judgment* by Hieronymus Bosch illustrates the artist's apocalyptic vision of some of the worst that humans can think, say, or do.

Department of Psychology, Harvard University, 33 Kirkland Street, Cambridge, MA 02138, USA. E-mail: wegner@wjh.harvard.edu

Intentions and Ironies: Best and Worst

Do we do the worst thing more often than other things? Fortunately for the proprietors of china shops, we do not. However, accumulating evidence on ironic processes of mental control (*6*) reveals conditions under which people commit precisely counterintentional errors. The prototypical error of this kind occurs when people are asked to keep a thought out of mind (e.g., "don't think about a white bear"). The thought often comes back. When asked to signal any return of that thought, people may indicate that it comes back about once per minute (*7*)—often to echo for yet longer periods (*8*) and, at the extreme, to return for days (*9*, *10*). Some people are better at such thought suppression than others (*11*, *12*), of course, and some try more than others (*13*), but keeping a thought out of mind remains a challenge for most of us even when we have only arbitrarily tried to suppress it.

Why would thought suppression be so hard? It does seem paradoxical: We try to put out of mind what we are thinking now, while still remembering at some level not to think of it later. The ironic process theory (*6*) suggests that we achieve this trick through two mental processes: The first is a conscious, effortful process aimed at creating the desired mental state. The person engaged in suppressing white bear thoughts, for example, might peruse the room or otherwise cast about for something, anything, that is not a white bear. Filling the mind with other things, after all, achieves "not thinking of a white bear."

As these distracters enter consciousness, though, a small part of the mind remains strangely alert to the white bear, searching for indications of this thought in service of ushering it away with more distractions. Ironic process theory proposes that this second component of suppression is an ironic monitoring process, an unconscious search for the very mental state that is unwanted. The conscious search for distractions and the unconscious search for the unwanted thought work together to achieve suppression—the conscious search doing the work and the unconscious search checking for errors.

The control system underlying conscious mental control is unique, however, in that its monitoring process can also produce errors. When distractions, stressors, or other mental loads interfere with conscious attempts at self-distraction, they leave unchecked the ironic monitor to sensitize us to exactly what we do not want. This is not a passive monitor, like those often assumed in control system theories, but rather is an active unconscious search for errors that subtly and consistently increases their likelihood via processes of cognitive priming (*14*). For example, when people are asked not to think about a target word while under pressure to respond quickly in a word association task, they become inclined to offer precisely that forbidden target word (*15*). Indeed, with time pressure people more often blurt out a word while suppressing it than when they are specifically asked to concentrate on it.

Fortunately, the ironic return of suppressed thoughts is not inevitable, or we would be plagued by every thought we had ever tried to put out of mind. We can stop thinking of things quite successfully when we have time to devote to the project and become absorbed in our self-distractions. The ironic rebound of suppressed thoughts after suppression is mainly evident when people abandon the attempt to suppress or are encouraged to revisit the suppressed thought (*16*, *17*). The ironic return of suppressed thoughts during suppression is found only sporadically when people are simply reporting their thoughts but is readily observed with measures of thought that are sensitive to automatic, uncontrollable indications of the thought (*18*).

For example, when people are asked to name the colors in which words are displayed and encounter a word they have been asked not to think about, they name the word's color more slowly—apparently because their attention is rapidly drawn to the word's meaning and so interferes with color-naming (*15*, *19*). Such automatic attention to suppressed thoughts surfaces in color-naming when people are under mental load (such as holding a five-digit number in mind) and can be found as an effect of load in many paradigms (*20*, *21*). Color-naming research reveals, though, that ironic monitoring processes are not limited only to suppression; they also occur during intentional concentration. People intentionally concentrating on particular words under load show slowed color-naming for words that are not concentration targets because these nontargets now pop more easily to mind (*19*). Perhaps this is why concentrating under pressure, such as during last-minute studying, seems to accentuate the clarity of every stray noise within earshot.

The ironic monitoring process also influences memory. Memories we try to forget can be more easily remembered because of the ironic results of our efforts, but they do this mainly when mental loads undermine conscious attempts to avoid the memories (*22*, *23*). People attempting to forget many items at once can do so with some success (*24*, *25*), perhaps because monitoring multiple control projects dilutes ironic monitoring effects (*26*). Functional magnetic resonance imaging studies show a similar disparity in brain activity: People trying to forget many targets show a suite of changes in brain activity associated with forgetting (*27*), whereas those trying not to think of a single target show specific monitoring-related activity of the anterior cingulate and dorsolateral prefrontal cortex (*28*, *29*). The brain regions subserving ironic and intentional processes are differentiable when people do targeted mental control tasks.

Taboos and Faux Pas: Worst Thoughts and Utterances

Ironic lapses of mental control often appear when we attempt to be socially desirable, as when we try to keep our minds out of the gutter. People instructed to stop thinking of sex, for example, show greater arousal (as gauged by finger skin conductance) than do those asked to stop thinking about a neutral topic. Indeed, levels of arousal are inflated during the suppression of sex thoughts to the same degree that they inflate during attempts to concentrate on such thoughts (*8*). In research on sexual arousal per se, male participants instructed to inhibit erections as they watched erotic films found it harder than they had hoped, so to speak—particularly if they imbibed a mental load in the form of a couple of alcoholic drinks (*30*). Ironic effects also may underlie the tendency of homophobic males to show exaggerated sexual arousal to homoerotic pictures (*31*).

The causal role of forbidden desires in ironic effects is clear in experimental research on the effects of imposed secrecy (*32*). People randomly paired to play "footsie" under the table in a laboratory study reported greater subsequent attraction to their assigned partner when they had been asked to keep their contact secret from others at the table, and survey respondents revealed similar effects of tainted love: a greater desire for past romantic partners with whom relationships had first started in secret (*33*). This desire seems to arise as an ironic emotional effect of suppression: People who are asked not to think about a specific old flame show greater psychophysiological arousal than do others when later allowed to think about that relationship (*34*).

Like forbidden romance, other occasions for social deception are a fertile source of ironic effects. People admonished to keep an item private in conversation, for example, become more likely to mention it; speakers asked to keep a target hidden from an addressee more often leaked its identity by making inadvertent reference to it—for example, describing the target in Fig. 2 as a "small triangle" and thereby revealing that the occluded object was a larger one (*35*). Interviewees with eating disorders who role-played not having a disorder for the interviewer also showed ironic effects. During the interview, they reported intrusive thoughts of eating and revealed preoccupation with the topic by rating the interviewer, too, as the likely victim of an eating disorder (*36*).

Another challenge for mental control is keeping a lid on our social prejudices. There is substantial evidence that racism, sexism, homophobia, and other prejudices can be expressed automatically after all, even when we try to control them (*37*, *38*). But the ironic process theory holds that unconscious urges to express such prejudices will be especially insistent when we try to control them under load. This possibility was initially documented in research that asked British participants to suppress their stereotypes of skinheads (white supremacists) and found that such stereotypes then rebounded—even leading experimental participants to sit far away from a skinhead in a waiting room (*39*). Ironic effects have since surfaced showing that expressions of prejudice against racial, ethnic, national, and gender groups are often prompted by attempts to be "politically correct" under mental load (*40*–*42*). The desire to be fair and unprejudiced, exercised in haste or distraction, can engender surprising levels of bias and prejudice.

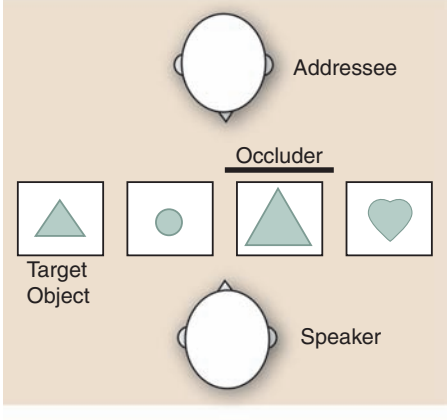

Fig. 2. Speaker who is asked to describe the mutually visible target becomes more likely to mention a clue to the hidden target that is irrelevant to the addressee (e.g., saying "small triangle" rather than "triangle") when instructed to conceal the identity of the target from the addressee. [Adapted from (*35*)]

Yips and Worries: Worst Movements and Emotions

Pressures to avoid the worst are not always a matter of doing what is socially desirable—they can arise in attempts to achieve self-imposed goals as well. The desire to succeed at a task defines the worst thing that could happen in that situation as failure at this task. So, when people grasp a string with a weight attached and try to keep this pendulum from swinging in one direction, they often find that the pendulum swings in just the way they hope to avoid (*43*). And, as predicted by ironic process theory, the pendulum is even more likely to swing in the unwanted direction when its holder is distracted by counting backward from 1000 by threes (Fig. 3).

Sports psychologists and coaches are familiar with ironic movement errors, counterintentional movements induced by the very desire to prevent them. Former major league baseball players Chuck Knoblauch, Steve Blass, and Rick Ankiel were famed for sporadic wild throws as well as for the desire to avoid them, Ankiel even calling his chronic error "the Creature" (*44*). In golf putting, the ironic tendency has a name (the "yips"), and golfers who are instructed to avoid a particular error (e.g., "don't overshoot") indeed make it more often when under load (*43*, *45*). Eye-tracking cameras reveal that soccer players who are instructed to avoid kicking a penalty shot to a particular part of the goal more often direct their gaze to the very area to be avoided (*46*). Perhaps the common sensation we get as we look over a precipice—that we are teetering toward the edge—is an accurate perception of our subtle ironic movements. (It may be best when poised at the brink, by the way, not to count backward from 1000 by threes.)

Worries and fears are also fertile ground for ironic effects. Unwanted emotions associated with thoughts not only provide a reason to avoid those thoughts but also prompt an unwanted emotional punch when the thoughts return. Emotions we put out of mind are experienced with unusual intensity when the emotional thoughts recur after suppression (*19*, *34*, *47*). Depressed mood is especially recalcitrant, recurring after suppression when reminders, negative events, or increased mental loads are encountered (*48*). And when anxious thoughts are suppressed under mental load, their return can rekindle anxiety with particular vigor (*49*).

Worry about falling asleep yields similar ironic effects: People urged to fall asleep as quickly as possible, but who are also given a mental load (in the form of Sousa march music), are particularly likely then to have trouble sleeping (*50*). The common observation that dreams center on unpleasant and emotionally disturbing topics makes

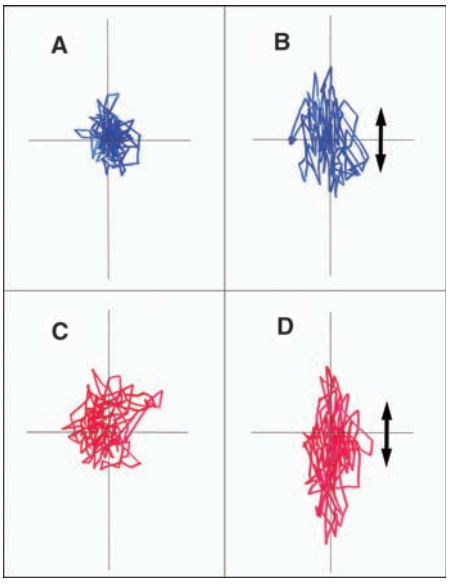

Fig. 3. Sample tracings of 30-s videos from below a handheld pendulum on a string when pendulum holder is asked to (**A**) hold it steady, (**B**) keep it from swinging parallel to the arrow, (**C**) hold it steady while counting backward from 1000 by threes, or (**D**) keep it from swinging parallel to the arrow while counting backward from 1000 by threes. [Figure based on data from (*43*).]

sense in this light: When people are instructed to suppress thoughts of neutral or emotional topics before sleep, they report more frequent dreaming about those topics (*51*–*53*). If we spontaneously choose to avoid unpleasant or worrisome thoughts in daytime, it makes sense that such thoughts would then populate our dreams.

Puzzling ironies arise too in response to pain. Usually, people exposed to painful stimulation report higher levels of felt pain when they direct their attention toward the pain. However, suppression of laboratory-induced pain can result in some ironic effects, including ironic increments in suppressed pain and ironic decrements in attended pain (*54*–*56*). Such effects are unreliable and have not been examined under variations in mental load, so conclusions are not yet clear (*57*, *58*). Caution should also be exercised in considering ironic effects of thinking about death. People suppress thoughts of death spontaneously or use strategies other than direct suppression, so ironic effects of suppressing thoughts of one's own death are not always evident (*59*). Research on such effects is complicated when natural attempts people make to gain mental control obscure the effects of experimental manipulations of control striving.

Putting the Worst Behind Us

The ubiquity of ironic effects suggests we should consider it something of a treat when we control ourselves successfully. According to ironic process theory, however, successful control is likely to be far more prevalent than ironic error because people often use effective strategies for control and deploy them under conditions that are not mentally loading. Ironic effects are often small, and the experimental production of ironic errors often depends on the introduction of artificial loads, time pressures, or other means of magnifying ironic effects. Even such amplifiers of ironic error may be overcome, however, in certain individuals with talents for mental control. People who are susceptible to hypnotic suggestion, for example, and who are given suggestions to control thoughts show heightened mental control without ironic effects (*60*, *61*).

The rest of us, however, who go through life without special talent for mental control, sometimes must turn to other tactics to overcome ironic error. Strategies people use to relax excessive striving for control, for example, show promise in reducing the severity of ironic effects. Potentially effective strategies include accepting symptoms rather than attempting to control them (*62*) and disclosing problems rather than keeping them secret (*63*). Therapies devised for improving mental control—or for helping people to relax it—remain largely untested, however, and there are enough ambiguities surrounding the translation of laboratory research into effective treatments that recommendations for clinical practice at this time are premature. Current research indicates only that, under certain conditions, we may be better able to avoid the worst in what we think, do, or say by avoiding the avoiding. Failing that, our best option is to orchestrate our circumstances so as to minimize mental load when mental control is needed.

References and Notes

1. E. A. Poe, "The imp of the perverse," *Graham's Lady's and Gentleman's Magazine* (July 1845), vol. 28, pp. 1–3.
2. S. Freud, in *The Standard Edition of the Complete Psychological Works of Sigmund Freud,* J. Strachey, Ed. (Hogarth, London, 1950), vol. 1, pp. 115–128.
3. W. James, *Mind* **4**, 1 (1879).
4. C. Baudoin, *Suggestion and Autosuggestion* (Dodd, Mead, New York, 1921).
5. C. Darwin, *On the Origin of Species by Means of Natural Selection* (Broadview, Petersborough, Canada, 2003).
6. D. M. Wegner, *Psychol. Rev.* **101**, 34 (1994).
7. D. M. Wegner, D. J. Schneider, S. Carter, T. White, *J. Pers. Soc. Psychol.* **53**, 5 (1987).
8. D. M. Wegner, J. W. Shortt, A. W. Blake, M. S. Page, *J. Pers. Soc. Psychol.* **58**, 409 (1990).
9. H. Trinder, P. M. Salkovskis, *Behav. Res. Ther.* **32**, 833 (1994).
10. P. Muris, H. Merckelbach, R. Horselenberg, *Behav. Res. Ther.* **34**, 501 (1996).
11. R. D. V. Nixon, J. Flood, K. Jackson, *Pers. Individ. Dif.* **42**, 677 (2007).
12. D. F. Tolin, J. S. Abramowitz, A. Przeworski, E. B. Foa, *Behav. Res. Ther.* **40**, 1255 (2002).
13. D. M. Wegner, S. Zanakos, *J. Pers.* **62**, 615 (1994).
14. E. T. Higgins, in *Unintended Thought*, J. S. Uleman, J. A. Bargh, Eds. (Guilford, New York, 1999), pp. 75–123.
15. D. M. Wegner, R. E. Erber, *J. Pers. Soc. Psychol.* **63**, 903 (1992).
16. J. S. Abramowitz, D. F. Tolin, G. P. Street, *Clin. Psychol. Rev.* **21**, 683 (2001).
17. E. Rassin, H. Merckelbach, P. Muris, *Clin. Psychol. Rev.* **20**, 973 (2000).
18. D. M. Wegner, in *Advances in Experimental Social Psychology*, M. Zanna, Ed. (Academic Press, San Diego, CA, 1992), vol. 25, pp. 193–225.
19. D. M. Wegner, R. E. Erber, S. Zanakos, *J. Pers. Soc. Psychol.* **65**, 1093 (1993).
20. A. C. Page, V. Locke, M. Trio, *J. Pers. Soc. Psychol.* **88**, 421 (2005).
21. L. S. Newman, K. J. Duff, R. F. Baumeister, *J. Pers. Soc. Psychol.* **72**, 980 (1997).
22. C. N. Macrae, G. V. Bodenhausen, A. B. Milne, R. L. Ford, *J. Pers. Soc. Psychol.* **72**, 709 (1997).
23. S. Najmi, D. M. Wegner, *Conscious. Cogn.* **17**, 114 (2008).
24. M. C. Anderson, C. Green, *Nature* **410**, 366 (2001).
25. D. M. Wegner, F. Quillian, C. E. Houston, *J. Pers. Soc. Psychol.* **71**, 680 (1996).
26. R. M. Wenzlaff, D. E. Bates, *Pers. Soc. Psychol. Bull.* **26**, 1200 (2000).
27. M. C. Anderson *et al.*, *Science* **303**, 232 (2004).
28. J. P. Mitchell *et al.*, *Psychol. Sci.* **18**, 292 (2007).
29. C. L. Wyland, W. M. Kelley, C. N. Macrae, H. L. Gordon, T. F. Heatherton, *Neuropsychologia* **41**, 1863 (2003).
30. H. B. Rubin, D. R. Henson, *Psychopharmacology (Berlin)* **47**, 123 (1976).
31. H. E. Adams, L. W. Wright Jr., B. A. Lohr, *J. Abnorm. Psychol.* **105**, 440 (1996).
32. J. D. Lane, D. M. Wegner, *J. Pers. Soc. Psychol.* **69**, 237 (1995).
33. D. M. Wegner, J. D. Lane, S. Dimitri, *J. Pers. Soc. Psychol.* **66**, 287 (1994).
34. D. M. Wegner, D. B. Gold, *J. Pers. Soc. Psychol.* **68**, 782 (1995).
35. L. W. Lane, M. Groisman, V. S. Ferreira, *Psychol. Sci.* **17**, 273 (2006).
36. L. Smart, D. M. Wegner, *J. Pers. Soc. Psychol.* **77**, 474 (1999).
37. A. G. Greenwald, M. R. Banaji, *Psychol. Rev.* **102**, 4 (1995).
38. J. A. Bargh, in *Dual Process Theories in Social Psychology*, S. Chaiken, Y. Trope, Eds. (Guilford, New York, 1999), pp. 361–382.
39. C. N. Macrae, G. V. Bodenhausen, A. B. Milne, J. Jetten, *J. Pers. Soc. Psychol.* **67**, 808 (1994).
40. M. J. Monteith, J. W. Sherman, P. G. Devine, *Pers. Soc. Psychol. Rev.* **2**, 63 (1998).
41. A. D. Galinsky, G. B. Moskowitz, *J. Exp. Soc. Psychol.* **43**, 833 (2007).
42. C. N. Macrae, G. V. Bodenhausen, *Annu. Rev. Psychol.* **51**, 93 (2000).
43. D. M. Wegner, M. Ansfield, D. Pilloff, *Psychol. Sci.* **9**, 196 (1998).
44. J. Merron, "Ankiel can't seem to conquer 'The Creature'" (2003), http://assets.espn.go.com/mlb/s/2003/0615/1568307.html.
45. D. L. Beilock, J. A. Afremow, A. L. Rabe, T. H. Carr, *J. Sport Exerc. Psychol.* **23**, 200 (2001).
46. F. C. Bakker, R. R. D. Oudejans, O. Binsch, J. Van der Kamp, *Int. J. Sport Psychol.* **37**, 265 (2006).
47. E. H. W. Koster, E. Rassin, G. Crombez, G. W. B. Naring, *Behav. Res. Ther.* **41**, 1113 (2003).
48. C. G. Beevers, R. M. Wenzlaff, A. M. Hayes, W. D. Scott, *Clin. Psychol. Sci. Pract.* **6**, 133 (1999).
49. D. M. Wegner, A. Broome, S. J. Blumberg, *Behav. Res. Ther.* **35**, 11 (1997).
50. M. E. Ansfield, D. M. Wegner, R. Bowser, *Behav. Res. Ther.* **34**, 523 (1996).
51. D. M. Wegner, R. M. Wenzlaff, M. Kozak, *Psychol. Sci.* **15**, 232 (2004).
52. F. Taylor, R. A. Bryant, *Behav. Res. Ther.* **45**, 163 (2007).
53. R. E. Schmidt, G. H. E. Gendolla, *Conscious. Cogn.* **17**, 714 (2008).
54. D. Cioffi, J. Holloway, *J. Pers. Soc. Psychol.* **64**, 274 (1993).
55. L. Goubert, G. Crombez, C. Eccleston, J. Devulder, *Pain* **110**, 220 (2004).
56. J. D. Eastwood, P. Gaskovski, K. S. Bowers, *Int. J. Clin. Exp. Hypn.* **46**, 77 (1998).
57. A. G. Harvey, B. McGuire, *Behav. Res. Ther.* **38**, 1117 (2000).
58. A. I. Masedo, M. R. Esteve, *Behav. Res. Ther.* **45**, 199 (2007).
59. J. Arndt, J. Greenberg, S. Solomon, T. Pyszczynski, L. Simon, *J. Pers. Soc. Psychol.* **73**, 5 (1997).
60. B. J. King, J. R. Council, *Int. J. Clin. Exp. Hypn.* **46**, 295 (1998).
61. R. A. Bryant, S. Wimalaweera, *Int. J. Clin. Exp. Hypn.* **54**, 488 (2006).
62. P. Bach, S. C. Hayes, *J. Consult. Clin. Psychol.* **70**, 1129 (2002).
63. J. W. Pennebaker, *Psychol. Sci.* **8**, 162 (1997).

64. Thanks to K. Gray, A. Heberlein, A. Jenkins, A. Knickman, K. Koh, and T. Wegner for helpful comments. This work was supported by National Institute for Mental Health grant MH 49127.

10.1126/science.1167346

Serengeti Birds Maintain Forests by Inhibiting Seed Predators

Gregory J. Sharam, A. R. E. Sinclair, Roy Turkington*

Tropical forests are declining and becoming fragmented (*1*, *2*). In Africa, they are subjected to fires, competition from grasses, and browsing and have low recruitment of trees (*3*, *4*). We report here the mechanism that contributes to the regeneration of riverine forests in the Serengeti ecosystem, Tanzania, and the destabilizing consequences when fire disturbance alters that mechanism by opening the forest canopy. Forest patches of mixed broadleaf trees occur naturally along rivers in East Africa, and in Serengeti some 70 to 80% have disappeared since 1950 (*5*). We have monitored forest tree density and bird species since 1966, and from 1997 to 2006 we monitored abundance of bird species, beetle attack on seeds, germination of seeds, and survival of tree seedlings in 18 patches of forest at different stages of canopy loss (figs. S1 to S3) and conducted experiments on seed viability (*6*). Total bird species dropped from 33 in forest patches to 18 in open-canopy patches ($P < 0.001$), largely because of the loss of frugivores from 16 to 6 species.

Because the number of forest bird species declined as tree density declined (Fig. 1A), we examined how this affected seed germination, seedling emergence, and recruitment in remaining closed-canopy undisturbed patches. The frugivores were generalists that ingested fruits of most trees, removed the pericarp, and either regurgitated seeds or excreted them. The proportion of all seeds on the forest floor that had been previously fed upon and dropped by birds declined from 70% in patches with closed canopy and high stem density to 3% in open forest and thickets with low stem density (Fig. 1B).

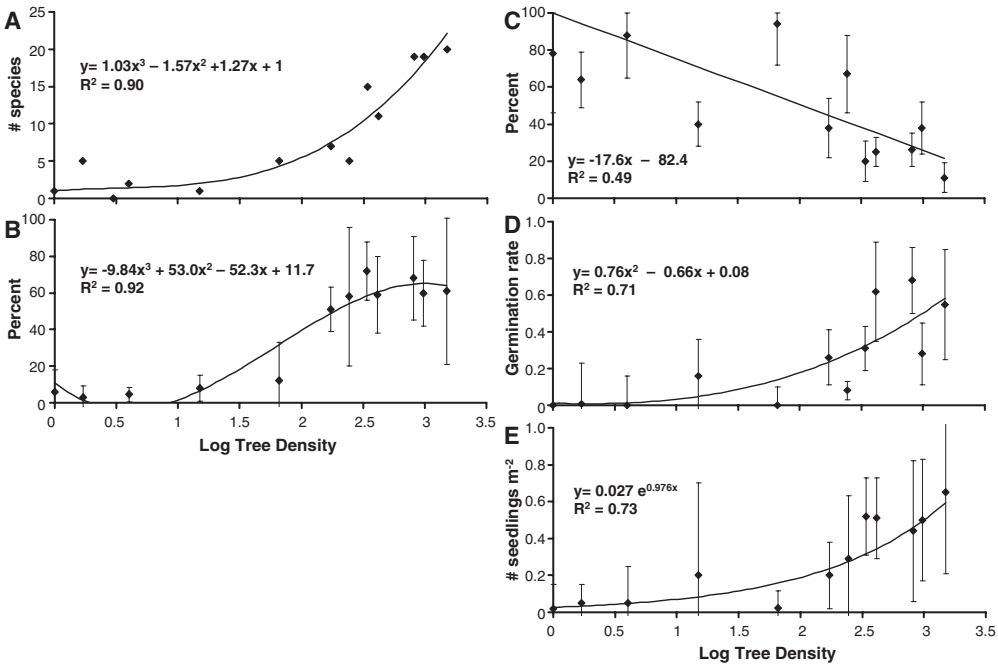

Fig. 1. Forest or thicket patches of differing tree density relative to (**A**) the number of forest bird species, (**B**) percent of fruits eaten by birds, (**C**) percent of seeds attacked by beetles, (**D**) seedling density (number/m^2 per year), and (**E**) density of recruits/m^2. Canopy tree density (± 1 SE) is a count of canopy and subcanopy trees.

Bruchid beetles are the main insect seed predators (*7*). Seeds still on the trees were not attacked by beetles, and seeds previously fed upon by birds only suffered an ~5% attack rate. The attack rate on uneaten seeds on the ground ranged from 68 to 92%. Because the proportion of seeds uneaten by birds in the total seed sample on the ground increased as tree density declined (Fig. 1B), the overall attack rate by beetles increased from 20 to 90% (Fig. 1C) as the canopy opened.

Seeds from the tree canopy and free from the effects of birds and beetles germinated at 56% ± 14% SE ($n = 250$). Seeds collected from the forest floor without beetle holes had a similar germination rate with pericarp (i.e., without bird feeding, 42% ± 8%, $n = 225$) or without pericarp (fed-upon by birds, 48% ± 6%, $n = 224$). Seeds that had been attacked by beetles did not germinate whether the fruit had been processed by birds ($n = 87$) or not ($n = 556$). Therefore, birds protected the seeds through their feeding, and in their absence beetles caused a major reduction of seed germination.

We then related seedling emergence per m^2 (Fig. 1D) and density of new recruits per m^2 (Fig. 1E) to stem density. Seedling density declined from a high of 0.3 to 0.7 new seedlings/m^2 per year in forest patches with high stem density (>1000 stems/ha) and a closed canopy to zero in forest patches with fewer than 20 stems/ha (Fig. 1D) (figs. S4 and S5). The density of recruits (beyond cotyledon emergence but <50 cm tall) followed the same pattern as that for seedlings, namely high density in dense patches (0.65 recruits/m^2) and low density (0.02 recruits/m^2) in patches with <20 stems/ha (Fig. 1E). Both the density of seedlings emerging (Fig. 1D) and the density of recruits (Fig. 1E) were in contrast to the proportion of seeds attacked by beetles (Fig. 1C). We conclude that forest-adapted birds, by consuming seeds, protect them from beetle attack. Consumption increased the germination rate and ultimately the density of seedlings and new recruits. This density in a closed forest provided sufficient recruitment to maintain the forest (*4*). Thus, the frugivorous birds are necessary for the maintenance of forests, and their absence could result in the continued disappearance of forests. In general, this study illustrates, first, how a stable community is maintained and, second, how it can unravel by a single disturbance. This causes a positive feedback loop of processes that, over decades, changes the ecosystem into a different state, despite the removal of the original disturbance. This unravelling has been widely observed (e.g., figs. S6 to S8, 1968 to 1999) and also measured at one site for 40 years (1966 to 2006) (fig. S9).

References and Notes

1. C. A. Chapman, L. J. Chapman, *Conserv. Biol.* **13**, 1301 (1999).
2. J. Terborgh *et al.*, *Science* **294**, 1923 (2001).
3. S. A. R. Mduma, A. R. E. Sinclair, R. Turkington, *J. Ecol.* **95**, 184 (2007).
4. G. Sharam, A. R. E. Sinclair, R. Turkington, *Biotropica* **38**, 599 (2006).
5. G. Sharam, thesis, University of British Columbia (2005).
6. Materials and methods are available as supporting material on *Science* Online.
7. R. A. Pellew, B. J. Southgate, *Afr. J. Ecol.* **22**, 73 (1984).
8. This work was funded by the Natural Sciences and Engineering Research Council of Canada.

Supporting Online Material

www.sciencemag.org/cgi/content/full/325/5936/51/DC1
Materials and Methods
Figs. S1 to S9

19 March 2009; accepted 7 May 2009
10.1126/science.1173805

Biodiversity Research Center, University of British Columbia, Vancouver, British Columbia V6T 1Z4, Canada.

*To whom correspondence should be adddressed. E-mail: royt@interchange.ubc.ca

Dissociable Components of Rule-Guided Behavior Depend on Distinct Medial and Prefrontal Regions

Mark J. Buckley,[1]*† Farshad A. Mansouri,[2]*† Hassan Hoda,[2] Majid Mahboubi,[2] Philip G. F. Browning,[1] Sze C. Kwok,[1] Adam Phillips,[2] Keiji Tanaka[2]

Much of our behavior is guided by rules. Although human prefrontal cortex (PFC) and anterior cingulate cortex (ACC) are implicated in implementing rule-guided behavior, the crucial contributions made by different regions within these areas are not yet specified. In an attempt to bridge human neuropsychology and nonhuman primate neurophysiology, we report the effects of circumscribed lesions to macaque orbitofrontal cortex (OFC), principal sulcus (PS), superior dorsolateral PFC, ventrolateral PFC, or ACC sulcus, on separable cognitive components of a Wisconsin Card Sorting Test (WCST) analog. Only the PS lesions impaired maintenance of abstract rules in working memory; only the OFC lesions impaired rapid reward-based updating of representations of rule value; the ACC sulcus lesions impaired active reference to the value of recent choice-outcomes during rule-based decision-making.

Although there have been recent advances in our understanding of how and where rules are represented in prefrontal cortex (PFC), disparity has emerged between findings from neurophysiology, neuropsychology, and neuroimaging as to the importance of different PFC regions. To address these issues, it is important to make distinctions between different kinds of rule-guided behavior. For instance, some behaviors involve following simple cued rules (e.g., stopping at a red light) wherein the presence of a particular stimulus instructs a fixed behavioral response. Experimental investigations of this category of rule-based behavior often utilize conditional learning tasks, such as arbitrary visuo-motor or visuo-visual mapping where animals acquire and maintain behavioral rules of the form "if A, then B" (with A being an instruction cue and B being the instructed motor response, or stimulus, that should be chosen, respectively). Although single-unit recording studies in macaque monkeys have found that neurons in both the dorsolateral PFC (dlPFC) and ventrolateral PFC (vlPFC) can encode such arbitrary rules (*1*–*3*) (Fig. 1B), human neuroimaging studies have observed activity within the vlPFC associated with the performance of similar tasks (*4*), and macaque lesion studies have established that the ventral PFC [vlPFC and orbitofrontal cortex (OFC)] is far more important than the dorsal PFC for supporting this kind of rule-based behavior (*5*–*8*).

Humans and nonhuman primates are also capable of learning to follow abstract rules wherein a rule generalizes to all the possible exemplars (*1*, *9*–*11*). For example, neurons throughout dlPFC, vlPFC, and OFC can encode, across a delay period, which of two different abstract rules ("matching" or "nonmatching" in this case) animals should apply to perform a task correctly at the end of the delay (*12*). Although there is no evidence of any quantitative differences in the proportions of such neurons in these different PFC regions of the macaque, when a human neuroimaging study adopted the same paradigm, activity associated with maintenance of specific rules across delays was observed in vlPFC but not elsewhere within the PFC (*13*). Another human neuroimaging study has similarly reported the involvement of only the inferior frontal gyral regions of the ventral PFC when rule-specific activation has to be maintained across a delay (*14*), and lesion studies in macaques have established that the ventral PFC regions, but not the dlPFC or anterior cingulate cortex (ACC), are necessary for acquisition of nonmatching rules (*15*–*17*). Thus the question arises: What, if any, aspect of rule-guided behavior is the dlPFC necessary to support in its own right?

In the paradigms discussed above, an animal knows which abstract rule to apply either because the rule remains constant or because it is instructed by a cue presented at the start of each trial. However, there are many everyday circumstances where we have to decide for ourselves which behavioral rule is most appropriate to follow under the circumstances we find ourselves in (for example, in deciding whether it remains appropriate to behave "in the same way" as others in a social setting). The Wisconsin Card Sorting Test (WCST) (*18*) has been used extensively in the clinic because it is a relatively simple task to administer and has long been believed to have utility [which has now been verified (*19*)] in contributing to the diagnosis of patients who are likely to suffer from PFC dysfunction owing to brain disease or damage. In the WCST, subjects first have to discover by trial and error which abstract rule they should follow; then they have to retain that rule in working memory so that they may continue to apply it on subsequent trials. This has to be done up until the point where the subject determines that the rule is no longer valid because it no longer elicits positive feedback; after which point, the subject must determine which alternative rule has become reinforced, and so on. A recent study of ours confirmed that dlPFC neurons in the vicinity of the principal sulcus (PS) in Brodmann's areas 46 and 9/46 of macaque PFC can maintain representations of uncued rules both within and between trials of a WCST analog (*20*). As in the human WCST, the rules are not cued at any time in our WCST analog either; rather, macaque monkeys receive "stay" or "switch" cues, by means of positive or negative feedback (Fig. 1A) after each choice, which they can use to determine whether they should either retain the current rule (stay) or change to the other rule (switch) in the next trial. In a recent human neuroimaging study in which participants were either directly told which rule to apply or alternatively were told to switch or stay with their previously chosen rule, greater additional activity was associated with the latter condition in the middle frontal gyrus, including area 46, part of dlPFC (*21*). Likewise, another study that compared free choice between rules with directly instructed rules, in the context of a working memory task, found greater delay activity in Brodmann's area 46 in the free-choice condition (*22*), as has a study in which subjects were able to freely choose which action to perform, or which stimuli to select (*23*). Thus, we hypothesized that an important factor determining the necessary involvement of the dlPFC in rule-guided decision-making may be the way in which abstract rules are set up. To determine whether the dlPFC is necessary for implementing uncued abstract rules held in working memory, we investigated the effects of lesions to different regions of dlPFC on the WCST analog.

To engage in self-initiated rule-guided decision-making, one needs to be able to adjust behavior flexibly in light of positive or negative feedback. Although neurons throughout swathes of frontal cortex have been observed to have activities related to reward value (*24*), those in the OFC, in particular, are believed to be most closely implicated in representing the reward value of stimuli or outcomes (*25*, *26*). It has recently been reported that neurons in the OFC might provide a relatively context-free value scale to facilitate comparison of the economic value to the animal of different "goods" (*27*, *28*). Nevertheless, it is clear that OFC lesions do not simply render animals unmotivated by reward or insensitive to the value of reward, as even animals with OFC lesions will work as hard as normal animals to earn food reward and will avoid choosing food items that are in view and on which they have been fed to satiety (*29*). So what is the specific

[1]Department of Experimental Psychology, University of Oxford, South Parks Road, Oxford, OX1 3UD, UK. [2]Cognitive Brain Mapping Laboratory, RIKEN Brain Science Institute, 2-1 Hirosawa, Wako, Saitama, Japan.

*These authors contributed equally to this work.
†To whom correspondence should be addressed. E-mail: buckley@psy.ox.ac.uk (M.J.B.); farshad@postman.riken.go.jp (F.A.M.)

role played by the OFC? Previous lesion studies in macaques have established that OFC-lesioned animals are impaired on tasks in which animals have to learn about changing stimulus-reward value associations, such as reinforcer devaluation paradigms, wherein the value of the food stuff associated with one object in the pair is subsequently devalued by feeding to satiety (*29*), and reversal learning paradigms in which the value of food items remain the same but the stimulus-reward reinforcement contingencies are changed (*17*, *29*, *30*). Performance on tasks in which there is a consistent relation between stimulus choice and outcomes, such as discrimination learning, is unaffected by OFC lesions (*5*, *29*). The role of the OFC also extends to learning about the changing value of instrumentally learned motor actions; OFC-lesioned animals are impaired in extinction after conditioning to variable interval schedules (*30*, *31*). We included an OFC group in this study to test the hypothesis that the role of the OFC might also extend to learning about the value of rules as is required in the WCST analog, in which maintaining continued successful choices cannot be based either on reference to the reward value of recently chosen stimuli or recently chosen actions, because both the identity and the position of the rewarded stimulus are randomly determined from trial to trial. Like the OFC, the anterior cingulate sulcus cortex (ACC_s) has also been implicated in reinforcement-guided decision-making, but in contrast to the OFC, it appears to be more important for making decisions on the basis of action values as opposed to stimulus values (*32*–*36*). But it is not yet known if the role of the ACC_s also extends to learning about the changing value of abstract rules, and so we also included an ACC_s-lesioned group in our investigation into the effects of discrete medial frontal and prefrontal cortical lesions on performance of the WCST analog.

Macaque lesion studies. Fourteen macaque monkeys were trained to perform an analog of the human WCST on a touch screen (Fig. 1A) (*37*). The currently reinforced rule was not directly cued at any time in this WCST analog; rather, animals had to discover for themselves by trial and error which rule was currently reinforced, then they had to maintain performance according to that rule across a series of trials until they attained 85% correct choices in a consecutive series of 20 trials, at which point an unannounced rule change was implemented and the next block of trials, with the other rule now reinforced, commenced. Each daily session comprised 300 trials, and before surgery, the 14 macaques were able to achieve a mean of 10 rule shifts per session with a median preoperative block length (i.e., trials taken to attain criterion on a rule) of 24 trials. The mean preoperative distribution of response types for the first 20 trials after every rule change is shown in Fig. 2. Note that animals rarely selected the stimulus that did not match the sample in either dimension; on average only 2.1% of animals' preoperative responses were of this type (which we called "nonperseverative" errors). Most of the animals' errors in the task were "perseverative" errors (defined here as a choice of the nonreinforced rule), and these errors accounted for 91% of the total errors. The dominance of perseverative errors on the very first trial after each unannounced rule change (Fig. 2) confirms that the animals could not predict when the unannounced rule change would occur. Also, the first unexpected instance of an absent reward (i.e., at the end of the first trial after a rule change) was on average insufficient to inform animals that the rule had changed (Fig. 2). Rather, the animals took a few trials to shift their behavior over to that of matching predominantly by the other rule. This failure of animals to change their behavior immediately after failing to receive a reward, the lack of which unambiguously signifies a change in reinforcement schedule, has also been observed in other task-shifting paradigms used with macaques (*33*). We likewise interpret this as further evidence that, to foraging animals, single outcomes (both negative and positive) are simply pieces of evidence that must be weighed against the recent history of experienced reinforcement to reach a decision as to whether a current behavior (to apply a particular rule in this case) is still optimal.

Experimental groups and general effects of PFC lesions on the WCST analog. On the basis of individuals' preoperative scores, we divided the animals into three groups of matched abilities, one group (PS group, $n = 4$, mean preoperative rule shifts per session = 9.8) received bilateral lesions of the PS within the inferior dlPFC; another group (ACC_s group, $n = 4$, mean preoperative rule shifts per session = 10.1) received bilateral lesions of the ACC_s within the medial frontal cortex; and the other animals (CON group, $n = 6$, mean preoperative rule shifts per session = 10) remained unoperated controls. In

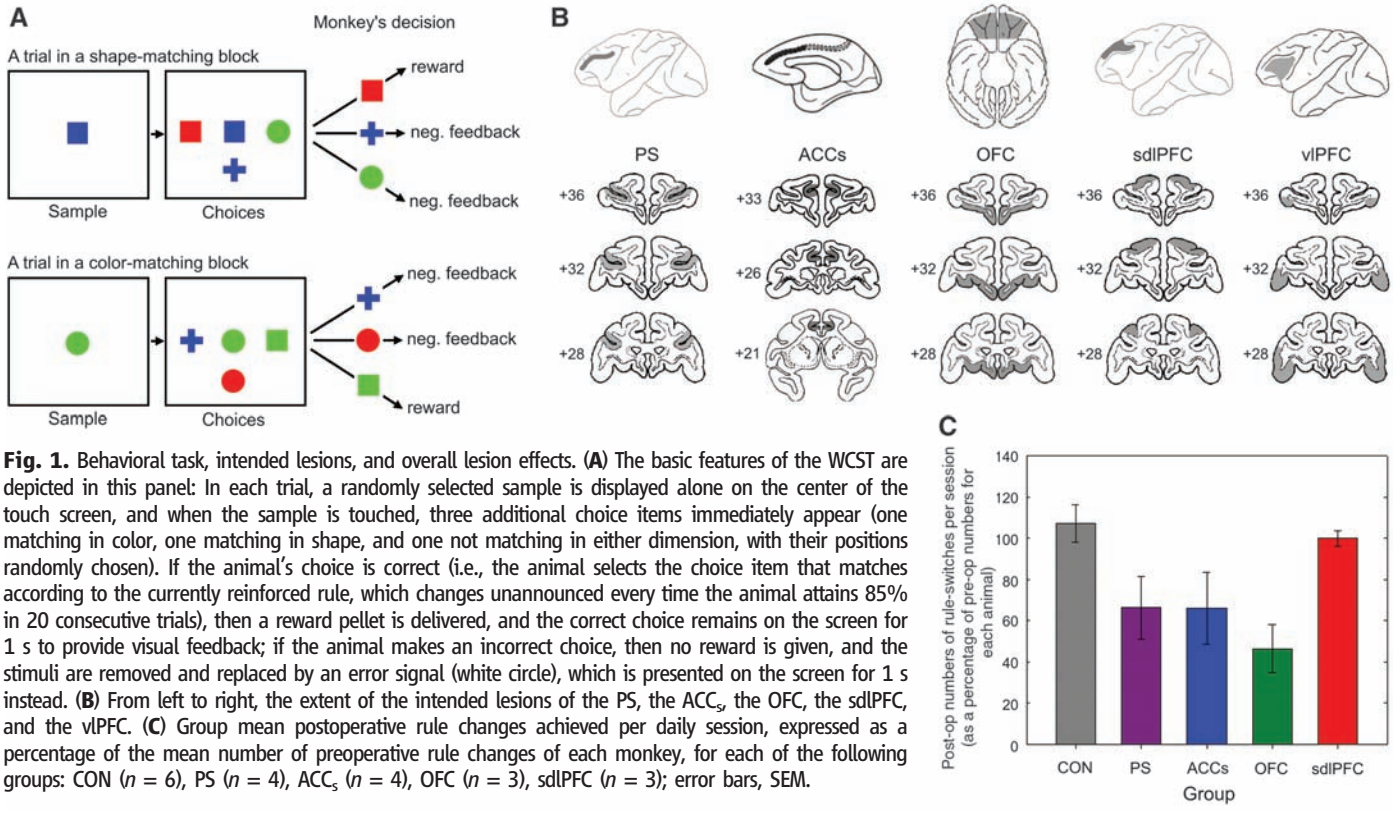

Fig. 1. Behavioral task, intended lesions, and overall lesion effects. (**A**) The basic features of the WCST are depicted in this panel: In each trial, a randomly selected sample is displayed alone on the center of the touch screen, and when the sample is touched, three additional choice items immediately appear (one matching in color, one matching in shape, and one not matching in either dimension, with their positions randomly chosen). If the animal's choice is correct (i.e., the animal selects the choice item that matches according to the currently reinforced rule, which changes unannounced every time the animal attains 85% in 20 consecutive trials), then a reward pellet is delivered, and the correct choice remains on the screen for 1 s to provide visual feedback; if the animal makes an incorrect choice, then no reward is given, and the stimuli are removed and replaced by an error signal (white circle), which is presented on the screen for 1 s instead. (**B**) From left to right, the extent of the intended lesions of the PS, the ACC_s, the OFC, the sdlPFC, and the vlPFC. (**C**) Group mean postoperative rule changes achieved per daily session, expressed as a percentage of the mean number of preoperative rule changes of each monkey, for each of the following groups: CON ($n = 6$), PS ($n = 4$), ACC_s ($n = 4$), OFC ($n = 3$), sdlPFC ($n = 3$); error bars, SEM.

the second stage of postoperative testing, the unoperated controls were divided into two matched-ability groups: One received bilateral lesions of the superior dlPFC (sdlPFC group, $n = 3$), whereas the other received bilateral lesions of the OFC (OFC group, $n = 3$). The intended lesions are depicted in Fig. 1B, and reproductions of the actual lesions, which were as intended, are shown in figs. S1 to S5. None of the lesioned groups were impaired on any of the control tasks [see supporting online material (SOM) text], which included color-matching or shape-matching for an entire session without rule shifts being imposed, confirming that their perceptual, motor, and attentional abilities were intact. However, after the lesions were introduced, the PS, ACC_s, and OFC groups were markedly impaired on the WCST analog; they achieved means of only 7.4, 6.7, and 5.5 rule shifts per postoperative session, respectively, compared with means of 10.1 and 11.7 rule shifts per session in the CON and sdlPFC groups at this stage of testing. The number of rule shifts achieved postoperatively is shown (Fig. 1C) as a percentage of the preoperative number attained for each group. As it was clear that the sdlPFC lesion had absolutely no effect on performance on this or any other measure of performance of the WCST analog, for all of the following statistical analyses the sdlPFC group was hereafter considered an operated control group that could be directly compared with the OFC group, as these two groups had experience identical to each other's. Designed comparisons using the pooled error term confirmed what is shown in Fig. 1C, namely, that both the PS group [$t(11) = 2.217$, $P = 0.024$, one-tailed] and the ACC_s group [$t(11) = 2.459$, $P = 0.023$, one-tailed] were significantly impaired relative to the CON group and that there was no difference in performance between the PS and ACC_s groups ($t < 1$). The OFC group was also significantly impaired [$t(4.32) = 4.3$, $P = 0.006$, one-tailed] relative to the sdlPFC group, whose performance did not change postoperatively ($t = 0$).

Two additional animals were trained preoperatively on our control task for the WCST analog (*37*), which required color- or shape-matching ability on alternate days but did not require rule changes within a daily session. Both animals were greatly impaired in implementing the rules they had learnt preoperatively after vlPFC lesions. This is consistent with previous studies that have reported that vlPFC-lesioned animals are impaired at both the learning and use of matching and nonmatching rules (*16*, *38*–*40*). The impairment in rule implementation after vlPFC lesions in the WCST analog is unlikely to be attributable largely to impoverished visual input into PFC, because the OFC is also well connected with visual association areas in the temporal lobe (*41*, *42*), and indeed, nonconditional learning tasks, such as concurrent visual discrimination learning, are not impaired by vlPFC lesions (*16*). It has been proposed that a fundamental role of the PFC is learning about the structure of complex tasks by a model-building approach (*43*); this gradual learning process allows the conditional or abstract rules that link stimuli with goals and the means to achieve them to be identified. Even after abstract rules have been acquired, the vlPFC may remain necessary to retain these linkages in the face of competing and, in the case of abstract rules, disruptive non–goal-directed learning processes elsewhere, that might otherwise bias animals to respond on the basis of rapidly acquired stimulus-response associations instead (*44*). The vlPFC has been proposed to be more important for learning and retaining rules based on abstractions as opposed to exemplars (*45*). This would be consistent with the known patterns of PFC afferents from visual association areas in the temporal lobes. The perirhinal region of the temporal lobe, where object-level representations of exemplars are believed to be represented (*46*), projects more heavily into OFC than vlPFC (*41*, *42*), whereas vlPFC receives relatively more of its input from the inferotemporal cortex, where representations are more feature-based than object-based (*47*).

The impairments in the PS, OFC, and ACC_s groups in the main experimental task noted above cannot be attributable to impaired rule-switching per se, as none of the groups (see fig. S6) made significantly more perseverative or nonperseverative errors in the trials immediately after rule switches ($P > 0.1$ for all Group × Stage interactions in two-way analysis of variance for all preoperative versus postoperative comparisons on numbers of perseverative or nonperseverative errors accumulated in the three trials that followed the first trial after each rule changed). Therefore, the underlying natures of the impairments in the PS, OFC, and ACC_s groups are explored in detail in the following sections.

The role of the PS in working memory for rule. Having observed the impairment in the PS, ACC_s, and OFC groups in adapting to rule shifts, we explored the respective role of these areas in WCST analog performance. In order to test our hypothesis that the PS lesion impairs working memory for uncued abstract rules, it is necessary to show that performance on the WCST analog relies on working memory for rule. To do this, we determined the extent to which animals were able to maintain a rule from one trial to the next in the WCST analog, depending on the interval that elapsed between trials. In these dedicated postoperative rule-memory sessions (see SOM text for details), the WCST analog proceeded as normal, except that from the second block of the day onward, whenever animals again attained the normal criterion level of performance on the current rule, instead of having the rule change at that point, the rule remained the same but the interval before the next trial was either lengthened by 5 s [that this delay length would impede working memory for the rule was informed by a prior preliminary investigation (see SOM text)] or the interval before the next trial remained the same duration as normal (6 s). We recorded the extent to which the animals in different groups applied the currently reinforced rule on the next trial (the rule itself did not change until the animal attained criterion for a second time, i.e., a minimum of 20 trials later). The CON and sdlPFC groups performed at 92.7% and 100% correct, respectively, on the first trial after the normal delay, whereas they performed at only 73.3% and 68.8% correct, respectively, on the first trial after the extended delay. That a relatively short lengthening of the delay between trials can cause such a significant performance decrement in unoperated controls [for CON: $t(5) = 3.92$, $P = 0.01$] confirms that between-trial rule remembrance in the WCST analog is mediated by short-term working memory. Next, we assessed how well the PS group performed under the same conditions (Fig. 3A). The performance of the PS group was not significantly different from chance levels of choice between the two matching rules after the 5 s longer interval ($t < 1$), and the PS group was significantly impaired relative to the CON group at remembering the rule across this slightly longer interval [Group × Delay, $F_{(1,8)} = 5.76$, $P = 0.04$]. The ACC_s and OFC groups, in comparison, did not perform significantly worse on the trial after the slightly longer interval [ACC_s: Group × Delay, $F_{(1,8)} = 2.89$, $P > 0.1$; OFC: Group × Delay, $F_{(1,4)} = 1.34$, $P > 0.1$]. We conclude that only the PS group had more fragile working memory for the abstract rule. Although previous studies have examined the effect of PFC lesions in the acquisition of extra-dimensional set-shifting abilities in the context of stimulus-reward associative learning toward exemplars (*48*) or toward categories (*49*), our study examines the importance of these PFC regions for supporting flexible switching between abstract rules based on short-term memory and outside of the context of associative learning.

The role of the OFC in representing the value of rules. If the OFC group were impaired at

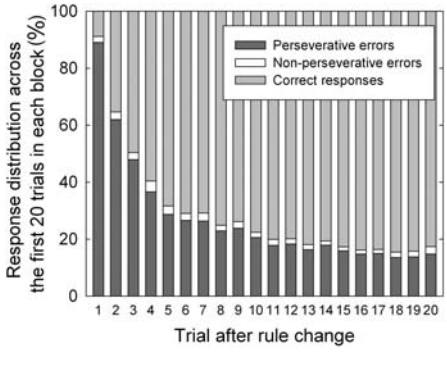

Fig. 2. Preoperative distribution of response types after rule changes occurred. Proportions of the three types of response (perseverative errors, nonperseverative errors, and correct responses) that were made in each of the first 20 trials of each block in the WCST analog averaged across the performance of all animals in all preoperative sessions.

updating the current value of rules in the WCST analog, then we would predict that once the value of rules was sufficiently established (i.e., after several consecutive correct responses had reinforced the value of the rule) that the OFC group might then be expected to be able to maintain a series of consecutive correct responses on the basis of remembering the rule itself (as the previous analysis showed that the OFC group have no deficit in rule remembrance). However, when the current rule value is not as well established to animals (i.e., after only one or a small number of consecutive correct responses have been made), deficits in the OFC animals' abilities to choose correctly might be prominent. Thus, we first scored the pre- and postoperative performance of each animal on EC + 1 trials, that is the percent correct on trials that followed a single correct response (C) that was itself preceded by an error (E), and we then scored how well animals could maintain correct responding after varying numbers (n) of consecutive correct responses after the initial errors, which constituted an $EC_n + 1$ analysis (with n ranging from 2 to 10). For both analyses, we included all trials in all blocks excluding the trials immediately after rule changes (responses in the first three trials in each block were not considered in these analyses). The performance of the OFC group on trials after a single reward (EC + 1) was 76.9% preoperatively, but no better than chance postoperatively (Fig. 3B); analyses confirmed that the OFC group was significantly and severely impaired [OFC: Group × Stage, $F_{(1,4)} = 16.81$, $P = 0.01$], whereas the numerical trends toward worse postoperative performance on EC + 1 in the PS and ACC_s groups did not attain statistical significance [PS: Group × Stage, $F_{(1,8)} = 4.18$, $P > 0.05$; ACC_s Group × Stage, $F_{(1,8)} = 1.66$, $P > 0.1$]. The $EC_n + 1$ data shows that the OFC group was also impaired postoperatively at maintaining a series of correct responses when the value of n in the $EC_n + 1$ was low (Fig. 4E); analyses confirmed a highly significant interaction between Group × Stage × n [$F_{(8,32)} = 4.27$, $P < 0.002$] with a significant linear trend component [$F_{(1,4)} = 11.74$, $P = 0.027$], showing that the magnitude of the impairment in the OFC group was inversely correlated with increasing values of n. None of the other lesioned groups showed the same pattern of postoperative deficit as the OFC group in the $EC_n + 1$ analysis (Fig. 4); both the PS group [Group × Stage, $F_{(1,8)} = 5.34$, $P = 0.05$; Group × Stage × n, $F < 1$] and the ACC_s group [Group × Stage, $F_{(1,8)} = 5.31$, $P = 0.05$; Group × Stage × n, $F < 1$] were more consistently impaired across all values of n in the $EC_n + 1$ analysis, which may be most parsimoniously accounted for as impairments in rule memory (see above) or in reference to the integrated outcome history of recent decisions (see below), respectively, deficits that are not seen in the OFC group. Further, the slope of the curves in Fig. 4E allows us to infer that, after receiving multiple rewards, the rate at which the OFC animals proceed to shift over to making consecutive correct choices according to the new rule is as rapid as controls, which confirms that the OFC group is not insensitive to reward per se, even if their overall sensitivity to initial reward is deficient. Further evidence that the OFC-lesioned animals are not insensitive to reward per se comes from another study (*34*), which showed that OFC-lesioned animals are not impaired in their responses after receiving a single reward (i.e., $n = 1$ of $EC_n + 1$) in a task in which animals had to make decisions between specific motor actions, as opposed to between rules.

We also calculated average response time (i.e., time elapsing between test-item appearance and screen touch) for each animal across the three different kinds of responses: perseverative errors, nonperseverative errors, and correct responses (Fig. 3C). Preoperatively, across all animals, the mean response times were 1231 ms for correct responses, 1689 ms for perseverative errors, and 1951 ms for nonperseverative errors; response times for both error types were significantly slower than correct response times [perseverative versus correct: $t(13) = 5.79$, $P < 0.001$; nonperseverative versus correct: $t(13) = 6.15$, $P < 0.001$], and nonperseverative error responses were significantly slower than perseverative errors [$t(13) = 3.14$, $P < 0.01$]. The response times in the OFC group were on average 287 ms slower for correct responses, 287 ms slower for perseverative errors, and 339 ms slower for nonperseverative responses than the response times recorded by the same animals preoperatively. This slowing of response times in the OFC group was significant and similar across all three response types [Stage × Group, $F_{(1,4)} = 8.06$, $P = 0.047$; Stage × Response Type × Group, $F < 1$]. However, this does not reflect a global lowering of motivation because OFC-lesioned animals' responses times were unchanged postoperatively [Stage × Group, $F < 1$; Stage × Response Type × Group, $F < 1$]

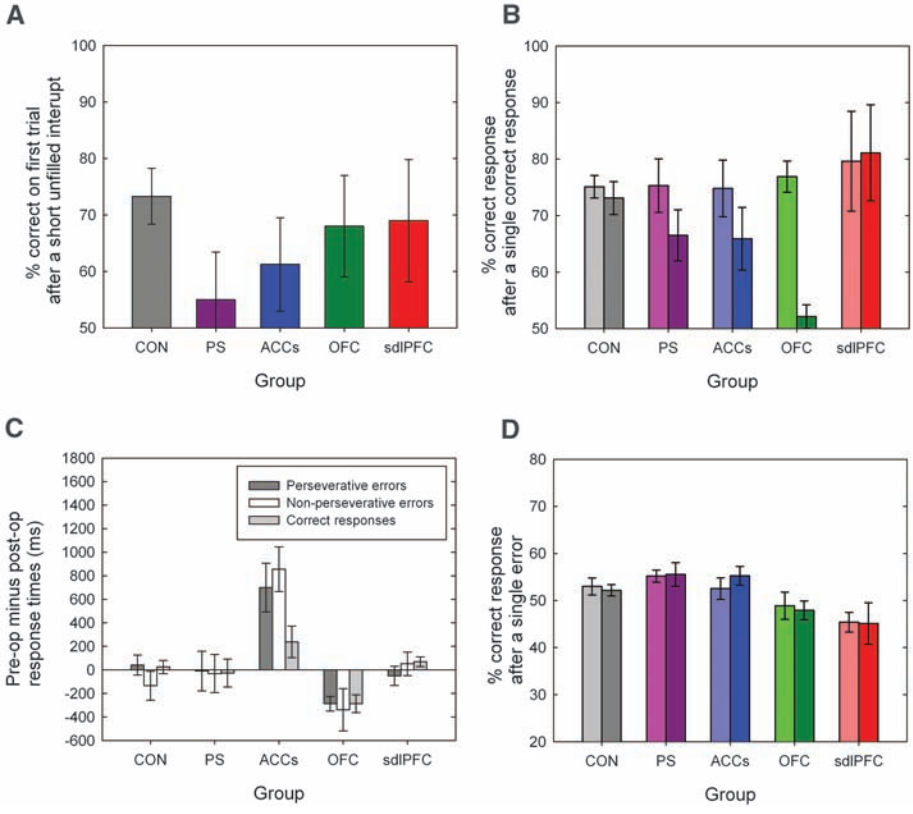

Fig. 3. Effects of different prefrontal lesions on different performance measures in the WCST analog. (**A**) Response on the first trial after a short unfilled interruption. Group mean postoperative percent correct performance on rare probe trials before which the intertrial interval after a correct response (normally 6 s) was lengthened by 5 s; chance level of choice (between the two matching rules) in this condition would equate to 50% correct. (**B**) Response after a single correct response. Group mean preoperative levels (light hues) and postoperative levels (dark hues) of correct responses on trials preceded by a single correct response (i.e., trials preceded by more than one correct response were excluded). (**C**) Response times. Group mean preoperative minus postoperative response times averaged across all trials according to the three different response types (perseverative errors, nonperseverative errors, and correct responses). (**D**) Response after a single error. Group mean preoperative levels (light hues) and postoperative levels (dark hues) of correct responses on trials after a single error trial that was itself preceded by a correct response. Error bars, SEM.

in control tasks without conflict between rules (*37*). In addition, previous studies have observed OFC-lesioned animals to be just as willing as unoperated animals to work for reward in a range of experimental tasks (*29*, *36*, *50*). The faster decisions in the CON group compared with the OFC group may be due to their being able to reach decisions more quickly in the presence of a heightened and more reliable bias in rule value, as opposed to any insensitivity to the signal value of reward per se. Consistent with the conclusions of previous studies of OFC lesions (*17*, *50*), our observations of a lack of perseveration after rule changes in the OFC group postoperatively lead us to rule out perseverative tendencies as the explanation for their deficits in adapting to rule shifts (Fig. 1C) and the findings in EC + 1 (Fig. 3B) and EC_n + 1 analyses (Fig. 4E). Our observations of slowed response times allow us to rule out a general lack of inhibition in OFC-lesioned macaques.

Rather than OFC being important for rule-value coding per se, as argued here, might there be an alternative explanation that could account for the pattern of data in the OFC group? For instance, it has been argued elsewhere (*45*) that OFC mediates behavior-guiding rules based on objects and so mediates learning about exemplars, whereas the vlPFC is more important for attaching value to abstractions (*48*). Thus, it is useful to consider whether the OFC might contribute to higher-order rules in the current study by coding outcomes for specific stimuli in the context of a particular rule in the WCST analog. Unlike in the intradimensional-extradimensional (ID-ED) shift paradigm (*48*), successful task performance in the WCST analog cannot arise through learning about the relative value of particular exemplars (e.g., "red square"), or indeed about the relative value of particular stimulus features (e.g., the color red) either (*49*), because the exemplar that is rewarded (and hence any features that are present while reward is given too) changes from trial to trial. Thus, whatever crucial contribution the OFC and vlPFC make toward performance of the WCST task, it cannot be within-block learning about the value of objects or the value of object features. In the SOM, we also argue against the idea that the OFC and vlPFC might contribute to decision-making in the WCST analog by representing the transient value of exemplars or stimulus features, respectively, within the context of an individual trial and within the context of a particular rule (see SOM text, discussion). In ruling out these alternative explanations, we believe that the most parsimonious explanation of the impairment in the OFC group is that these lesioned animals are unable to rapidly update rule-value representations as efficiently as controls and need a greater number of rewards to do so.

The role of the ACC in rule-based decision-making. One previous proposal regarding the role of the ACC was that it might be important for error detection and the enabling of subsequent error correction [see (*51*) for a review]. Here, we found that ACC_s lesions had no effect on the performance on trials that followed immediately after errors. Indeed, none of the lesioned groups showed any postoperative change in performance on trials that followed single errors that were themselves preceded by a correct response (Group × Stage: $F < 1$ for all groups) (Fig. 3D). In all groups, the effect of a single error in this task was the same, that is, to "reset" the animals' performance on the next trial back close to chance level of selection between the two rules. Previous studies have also refuted the hypothesis that the ACC is important only for error detection and correction because ACC lesions have been observed to impair reward-guided action selection (*52*). Another influential hypothesis regarding the role of the ACC is that this brain region is important for conflict monitoring (*53*). However, a recent macaque lesion study of our own showed that ACC_s lesions leave intact animals' abilities to detect and respond to different levels of conflict (*54*). Thus, we interpret the deficits in the ACC_s group in the present experiment as deficits in response selection and decision-making, a notion explored in more detail below.

First, we found that the ACC_s group were impaired across all values of n in our EC_n + 1 analysis of the WCST analog performance data [Group × Stage, $F_{(1,8)} = 5.31$, $P = 0.05$; Group × Stage × n, $F < 1$], which indicated that they are impaired relative to controls at maintaining extended sequences of correct choices between abstract rules. This kind of EC_n + 1 analysis was recently used elsewhere to show that ACC_s lesions produced a similar pattern of impairment in a reinforcement-guided decision-making task that necessitated making decisions between motor responses (*33*); however, another study showed that ACC_s lesions do not impair reinforcement-guided decision-making in a task where the choices were between stimuli (*36*). These differences indicate that the OFC and ACC_s are more

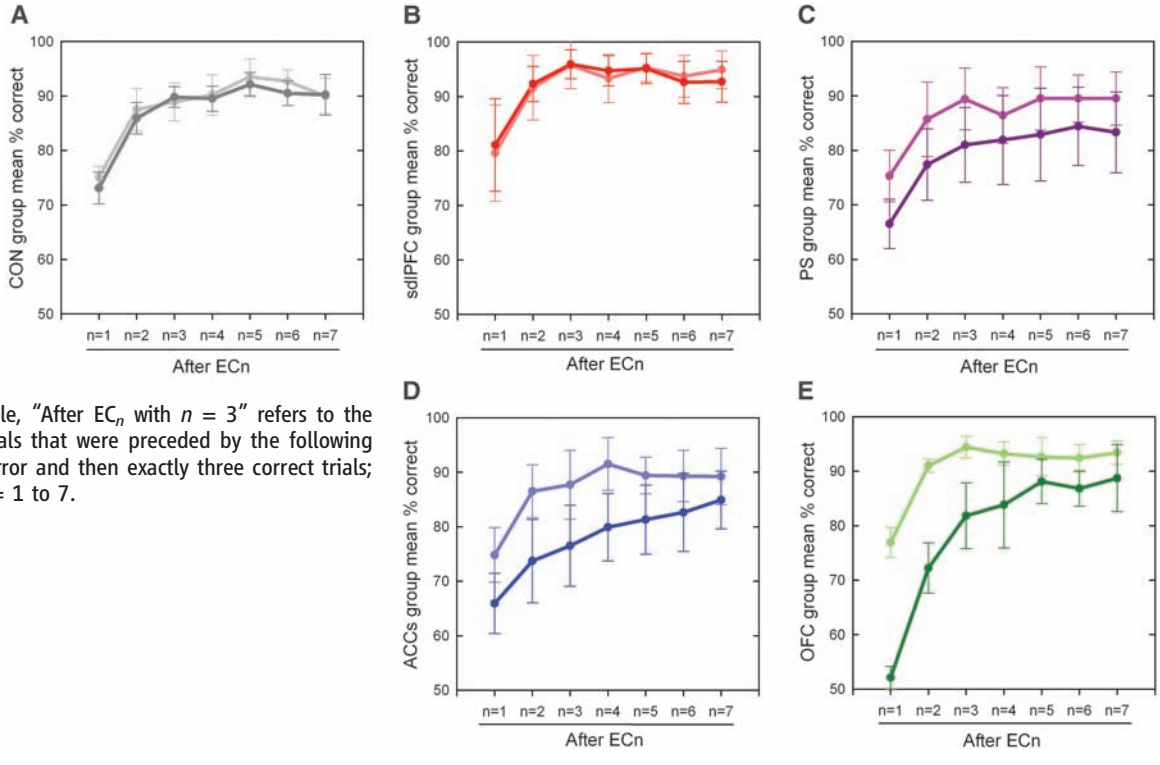

Fig. 4. Sustaining rewarded behavior. For each of the five groups, (**A**) CON, (**B**) sdlPFC (lesion), (**C**) PS (lesion), (**D**) ACC_s (lesion), and (**E**) OFC (lesion), the mean preoperative (light hues) and postoperative (dark hues) performance on trials are depicted depending on how many (*n*) consecutive correct responses (C) lay between an initial error trial (E) and that trial. For example, "After EC_n with $n = 3$" refers to the mean performance on trials that were preceded by the following sequence of trials: one error and then exactly three correct trials; values are plotted for $n = 1$ to 7.

important for reward-based decision-making between stimuli and actions, respectively (*34*, *35*), but this dichotomy alone does not provide an account of why the ACC_s group is impaired on the WCST analog. The reason for the impairment in the ACC_s group on the WCST analog might be related instead to another difference between the ACC and the OFC, namely, that the ACC may be more important than the OFC for representing more highly integrated and "context-dependent" representations of choice-outcome values (*55*). Whereas ACC representations of choice-outcome values may be more dependent on the recent history of the monkey's responses and rewards and the context of changing environmental constraints, the OFC may represent indices of value in a relatively less integrated and more context-independent manner. For example, OFC neurons in macaques are reported to represent goods on a common value-scale independent of what other goods are available (*28*), and OFC neurons in rats appear to represent the costs of a choice independent from the magnitude of the reward (*56*). Integrated choice outcomes reflect costs as well as benefits, and both may vary depending on the environment context; ACC lesions have been observed to impair animals' cost-benefit decision-making in rodents (*57*), and human neuroimaging studies have implicated the ACC in representing estimates of environmental volatility (*58*), a statistic that animals make reference to when determining the degree to which recent outcomes should be allowed to influence subsequent choices. Thus, the ACC has been proposed to be involved in context-driven estimations of the uncertainty of obtaining reward (*55*, *59*). The impairments in the $EC_n + 1$ analysis in the current study may also reflect animals' being uncertain about the value of repeating previously successful choices; this may be attributable to deficits in postoutcome updating of, or predecision referral to, representations of the extent to which recent outcomes should influence future decisions.

Second, unlike the OFC-lesioned animals who were reported to respond slower postoperatively in the preceding section, the response times in the PS group were unchanged postoperatively ($F < 1$ for all interactions involving Stage and Group with Rule and/or Response-type factors), whereas those of the ACC_s group were significantly faster [Stage × Group, $F_{(1,8)} = 20.58$, $P < 0.01$] for both perseverative errors [$F_{(1,8)} = 11.21$, $P = 0.01$] and nonperseverative error responses [$F_{(1,8)} = 28.05$, $P < 0.01$], but were unchanged for correct responses [$F_{(1,8)} = 2.72$, $P > 0.1$] (Fig. 3C). That this might reflect general disinhibition in the ACC_s can be ruled out because the response times of the ACC_s group were unchanged in our control tasks described in (*37*) (Stage × Group, $F < 1$; Stage × Response type × Group, $F < 1$). In addition, we have previously reported data confirming that ACC_s-lesioned animals do not exhibit selective disinhibition under conditions of high cognitive load (*54*); in this study, the difference in response time between conditions of high and low cognitive load was observed to be no different in ACC_s compared with unoperated controls. Rather, this selective quickening of response times in erroneous trials in the ACC_s group is further consistent with the idea that errors are commissioned in this group when the animals fail to complete the normal processes of response selection, as outlined above, when cognitively challenged.

Summary and conclusions. This lesion study has shown that macaque PS, OFC, ACC, and vlPFC (but not sdlPFC) all play indispensable, but different, roles in rule-guided behavior. Our data confirm that implementing previously acquired abstract rules is crucially dependent on the vlPFC region, and we propose that the vlPFC may support abstract rule implementation by biasing behavior toward such acquired rules and away from the influence of competing concrete stimulus-reward associations mediated by other areas. Our study also showed that among all the areas we targeted, only the PS region was necessary to support working memory for abstract rules. We propose that this region of dlPFC is important when subjects have to select an abstract rule themselves and then actively maintain a representation of the chosen rule in working memory in order to bias behavior away from other competing rules. This finding extends the known range of functions crucially supported by the PS beyond spatial working memory [see SOM text, discussion, and (*54*)]. Our OFC lesion was the only target lesion that impaired animals' responses after single rewards, and we argue that the pattern of data after OFC lesions supports the hypothesis that the role of the OFC extends to representing the value of rules and that the OFC is necessary to rapidly update rule value on the basis of reinforcement. The pattern of deficits after ACC_s lesions was consistent with a deficit in response selection and reference to integrated representations of the outcome of rule selection, which extends the known role of the ACC_s to rule-based decision-making. In contrast to these lesion effects, the sdlPFC lesion was unique in the areas we investigated in that it was the only region that proved not to be crucially involved in any aspect of the WCST analog. The role of the sdlPFC deserves further investigation, as lesions to this region in macaques, to date, have only been shown to impair working-memory tasks that involve monitoring externally or self-ordered choices (*60*) (see SOM text, discussion). Nevertheless, our results indicate that in tasks requiring cognitive flexibility to adapt to the rule changes, there is a functional dissociation even in the dlPFC.

These dissociations and double-dissociations refute the idea that there may be no real specialization of function within the PFC (*61*). One PFC region that we did not target in the current study is the frontopolar cortex (FPC). The FPC has not yet been targeted selectively by nonhuman primate lesion studies, but human neuropsychological patient-testing studies have reported that patients with lesions that include the FPC region are associated with greater incidence of rule-breaking behaviors and deficits in the prospective memory component of multitasking (*62*). Although human patient neuropsychology is limited because lesions are not circumscribed to cytoarchitectural regions of interest, such studies do provide some evidence of fractionalization of function within the human PFC (*62*); indeed, with regard to abstract rules, patients whose lesions are more rostrally located are reported to be more impaired in higher-order abstract rules (*63*). The precise role of the FPC remains to be verified, but it has been suggested that the FPC may lie at the top of a processing hierarchy of rule-guided behavior, possibly important for implementing the most complex (higher-order) rules or for selecting between multiple nested abstract rules in branching or multitasking paradigms (*64*–*66*). Here, in a species capable of flexible switching between abstract rules, we used the animal lesion approach where highly circumscribed lesions can be placed within anatomical regions of interest to demonstrate how a range of different PFC and medial frontal regions contribute in different ways to separable cognitive processes involved in rule-guided behavior. Our task is the closest nonhuman primate analog to date of the human WCST, which has been used extensively in the clinic because of its efficacy in diagnosing frontal lobe dysfunction (*19*), and this study offers a bridge between neurophysiological investigations of the mechanisms of rule-guided behavior in nonhuman primates and human neuropsychological and clinical studies.

References and Notes

1. W. F. Asaad, G. Rainer, E. K. Miller, *J. Neurophysiol.* **84**, 451 (2000).
2. S. P. Wise, E. A. Murray, *Trends Neurosci.* **23**, 271 (2000).
3. M. Watanabe, *Exp. Brain Res.* **80**, 296 (1990).
4. I. Toni, M. F. S. Rushworth, R. E. Passingham, *Exp. Brain Res.* **141**, 359 (2001).
5. T. J. Bussey, S. P. Wise, E. A. Murray, *Behav. Neurosci.* **115**, 971 (2001).
6. E. A. Murray, T. J. Bussey, S. P. Wise, *Exp. Brain Res.* **133**, 114 (2000).
7. M. Petrides, *Behav. Brain Res.* **5**, 407 (1982).
8. D. Gaffan, S. Harrison, *Behav. Brain Res.* **31**, 207 (1989).
9. I. M. White, S. P. Wise, *Exp. Brain Res.* **126**, 315 (1999).
10. E. Hoshi, K. Shima, J. Tanji, *J. Neurophysiol.* **80**, 3392 (1998).
11. E. Hoshi, K. Shima, J. Tanji, *J. Neurophysiol.* **83**, 2355 (2000).
12. J. D. Wallis, K. C. Anderson, E. K. Miller, *Nature* **411**, 953 (2001).
13. S. A. Bunge, I. Kahn, J. D. Wallis, E. K. Miller, A. D. Wagner, *J. Neurophysiol.* **90**, 3419 (2003).
14. K. Sakai, R. E. Passingham, *Nat. Neurosci.* **6**, 75 (2003).
15. J. Bachevalier, M. Mishkin, *Behav. Brain Res.* **20**, 249 (1986).
16. D. M. Kowalska, J. Bachevalier, M. Mishkin, *Neuropsychologia* **29**, 583 (1991).
17. M. Meunier, J. Bachevalier, M. Mishkin, *Neuropsychologia* **35**, 999 (1997).
18. R. K. Heaton, *Wisconsin Card Sorting Test Manual* (Psychological Assessment Resources, Odessa, FL, 1981).
19. D. T. Stuss *et al.*, *Neuropsychologia* **38**, 388 (2000).
20. F. A. Mansouri, K. Matsumoto, K. Tanaka, *J. Neurosci.* **26**, 2745 (2006).

21. B. U. Forstmann, M. Brass, I. Koch, D. Y. von Cramon, *Neuropsychologia* **43**, 943 (2005).
22. S. L. Bengtsson, J. D. Haynes, K. Sakai, M. J. Buckley, R. E. Passingham, *Cereb. Cortex* (2009).
23. J. B. Rowe, K. E. Stephan, K. Friston, R. S. J. Frackowiak, R. E. Passingham, *Cereb. Cortex* **15**, 85 (2005).
24. M. R. Roesch, C. R. Olson, *J. Neurophysiol.* **90**, 1766 (2003).
25. L. Tremblay, W. Schultz, *Nature* **398**, 704 (1999).
26. M. R. Roesch, C. R. Olson, *Science* **304**, 307 (2004).
27. C. Padoa-Schioppa, J. A. Assad, *Nature* **441**, 223 (2006).
28. C. Padoa-Schioppa, J. A. Assad, *Nat. Neurosci.* **11**, 95 (2008).
29. A. Izquierdo, R. K. Suda, E. A. Murray, *J. Neurosci.* **24**, 7540 (2004).
30. C. M. Butter, *Physiol. Behav.* **4**, 163 (1969).
31. C. M. Butter, M. Mishkin, H. E. Rosvold, *Exp. Neurol.* **7**, 65 (1963).
32. K. Shima, J. Tanji, *Science* **282**, 1335 (1998).
33. S. W. Kennerley, M. E. Walton, T. E. J. Behrens, M. J. Buckley, M. F. S. Rushworth, *Nat. Neurosci.* **9**, 940 (2006).
34. P. H. Rudebeck *et al.*, *J. Neurosci.* **28**, 13775 (2008).
35. P. H. Rudebeck, E. A. Murray, *J. Neurosci.* **28**, 8338 (2008).
36. P. H. Rudebeck, M. J. Buckley, M. E. Walton, M. F. S. Rushworth, *Science* **313**, 1310 (2006).
37. Materials and methods are available as supporting material on *Science* Online.
38. M. F. S. Rushworth, P. D. Nixon, M. J. Eacott, R. E. Passingham, *J. Neurosci.* **17**, 4829 (1997).
39. M. Mishkin, F. J. Manning, *Brain Res.* **143**, 313 (1978).
40. R. Passingham, *Brain Res.* **92**, 89 (1975).
41. S. T. Carmichael, J. L. Price, *J. Comp. Neurol.* **363**, 642 (1995).
42. M. J. Webster, J. Bachevalier, L. G. Ungerleider, *Cereb. Cortex* **4**, 470 (1994).
43. N. D. Daw, Y. Niv, P. Dayan, *Nat. Neurosci.* **8**, 1704 (2005).
44. E. K. Miller, T. J. Buschman, in *Neuroscience of Rule-Guided Behavior*, S. A. Bunge, J. D. Wallis, Eds. (Oxford Univ. Press, New York, 2008), pp. 419–440.
45. S. P. Wise, E. A. Murray, C. R. Gerfen, *Crit. Rev. Neurobiol.* **10**, 317 (1996).
46. M. J. Buckley, D. Gaffan, *Trends Cogn. Sci.* **10**, 100 (2006).
47. K. Tanaka, *Annu. Rev. Neurosci.* **19**, 109 (1996).
48. R. Dias, T. W. Robbins, A. C. Roberts, *Nature* **380**, 69 (1996).
49. T. L. Moore, S. P. Schettler, R. J. Killiany, D. L. Rosene, M. B. Moss, *Behav. Neurosci.* **123**, 231 (2009).
50. Y. Chudasama, J. D. Kralik, E. A. Murray, *Cereb. Cortex* **17**, 1154 (2006).
51. M. F. S. Rushworth, M. E. Walton, S. W. Kennerley, D. M. Bannerman, *Trends Cogn. Sci.* **8**, 410 (2004).
52. K. A. Hadland, M. F. S. Rushworth, D. Gaffan, R. E. Passingham, *J. Neurophysiol.* **89**, 1161 (2003).
53. M. M. Botvinick, T. S. Braver, D. M. Barch, C. S. Carter, J. D. Cohen, *Psychol. Rev.* **108**, 624 (2001).
54. F. A. Mansouri, M. J. Buckley, K. Tanaka, *Science* **318**, 987 (2007).
55. M. F. S. Rushworth, T. E. J. Behrens, *Nat. Neurosci.* **11**, 389 (2008).
56. M. R. Roesch, A. R. Taylor, G. Schoenbaum, *Neuron* **51**, 509 (2006).
57. M. E. Walton, D. M. Bannerman, K. Alterescu, M. F. S. Rushworth, *J. Neurosci.* **23**, 6475 (2003).
58. T. E. J. Behrens, M. W. Woolrich, M. E. Walton, M. F. S. Rushworth, *Nat. Neurosci.* **10**, 1214 (2007).
59. F. A. Mansouri, K. Tanaka, M. J. Buckley, *Nat. Rev. Neurosci.* **10**, 141 (2009).
60. M. Petrides, *J. Neurosci.* **15**, 359 (1995).
61. D. Gaffan, *Philos. Trans. R. Soc. London Ser. B Biol. Sci.* **357**, 1111 (2002).
62. P. W. Burgess, E. Veitch, A. D. Costello, T. Shallice, *Neuropsychologia* **38**, 848 (2000).
63. D. Badre, J. Hoffman, J. W. Cooney, M. D'Esposito, *Nat. Neurosci.* **12**, 515 (2009).
64. D. Badre, *Trends Cogn. Sci.* **12**, 193 (2008).
65. E. Koechlin, A. Hyafil, *Science* **318**, 594 (2007).
66. P. W. Burgess, S. J. Gilbert, I. Dumontheil, *Philos. Trans. R. Soc. London B Biol. Sci.* **362**, 887 (2007).

67. This research was jointly supported by a Royal Society University Research Fellowship (M.J.B.), a U.K. Medical Research Council (MRC) project grant (M.J.B.), a grant-in-aid for Scientific Research on Priority Areas from the Ministry of Education, Culture, Sports, Science, and Technology of Japan (K.T.), and an MRC program grant held by D. Gaffan, whom we thank for encouragement and support. We also wish to thank M. G. Baxter for assistance with anesthesia, and G. J. Daubney, K. Rockland, N. Ichinohe, H. Mashiko, and Y. Abe for assistance in preparing tissues for histology.

Supporting Online Material

www.sciencemag.org/cgi/content/full/325/5936/52/DC1
Materials and Methods
SOM Text
Figs. S1 to S6
References

17 February 2009; accepted 26 May 2009
10.1126/science.1172377

REPORTS

H_2O at the Phoenix Landing Site

P. H. Smith,[1]* L. K. Tamppari,[2] R. E. Arvidson,[3] D. Bass,[2] D. Blaney,[2] W. V. Boynton,[1] A. Carswell,[4] D. C. Catling,[5] B. C. Clark,[6] T. Duck,[7] E. DeJong,[2] D. Fisher,[8] W. Goetz,[9] H. P. Gunnlaugsson,[10] M. H. Hecht,[2] V. Hipkin,[11] J. Hoffman,[12] S. F. Hviid,[9] H. U. Keller,[9] S. P. Kounaves,[13] C. F. Lange,[14] M. T. Lemmon,[15] M. B. Madsen,[16] W. J. Markiewicz,[9] J. Marshall,[17] C. P. McKay,[18] M. T. Mellon,[19] D. W. Ming,[20] R. V. Morris,[20] W. T. Pike,[21] N. Renno,[22] U. Staufer,[23] C. Stoker,[18] P. Taylor,[24] J. A. Whiteway,[24] A. P. Zent[18]

The Phoenix mission investigated patterned ground and weather in the northern arctic region of Mars for 5 months starting 25 May 2008 (solar longitude between 76.5° and 148°). A shallow ice table was uncovered by the robotic arm in the center and edge of a nearby polygon at depths of 5 to 18 centimeters. In late summer, snowfall and frost blanketed the surface at night; H_2O ice and vapor constantly interacted with the soil. The soil was alkaline (pH = 7.7) and contained $CaCO_3$, aqueous minerals, and salts up to several weight percent in the indurated surface soil. Their formation likely required the presence of water.

The Phoenix mission, the first of NASA's Scout class, landed inside the arctic circle of Mars on 25 May 2008 at 23:38:24 UTC during the late northern spring. Phoenix was designed to verify the presence of subsurface H_2O ice (*1*) that was previously predicted on the basis of thermodynamic principles (*2*, *3*) and was mapped at low resolution (~500 km) within 1 m of the surface by using Odyssey's Gamma-Ray Spectrometer (GRS) instrument (*4*–*6*). Here, we address the properties of subsurface ice as well as the interaction of atmospheric water with the surface soil and the evidence that water modified this soil in the past.

Phoenix landed at 68.22°N, 234.25°E (areocentric) at an elevation of –4.1 km (referenced to Mars Orbiter Laser Altimeter areoid) on a valley floor covered by the Scandia Formation estimated to be Amazonian in age, a deposit that surrounds the northern margin of a shield volcano named Alba Patera (*7*, *8*). The Scandia Formation is interpreted as volcanic ash erupted from Alba Patera and/or as ancient polar deposits (*9*). The site also contains eroded ejecta deposits from a 10-km-diameter, bowl-shaped crater, Heimdal (fig. S1). Phoenix landed on darker ejecta deposits 20 km southwest of the crater.

The dominance of polygonal ground at the landing site (Fig. 1A) is consistent with the presence of widespread, shallow, cohesive icy soil that has undergone seasonal or longer-term freezing.

[1]Lunar and Planetary Laboratory, University of Arizona, Tucson, AZ 85721, USA. [2]Jet Propulsion Laboratory, California Institute of Technology, Pasadena, CA 91109, USA. [3]Department of Earth and Planetary Sciences, Washington University, St. Louis, MO 63130, USA. [4]Optech Incorporated, Vaughan, Ontario L4K 5Z8, Canada. [5]University of Bristol, Bristol BS8 1RJ, UK, and Department of Earth and Space Sciences, University of Washington, Seattle, WA 98195, USA. [6]Space Science Institute, Boulder, CO 80301, USA. [7]Dalhousie University, Halifax, Nova Scotia B3H 1Z9, Canada. [8]Geological Survey of Canada and University of Ottawa, Ottawa, Ontario K1A 0E8, Canada. [9]Max Planck Institute for Solar System Research, 31791 Katlenburg-Lindau, Germany. [10]Institute of Physics and Astronomy, University of Aarhus, DK-8000 Aarhus C, Denmark. [11]Canadian Space Agency, Saint-Hubert, Quebec J3Y 8Y9, Canada. [12]University of Texas–Dallas, Richardson, TX 75080, USA. [13]Tufts University, Medford, MA 02155, USA. [14]University of Alberta, Edmonton, Alberta T6G 2H1, Canada. [15]Texas A&M University, College Station, TX 77843, USA. [16]Earth and Planetary Physics, University of Copenhagen, 2100 Copenhagen, Denmark. [17]SETI Institute, Mountain View, CA 94043, USA. [18]NASA Ames Research Center, Mountain View, CA 94035, USA. [19]University of Colorado, Boulder, CO 80309, USA. [20]NASA Johnson Space Center, Houston, TX 77058, USA. [21]University of Michigan, Ann Arbor, MI 48109, USA. [22]Imperial College, London SW7 2AZ, UK. [23]Institute of Microtechnology, University of Neuchâtel, 2002 Neuchâtel, Switzerland, and Micro and Nano Engineering Laboratory, Delft University of Technology, 2628 CD Delft, Netherlands. [24]York University, Toronto, Ontario M3J 1P3, Canada.

*To whom correspondence should be addressed. E-mail: psmith@lpl.arizona.edu

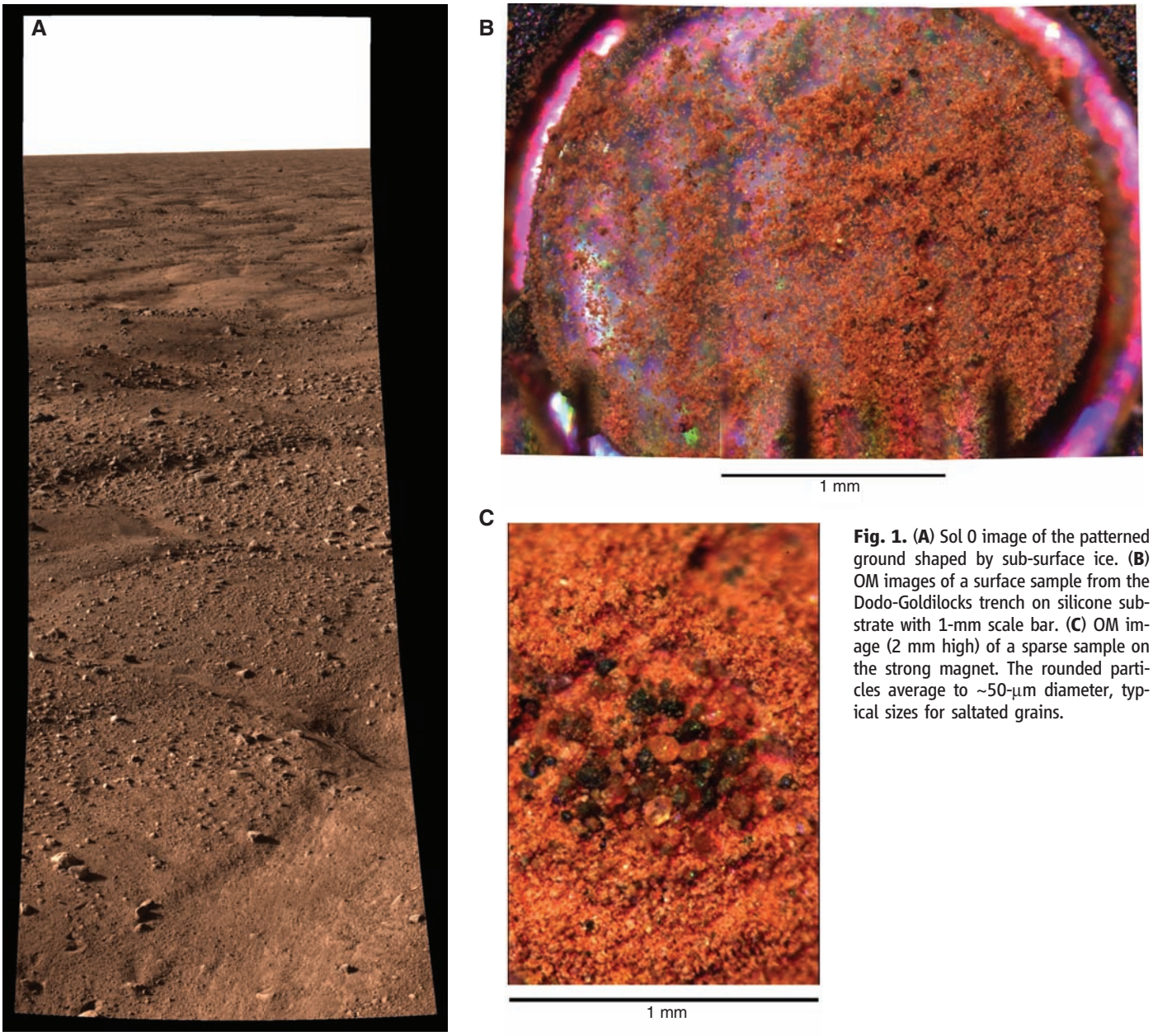

Fig. 1. (**A**) Sol 0 image of the patterned ground shaped by sub-surface ice. (**B**) OM images of a surface sample from the Dodo-Goldilocks trench on silicone substrate with 1-mm scale bar. (**C**) OM image (2 mm high) of a sparse sample on the strong magnet. The rounded particles average to ~50-μm diameter, typical sizes for saltated grains.

Contraction cracks fill with aeolian sediments and are not able to close when the icy soil warms, causing bulging of the polygon interiors (*10*). The troughs between the 2- to 3-m diameter polygons have depths of 20 to 50 cm relative to the centers. Small rocks are abundant and generally associated with troughs, but larger rocks (>1 m) are rare. A small amount of adsorbed or volumetrically bound water in the surface layer is implied by near-infrared (NIR) data from the OMEGA (Observatoire pour la Minéralogie, l'Eau, les Glaces, et l'Activité imaging spectrometer on Mars Express) and CRISM (Compact Reconnaissance Imaging Spectrometer for Mars on Mars Reconnaissance Orbiter) orbiting spectrometers at this site.

The 2.35-m Robotic Arm (RA) and associated Icy Soil Acquisition Device (ISAD) were used to excavate a dozen trenches (*11*) to the north and northeast of the lander. The upper few cm of soil is crusted, and clods were observed around the trenches and inside the RA scoop. Special procedures were developed, the "sprinkle" techniques, to reduce the clumpiness of the delivered samples.

Optical Microscope (OM) images (Fig. 1B) show particles that are the components of the soil; by number, the dominant size consists of reddish fine-grained agglomerates <10 μm across. These small particles are just under the resolution limit of the OM, but Atomic Force Microscope (AFM) imaging shows that many particles have a platy morphology (fig. S4). A second size distribution likely of different origin includes magnetic (20 to 100 μm) particles (Fig. 1C); many are black, suggesting magnetite, whereas others are brownish and less opaque. These larger particles are rounded and likely weathered by saltation. In terms of soil mass, 20% is in the reddish small particles and the other 80% in the larger particles.

The soil is likely of aeolian origin, but the crust that produces the clods formed in place. The mechanical properties are similar to those found by the Viking Lander 2 (*12*). The cloddy nature of the soil may be a consequence of cementation by carbonates (*13*) and other salts in association with small amounts of water. Because no ripples or dunes are seen, the landscape is likely deflated: Dust devils observed by Phoenix (fig. S5) scour the surface mobilizing airfall dust.

The diffusion of H_2O vapor into and out of the regolith during diurnal and seasonal cycles may produce unfrozen films of water around

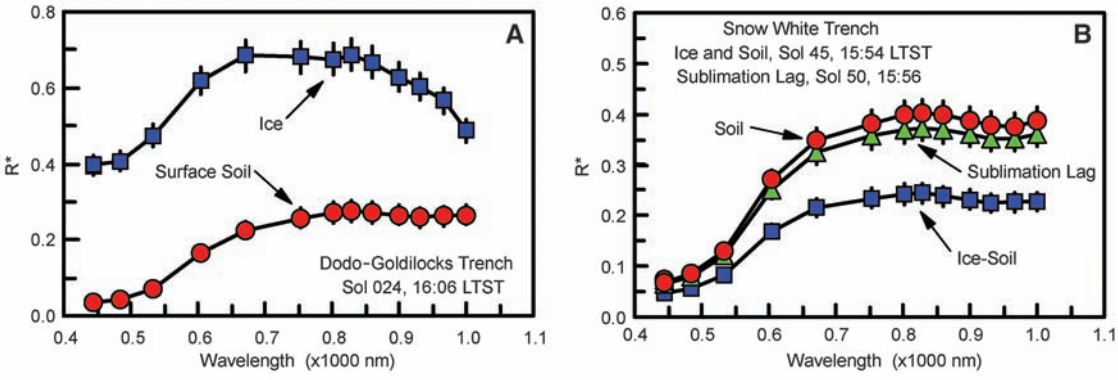

Fig. 2. Spectra reveal two different concentrations of ice mixed with soil. Error bars indicate 1σ uncertainties. (**A**) The Dodo-Goldilocks trench matches high-albedo ice with a minor soil component (<2%) compared with nearby ice-free soil exposed in the trench bottom. (**B**) The spectra in the Snow White trench correspond to low-albedo ice with a major soil component, and nearby ice-free surface soil exposed in the trench bottom and to the sublimation lag developed 5 sols later at the same location as the ice.

soil particles (*14*). The Thermal and Electrical Conductivity Probe (TECP) electrical conductivity measurements were consistent with a fully open circuit, implying that there was no effective transport of charge carriers on the scale of 15 mm. Nighttime increases in regolith dielectric permittivity, observed during the latter half of the mission (mid to late summer), imply an overnight accumulation of H_2O molecules.

A surface sample taken from the Dodo trench (fig. S8) shows two regions of water release in the Thermal and Evolved-Gas Analyzer (TEGA) oven (fig. S6, A and B): a low-temperature release from 295° to 735°C and a high-temperature release beginning near 735°C. Both indicate the presence of hydrous minerals or phases. The low-temperature region is likely indicative of phases that formed through aqueous processes. Candidate phases include iron oxyhydroxides (e.g., goethite dehydroxylation onset around 250°C), smectites (e.g., nontronite dehydroxylation onset around 300°C), kaolinite (dehydroxylation onset from 400° to 550°C depending on crystallinity), iron sulfates (e.g., jarosite dehydroxylation onset near 400°C), and magnesium sulfates (e.g, kieserite loss of crystalline water near 350°C).

The high-temperature region may reflect the presence of phases that have formed by aqueous or rock-forming processes. Candidates are smectites (e.g., montmorillonite dehydroxylation from 600° to 800°C and saponite dehydroxylation near 700° to 800°C), chlorites, talc (dehydroxylation from 750° to 850°C), serpentines (e.g., antigorite dehydroxylation from 600° to 800°C), and amphiboles (e.g., dehydroxylation near 1000°C).

TEGA has not detected low-temperature release of H_2O in the surface soils. A null detection below 295°C implies an arid soil with no adsorbed water or interstitial ice. This is unexpected because perchlorate salts (*15*) are expected to bind six to eight H_2O molecules at these cold temperatures and orbital observations detect a strong 3-μm water absorption band. TECP indicates that the soil is adsorbing water vapor at night.

Bright material was seen in one trench (Dodo-Goldilocks) at a depth of 4 to 5 cm. This material had a broad ≥1-μm absorption (*16*) and was bright in the blue filter (<0.5 μm), consistent with coarse-grained H_2O ice containing a few percent of dust

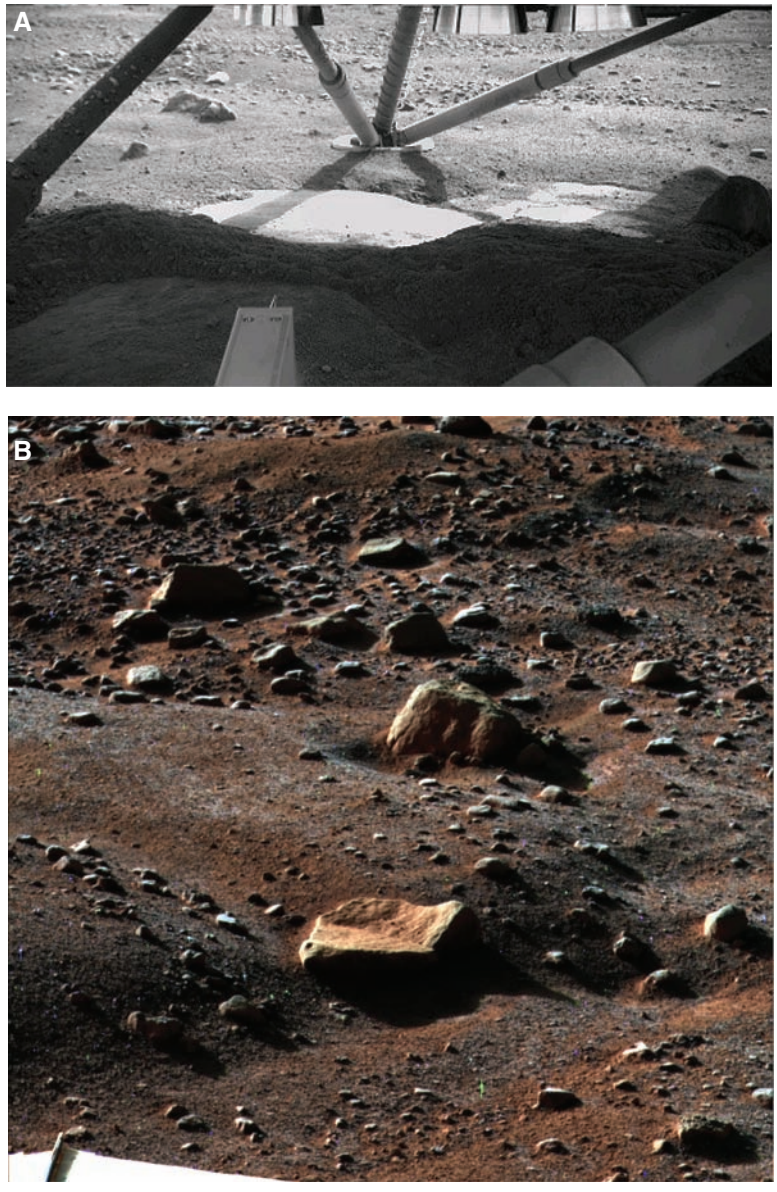

Fig. 3. (**A**) An image taken by the RA camera pointed under the lander, showing the ice table exposed by the thrusters. (**B**) Nighttime image of surface frost from sol 80 (L_s = 113°).

(Fig. 2A). Other trenches showed a weaker spectral contrast. In the Snow White trench, the ISAD scraped into a hard, icy layer that appeared to be pore ice (Fig. 2B); its albedo varied from midday to early morning (fig. S7, A and B) likely because of photometric changes in the illumination angle.

In Dodo-Goldilocks, several chunks of bright material 1.5 to 2 cm across were dislodged by the RA on sol 20 (*17*) and had disappeared by sol 24 without any obvious residue (fig. S8, A and B). This is expected for H_2O ice. Over the next 2 months, the material in the trench sublimated by several mm (fig. S8C). Pore ice has been predicted by thermodynamical arguments (*18*), but the exposure of nearly pure ice usually requires a liquid phase or brine on Earth. If dominant in the region, this supports the Odyssey GRS conclusion that ice concentrations exceed pore ice (*5*, *19*, *20*).

Because attempts to collect and to deliver ice-cemented soil materials to the TEGA ovens were not successful, we sampled sublimated till material at the bottom of one trench (Snow White) on sol 63. A small, endothermic peak was observed (fig. S9) coincident with the melting of ice with an onset temperature at –2°C and a peak around 6°C. Evolved water was recorded by TEGA's mass spectrometer as the temperature increased from –20° to +35°C.

Integration of the endothermic peak provides an estimate of the enthalpy of 0.35 J, which corresponds to 1.0 mg of water ice. If we assume that the TEGA oven was full, this sample contained ~2% ice. Because this sample was a sublimated lag, this does not represent the ice concentration in the ice layer.

Early in the mission, the RA pointed its camera under the lander to assess the footpad stability and captured an image of the ice table excavated by the 12 thrusters (Fig. 3A and fig. S3). The curved shadow of the strut provides a means to estimate its depth as 5 cm. The strut to the left of the image shows a number of blobs that have been interpreted as liquid brine splashed onto the strut during the last few seconds of landing (*21*). Perchlorate brines can have eutectic temperatures as low as –70°C once the perchlorate concentration reaches 30 to 50%. The planetary distribution of brines is unknown, if they exist at all, but salts do tend to concentrate with the presence of small amounts of water.

Atmospheric water vapor was measured regularly by using the TECP (fig. S10). Water vapor partial pressure remained near 2 Pa throughout most days, dropping rapidly at 18. local true solar time (LTST) to a minimum of <0.05 at 1.5 LTST. Vapor pressure of 2 Pa is about that of saturation over ice at 210 K. The water vapor measurements and 2-m air temperatures suggest that the typical mid-sol relative humidity was ~5%. The air was close to saturation at night early in the mission and was saturated toward the end, as seen via ground fog and low clouds (*22*). Surface temperatures are expected to be colder than those measured at 2 m, and indeed frost formation was observed in the second half of the mission (Fig. 3B).

Water ice clouds were detected by the light detection and ranging (LIDAR) (*23*) instrument as layers of enhanced back scatter. Near summer solstice, the most prominent clouds were detected at heights above 10 km. As the season progressed and the polar atmosphere cooled, clouds formed in the boundary layer in late summer [after solar longitude of Mars (L_s) = 117°], and fall streaks are clearly seen in the LIDAR observations (*22*). Late at night water ice was observed to fall from the clouds at 4 km altitude, and ground fogs were seen in the lower ~700 m of atmosphere (*22*). This diurnal cycle deposited ice onto the surface at night, reducing the vapor pressure to low values (fig. S10), sublimated it in the morning, and redistributed it throughout the planetary boundary layer in the turbulent afternoon. Near midnight, ice clouds formed and precipitated a portion of the atmospheric H_2O back to the surface in the early morning.

Orbital dynamics and particularly obliquity variations strongly influence the martian climate (*24*) and offer the possibility of liquid water in the recent past. As the obliquity exceeds 30°, the polar cap becomes warmer and increasingly unstable, releasing water vapor into the atmosphere. Models predict a wetter environment when the summer temperatures are able to exceed 0°C (*25*).

The pressure at the Phoenix landing site is always higher than the triple point pressure. Several lines of evidence support liquid films of water in the soil in the recent past: $CaCO_3$ identified by TEGA (*13*) likely forms in a wet environment, segregated ice (fig. S8, A to C) is a signature of frozen liquid water, soil is often cemented by wetted soils, and the likelihood of thicker snowfalls melting during the warmer days at high obliquity. This evidence for periodic liquid water in an alkaline environment with a sprinkling of various salts and a perchlorate energy source (*15*) implies that this region could have previously met the criteria for habitability during favorable Milankovich cycles.

References and Notes

1. P. H. Smith *et al.*, *J. Geophys. Res.* **113**, 10.1029/2008JE003083 (2008).
2. M. T. Mellon, B. M. Jakosky, *J. Geophys. Res.* **100**, 11781 (1995).
3. R. B. Leighton, B. C. Murray, *Science* **153**, 136 (1966).
4. I. G. Mitrofanov *et al.*, *Science* **300**, 2081 (2003).
5. W. V. Boynton *et al.*, *Science* **297**, 81 (2002); published online 30 May 2002 (10.1126/science.1073722).
6. W. Feldman *et al.*, *Science* **297**, 75 (2002); published online 30 May 2002 (10.1126/science.1073541).
7. R. E. Arvidson *et al.*, *J. Geophys. Res.* **113**, E00A03 (2008).
8. K. L. Tanaka, J. A. Skinner Jr., T. M. Hare, *U.S. Geol. Surv. Sci. Inv. Map (SIM) 2888* (2005).
9. K. Seelos *et al.*, *J. Geophys. Res.* **113**, E00A13 (2008).
10. M. T. Mellon *et al.*, *J. Geophys. Res.* **113**, E00A23 (2008).
11. R. Bonitz *et al.*, *J. Geophys. Res.* **113**, E00A01 (2008).
12. H. Moore *et al.*, *U.S. Geol. Surv. Prof. Pap.* 1389 (1987).
13. W. V. Boynton *et al.*, *Science* **325**, 61 (2009).
14. A. Zent, *Icarus* **196**, 385 (2008).
15. M. H. Hecht *et al.*, *Science* **325**, 64 (2009).
16. The longest wavelength filter available is at 1 μm, and the trend was downward.
17. A martian solar day has a mean period of 24 hours 39 min 35.244 s and is referred to as a sol to distinguish this from a ~3% shorter solar day on Earth.
18. M. T. Mellon *et al.*, *J. Geophys. Res.* **113**, E00A25 (2008).
19. W. C. Feldman *et al.*, *Geophys. Res. Lett.* **34**, 10.1029/2006GL028936 (2007).
20. D. A. Fisher, *Icarus* **179**, 387 (2005).
21. N. Renno *et al.*, *Lunar Planet. Sci. Conf.* **XL** (abstr. 1440) (2009).
22. J. A. Whiteway *et al.*, *Science* **325**, 68 (2009).
23. J. Whiteway *et al.*, *J. Geophys. Res.* **113**, 10.1029/2007JE003002 (2008).
24. J. A. Laskar *et al.*, *Icarus* **170**, 343 (2004).
25. R. M. Haberle, J. R. Murphy, J. Shaeffer, *Icarus* **161**, 66 (2003).

26. We thank our project manager, B. Goldstein; the Jet Propulsion Laboratory team; and our aerospace partner, Lockheed Martin. The University of Arizona supported Phoenix throughout the mission. We appreciate the help of the orbiter teams, in particular, the THEMIS (Thermal Emission Imaging System) team [P. Christensen, principal investigator (PI)] and the HiRISE (High-Resolution Imaging Science Experiment) team (A. McEwen, PI). Funding for this research came from NASA and the Canadian Space Agency.

Supporting Online Material

www.sciencemag.org/cgi/content/full/325/5936/58/DC1
Materials and Methods
Figs. S1 to S10
References

16 February 2009; accepted 1 June 2009
10.1126/science.1172339

Evidence for Calcium Carbonate at the Mars Phoenix Landing Site

W. V. Boynton,[1]* D. W. Ming,[2] S. P. Kounaves,[3] S. M. M. Young,[3]† R. E. Arvidson,[4] M. H. Hecht,[5] J. Hoffman,[6] P. B. Niles,[2] D. K. Hamara,[1] R. C. Quinn,[7] P. H. Smith,[1] B. Sutter,[10] D. C. Catling,[8,9] R. V. Morris[2]

Carbonates are generally products of aqueous processes and may hold important clues about the history of liquid water on the surface of Mars. Calcium carbonate (approximately 3 to 5 weight percent) has been identified in the soils around the Phoenix landing site by scanning calorimetry showing an endothermic transition beginning around 725°C accompanied by evolution of carbon dioxide and by the ability of the soil to buffer pH against acid addition. Based on empirical kinetics, the amount of calcium carbonate is most consistent with formation in the past by the interaction of atmospheric carbon dioxide with liquid water films on particle surfaces.

The key to understanding Mars' past climate is the study of secondary minerals that have formed by reaction with volatile compounds such as H_2O and CO_2. A wet and warmer climate during the early history of Mars, coupled with a much denser CO_2 atmosphere,

are ideal conditions for the aqueous alteration of basaltic materials and the subsequent formation of carbonates (*1*, *2*). Although Mg- and Ca-rich carbonates are expected to be thermodynamically stable in the present martian environment (*3*, *4*), there have been few detections of carbonates on the surface by orbiting or landed missions to Mars. Earth-based thermal emission observations of Mars were the first to indicate the presence of carbonates in the martian dust (1 to 3 volume percent) (*5*). Mg-rich carbonates have been suggested to be a component [2 to 5 weight percent (wt %)] of the martian global dust based on the presence of a 1480 cm^{-1} absorption feature in orbital thermal emission spectroscopy (*6*). A similar feature was observed in brighter, undisturbed soils by the Miniature Thermal Emission Spectrometer on the Gusev plains (*7*). Mg-rich carbonates have recently been identified in the Nili Fossae region by the Compact Reconnaissance Imaging Spectrometer for Mars instrument onboard the Mars Reconnaissance Orbiter (*8*), prompting the idea that the Mg-rich carbonates in the dust might be due to the eolian redistribution of surface carbonates. Carbonates have also been confirmed as aqueous alteration phases in martian meteorites (*9*–*11*).

Here, we describe observations made by instruments on the Phoenix Lander relevant to the identification of calcium carbonate in the soil: the Thermal and Evolved-Gas Analyzer (TEGA), which is similar to the TEGA instrument flown on the Mars Polar Lander (*12*), and the Microscopy, Electrochemical, and Conductivity Analyzer (MECA) (*13*). TEGA consisted of eight thermal analyzer cells that each contained an oven in which samples were heated up to 1000°C at a controlled ramp rate, with the necessary power recorded for calorimetry. Any gases that were generated from the heated samples were carried to the evolved-gas analyzer by a N_2 carrier gas maintained at 12 mbar oven pressure (*14*). The MECA contained a Wet Chemistry Laboratory (WCL) that consisted of four analyzer cells, each of which added an aqueous solution to the soil and measured electrchemical parameters such as pH and the concentrations of various ions before and after the addition of various chemical reagents.

Soils analyzed by TEGA have similar thermal and evolved gas behaviors. Here, we focus on a subsurface sample dubbed Wicked Witch (*15*). We looked for an endothermic phase transition by fitting a curve to the oven power as a function of temperature and looked for differences from the smooth baseline fit. For the thermal analysis of a sample we routinely heated the oven containing the sample a second time with an identical temperature ramp within a day or two after the initial heating and compared the results to check for background transitions that occurred in the oven itself.

A clear endothermic peak is seen between 725°C and 820°C, and there is another one between about 860°C and 980°C (Fig. 1). The phase responsible for the 860°C peak is unidentified at this time. The most likely phase candidate for the 725°C endothermic reaction is a calcium-rich carbonate mineral phase (e.g., calcite, ikaite, aragonite, or ankerite) (*16*). The area of the endothermic peak is about 6 J. Based on the calcite decomposition enthalpy of 2550 J/g (*17*) we estimate that there is 2.4 mg of $CaCO_3$ in the sample. For a TEGA oven volume of 0.052 cm^3, full with a 1 g/cm^3 sample, the concentration of $CaCO_3$ is about 4.5 wt % (*18*).

The amount of CO_2 generated during the heating is shown in Fig. 2. There is a low-temperature release between 400°C and 680°C, which may be due to Mg or Fe carbonate, adsorbed CO_2 contained in a zeolite type phase, or organic molecules that are converted to CO_2 by oxidants in the soil. We made an independent estimate of the amount of $CaCO_3$ from the amount of CO_2 generated at higher temperatures. The majority of the high-temperature gas release appears to happen at a temperature higher than that of the oven phase transition (Fig. 2). There is a time lag of about 3 min or 60° for the gas to reach the EGA, but the observed time lag is greater than expected (*19*). Pending laboratory studies, this time lag may represent an interaction between the CO_2 and the walls of the plumbing. The area under the peak corresponds to 0.66 mg of CO_2, which implies a concentration of 3 wt % $CaCO_3$ in the sample. Based on the combined calorimetry and evolved gas results, the Wicked Witch sample has on the order of 3 to 5 wt % $CaCO_3$.

The WCL was designed to perform an assay for carbonate using classical wet chemical methods based on sample acidification. After 25 mL of water and a calibrant were added to the WCL beaker, soil was added and the pH was measured for a period of time. After a 4-sol freeze and subsequent thaw, 2.5×10^{-5} mole of 2-nitrobenzoic acid was dispensed into the soil solution (*20*). The pH was monitored by two ion selective polymer membrane pH electrodes and an iridium oxide pH electrode (*12*). Based on the acid dissociation constant (pK_a) of 2-nitrobenzoic acid, the pH of the WCL solution should be 3.2 after acid addition in the absence of buffering.

After a surface sample dubbed Rosy Red (*15*) was added, the pH of the WCL leaching solution rose to 7.7 ± 0.5, a value consistent with the pH of a carbonate buffered solution and a partial pressure of CO_2 (P_{CO_2}) of ~0.3 mbar in the WCL headspace (Fig. 3A). Over the course of sols 30 to 34, the pH reading decreased slightly to pH 7.5 ± 0.5, possibly due to changes in headspace P_{CO_2}, temperature, or intrinsic sensor drift. The addition of acid to the sample solution did not change the pH, confirming that the system is buffered by carbonate (Fig. 3B). The addition of the acid was confirmed by WCL cyclic voltammetry measurements, which detect the presence of 2-nitrobenzoic acid in solution. If calcium carbonate is the only saturated carbonate species present and thermodynamically independent of other equilibrium reactions, its solubility product Ksp will determine the upper limit of Ca^{2+} concentration in solution. The measured Ca^{2+} concentration in the Rosy Red soil solution of $5.5(\pm3.0) \times 10^{-4}$ M is consistent with a P_{CO_2} of ~0.3 mbar and a saturated calcium carbonate solution (*21*).

Assuming that a 1 cm^3 sample with a density of 1 g/cm^3 was added to the WCL cell, equilib-

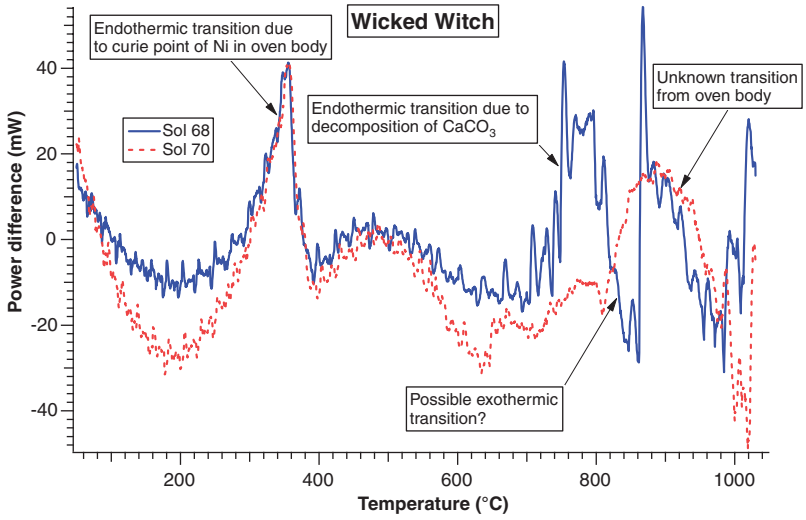

Fig. 1. Plot of differential power (relative to a degree 4 polynomial fit) for the subsurface sample dubbed Wicked Witch.

[1]Lunar and Planetary Laboratory, University of Arizona, Tucson, AZ 85721, USA. [2]Johnson Space Center, Houston, TX 77058, USA. [3]Department of Chemistry, Tufts University, Medford, MA 02155, USA. [4]Department of Earth and Planetary Sciences, Washington University, Saint Louis, MO 63130, USA. [5]Jet Propulsion Laboratory, Pasadena, CA 91109, USA. [6]Department of Physics, University of Texas at Dallas, Richardson, TX 75083, USA. [7]SETI Institute, NASA Ames Research Center, Moffett Field, CA 94035, USA. [8]Department of Earth Sciences, University of Bristol, Bristol BS8 1RJ, UK. [9]Department of Earth and Space Sciences, University of Washington, Seattle, WA 98195, USA. [10]Jacobs Engineering and Science Contract Group, NASA Johnson Space Center, Houston, TX 77058, USA.

*To whom correspondence should be addressed. E-mail: wboynton@LPL.Arizona.edu

†Present address: Department of Chemistry, University of New Hampshire, Durham, NH 03824, USA.

rium calculations based on the measured ion concentrations in solution and the quantity of acid added show that the amount of calcium carbonate needed to neutralize the acid is 0.3% by weight. Lacking a full titration of the amount of carbonate, this quantity is only a lower limit to the concentration of calcium carbonate in the soil. Two other samples, both subsurface samples from the Sorceress location (similar to Wicked Witch), were shown also to contain ≥ 0.3% of calcium carbonate by weight. The WCL results are entirely consistent with the TEGA calorimetry and evolved-gas data, which strongly suggest the presence of calcium carbonate in the soils around the Phoenix landing site.

Low-temperature carbonate dissolution and precipitation are among the most important pedogenic processes in terrestrial semiarid to arid soils (*22*). Carbonates precipitate as coatings on soil particles and in soil pores that can result in cementation of particles. Calcium carbonate generally precipitates by reaction of CO_2-charged water with Ca^{2+} released by dissolution of parent materials. Soils at the Phoenix landing site are in physical proximity to an ice-cemented soil layer several cm under the surface and are covered with a surface frost during the winter. These water reservoirs suggest the diffusion of water vapor through the soils (*23*) and the possibility of films of unfrozen water on particle surfaces. The latter can weather basaltic minerals and mobilize ions (*24*, *25*). Given that atmospheric CO_2 would dissolve in these thin films, calcium carbonate would precipitate if the water film becomes supersaturated. These precipitation events may be facilitated by the evaporation of the thin films during diurnal or seasonal cycles and may be much more frequent during periods of high obliquity (*26*). Another possibility for the formation of calcium carbonate is by hydrothermal aqueous alteration associated with an impact event or other thermal source (e.g., volcanic). An impact event into a volatile-rich target (i.e., ice and ice-cemented sediments) would rapidly melt and/or vaporize the ice, resulting in localized hydrothermal conditions. The Phoenix landing site lies on the ejecta of the Heimdall crater, which is located 20 km away. Consequently, calcium carbonate formed in the subsurface may have been transported to the Phoenix site by the excavation of subsurface material during the impact event that formed Heimdall. In this case, calcium carbonate has persisted in the soil since the impact event, ~0.5 billion years ago (*27*).

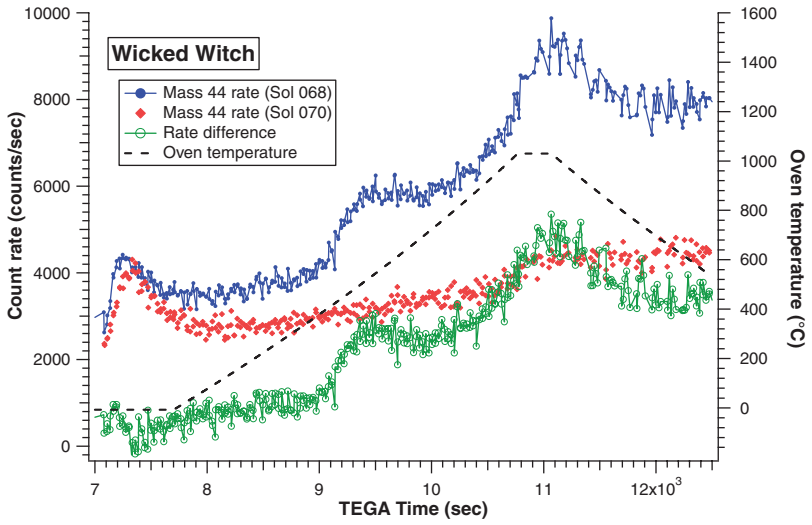

Fig. 2. Plot of Mass 44 (CO_2) count rate and temperature versus run time. The first peak is atmospheric CO_2 that diffuses into the oven and plumbing overnight; the second may be due to carbonates with a low decomposition temperature (e.g., $FeCO_3$ or $MgCO_3$). The high temperature peak is due to decomposition of $CaCO_3$.

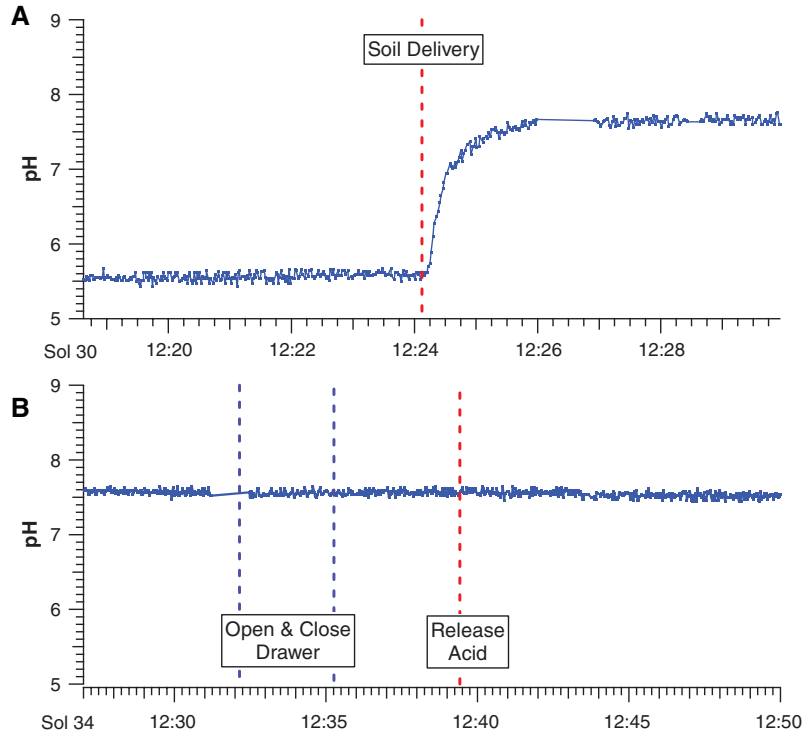

Fig. 3. Plot of pH versus local Mars time (**A**) upon soil delivery and (**B**) upon addition of 2-nitrobenzoic acid.

There are nonaqueous processes that can form carbonates, but the reaction rates appear to be far too small to account for the amount of calcium carbonate that we find (*28*). The presence of several percent by mass of calcium carbonate in the soil at the Phoenix site is of the expected magnitude if there has been periodically wet or damp martian soil in the geologic past, but it is difficult to produce under current martian conditions. This inference applies even if the calcium carbonate has been transported to the Phoenix site by wind, because the calcium carbonate would still have formed in damp or wet soil elsewhere on Mars. Two possible objections are (i) that the carbonate might be magmatic (e.g., carbonatites) and (ii) that the soil particles might have an abnormally large specific surface area, which would make a larger mass fraction of dry carbonate formation more feasible. There is, however, no evidence to support either objection. For the latter, preliminary analysis of microscopic imagery (*29*) indicates a modest specific surface area. Consequently, the simplest explanation is that the amount of carbonate provides geochemical evidence of past liquid water.

The presence of calcium carbonate in the soil has implications for our understanding of Mars. Calcium carbonate buffers an alkaline pH, which is similar to that of many habitable environments, notably terrestrial seawater. Another implication of the presence of calcium carbonate is that various ions may be adsorbed at exposed Ca^{2+} lat-

tice sites of calcium carbonate and affect Mars' soil geochemistry, and calcium carbonate can cement small soil grains and change the physical properties of the surface of Mars.

References and Notes

1. J. B. Pollack *et al*., *Icarus* **71**, 203 (1987).
2. D. C. Catling *et al*., *J. Geophys. Res.* **104**, 16453 (1999).
3. J. L. Gooding, *Icarus* **33**, 483 (1978).
4. M. C. Booth, H. H. Kieffer, *J. Geophys. Res.* **83**, 1809 (1978).
5. J. B. Pollack *et al*., *J. Geophys. Res.* **95**, 14595 (1990).
6. J. L. Bandfield *et al*., *Science* **301**, 1084 (2003).
7. P. R. Christensen *et al*., *Science* **305**, 837 (2004).
8. B. L. Ehlmann *et al*., *Science* **322**, 1828 (2008).
9. J. C. Bridges, M. M. Grady, *Meteorit. Planet. Sci.* **34**, 407 (1999).
10. J. C. Bridges, M. M. Grady, *Earth Planet. Sci. Lett.* **176**, 267 (2000).
11. J. C. Bridges *et al*., *Space Sci. Rev.* **96**, 365 (2001).
12. W. V. Boynton *et al*., *J. Geophys. Res.* **106**, 17,683 (2001).
13. S. P. Kounaves *et al*., *J. Geophys. Res.* **113**, 10.1029/2008JE003084 (2009).
14. J. H. Hoffman *et al*., *J. Am. Soc. Mass Spectrom.* **19**, 1377 (2008).
15. R. E. Arvidson *et al*., Abstr. 1067, 40th Lunar and Planetary Science Conference, The Woodlands, TX, 23 to 27 March 2009.
16. The onset temperature for this endothermic peak is similar to the calcite decomposition onset temperature of 738°C measured in the TEGA engineering qualification model (*17*). Other carbonates have decomposition temperatures that are lower than that of calcite.
17. In a calibration run on the TEGA engineering qualification model with a known amount of calcite, we found the heat of transition to be 2550 J/g, which implies 2.4 mg of $CaCO_3$ in the Wicked Witch sample.
18. Estimation of the concentration of calcium carbonate in the sample is uncertain because the mass of sample in the oven is not tightly constrained. We estimate that this error is on the order of ± 25%.
19. The cause of this delay will be explored in planned laboratory experiments in the future. The plumbing temperatures are heated to greater than 35°C, so one would not expect CO_2 to condense out on any plumbing surfaces. The sol 70 run shows that this effect is not due to a background signal.
20. A martian solar day has a mean period of 24 hours 39 min 35.244 s and is referred to as a sol to distinguish this from a ~3% shorter solar day on Earth.
21. W. L. Lindsay, *Chemical Equilibria in Soils* (Blackburn Press, Caldwell, NJ, 1979).
22. H. Doner, P. Grossl, in J. B. Dixon, D.G. Schulze, *Soil Mineralogy with Environmental Applications* (SSSA, Madison, WI, 2002), pp. 199–228.
23. D. Fisher, *Icarus* **179**, 387 (2005).
24. D. M. Anderson, L. W. Gatto, F. C. Ugolini, *Antarct. J.* **30**, 114 (1972).
25. J. L. Gooding, in *International Workshop on Antarctic Meteorites* (Lunar and Planetary Institute, Houston, TX, 1986), pp. 48–54.
26. A. Zent, *Icarus* **196**, 385 (2008).
27. T. L. Heet, R. E. Arvidson, M. Mellon, Abstr. 1114, 40th Lunar and Planetary Science Conference, The Woodlands, TX, 23 to 27 March 2009.
28. A previous experiment suggested that carbonate could form in relatively dry Mars-like conditions as submicrometer coatings on soil particles (*5*). However, the results from this study cannot be extrapolated over time because the experiments did not proceed beyond a monolayer of carbonate. A more comprehensive experimental study under Mars-like conditions showed that, in a given time span, carbonate forms on the surface of basaltic particles in an amount that increases with the thickness of films of water around the particles (*30*, *31*). Growth of more than a monolayer of carbonate occurs with logarithmic reaction kinetics. For damp or wet conditions (meaning 0.1 to 0.5 g H_2O per g soil, equivalent to 10^2 to 10^3 monolayers of water), the number of CO_2-reacted monolayers of substrate, L, per particle is found empirically to follow the relationship (*30*, *32*) $L(t) = D\log10(1 + t/t0)$ (Eq. 1). Here, the constant of proportionality D is ~1 monolayer CO_2/log10t for powdered basalt, while $t0$, which represents a time scale for CO_2 adsorption or dissolution in H_2O, is ~10^{-2} to 10^{-3} days. Because the Phoenix site contains material that was likely ejected from the nearby Heimdall crater up to 0.6 billion years ago (*27*), or 2.2×10^{11} (Earth) days ago, the number of monolayers reacting with CO_2 can be calculated from Eq. 1 as ~13 to 14. By stoichiometry, 1 mol of CO_2 generates 1 mol of carbonate, so it follows that the mass fraction, F, of carbonate produced under these "damp" or "wet" soil conditions would be $F = M \times [(L\ A_s/A)/N_A]$ (Eq. 2), where M is the molar mass of carbonate (100 g/mol for $CaCO_3$), A_s is the specific surface area of the particles, $A = 2 \times 10^{-19}$ m^{-2} $molecule^{-1}$ is the area taken up by a CO_2 molecule in reaction with the surface (*32*), and N_A is Avogadro's number. Basalt glasses pulverized to 0.1 to 1 micrometer size have A_s ~1 to 10 m^2/g (*33*), whereas 17 m^2/g was estimated for Viking lander 1 soil (*34*). Substituting numerical values into Eq. 2 gives a carbonate mass fraction up to 20 wt % for continuously "wet" conditions. In contrast, under persistently dry or vapor conditions (meaning zero to a few monolayers of H_2O), the fraction of carbonate produced is smaller because the kinetic coefficient D is smaller. D was measured up to 0.07 monolayers CO_2/log10t at 6.6 mbar and –15°C (*24*), giving up to 0.8 wt % in Eq. 2. Other values of D for dry or vapor conditions ranged from ~0.01 to 0.2, but high values occurred only at higher CO_2 pressures, up to 995 mbar (*32*).
29. H. U. Keller *et al*., Abstr. 1671, 40th Lunar and Planetary Science Conference, The Woodlands, TX, 23 to 27 March 2009.
30. S. K. Stephens, *Proc. Lunar Planet. Sci. Conf.* **XXVI**, 1355 (1995).
31. S. K. Stephens, thesis, California Institute of Technology, Pasadena (1995).
32. A. L. McClellan, H. F. Harnsberger, *J. Colloid Interface Sci.* **23**, 577 (1967).
33. C. Papelis, W. Um, C. E. Russell, J. B. Chapman, *Colloids Surf. A Physicochem. Eng. Asp.* **215**, 221 (2003).
34. E. V. Ballou *et al*., *Nature* **271**, 644 (1978).

35. We acknowledge the work of the Robotic Arm team in delivering the samples to TEGA and WCL and the contributions of the engineers, scientists, and managers who made these instruments and the analysis of their data possible, including H. Enos, C. Fellows, K. Harshman, M. Finch, M. Williams, M. Fitzgibbon, G. Droege, J. M. Morookian, V. Lauer, D. C. Golden, R. Chaney, H. Hammack, L. Brooks, M. Mankey, K. Gospodinova, J. Kapit, C. Cable, P. Chang, E. Coombs, and S. Stroble. The Phoenix Mission was led by the University of Arizona, Tucson, on behalf of NASA and was managed by NASA's Jet Propulsion Laboratory, California Institute of Technology, of Pasadena, CA. The spacecraft was developed by Lockheed Martin Space Systems, Denver.

25 February 2009; accepted 8 June 2009
10.1126/science.1172768

Detection of Perchlorate and the Soluble Chemistry of Martian Soil at the Phoenix Lander Site

M. H. Hecht,[1]* S. P. Kounaves,[2] R. C. Quinn,[3] S. J. West,[4] S. M. M. Young,[2]† D. W. Ming,[5] D. C. Catling,[6,7] B. C. Clark,[8] W. V. Boynton,[9] J. Hoffman,[10] L. P. DeFlores,[1] K. Gospodinova,[2] J. Kapit,[2] P. H. Smith[9]

The Wet Chemistry Laboratory on the Phoenix Mars Lander performed aqueous chemical analyses of martian soil from the polygon-patterned northern plains of the Vastitas Borealis. The solutions contained ~10 mM of dissolved salts with 0.4 to 0.6% perchlorate (ClO_4) by mass leached from each sample. The remaining anions included small concentrations of chloride, bicarbonate, and possibly sulfate. Cations were dominated by Mg^{2+} and Na^+, with small contributions from K^+ and Ca^{2+}. A moderately alkaline pH of 7.7 ± 0.5 was measured, consistent with a carbonate-buffered solution. Samples analyzed from the surface and the excavated boundary of the ~5-centimeter-deep ice table showed no significant difference in soluble chemistry.

The elemental composition of the martian surface has been measured in situ by the two Viking landers (*1*), the Mars Pathfinder lander (*2*), and the two Mars Exploration Rovers, Spirit and Opportunity (*3*, *4*) with the use of x-ray fluorescence spectrometry. Elemental analysis does not, however, predict the solution chemistry of the soil (*5*), which is important because it is the soluble constituents that are of primary importance to biological activity, prebiotic organic synthesis, and the thermophysical properties of any liquid solution. The only prior aqueous experiments were by the Viking missions in 1976, but these focused on specific protocols

[1]Jet Propulsion Laboratory, California Institute of Technology, Pasadena, CA 91109, USA. [2]Department of Chemistry, Tufts University, Medford, MA 02155, USA. [3]SETI Institute, NASA Ames Research Center, Moffett Field, CA 94035, USA. [4]Invensys Process Systems, Foxboro, MA 02035, USA. [5]Astromaterials Research and Exploration Science Directorate, NASA Johnson Space Center, Houston, TX 77058, USA. [6]Department of Earth Sciences, University of Bristol, Wills Memorial Building, Bristol BS8 1RJ, UK. [7]Department of Earth and Space Sciences, University of Washington, Seattle, WA 98195, USA. [8]Space Science Institute, Boulder, CO 80301, USA. [9]Lunar and Planetary Laboratory, University of Arizona, Tucson, AZ 85721, USA. [10]Department of Physics, University of Texas at Dallas, Richardson, TX 95080, USA.

*To whom correspondence should be addressed. E-mail: michael.h.hecht@jpl.nasa.gov
†Present address: Chemistry Department, University of New Hampshire, Durham, NH 03824, USA.

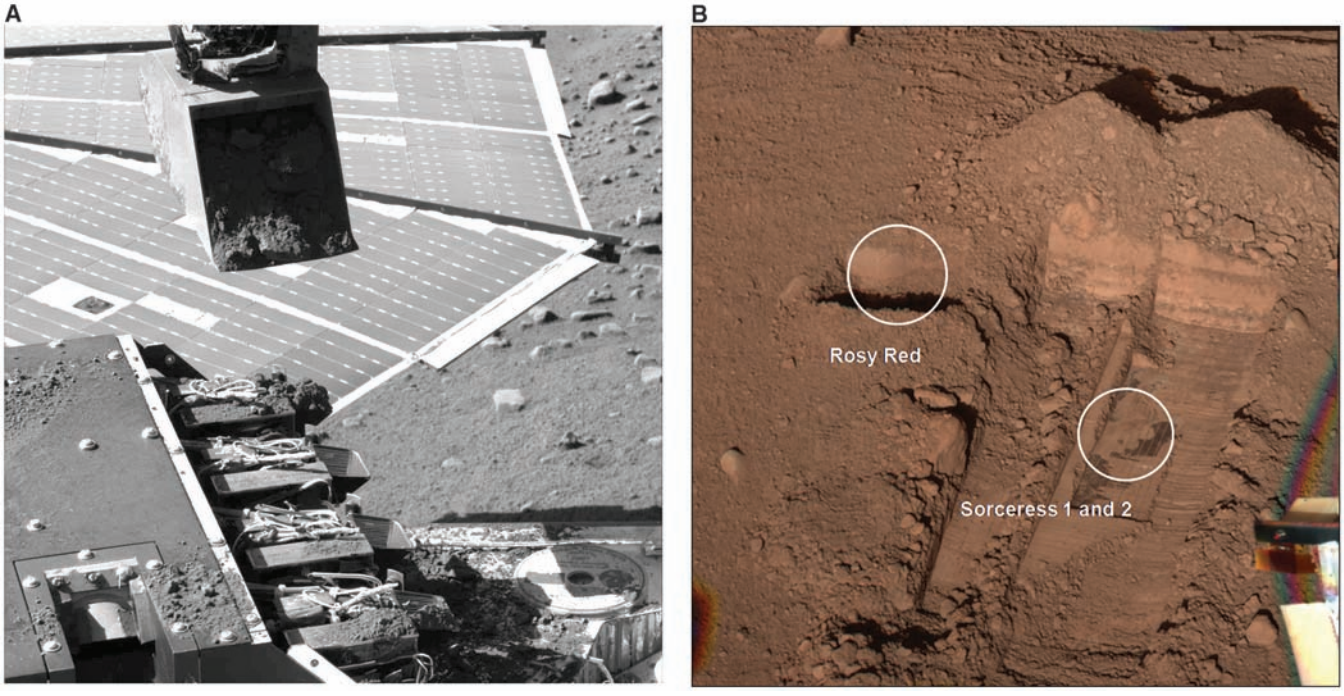

Fig. 1. (**A**) The Phoenix robotic arm is poised to deliver a sample to one of the four WCL cells. The sample previously delivered to the cell on the far end did not successfully pass through the screen, and this cell was used as a blank. The single chute in the foreground is for the delivery of samples to the microscopes. The SSI image is from sol 102; the length of the box is 35 cm. (**B**) The three successful WCL samples were acquired by the Phoenix robotic arm and delivered from the locations shown in this image. The picture is a mosaic of two SSI images acquired on sol 31 at wavelengths of 600, 530, and 480 nm to approximate RGB color. The first WCL sample (Rosy Red), from the small divot on the left, consisted primarily of surface material. The second and third samples (Sorceress 1 and 2) were acquired by scraping at the ice-soil boundary from the large trench on the right (Snow White).

seeking to detect metabolic processes indicative of life (*6*, *7*), and only evolved gases were analyzed.

The Phoenix spacecraft (*8*) landed in the northern plains of Mars on 25 May 2008 carrying several soil analysis instruments, among them a Wet Chemistry Laboratory (WCL). The four single-use cells (*9*) comprising the WCL were part of the Microscopy, Electrochemistry, and Conductivity Analyzer (MECA) instrument suite (*10*, *11*). Samples from the landing site, which was dominated by several centimeters of a loosely consolidated regolith above a hard, icy sheet of permafrost, were excavated by a robotic arm. The WCL analyzed three of those samples (Fig. 1).

Using ion-selective electrodes (ISEs) (*12*), the WCL measured solution concentration of the cations Ca^{2+}, Mg^{2+}, K^{+}, NH_4^{+}, and Na^{+}; the H^{+} ion (pH); and the halide ions, Cl^{-}, Br^{-}, and I^{-}. A Hofmeister anion ISE was intended to monitor nitrate from a $LiNO_3$ reference electrolyte that was part of the leaching solution, but was ultimately used for perchlorate detection (*13*). Other electrodes measured total conductivity and oxidation-reduction potential, performed cyclic voltammetry (in part to detect soluble iron), and redundantly measured halide concentration with chronopotentiometry. Deployable $BaCl_2$ crucibles were included to detect sulfate by titration using a Ba^{2+} ISE.

Each WCL analysis was designed to extend over two nonconsecutive martian solar days (sols) (*14*), with up to 10 hours of operation during each sol. On the first sol, 25 ml of an aqueous leaching solution containing micromolar levels of calibrant ions was thawed and delivered to the sensor-lined beaker, which was maintained at a temperature of 5° to 10°C. A standard addition of soluble salts provided a second calibration point (except for the sample Sorceress 1, where the addition apparently failed), and then up to 1 cm^3 of

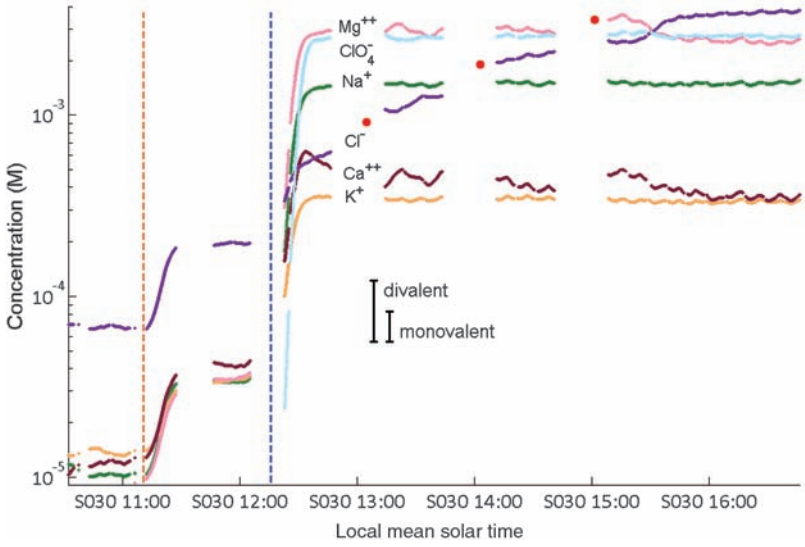

Fig. 2. Sensor response for the analysis of a 1-cc sample (Rosy Red on sol 30) after delivery to 25 ml of solution in the WCL. The responses of the sensors are shown after filtering, determination of activity from the calibration, and conversion to solution concentration with the Debye-Hückel formula. The first vertical dashed line marks delivery of a crucible containing calibration salts; the second dashed line marks the sample addition. Red circles are chloride measurements using chronopotentiometry. The time axis is labeled by sol and local mean solar time. The small error bar is typical for monovalent ions, and the larger error bar is for divalent ions (relative errors are smaller). The slow increase in Cl^{-} is attributed to a source within the WCL assembly, not the martian soil. For ClO_4, a small contribution due to interference from NO_3 in the leaching and calibration solutions has been subtracted.

soil was added and allowed to equilibrate with the solution as it was stirred and monitored. Results from the two calibration solutions were compared to prelaunch data to determine an intercept (pivot) voltage for the logarithmic scale and to verify that there were no significant changes from the predetermined slope. The nominal slope at 25°C is 59/*n* mV per decade of concentration, where *n* is the ion charge. A systemic error estimated at less than ±5 mV, resulting from the determination of the slope and pivot voltage, corresponds to a 20% error in concentration for monovalent ions and 50% for divalent ions (*15*).

All sensors responded promptly upon addition of soil to the solution (Fig. 2 and Table 1). Allowing for variable sample sizes (for Sorceress 1 the sample drawer was only two-thirds to three-fourths full), the differences among the samples were not significant. The most striking response was the increase of the Hofmeister lipophilicity series anion sensor signal by three orders of magnitude, attributed to the perchlorate ion at an average concentration level of 2.4 (±0.5) mM (*16*). The concentrations of Mg^{2+}, Na^{+}, and K^{+} in the solution increased over the initial calibrant concentrations by an average of 3.3 (±1.7), 1.4 (±0.3), and 0.39 (±0.08) mM, respectively. The Ca^{2+} signal decreased from its calibration level, a behavior characteristic of the Ca^{2+} ISE in the presence of perchlorate (*17*, *18*). The true level of Ca^{2+} was estimated as 0.60 (±0.3) mM from laboratory calibration of the Ca^{2+} sensor in the presence of the measured concentration of perchlorate. For Cl^{-}, an increase of 0.47 (±0.09) mM relative to the calibrant level was observed upon soil addition. Over the course of the experiment the Cl^{-} level appeared to slowly increase, but the observation of similar behavior in an empty cell suggests that leakage from the $BaCl_2$ crucibles is the most likely explanation (*19*). Thus, we only attribute to mineralogical chloride the prompt increase in Cl^{-} after soil addition.

The pH of all three samples at the partial pressure of CO_2 of the sample cell (~3 mbar) was 7.7 (±0.5). Although Mars rover results led to inferences of widespread acidic soil (*20*), Viking data analysis suggested a pH consistent with the WCL result (*21*). The pH of the soil solution was not measurably affected by addition of 4 mg of 2-nitrobenzoic acid, with a pK_a of 2.2; this result indicates that the soil provides pH buffering at ≥1 mM, most likely by calcium carbonate in the soil (*22*). The leaching solution itself is unbuffered.

The measurement strategy of the WCL experiment was to identify as many major anions and cations as possible, and to measure the overall conductivity of the sample solution in order to identify gaps. Discrepancies among cation, anion, and conductivity measurements imply the presence of unmeasured ionic species. The activity-weighted concentrations of only the measured ions predict conductivity of about one-half the measured total solution conductivity (Table 1), which suggests that any unmeasured constituents are of comparable or lower concentrations than those measured directly. Although charge balancing in complex fluids can be problematic, comparison of the charge concentration associated with anions and cations suggests that the missing species are anions. Bicarbonate could account for this entire deficit, but soluble sulfate is also a candidate. Measurements by Viking Lander 1 (*1*), the Mars rovers (*23*–*25*), and near-infrared spectroscopy of the martian surface (*26*, *27*) suggest a soil sulfur content of 5 to 9 weight % SO_4, at a uniform molar ratio for S:Cl of 4:1. Although it cannot be assumed that soils encountered by Phoenix and by the Mars rovers are the same, the complete absence of sulfate at the Phoenix site would nonetheless be surprising. If the entire anion deficit were sulfate, it would constitute ~0.8% of the total sample mass, so if sulfate is present in the soil at higher concentrations, it must be in a sparingly soluble form such as $CaSO_4$.

Independent evidence for perchlorate was provided by the Thermal and Evolved Gas Analyzer (TEGA) (Fig. 3) (*22*). Although oxygen, sulfur, and hydrazine (from thrusters) are candidate fragment ions for mass 32, the observed temperature range (325° to 625°C) is consistent with O_2 evolution by the thermal decomposition of perchlorate salts, as demonstrated both in a laboratory testbed (*28*) and by literature values (*29*). Hydrazine would evolve at lower temperature, and no other S fragments (e.g., $^{32}S^{16}O_2^{+}$, $^{32}S^{16}O^{+}$) were detected during the ramp.

The characteristics of perchlorate salts derive largely from the chemical energy stored in the highly metastable, fully oxidized molecule, which at high temperature is used for rocket fuel and generation of breathing oxygen. At low temperature, in aqueous solution, most perchlorates are soluble and do not readily react or precipitate. This affinity for water suggests that a history of liquid water would be indicated by sharp gradients in evaporitic perchlorate salt concentration. The homogeneous perchlorate concentration found at two depths at the Phoenix site argues against such a history. If liquid water were present in the past, aeolian mixing, cryoturbation, or subsequent influx of perchlorate have since obscured the record.

The distribution of cations in the solution suggests that at least some of the perchlorate in

Table 1. Ion concentration determined shortly after addition of each of the three samples. Quantities in the last seven rows are derived from concentrations. Concentration error is ±20% (monovalent ions) or ±50% (divalent ions). Total charge includes Li^{+} and NO_3^{-} from the leaching solution. The Sorceress 1 sample volume was smaller than the others (i.e., more dilute) by an estimated 25 to 35% and is therefore not included in the average. The pH reading from Sorceress 2 was comparable to the others, but noisy. Note that measured conductivity also includes ions from the leaching solution.

	Rosy Red	Sorceress 1	Sorceress 2	Average
Na^{+} (mM)	1.4	1.10	1.4	1.4
K^{+} (mM)	0.36	0.17	0.39	0.38
Ca^{2+} (mM)	0.55	0.42	0.6	0.58
Mg^{2+} (mM)	2.9	2.20	3.7	3.3
Cl^{-} (mM)	0.6	0.24	0.47	0.54
ClO_4^{-} (mM)	2.6	2.10	2.2	2.4
Conductivity (μS/cm)	NA	1000	1400	1400
pH	7.7	7.6	—	7.7
Equivalent conductivity at 25°C (μS/cm)	NA	1370	1900	1900
ClO_4^{-} mass (mg)	6.50	5.25	5.50	6.00
Conductivity at 25°C (calculated, μS/cm)	815	636	918	866
Total cation charge (mM)	9.66	7.51	11.39	10.53
Total anion charge (mM)	4.30	3.44	3.77	4.04
Anion deficit, if monovalent (mM)	5.36	4.07	7.62	6.49
Anion deficit, if divalent (mM)	2.68	2.04	3.81	3.25

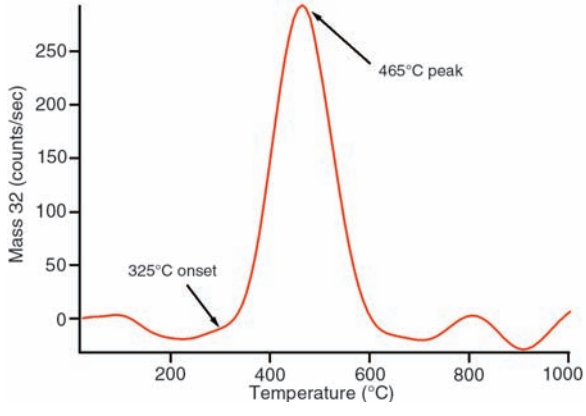

Fig. 3. Evolved mass 32 (O_2) analysis for the Baby Bear surface sample from TEGA. The curve is the difference between the first high-temperature ramp and the second-day reheat for the high-temperature ramp.

the soil is in the form of $Mg(ClO_4)_2$ or $Ca(ClO_4)_2$. Alkaline earth perchlorate salts have a strongly exothermic affinity for water, are deliquescent, and have eutectic freezing points in the range of −70°C (*30*, *31*). The dynamics of thermally driven exchange of water vapor between the buried ice and the overlying perchlorate-rich soil may make a wet super-eutectic solution possible at certain temperatures, possibly explaining the time-varying cohesiveness of the soil at the Phoenix site (*32*). If, as was found by Phoenix, most of the chlorine on Mars is in the form of perchlorate, it lends support to the conjecture that low-temperature brines, stable at or below the present-day mean martian frost-point, may be responsible for contemporary liquid-mediated processes such as gully formation (*33*).

The deliquescent properties of perchlorate salts may also play a role in controlling soil and atmosphere water content. Hydrogen levels measured by Odyssey's Gamma Ray Spectrometer (GRS), corresponding to several percent of water in martian surface soil over large swaths of equatorial Mars, have been attributed to hydrated salts (*34*). Subsequently, the concentration of chlorine was mapped and found to correlate with the hydrogen (*35*). In the form of $Mg(ClO_4)_2$, perchlorate in equilibrium with the martian atmosphere would be coordinated as a mixture of hexahydrate and octahydrate, depending on temperature and humidity (*30*), such that the mass of water would be 3 to 4 times that of the chlorine, a value similar to the GRS ratios. At the Phoenix site, perchlorate in this form would take up and release more water with temperature than the entire peak summer column density in the atmosphere, which suggests that it may even be a factor in zonal control of atmospheric humidity.

Several microorganisms on Earth are known to harvest energy by anaerobic reduction of the perchlorate molecule (*36*, *37*). Under martian conditions, perchlorate does not readily oxidize organics (although the presence of perchlorate salts may indicate a vigorous oxidant-forming chemistry in the martian atmosphere or on the surface), but the low water activity associated with such a strongly desiccating substance may inhibit many forms of life. The high-temperature oxidizing properties of perchlorate will, however, promote combustion of organics in pyrolytic experiments, compromising the ability of Phoenix's TEGA experiment to readily detect organics (*38*) and possibly affecting the Viking mass spectrometer experiments (*39*).

If perchlorate on Mars has a photochemical origin similar to that on Earth (*40*), and if the chlorine directly originates from volcanic gas, then perchlorates are likely to be characteristic only of later geologic time because on early Mars volcanism would have produced a reducing atmosphere (*41*). Perchlorate may be favored at high latitudes if ice is important as a reaction surface for adsorbed species or if its formation depends on ozone, which is barely detectable in the tropics but is abundant in the spring-winter circumpolar regions (*42*, *43*).

In summary, aqueous chemical analysis of martian soil has revealed that most of the soluble chlorine is in the form of perchlorate. This finding has possible relevance to water sequestration, control of soil and atmospheric humidity, gully formation, habitability, and resource use for human exploration.

References and Notes

1. B. C. Clark *et al*., *J. Geophys. Res.* **87**, 10059 (1982).
2. H. J. Wänke, J. Brückner, G. Dreibus, R. Rieder, I. Ryabchikov, *Space Sci. Rev.* **96**, 317 (2001).
3. R. Gellert *et al*., *Science* **305**, 829 (2004).
4. R. Rieder *et al*., *Science* **306**, 1746 (2004).
5. In using the term soil to denote unconsolidated surface materials on Mars, we follow the convention of (*44*). The presence of organic materials is not implied.
6. V. I. Oyama, B. J. Berdahl, *J. Geophys. Res.* **82**, 4669 (1977).
7. G. V. Levin, P. A. Straat, *J. Geophys. Res.* **82**, 4663 (1977).
8. P. H. Smith *et al*., *Science* **325**, 58 (2009).
9. S. P. Kounaves *et al*., *J. Geophys. Res.* **114**, E00A19 (2009).
10. M. H. Hecht *et al*., *J. Geophys. Res.* **113**, E00A22 (2008).
11. A. Zent *et al*., *J. Geophys. Res.* **114**, E00A27 (2009).
12. Following the Nernst equation, the ISE voltage response is logarithmic in concentration over several orders of magnitude of concentration, making ISEs well suited for analysis of a solution of unknown composition. Most of the ISEs in the WCL use polyvinyl chloride membranes doped with ionophores that respond predominantly to one ionic species. In a complex mixture, the ISEs may respond to more than one species. Processing of the signal requires the use of selectivity coefficients to deconvolve the response.
13. The relative sensitivity of the Hofmeister series ISE to perchlorate over nitrate is 1000:1, and substantial quantities of perchlorate will overwhelm any other signal. If, as was observed, >1 mM perchlorate accounts for the observed signal, it would require >1000 mM nitrate to produce the same response. This would correspond to more than the mass of the entire sample.
14. A martian solar day has a mean period of 24 hours 39 min 35.244 s and is referred to as a sol to distinguish this from a ~3% shorter solar day on Earth.
15. The slope of the Nernst relationship is consistent with preflight calibration, but the reference (pivot) point can shift and must be calibrated relative to the reference solution. The 5-mV error is a conservative estimate of the accuracy of that calibration and combines the effects of noise and drift. It does not reflect a standard deviation.
16. Possible sources of perchlorate contamination, such as pyrotechnic devices, have been systematically eliminated as explanations for the signal. The only source of perchlorate sufficient to produce the measured level in soil would be the third-stage rocket engine, which is many levels of protection removed from the lander and uses ammonium perchlorate (which was not detected by the WCL). The lander retrorockets use hydrazine as fuel.
17. S. P. Kounaves *et al*., *J. Geophys. Res.* **108**, 5077 (2003).
18. M. H. Lee *et al*., *Anal. Chem.* **74**, 2603 (2002).
19. In view of the rapid dissolution of other measured salts, the typical rapid solubility of chloride salts, and the absence of a measurable cation with a corresponding increase (whereas Ba could have precipitated out as a sulfate), mineralogical explanations of this behavior are unlikely. Explanations such as the decomposition of intermediate oxidation states of chlorine were also examined and rejected.
20. J. A. Hurowitz, S. M. McLennan, *Earth Planet. Sci. Lett.* **260**, 432 (2007).
21. R. Quinn, J. Orenberg, *Geochim. Cosmochim. Acta* **57**, 4611 (1993).
22. W. V. Boynton *et al*., *Science* **325**, 61 (2009).
23. B. C. Clark *et al*., *Earth Planet. Sci. Lett.* **240**, 73 (2005).
24. D. W. Ming *et al*., *J. Geophys. Res.* **113**, E12S39 (2008).
25. R. Gellert *et al*., *J. Geophys. Res.* **111**, E02S05 (2006).
26. J.-P. Bibring *et al*., *Science* **307**, 1576 (2005); published online 17 February 2005 (10.1126/science.1108806).
27. Y. Langevin, F. Poulet, J.-P. Bibring, B. Gondet, *Science* **307**, 1584 (2005); published online 17 February 2005 (10.1126/science.1109091).
28. H. V. Lauer Jr. *et al*., *Lunar Planet. Sci. Conf. XL*, abstr. 2196 (2009).
29. J. D. Devlin, P. J. Herley, *Thermochim. Acta* **104**, 159 (1986).
30. L. M. Besley, G. A. Bottomley, *J. Chem. Thermodyn.* **1**, 13 (1969).
31. O. N. Pestova *et al*., *Russ. J. Appl. Chem.* **78**, 409 (2005).
32. Soil clumping was first noted on sol 7 from the first sample scooped by the robotic arm. Images showed that clumps of soil left in the scoop and on the lander deck developed cracks and became friable within a sol. Although soil adhesion may be due to electrostatic forces, these should not be time-dependent (unless the soil is strongly pyroelectric), whereas salt cement would be expected to dehydrate to create more friable soil.
33. L. P. Knauth, D. M. Burt, *Icarus* **158**, 267 (2002).
34. W. C. Feldman *et al*., *J. Geophys. Res.* **109**, E09006 (2004).
35. J. M. Keller *et al*., *J. Geophys. Res.* **111**, E03S08 (2006).
36. J. D. Coates, L. A. Achenbach, *Nat. Rev. Microbiol.* **2**, 569 (2004).
37. M. Ader *et al*., *Earth Planet. Sci. Lett.* **269**, 605 (2008).
38. D. W. Ming *et al*., *Lunar Planet. Sci. Conf. XL*, abstr. 2241 (2009).
39. K. Biemann, *Proc. Natl. Acad. Sci. U.S.A.* **104**, 10310 (2007).
40. Natural perchlorate in terrestrial soils is rare but occurs in arid environments including the Atacama Desert at levels up to 0.6 weight % (*45*), deserts of West Texas (*46*), and Bolivian playas (*47*). Atacama perchlorate is attributed to the photochemical reaction of ozone with volatile chlorine species in the atmosphere (*48*, *49*). Perchloric acid ($HClO_4$) is a stable end product of atmospheric chemistry because of its resistance to photolysis (*50*) and occurs in sulfate aerosols in Earth's stratosphere at abundances of 0.5 to 5 parts per trillion (*51*). Similarly, photochemical processes in the martian atmosphere generate H_2O_2, O_3, OH, HO_2, O, and other oxidizing species (*52*, *53*), whereas ultraviolet action on mineral surfaces produces radicals, providing an environment conducive to oxidation of chlorine species. Volatile chlorine could originate from volcanic HCl or through aqueous reactions of chloride salts with sulfuric acid to produce sulfate salts; alternatively, heterogeneous reactions could be important.
41. K. Zahnle, R. M. Haberle, D. C. Catling, J. F. Kasting, *J. Geophys. Res.* **113**, E11004 (2008).
42. C. A. Barth *et al*., *Science* **179**, 795 (1973).
43. S. Perrier *et al*., *J. Geophys. Res.* **111**, E09S10 (2006).
44. A. Banin, B. C. Clark, H. Wänke, in *Mars*, H. H. Kieffer *et al*., Eds. (Univ. of Arizona Press, Tucson, AZ, 1992), pp. 594–625.
45. G. E. Eriksen, *U.S. Geol. Surv. Prof. Pap. 1188* (1981).
46. P. K. Dasgupta, *Environ. Sci. Technol.* **39**, 1569 (2005).
47. G. J. Orris *et al*., *U.S. Geol. Surv. Open File Rep. 03-314* (2003).
48. H. M. Bao, B. H. Gu, *Environ. Sci. Technol.* **38**, 5073 (2004).
49. J. K. Bohlke *et al*., *Anal. Chem.* **77**, 7838 (2005).
50. R. Simonaitis, J. Heicklen, *Planet. Space Sci.* **23**, 1567 (1975).
51. D. M. Murphy, D. S. Thomson, *Geophys. Res. Lett.* **27**, 3217 (2000).
52. D. M. Hunten, *J. Mol. Evol.* **14**, 71 (1979).
53. Y. L. Yung, W. B. DeMore, *Photochemistry of Planetary Atmospheres* (Oxford Univ. Press, Oxford, 1999).

54. We thank J. M. Morookian, C. Cable, P. Grunthaner, A. Fisher, X. Wen, D. Morris, M. Lemmon, the Phoenix Robotic Arm team, and other contributors to MECA and Phoenix. The Phoenix Mission was led by the University of Arizona, Tucson, on behalf of NASA and was managed by NASA's Jet Propulsion Laboratory, California Institute of Technology, of Pasadena, CA. The spacecraft was developed by Lockheed Martin Space Systems, Denver.

18 February 2009; accepted 26 May 2009
10.1126/science.1172466

Mars Water-Ice Clouds and Precipitation

J. A. Whiteway,[1]* L. Komguem,[1] C. Dickinson,[1] C. Cook,[1] M. Illnicki,[1] J. Seabrook,[1] V. Popovici,[1] T. J. Duck,[2] R. Davy,[1] P. A. Taylor,[1] J. Pathak,[1] D. Fisher,[3] A. I. Carswell,[4] M. Daly,[5] V. Hipkin,[6] A. P. Zent,[7] M. H. Hecht,[8] S. E. Wood,[9] L. K. Tamppari,[8] N. Renno,[10] J. E. Moores,[11] M. T. Lemmon,[12] F. Daerden,[13] P. H. Smith[11]

The light detection and ranging instrument on the Phoenix mission observed water-ice clouds in the atmosphere of Mars that were similar to cirrus clouds on Earth. Fall streaks in the cloud structure traced the precipitation of ice crystals toward the ground. Measurements of atmospheric dust indicated that the planetary boundary layer (PBL) on Mars was well mixed, up to heights of around 4 kilometers, by the summer daytime turbulence and convection. The water-ice clouds were detected at the top of the PBL and near the ground each night in late summer after the air temperature started decreasing. The interpretation is that water vapor mixed upward by daytime turbulence and convection forms ice crystal clouds at night that precipitate back toward the surface.

The seasonal hydrological cycle on Mars is most evident in the Arctic region, where the atmospheric water vapor abundance increases to a maximum in midsummer after the seasonal ground ice cover reaches a minimum (*1*). The water returns to the surface as the atmosphere cools in late summer, but it has not previously been known whether this process involves clouds and precipitation as on Earth. Observations of water vapor and temperature during the Viking missions indicated that the atmosphere would be saturated with respect to water ice at night (*2*, *3*), and it was suggested that the precipitation of ice crystals could be an important factor for the exchange of water between the atmosphere and surface (*4*). Here we report on experimental evidence that clouds and precipitation play a role in the exchange of water between the atmosphere and ground on Mars.

The Phoenix mission (*5*, *6*) obtained measurements from the surface in the Arctic region of Mars (68.22°N, 234.25°E). The spacecraft landed before the summer solstice on Mars and operated over the next 5 months. This period encompasses the midsummer peak and decline in the abundance of atmospheric water vapor, so it was possible to observe the local processes that contribute to the water cycle. The Phoenix mission included a light detection and ranging (LIDAR) instrument (*7*) that emitted pulses of laser light upward into the atmosphere and detected the backscatter from dust and clouds. An essential capability of the LIDAR was that it could resolve the internal structure of water-ice clouds that drifted past the landing site.

Daytime LIDAR observations mainly detected dust in the atmosphere. The measurements on the 45th sol (*8*) after landing were typical for moderate dust loading with no clouds (Fig. 1A). The dust was distributed evenly up to a height of 4 km because of the daytime vertical mixing produced by convection and turbulence within the planetary boundary layer (PBL). The atmospheric dust loading reached a peak around the summer solstice and then generally decreased. On sol 97 [solar longitude of Mars (L_s) = 121°], the dust loading within the PBL was reduced by a factor of 3 in comparison with that on sol 45 (Fig. 1A).

During the period around the summer solstice, clouds were observed sporadically and mainly above heights of 10 km. Moving into late summer, 50 sols after the solstice (L_s = 113°), the LIDAR detected a regular pattern of cloud formation each night within the PBL. A shallow surface-based cloud formed near midnight (Mars local solar time), and a second cloud layer formed after 1 a.m. at heights around 4 km. On sol 99 (L_s = 122°), there was a clear enhancement in the extinction coefficient due to the presence of clouds in the height range from 3 to 4 km and in the layer up to 1 km above the ground (Fig. 1B). The observed clouds formed at an estimated temperature of around –65°C (Fig. 1C), which is consistent with clouds that are composed of water-ice crystals (the frost point for carbon dioxide is less than –120°C). On each sol during the second half of the mission (L_s = 113° to 150°), clouds remained through the early morning hours and then dissipated when the atmosphere warmed sufficiently during the daytime. As the summer progressed toward autumn and the air temperature decreased, the clouds persisted longer into the morning hours and ex-

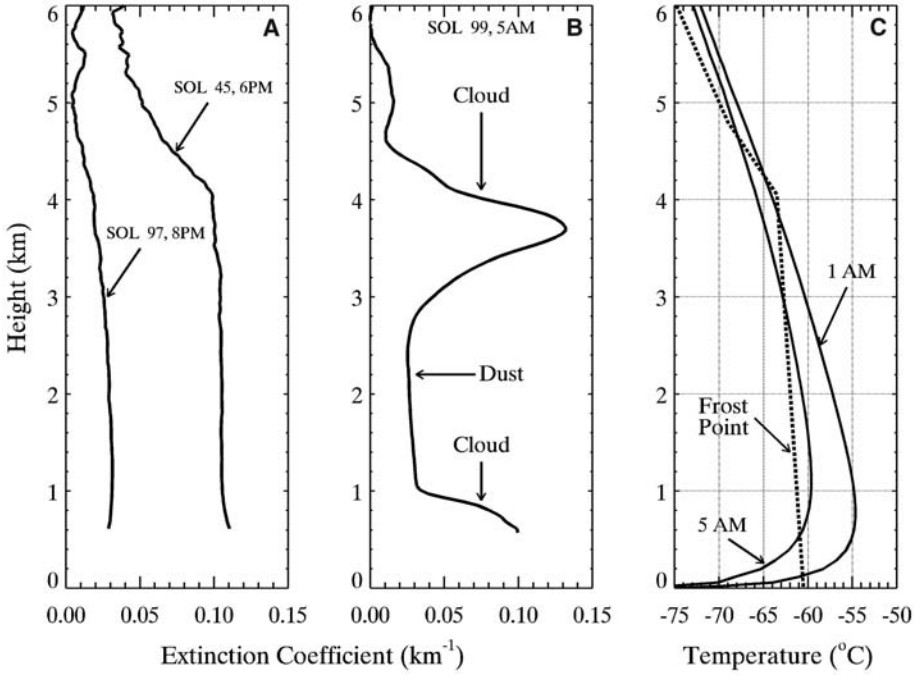

Fig. 1. (**A** and **B**) Profiles of the optical extinction coefficient (*9*) derived from the LIDAR backscatter signal at wavelength 532 nm for sols 45 (L_s = 97°), 97 (L_s = 121°), and 99 (L_s = 122°). Each profile is averaged over 1 hour and smoothed for a vertical resolution of 40 m. (**C**) Height profiles of atmospheric temperature estimated with a numerical simulation model of the martian PBL (*19*, *20*), and an estimate of the profile of frost point temperature.

[1]Department of Earth and Space Science and Engineering, York University, Toronto, Ontario, Canada. [2]Department of Physics and Atmospheric Science, Dalhousie University, Halifax, Nova Scotia. [3]National Glaciology Group, Geological Survey of Canada, Natural Resources Canada, Ottawa, Ontario, Canada. [4]Optech, Vaughan, Ontario, Canada. [5]MacDonald, Dettwiler and Associates (MDA), Brampton, Ontario, Canada. [6]Canadian Space Agency (CSA), St-Hubert, Quebec, Canada. [7]NASA Ames Research Center, Moffett Field, CA, USA. [8]Jet Propulsion Laboratory, California Institute of Technology, Pasadena, CA, USA. [9]Department of Earth and Space Sciences, University of Washington, Seattle, WA, USA. [10]Department of Atmospheric, Oceanic and Space Sciences, University of Michigan, Ann Arbor, MI, USA. [11]Department of Planetary Sciences, University of Arizona, Tucson, AZ, USA. [12]Department of Atmospheric Sciences, Texas A&M University, College Station, TX, USA. [13]Belgian Institute for Space Aeronomy (BIRA-IASB), Brussels, Belgium.

*To whom correspondence should be addressed. E-mail: whiteway@yorku.ca

tended further toward the ground. Clouds were not detected in the late afternoon or evening.

The outline and internal structure of the clouds that drifted above the Phoenix landing site are seen in the contour of the backscatter coefficient (*9*). On sol 99 (Fig. 2A), the most striking features are the tilted vertical streaks after 05:00 (Mars local time). This pattern is consistent with ice crystals precipitating from the cloud and eventually sublimating in the subsaturated air below the cloud. Such fall streaks are a well-known feature in observations of cirrus clouds on Earth.

In the early morning hours on sol 109, the LIDAR observed clouds and precipitation that extended all the way to the ground (Fig. 2B). In the period between 03:10 and 03:50, there were water-ice clouds at the top of the PBL (at heights of 3 to 5 km) and at ground level. In the next LIDAR run, from 05:16 to 05:45, the base of the observed cloud had dropped to a height of about 1.5 km, and there were precipitation fall streaks starting at 05:30 that extended down through the ground-level cloud. The LIDAR is not able to measure below about 50 m because of the geometry of the transmitter/receiver overlap. It is reasonable to assume that the ice crystals would have continued to descend through the saturated air to reach the surface. The essential point here is that precipitation moves water toward the surface from heights of up to 5 km (*10*).

In the period around sol 99 (L_s = 122°), clouds were observed only after 01:00, so we take this as the time when clouds were initially forming. The average fall speed required to produce a fall streak length of 1.2 km (Fig. 2A) after 4 hours is consistent with an ellipsoidal ice particle with an aspect ratio of 3 and volume equivalent to a sphere with a radius of 35 μm (*11*). This approximates a columnar ice crystal 42 μm wide and 127 μm long, which is similar to ice crystals that have been sampled in cirrus clouds on Earth (*12*, *13*). The comparison is not surprising, because cirrus clouds on Earth form at a similar temperature and water vapor density.

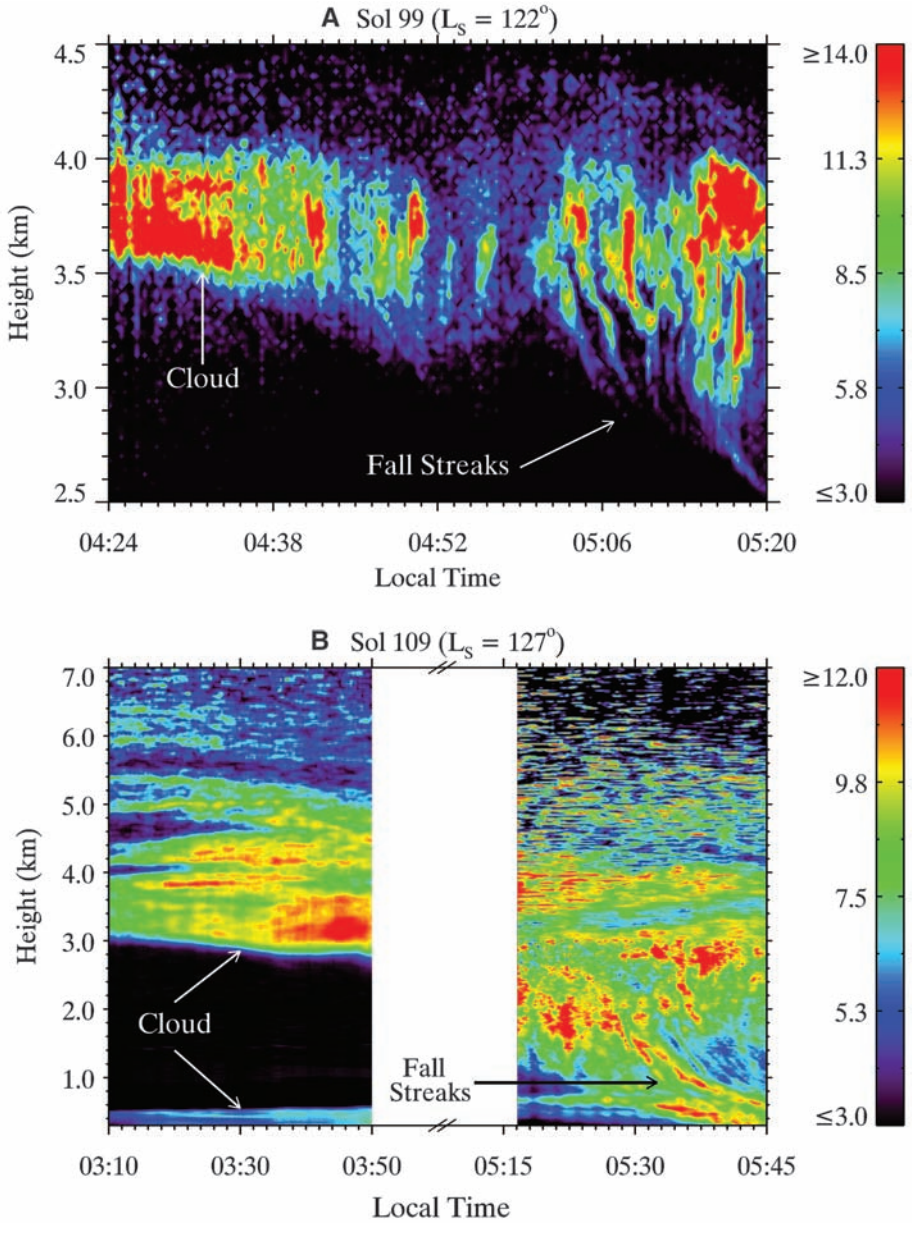

Fig. 2. Contour plots of backscatter coefficient (×10^{-6} m^{-1} sr^{-1}) derived from the LIDAR backscatter signal (*9*) at wavelength 532 nm on mission sols 99 (L_s = 122°) (**A**) and 109 (L_s = 127°) (**B**).

The extinction coefficient represents the effective cross-sectional area of the ice crystals per unit of volume and, assuming spherical particles, the ice water content can be calculated as IWC = $4\sigma R_{eff}\rho/3Q$. σ is the extinction coefficient; R_{eff} is the effective radius, which we assumed to be 35 μm based on the calculation of fall speed; Q is the scattering efficiency, which has a value of 2; and ρ is the density of water ice. The enhancement in the extinction coefficient due to the cloud in the average signal profile (Fig. 1B) has a peak value of 0.1 km^{-1}, but the range is from 0.07 to 0.27 km^{-1} in profiles with shorter averages. The corresponding estimates of IWC for spherical particles are in the range of 1.5 to 5.8 mg m^{-3}, and this is also similar to measurements of cirrus clouds on Earth (*14*). The spherical assumption can be avoided by using the empirical relationship between the extinction coefficient and IWC that was derived from aircraft in situ measurements in cirrus clouds (*14*): IWC = 119 $\sigma^{1.22}$. This gives a similar range of values: 1.0 to 5.3 mg m^{-3}. Using the empirical relationship, the amount of ice water integrated in the vertical (from the mean profile of Fig. 1B) is 1.9 g m^{-2}, which has the same value in units of precipitable micrometers (pr-μm) of water. This is more than substantial enough to play a role in the seasonal decreasing trend of about 0.5 pr-μm per sol in the local column water vapor (from L_s = 120° to 160°) measured from orbit (*1*).

We estimated the amount of water vapor within the PBL from the height and time of cloud formation, combined with the simulated temperature. For cloud formation commencing at 01:00 at a height of 4 km, the simulated temperature is –64.3°C (Fig. 1C), and the corresponding saturated vapor pressure is 0.61 Pa. The threshold relative humidity over ice for nucleation on desert dust has been measured in the laboratory to be in the range from 110 to 130% (*15*). Thus, we assumed that the water vapor pressure at a height of 4 km when the cloud started to form was 20% greater than the saturated value: 0.61 × 1.2 = 0.73 Pa. At the height of 4 km, the water vapor volume mixing ratio before cloud formation is 0.73/522 = 0.0014, where the model atmospheric pressure is 522 Pa. The uncertainty in this estimate is about ±20%, based on the range in the possible cloud formation times and the ice nucleation threshold. It is also assumed here that water vapor was well mixed throughout the PBL by the daytime

turbulence and convection, so that in the early evening, the mixing ratio of water vapor was approximately constant up to a height of 4 km. Above the cloud top, the water vapor partial pressure would have been below the saturation value because clouds were not observed at those heights. The corresponding height profile of frost point temperature (before cloud formation) is shown in Fig. 1C. The integrated amount of water vapor within the PBL (from the ground to 4 km) before cloud formation on sol 99 (L_s = 122°) can be estimated from the analysis above to be 35 pr-μm. This is a substantial fraction of the total atmospheric column water vapor (40 to 50 pr-μm) measured from orbit at the latitude of Phoenix in previous years (*1*, *16*). Solar radiation measurements during the Pathfinder mission also indicated that atmospheric water vapor was confined near the ground (*17*).

We also used the simulated temperature profiles in Fig. 1C to estimate the IWC in the clouds. At 05:00 and a height of 4 km, the simulated temperature is –66°C and the saturated vapor density is 5 mg m^{-3}. The threshold value of vapor density at cloud formation (time 01:00) was 7.6 mg m^{-3}. The difference of 2.6 mg m^{-3} is an estimate of the IWC in the cloud, and this is within the range of IWC derived from the LIDAR measurements.

Our estimate of the water content of the PBL is consistent with independent measurements. The Thermal and Electrical Conductivity Probe instrument (*18*) on Phoenix measured the partial pressure of water vapor near the ground to have values up to 2 Pa during the daytime and less than 0.1 Pa at night, with a diurnal average of 0.9 Pa (*6*). The water vapor volume mixing ratio in the mixed boundary layer would be greater than the average at ground level (0.0012), because the vertical mixing occurs mainly during the daytime. Also, if the water vapor volume mixing ratio was 0.0016 throughout the PBL, then the integrated amount up to a height of 4 km would be 40 pr-μm, and this is an upper limit because it is within the measured range of the total atmospheric column water vapor (*1*, *16*). Our estimate of the volume mixing ratio at the top of the PBL (0.0014) is within the range of plausible values.

The Phoenix LIDAR observations have demonstrated that water-ice crystals grow large enough to precipitate through the atmosphere of Mars. In the early morning hours, the clouds formed at ground level and at heights around 4 km because these were the coldest parts of the PBL (Fig. 1C). The cloud was capped at the top of the PBL because daytime turbulent mixing does not transport moisture above that height. The overall process was that water ice was transported downward by precipitation at night, it sublimated in the morning, and then the vapor was mixed back up through the PBL by turbulence and convection during the daytime. The clouds and precipitation act to confine water within the PBL. Eventually the ice clouds would have persisted within the PBL throughout the daytime, and water ice would have remained deposited on the ground. As the depth of the PBL decreased in late summer, this local process would contribute to the seasonal decrease in atmospheric water vapor (*1*).

References and Notes

1. M. D. Smith *et al.*, *J. Geophys. Res.* **107**, 5115 10.1029/2001JE001522 (2002).
2. D. Davies, *J. Geophys. Res.* **84**, 8335 (1979).
3. J. Ryan *et al.*, *J. Geophys. Res.* **87**, 7279 (1982).
4. R. A. Kahn, *J. Geophys. Res.* **95**, 14677 (1990).
5. P. H. Smith *et al.*, *J. Geophys. Res.* **113**, E00A18 (2008).
6. P. H. Smith *et al.*, *Science* **325**, 58 (2009).
7. J. A. Whiteway *et al.*, *J. Geophys. Res.* **113**, E00A08 10.1029/2007JE003002 (2008).
8. A sol is a martian day, with a length of 24.6 hours. Phoenix landed 30 sols before the Mars summer solstice, when solar longitude is L_s = 90°.
9. Materials and methods are available as supporting material on *Science* Online.
10. Further evidence of precipitation was observed in images of low-level clouds (supporting online material text).
11. N. A. Fuchs, *The Mechanics of Aerosols* (Pergamon, New York, 1964).
12. J. A. Whiteway *et al.*, *Geophys. Res. Lett.* **31**, L24102 (2004).
13. M. W. Gallagher *et al.*, *Q. J. R. Meteorol. Soc.* **131**, 1143 (2005).
14. A. J. Heymsfield *et al.*, *Geophys. Res. Lett.* **32**, L10807 (2005).
15. P. R. Field *et al.*, *Atmos. Chem. Phys.* **6**, 2991 (2006).
16. H. Tschimmel *et al.*, *Icarus* **195**, 557 (2008).
17. D. V. Titov *et al.*, *J. Geophys. Res.* **104**, 9019 (1999).
18. A. P. Zent *et al.*, *J. Geophys. Res.* **114**, E00A27 (2009).
19. R. Davy *et al.*, *J. Geophys. Res.* **114**, D04108 (2009).
20. For the simulations used here, the upper-level wind was assumed to be as 5 m s^{-1}. The temperature and pressure at ground level were matched to the Phoenix in situ measurements, and the height distribution of dust was based on the Phoenix LIDAR observations. The model predicts a PBL depth of 4 km, which is consistent with the LIDAR daytime dust observations (Fig. 1A).

21. We acknowledge contributions to landed operations from the engineering staff at the CSA (P. Allard, C. Brunet, D. Cormier, I. Tremblay, and E. Vachon) and MDA Space Missions (D. Hill, L. Clark, A. Kerr, and R. McCoubrey). This work was enabled by funding from the CSA under contract 9F007-070437/001/SR. The Phoenix mission was led by the University of Arizona, on behalf of NASA, and managed by the Jet Propulsion Laboratory.

Supporting Online Material

www.sciencemag.org/cgi/content/full/325/5936/68/DC1
Materials and Methods
SOM Text
Fig. S1
Movie S1
References

16 February 2009; accepted 27 May 2009
10.1126/science.1172344

A Coherent Single-Hole Spin in a Semiconductor

Daniel Brunner,[1] Brian D. Gerardot,[1] Paul A. Dalgarno,[1] Gunter Wüst,[1] Khaled Karrai,[2] Nick G. Stoltz,[3] Pierre M. Petroff,[3] Richard J. Warburton[1,4]*

Semiconductors have uniquely attractive properties for electronics and photonics. However, it has been difficult to find a highly coherent quantum state in a semiconductor for applications in quantum sensing and quantum information processing. We report coherent population trapping, an optical quantum interference effect, on a single hole. The results demonstrate that a hole spin in a quantum dot is highly coherent.

Semiconductor heterostructures can be designed to confine electrons, holes, and photons in specific ways. Post-growth processing enables the creation of individual devices and their interconnection into fully functional circuits. However, it is not yet clear whether these material advantages can be exploited in a new class of device whose operation depends on the controlled manipulation of coherent quantum states. Achieving the necessary coherence poses considerable challenges.

In bulk semiconductors and quantum wells, individual quantum states lose coherence rapidly through an interaction with the lattice vibrations, or phonons. An electron spin interacts only indirectly via the spin-orbit interaction with the phonons and emerges as a strong candidate quantum bit (qubit) (*1*). However, to suppress the spin-orbit interaction, the electron must be tightly confined to a nanoscopic quantum dot (*2*–*4*). But in GaAs, the semiconductor with the best materials properties, the electron spin now interacts with 10^4 to 10^5 nuclear spins, too few for cancellation of the hyperfine interaction and too many for each nuclear spin to be used as a resource. The nuclear spins create a fluctuating effective magnetic field, the Overhauser field. The electron spin precesses in the Overhauser field such that the time-averaged coherence time, T_2*, is small, just ~10 ns (*5*–*7*), much less than the intrinsic decoherence time, T_2, which is around 1 μs (*8*, *9*). This difficulty represents a stumbling block in engineering a coherent semiconductor spin state.

[1]School of Engineering and Physical Sciences, Heriot-Watt University, Edinburgh EH14 4AS, UK. [2]Department für Physik der Ludwig-Maximilians-Universität, Geschwister-Scholl-Platz 1, 80539 Munich, Germany. [3]Materials Department, University of California, Santa Barbara, CA 93106, USA. [4]Department of Physics, University of Basel, Klingelbergstrasse 82, 4056 Basel, Switzerland.

*To whom correspondence should be addressed. E-mail: r.j.warburton@hw.ac.uk

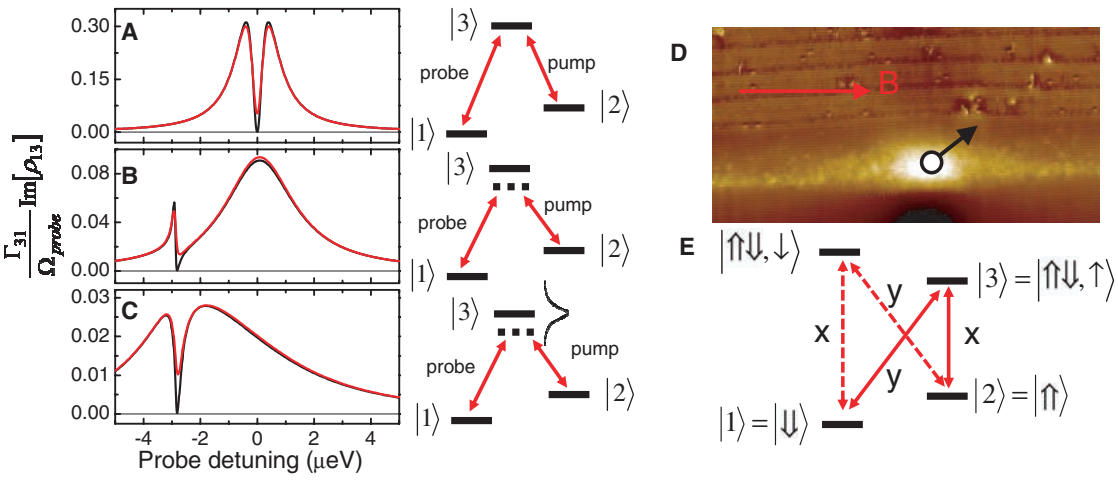

Fig. 1. (**A**) Calculated probe absorption spectrum in the presence of an on-resonant pump laser in a Λ system. The dip represents CPT; ρ is the density matrix. (**B**) As for (A) but with a detuned pump. The model uses Rabi energies $\hbar\Omega_{pump}$ = 1.0 μeV, $\hbar\Omega_{probe}$ = 0.45 μeV, radiative decay rates $\hbar\Gamma_{31}$ = $\hbar\Gamma_{32}$ = ½$\hbar\Gamma_r$ = 0.50 μeV with a lower-level coherence time T_2 = 1 μs (black line), and T_2 = 10 ns (red line). (**C**) Calculated probe absorption with the same parameters as (B) but also including a spectral wandering of level |3⟩ with Lorentzian probability distribution with full width Γ_X = 6 μeV. (**D**) A cross-sectional scanning tunneling image (80 nm by 40 nm) of a quantum dot, showing schematically a single hole and a magnetic field *B* applied in the plane along the *x* direction. [Image: Murat Bozkurt and Paul Koenraad] (**E**) The quantum states of the hole: |1⟩ and |2⟩ are the hole spin eigenvectors in the *x* basis, split by the Zeeman effect; the upper levels are X^{1+} excitons consisting of two spin-paired holes and an unpaired electron with spin ±½, again in the *x* basis. The optical transitions are linearly polarized along either the *x* or *y* direction. Two Λ systems are established (solid and dashed lines).

An alternative is to use a hole spin in an attempt to bypass the interaction with the nuclear spins (*10*–*16*). A hole state is constructed from a p-type atomic wave function that conveniently goes to zero at the location of the nuclei, suppressing the contact part of the hyperfine interaction (*14*). Furthermore, in a quantum dot, the hole spin–phonon interaction is weak because the strong quantization reduces the admixture of heavy and light hole states (*11*, *13*).

We conducted an experiment that is sensitive to hole spin coherence. We observed a quantum interference phenomenon, the "visibility" of which depends directly on the hole spin coherence (*17*). The interference arises in the optical spectroscopy of a Λ system, a quantum system consisting of three states, |1⟩, |2⟩, and |3⟩, with optical transitions between |1⟩ ↔ |3⟩ and |2⟩ ↔ |3⟩ (Fig. 1A). In our case, states |1⟩ and |2⟩ correspond to Zeeman-split hole spin states, and state |3⟩ corresponds to an exciton. A "pump" laser [Rabi energy $\hbar\Omega_{pump}$, where $\hbar$ is Planck's constant divided by 2π] drives the |2⟩ ↔ |3⟩ transition, and a "probe" laser [Rabi energy $\hbar\Omega_{probe}$] drives the |1⟩ ↔ |3⟩ transition. The interference occurs when the frequency difference of the lasers matches the |1⟩-|2⟩ splitting, the two-photon resonance. In this case, the amplitude of state |3⟩ undergoes a destructive interference, and a dark state—an admixture consisting only of states |1⟩ and |2⟩—results. This phenomenon, coherent population trapping (CPT) (*7*, *17*–*20*), is the underlying basis for electromagnetically induced transparency (*21*) and is revealed by a dip in the probe absorption spectrum, provided that the coherence of states |1⟩ and |2⟩ is high enough. Specifically, when $\Gamma_r > \Omega_{pump} > \Omega_{probe}$, the probe absorption acquires a dip with energy width $\hbar\Omega^2_{pump}/\Gamma_r$ where Γ_r is the spontaneous emission rate from state |3⟩ (Fig. 1A). This width sets the sensitivity of the experiment to the decoherence rate γ of state |2⟩ with respect to |1⟩: For $\gamma << \Omega^2_{pump}/\Gamma_r$ the signal in the dip goes to zero, but for $\gamma >> \Omega^2_{pump}/\Gamma_r$ the dip is washed out (Fig. 1A). Previous observations of CPT in semiconductors have not achieved a perfect dip because in each case the dephasing was too rapid (*7*, *18*–*20*).

Our experiments are performed on single InGaAs dots in a GaAs matrix (Fig. 1D), loading a single hole into a single dot and probing the exciton transitions resonantly with laser spectroscopy (*22*). To establish a Λ system, we apply a magnetic field in the *x* direction, in the growth plane, which allows optical transitions from both hole spin states to both exciton states (*23*) (Fig. 1E). Once the Zeeman splitting of the exciton states is larger than the linewidths, two Λ systems can be established. We work with the one at lower energy (Fig. 1E). At zero magnetic field and with one linearly polarized laser, there is an absorption peak at the exciton resonance. In magnetic field, this resonance disappears through optical pumping (*4*, *23*). However, a "double resonance" can be located by driving the dot simultaneously with a second laser: When both lasers come into resonance, one with the |1⟩ ↔ |3⟩ transition and the other with the |2⟩ ↔ |3⟩ transition, optical pumping is suppressed and a probe absorption signal reappears. Upon locating the double resonance, we then look for the CPT dip.

In the example data at a magnetic field of 2.3 T (Fig. 2), there is a pronounced and narrow dip in the probe spectrum. To prove that the dip arises from CPT, we detuned the pump laser (Fig. 3, A to C). Figure 3D shows that the energy shift of the dip in the probe spectrum equals the energy shift of the pump, as expected for a two-photon resonance. There are a number of features in Fig. 2. First, the dot is rendered transparent at the two-photon resonance. Such a clear destructive interference is only possible with a highly coherent hole spin state. Second, the CPT dip clearly survives the broadening of the exciton resonance, which is as large as 6 μeV for this particular dot.

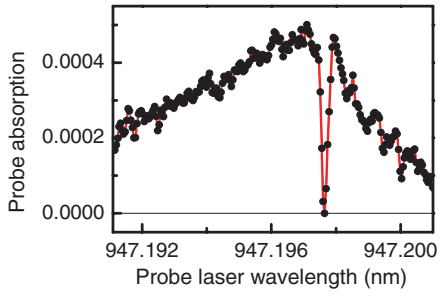

Fig. 2. Measured probe absorption spectrum (differential reflectivity) in the presence of a close-to-resonant weak pump laser on a single quantum dot containing a single hole. The pronounced dip signifies CPT. The measured Rabi energies are $\hbar\Omega_{pump}$ = 0.75 ± 0.25 μeV and $\hbar\Omega_{probe}$ = 0.34 ± 0.15 μeV; radiative decay time, 0.4 ± 0.2 ns; magnetic field, 2.3 T; integration time per point, 5 s; temperature, 4.2 K.

Third, for nonzero pump detunings, the form of the probe absorption spectrum does not follow the atomic physics model (Fig. 1B). Instead of a maximum signal located close to zero probe detuning (Fig. 1B), we find that the maximum signal is always close to the CPT dip (Fig. 3, A and C). Furthermore, for positive pump detunings, the probe absorption falls more rapidly on the positive detuning side than on the negative side, a situation reversed for negative pump detunings.

The CPT dip allows us to make a quantitative statement on the hole spin coherence time T_2* (*17*). To eliminate systematic errors, it is first necessary to understand the entire probe spectrum (Fig. 3, A to C). The missing factor in Fig. 1, A and B, is a description of the broadening of state |3⟩, the exciton. Including subnanosecond dephasing in level |3⟩ fails; this simply smears out the curves in Fig. 1, A and B. The experiment itself points to the resolution of this problem. The

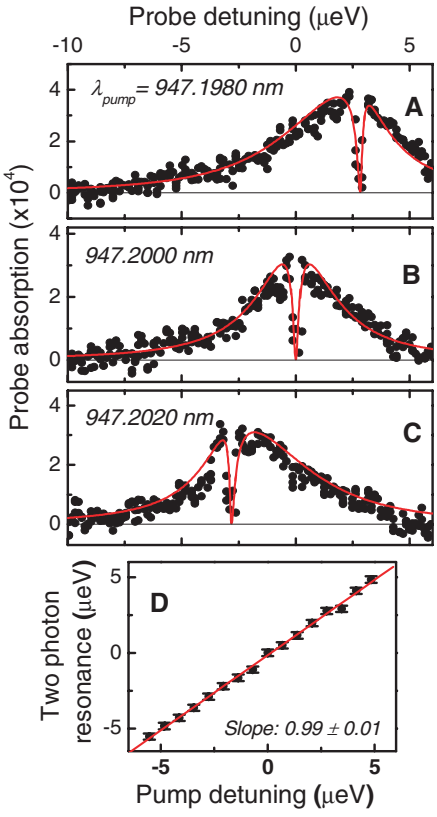

Fig. 3. CPT of a single-hole spin at 3.0 T and 4.2 K with Zeeman splitting 18.38 μeV using the same dot and Rabi energies as Fig. 2. The points show the measured absorption against probe laser detuning for three different pump wavelengths, one blue-detuned from the resonance (**A**), one close to resonance (**B**), and one red-detuned (**C**). The solid lines are fits to the calculated response for pump detunings of +2.831 μeV (A), 0.000 μeV (B), and −2.820 μeV (C); $\hbar\Omega_{pump}$ = 1.0 μeV, $\hbar\Omega_{probe}$ = 0.45 μeV, $\hbar\Gamma_{31} = \hbar\Gamma_{32}$ = 0.50 μeV, $\hbar\gamma_3$ = 0 (pure dephasing rate of state $|3\rangle$), $\hbar\gamma_2$ = 0.00067 μeV, Γ_X = 6.0 μeV, and field scattering ratio α = 0.01 (*22*). (**D**) Measured detuning of the probe laser at the CPT dip plotted against pump laser detuning with a linear fit.

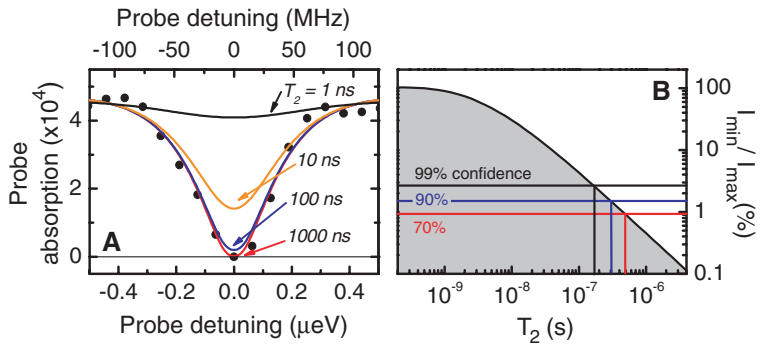

Fig. 4. (**A**) Data from Fig. 2 versus the calculated response (solid line) for several values of hole spin T_2. The theory uses the same parameters as in Fig. 3. (**B**) The calculated signal in the dip divided by the maximum signal (at zero pump detuning) as a function of hole spin T_2 (solid line). Experimental minimum/maximum signal ratios for confidence levels of 99%, 90%, and 70% are shown with horizontal lines.

narrow CPT dip amid the broad exciton resonance suggests that the exciton undergoes a spectral wandering with little if any effect on the hole spin splitting. Once the two-photon resonance condition is satisfied, it remains satisfied even as the exciton energy fluctuates. To confirm this view, we convoluted the density matrix calculation with a probability distribution in the detunings to describe the fluctuations of the exciton energy, slow relative to radiative recombination but fast relative to the experimental integration (*22*). The convolution made surprisingly large changes to the probe spectrum (Fig. 1C) and reproduced all the features in the experiment. We achieved excellent fits to the probe absorption curves (Fig. 3, A to C), reproducing both the width of the CPT dip and the overall line shape.

The minimum signal in the dip depends on the hole spin coherence. Figure 4A shows the results of the theory for various T_2 values along with the data of Fig. 2, allowing an immediate and robust conclusion that T_2* is at least 100 ns. To quantify this upper bound further, we used the average of the ratio of the minimum to the maximum signal, I_{min}/I_{max}, from 10 data sets: (0.11 ± 2.07)%. Figure 4B plots the calculated I_{min}/I_{max} versus T_2. The constraints on the parameters are that they must be compatible with the auxiliary experiments (*22*) and that they reproduce the overall line shapes in Fig. 3. This implies that any systematic error is less than the random error in the measurement of the small signal in the dip. The data in Fig. 4 reveal upper bounds to T_2 associated with probabilities calculated from the random error, for example, $T_2 \geq 490$ ns with 70% probability. With the current data, the probability that T_2 exceeds 1 μs is about 40%.

The CPT dip (Fig. 2 and Fig. 3, A to C) has a linewidth of just 0.35 μeV (85 MHz), ushering semiconductor optical spectroscopy into the domain of atomic physics with applications as frequency standards (*24*), ultrasensitive magnetometers (*25*), "slow light" photon storage devices (*21*), and coherent spin rotations via stimulated Raman adiabatic passage (*26*). The coherence of the hole spin points to applications in quantum information. A two-qubit device is possible with hole spins in tunnel-coupled quantum dot molecules (*27*).

The contact hyperfine interaction is not the only interaction between a quantum dot spin and the nuclear spins. There is also a dipole-dipole interaction. Recent theory suggests that the coupling coefficient of the heavy hole dipole-dipole hyperfine interaction is by no means negligible (*28*), but the interaction has an Ising form. For electrons, loss of phase arises through the component of the Overhauser field along the direction of the applied field. For a heavy hole spin with an Ising interaction, the Overhauser field lies in the growth direction, *z*, and has a benign effect in the presence of a large applied field in the *x* direction. Our data are consistent with this picture, but further work is required to establish its validity.

References and Notes

1. R. Hanson, L. P. Kouwenhoven, J. R. Petta, S. Tarucha, L. M. K. Vandersypen, *Rev. Mod. Phys.* **79**, 1217 (2007).
2. M. Kroutvar *et al.*, *Nature* **432**, 81 (2004).
3. S. Amasha *et al.*, *Phys. Rev. Lett.* **100**, 046803 (2008).
4. J. Dreiser *et al.*, *Phys. Rev. B* **77**, 075317 (2008).
5. I. A. Merkulov, A. L. Efros, M. Rosen, *Phys. Rev. B* **65**, 205309 (2002).
6. M. H. Mikkelsen, J. Berezovsky, N. G. Stoltz, L. A. Coldren, D. D. Awschalom, *Nat. Phys.* **3**, 770 (2007).
7. X. Xu *et al.*, *Nat. Phys.* **4**, 692 (2008).
8. J. R. Petta *et al.*, *Science* **309**, 2180 (2005); published online 1 September 2005 (10.1126/science.1116955).
9. A. Greilich *et al.*, *Science* **313**, 341 (2006).
10. S. Laurent *et al.*, *Phys. Rev. Lett.* **94**, 147401 (2005).
11. D. V. Bulaev, D. Loss, *Phys. Rev. Lett.* **95**, 076805 (2005).
12. M. Syperek *et al.*, *Phys. Rev. Lett.* **99**, 187401 (2007).
13. D. Heiss *et al.*, *Phys. Rev. B* **76**, 241306 (2007).
14. B. D. Gerardot *et al.*, *Nature* **451**, 441 (2008).
15. A. J. Ramsay *et al.*, *Phys. Rev. Lett.* **100**, 197401 (2008).
16. B. Eble *et al.*, *Phys. Rev. Lett.* **102**, 146601 (2009).
17. A. Imamoglu, *Phys. Stat. Sol. B* **243**, 3725 (2006).
18. M. D. Frogley, J. F. Dynes, M. Beck, J. Faist, C. C. Phillips, *Nat. Mater.* **5**, 175 (2006).
19. K. M. C. Fu, C. Santori, C. Stanley, M. C. Holland, Y. Yamamoto, *Phys. Rev. Lett.* **95**, 187405 (2005).
20. M. C. Phillips *et al.*, *Phys. Rev. Lett.* **91**, 183602 (2003).
21. M. Fleischhauer, A. Imamoglu, J. P. Marangos, *Rev. Mod. Phys.* **77**, 633 (2005).
22. See supporting material on *Science* Online.
23. X. Xu *et al.*, *Phys. Rev. Lett.* **99**, 097401 (2007).
24. R. Wynands, A. Nagel, *Appl. Phys. B* **68**, 1 (1999).
25. M. O. Scully, M. Fleischhauer, *Phys. Rev. Lett.* **69**, 1360 (1992).
26. K. Bergmann, H. Theuer, B. W. Shore, *Rev. Mod. Phys.* **70**, 1003 (1998).
27. E. A. Stinaff *et al.*, *Science* **311**, 636 (2006); published online 11 January 2006 (10.1126/science.1121189).
28. J. Fischer, W. A. Coish, D. V. Bulaev, D. Loss, *Phys. Rev. B* **78**, 155329 (2008).

29. Supported by the UK Engineering and Physical Sciences Research Council and the Royal Society of Edinburgh.

Supporting Online Material

www.sciencemag.org/cgi/content/full/325/5936/70/DC1
Materials and Methods
References

17 March 2009; accepted 21 May 2009
10.1126/science.1173684

Self-Assembling Sequence-Adaptive Peptide Nucleic Acids

Yasuyuki Ura,[1] John M. Beierle,[1] Luke J. Leman,[1] Leslie E. Orgel,[2] M. Reza Ghadiri[1]*

Several classes of nucleic acid analogs have been reported, but no synthetic informational polymer has yet proven responsive to selection pressures under enzyme-free conditions. Here, we introduce an oligomer family that efficiently self-assembles by means of reversible covalent anchoring of nucleobase recognition units onto simple oligo-dipeptide backbones [thioester peptide nucleic acids (tPNAs)] and undergoes dynamic sequence modification in response to changing templates in solution. The oligomers specifically self-pair with complementary tPNA strands and cross-pair with RNA and DNA in Watson-Crick fashion. Thus, tPNA combines base-pairing interactions with the side-chain functionalities of typical peptides and proteins. These characteristics might prove advantageous for the design or selection of catalytic constructs or biomaterials that are capable of dynamic sequence repair and adaptation.

Although several classes of nucleic acid analogs have been reported (*1*–*6*), nearly all previously postulated mechanisms for constructing nucleic acid oligomers invoke an irreversible covalent backbone assembly of nucleobase-containing monomers or fragments. We envisioned that a fundamentally different oligomer assembly mechanism relying on dynamic covalent chemistry (*7*–*19*) could involve the reversible anchoring of nucleobase units onto independently preformed backbone structures (*20*). In the present study, we investigate an oligomer system based on a simple repeating dipeptide backbone motif (*1*). The design features cysteine residues at alternating amino acid positions to provide the anchor for reversible tethering of nucleobase thioester monomers from solution via transthioesterification reactions. Although a number of reversible covalent reactions could be employed for nucleobase anchoring, thioester exchange was chosen for its chemoselective and relatively fast reaction kinetics, prebiotic relevance, and because it allowed the employment of a natural amino acid (Cys) for anchoring [see fig. S7 for molecular models supporting the structural compatibility of thioester peptide nucleic acid (tPNA) for interstrand base pairing with complementary oligonucleotides]. A variety of amino acid residues can be used at the flanking positions of the backbone (Glu, Asp, Arg, and Gly residues were employed here) to provide the appropriate spacing between Cys residues (*1*), improved aqueous solubility, backbone flexibility, and/or electrostatic properties for improved interactions with nucleic acids (Fig. 1). Because our studies experimentally establish a process involving peptides as the integral component for the spontaneous assembly of informational oligomers, it is tantalizing to speculate about the possible interdependence of peptides and nucleic acids at the advent of primordial (pre-RNA World) genetic systems (*21*–*24*).

[1]Department of Chemistry and The Skaggs Institute for Chemical Biology, The Scripps Research Institute, 10550 North Torrey Pines Road, La Jolla, CA 92037, USA. [2]The Salk Institute for Biological Studies, P.O. Box 85800, San Diego, CA 92186, USA.

*To whom correspondence should be addressed. E-mail: ghadiri@scripps.edu

We initially investigated the assembly of the adenine thioester (500 μM) (see fig. S1 for nucleobase syntheses) onto $(Glu\text{-}Cys)_{10}$ peptide **1** (100 μM) (*25*). Because peptide **1** contains 10 Cys residues, the nucleobase thioester was present in just 0.5 equivalents relative to Cys in this reaction. The anchoring reaction was rapid and efficient, generating a bell-shaped distribution of substituted peptides within 30 min, as determined by matrix-assisted laser desoption/ionization–time-of-flight mass spectrometry (MALDI-TOF MS) (Fig. 2A). When the nucleobase thioester was present in a twofold excess or higher ratio relative to Cys, the fully substituted 10-mer and 9-mer substituted tPNA strands predominated after 30 min (Fig. 2A). Product distributions did not change when analyzed after longer reaction times. These results are consistent with reports indicating that equilibrium in dynamic combinatorial thioester libraries is typically reached within 15 min (*26*–*28*).

Having established that peptide **1** rapidly and efficiently anchors adenine thioester monomers from solution via transthioesterification, we next assessed the capacity of this assembled tPNA strand to bind complementary sequences of DNA and RNA. We prepared tPNA strands by incubating peptide **1** (100 μM) and adenine thioester (2 mM, twofold excess relative to Cys residues) in neutral aqueous solution at 25°C for 30 min. Next, we added a dT_{20} DNA strand (100 μM) to the reaction solution, diluted the mixture 25-fold, and cooled it to 2°C for ultraviolet (UV) thermal denaturation analysis. The sample exhibited a hyperchromic melting profile consistent with a cooperative helix-to-coil transition, with an observed melting temperature (T_m) of 34°C (Fig. 2B). No change in absorbance was apparent in numerous control spectra (Fig. 2B), indicating that the observed transition occurred only when the peptide, nucleobase thioester, and complementary DNA strand were simultaneously present in the reaction mixture. In an otherwise identical reaction involving the (noncomplementary) dA_{20} template instead of dT_{20}, we did not observe any cooperative melting transition, which thus indicated base-pairing selectivity.

To further support the hypothesis that the observed pairing interaction was dependent on anchoring of nucleobase species to peptide **1**, we examined a series of reactions involving dT_{20} (5 μM), peptide **1** (5 μM), and increasing concentrations of the adenine thioester (0, 25, 50, or 100 μM). Only the reactions employing 50 or 100 μM thioester exhibited cooperative

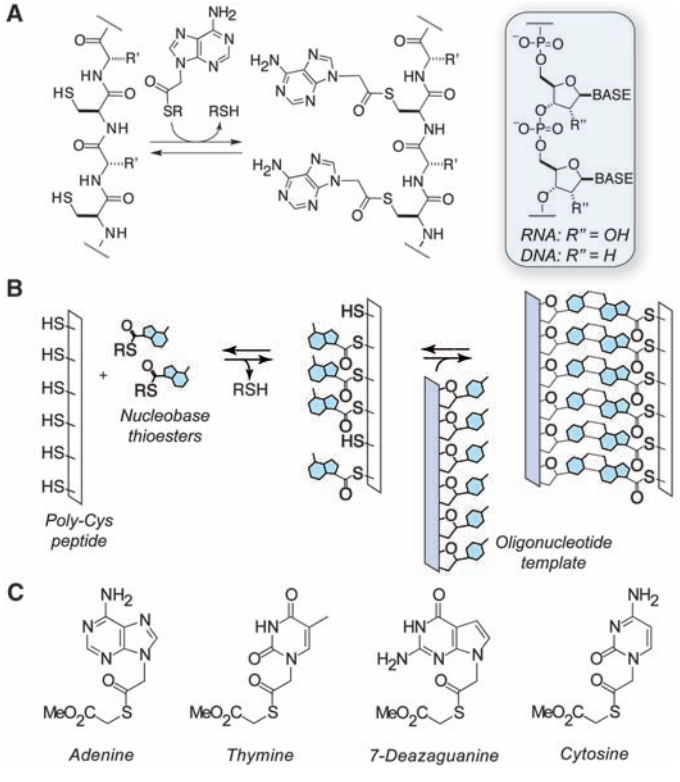

Fig. 1. Chemical structure and assembly mechanism of the dynamic oligomers. (**A**) Mechanism for reversible covalent assembly of the oligomers via anchoring of thioester-derived recognition units (adenine is shown) onto an oligopeptide backbone. RNA and DNA structures are drawn for comparison (in the box at right). (**B**) Illustration of oligomer assembly and binding to a complementary oligonucleotide template. (**C**) Structures of the nucleobase thioester monomers used in the present study. Me, methyl.

transitions (fig. S2), as would be expected considering that the number of substitutions per peptide is probably five or fewer under the more limiting concentrations of nucleobase thioester. With shorter DNA dT_{10} or RNA rU_{20} templates, cooperative melting transitions were also observed (Table 1). A Job plot analysis for peptide **1** with dT_{10} or dT_{20} indicated binding in the expected 1:1 or 2:1 ratios, respectively (fig. S3).

We next investigated the effects of backbone chirality, charge, spacing of the Cys side chains, flexibility, and length by preparing an expanded series of peptide backbones for analysis (Table 1). We observed cooperative melting transitions for each of the more than 20 sequences tested. Sequences **2** through **5** surveyed different combinations of amino acid chirality in the repeating dipeptide unit; higher T_m's were observed for the homochiral peptides (**2** and **5**) than for the heterochiral backbones (**3** and **4**) (fig. S2). Replacing the Glu residues of peptides **1** and **2** with Arg (sequences **7** and **8**) resulted in substantially heightened T_m values, whereas replacing Glu with Asp (sequence **6**) had little effect on the observed T_m, as might be expected based on electrostatic considerations. We synthesized peptides **9** through **12** to introduce backbone conformational flexibility by incorporating Gly residues. However, the Gly residues replace negatively charged Glu in sequence **9** and positively charged Arg in sequences **10** through **12**, so the observed increase in T_m for **9** relative to **2** and decreases in T_m for **10** through **12** relative to **8** probably result from electrostatic changes rather than from conformational effects.

We next prepared peptides **13** through **22**, in which the length of the backbone varied from 4 to 20 Cys residues. T_m values rose with backbone length (Fig. 2C), a trend probably due to the capacity of the longer backbones to anchor a greater number of nucleobase units for interaction with the oligonucleotide strand. We further prepared sequences **23** and **24** to study the effects of altered

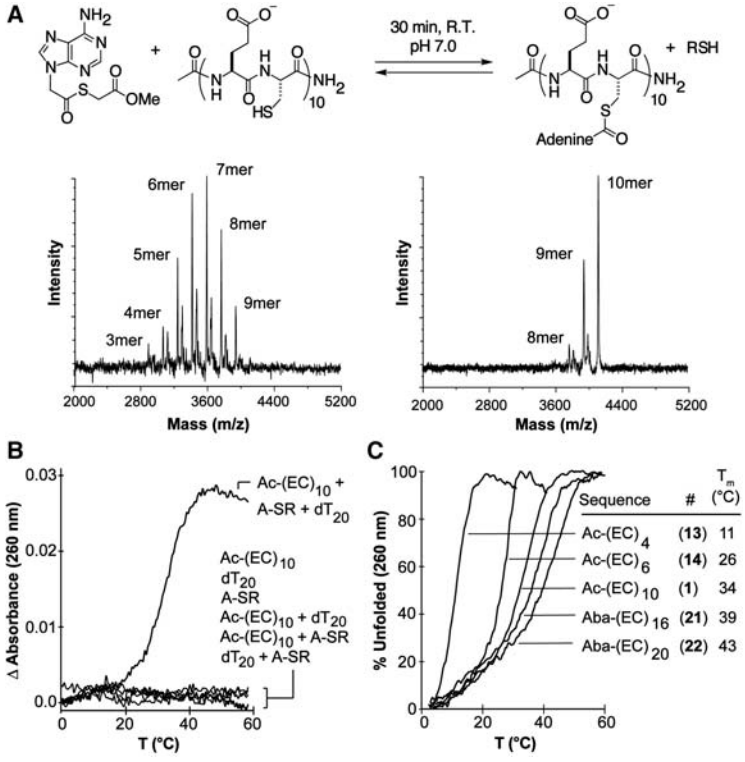

Fig. 2. Establishing oligomer assembly and DNA pairing properties. (**A**) Reaction scheme and corresponding MALDI-TOF MS spectra demonstrating adenine thioester anchoring to peptide **1** in reactions containing 0.5 equivalents (left) or 2 equivalents (right) of adenine thioester relative to Cys residues. "7mer" refers to peptides containing seven adenine bases tethered to Cys side chains. m/z, mass/charge ratio. (**B**) UV thermal denaturation curves for solutions containing various combinations of peptide **1** (5 μM), adenine thioester ("A-SR," 100 μM), and dT_{20} (5 μM). (**C**) Thermal denaturation curves demonstrating the effect of peptide backbone length on T_m values. "Aba" refers to 4-acetamidobenzoic acid, which was incorporated in some cases to facilitate peptide concentration determination. The DNA present in all cases is dT_{20}.

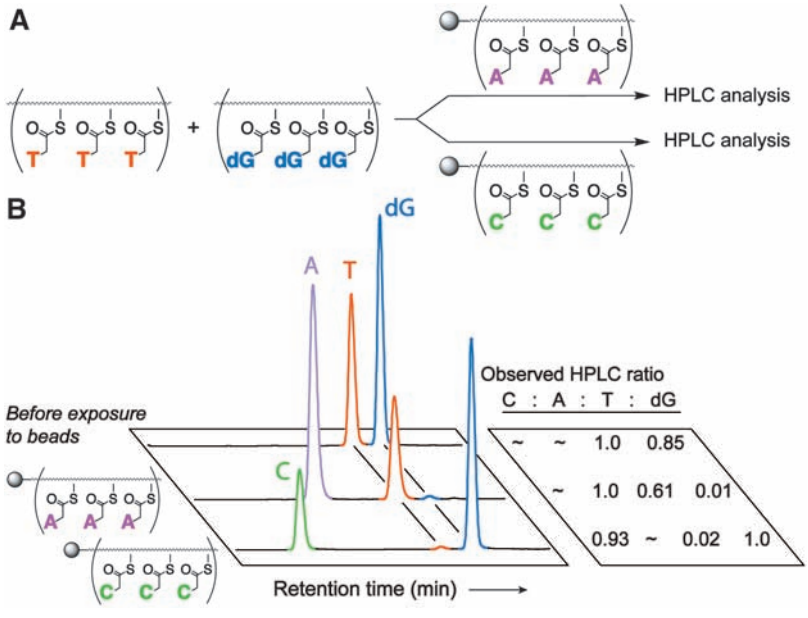

Fig. 3. Establishing specific self-pairing interactions among the assembled tPNA oligomers. (**A**) Schematic diagram illustrating the pull-down assay used to characterize oligomer self-pairing (nucleobase thioesters: T, thymine; A, adenine; C, cytosine; dG, 7-deazaguanine). After the 1-hour incubation, the beads were washed to remove those peptide strands not associated with the bead-bound tPNA sequences. Next, isobutylamine was added to the beads to cleave the nucleobase thioesters anchored to the peptide strands via aminolysis. Subsequent HPLC analysis of the cleavage products allowed quantification of the resultant nucleobase amides relative to one another. (**B**) HPLC analyses of the assay indicating that oligomers substituted with complementary nucleobases pair with high selectivities. Similar high selectivities were observed when the assay was carried out instead with the 7-deazaguanine and thymine bases anchored to the immobilized peptides and the adenine- and cytosine-substituted strands free in solution.

structural and hydrogen bonding properties of the repeating backbone unit. Peptide **23** has a seven-atom backbone repeat (in contrast to the six-atom repeat in the backbones of oligo-dipeptides and oligonucleotides) as a result of the incorporated isoaspartic acid residue (see fig. S4 for structure). The somewhat lower T_m values for sequence **23** relative to peptides **2** or **6** may, therefore, stem from a less favorable nucleobase spacing and/or from the increased proximity of the carboxylate side chain to the backbone/oligonucleotide duplex. The repeating unit of peptide **24** includes sarcosine, the N-methylated derivative of glycine. N-methylation of a backbone amine prevents the formation of hydrogen bonds and reduces the barrier to amide cis/trans isomerization; these factors probably contribute to the observed increase in T_m for **24** relative to non-methylated sequence **10**. Overall, the above studies indicate that a broad range of amino acid residues is permissible in the tPNA backbone. Therefore, tPNA seems to be unique among oligonucleotide analogs in simultaneously exhibiting base-pairing interactions and expressing side chain functionalities of typical peptides and proteins. These characteristics might be advantageous for the future design or selection of catalytic tPNA constructs reminiscent of protein enzymes or ribozymes.

In addition to characterizing the cross-pairing interactions between the tPNA oligomers and oligonucleotides, we also confirmed the ability of the tPNA strands to self-pair. Self-pairing is an important criterion for a putative primordial genetic polymer, because sequence-specific self-recognition and templating would have been necessary for a polymer to propagate genetic information before the advent of RNA. Initial studies aimed at establishing self-pairing interactions using analyses by UV or circular dichroism spectroscopy proved inconclusive because the observed spectral changes were of low magnitude and were probably complicated by thioester hydrolysis; these observations suggest that the tPNA homoduplex may not exhibit strong hyperchromic shifts upon denaturation or may have a poorly defined structure. We therefore carried out a series of pull-down experiments in which an N-terminally biotinylated $(Glu\text{-}Cys)_{10}$ peptide was immobilized onto a solid support and substituted with one of the four nucleobases (7-deazaguanine was used in place of guanine to avoid the possibility of forming of G-quadruplex type structures but still retain the Watson-Crick specificity of guanine). The immobilized, nucleobase-substituted peptide was then incubated with a solution containing two or three differentially substituted $(Glu\text{-}Cys)_{20}$ peptides to afford direct binding competitions (Fig. 3). In each case, the immobilized adenine-, thymine-, cytosine-, or 7-deazaguanine–substituted peptides specifically retained those strands substituted with the Watson-Crick complementary nucleobase; observed selectivities for the complementary base over noncomplementary bases were typically ≥10:1 (Fig. 3). Furthermore, the observed amount of a 7-deazaguanine–substituted strand retained by an immobilized cytosine-substituted peptide was reduced by about half when a non-immobilized cytosine-substituted peptide was also included in the incubation solution, as would be expected due to partitioning of the 7-deazaguanine–substituted strand between the competing complementary strands in solution and on the solid support. Analysis of an immobilized 7-deazaguanine–substituted peptide with a bound cytosine-substituted strand at regularly increasing temperatures indicated a T_m of ~15 to 20°C (fig. S5). Because the substituted peptides were purified after the nucleobase anchoring reaction, the absence of free nucleobase thioester and thiol in these self-pairing studies makes it unlikely that thioester exchange occurred among the substituted peptides.

Finally, we investigated the potential for dynamic nucleobase exchange and template-directed assembly processes in the tPNA strands. Initial experiments confirmed the capacity for nucleobase exchange by showing that the ratio of nucleobases anchored to peptide **1** changed by severalfold over a few hours in response to the addition of one of the nucleobase thioesters in excess (fig. S6). A much more interesting driving force that could, in principle, influence tPNA assembly is the presence of a template strand complementary in sequence to a subset of the reversibly assembled oligomers. As with other dynamic libraries, those oligomers that bind to the template would be sequestered from the equilibrium, driving the reaction to re-equilibrate, and thereby amplifying species that bind the oligonucleotide. We investigated this possibility by mixing the adenine and 7-deazaguanine nucleobase thioesters in solution with peptide **9**, splitting the reaction mixture, and then adding a different DNA template to each solution. In the

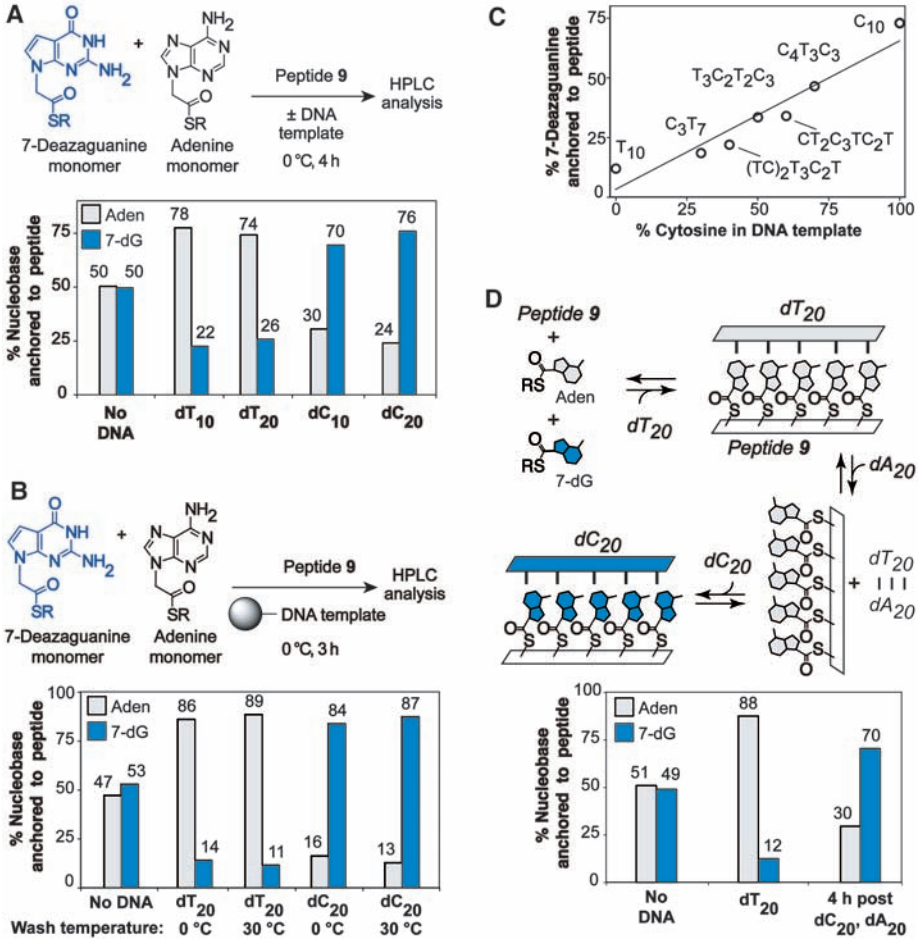

Fig. 4. Template-directed assembly and dynamic sequence remodeling reactions. (**A**) Outcome of incubation of peptide **9** with various DNA templates in the presence of adenine and 7-deazaguanine thioesters, analyzed by HPLC to determine the ratio of nucleobases anchored to the peptide. On the basis of independent experiments run in duplicate, errors are estimated to be less than 8% for all data shown. (**B**) Same as (A), except employing immobilized DNA templates. After 3 hours, the immobilized duplexes were washed at the temperatures shown and analyzed by HPLC. (**C**) Template-directed assembly reactions using immobilized mixed sequence DNA templates (template sequences are shown in the figure). (**D**) Outcome of incubation of peptide **9** with adenine and 7-deazaguanine thioesters, initially in the presence of a dT_{20} template for 2 hours, and after 4 additional hours in the presence of dA_{20} and dC_{20} DNA strands, leaving only the dC_{20} strand available to serve as template because of duplex formation between dT_{20} and dA_{20}. HPLC analysis of the oligomers before and 4 hours after addition of the dA_{20} and dC_{20} strands indicated substantial sequence remodeling in response to the available templates.

absence of a template, the ratio of bases anchored to the peptide after four hours at 0°C was approximately 1:1, as determined by high-performance liquid chromatography (HPLC) analysis. In contrast, anchored adenine species were selectively enriched to a ~3:1 ratio when dT_{10} or dT_{20} were present, whereas anchored 7-deazaguanine moieties were elevated to a similar ~3:1 ratio in the presence of a dC_{10} or dC_{20} template (Fig. 4A). These results are consistent with a template-directed assembly process in which Watson-Crick pairing interactions of the nucleobase-substituted tPNA strands with the DNA template favor the incorporation of complementary units to the peptide at equilibrium. Nearly identical nucleobase ratios were observed for aliquots of the reaction removed at 2 hours, suggesting that equilibrium is reached within 2 hours in such reactions.

One explanation for the observed 3:1 templating ratios in the above reactions is that all the assembled oligomers in solution contain anchored nucleobases in a ratio of 3:1; alternatively, the observed ratio could represent a composite value of a more complex mixture of equilibrating oligomers, some of which have a higher proportion of the complementary nucleobase and are bound to the template, and some of which have a lower proportion of the complementary base and are not bound to the template. To distinguish between these two possibilities, we prepared several DNA templates having a biotin tag. This allowed us to immobilize the DNA templates on streptavidin beads and thereby selectively retain and analyze only those assembled oligomers that bound to the template strands (Fig. 4B) (*16*). After washing away unbound peptide species, the observed nucleobase ratio for oligomers retained by the DNA template improved in the presence of both dT_{20} and dC_{20} such that the complementary bases represented nearly 90% of the bases anchored to the peptide backbone (Fig. 4B). Washing the immobilized template/oligomer duplexes at increasing temperatures only slightly improved the observed nucleobase selectivities, suggesting that the duplex-bound oligomers are relatively uniform in nucleobase constitution.

We further prepared a series of biotinylated mixed-sequence DNA templates containing different ratios of cytosine and thymine nucleotides to investigate templated-assembly reactions involving more complex templates (see Fig. 4C for template sequences). After carrying out assembly reactions using these templates with peptide **9** as described above, we observed a linear relation between the percentage of cytosine nucleotides present in the DNA template and the percentage of 7-deazaguanine thioester anchored to the peptide at equilibrium (Fig. 4C). This finding supports the potential of the oligomers to sequence-specifically assemble in response to mixed-sequence templates, although more rigorous evaluations of this possibility will probably require methods to sequence the assembled tPNA oligomers.

Adaptability is a characteristic feature of living systems and could be an advantageous property for new materials or prebiotic informational oligomers. To further demonstrate the unique dynamic features of the tPNA oligomers, we carried out an experiment involving selective pressures (DNA template strands) that change over the course of the reaction. Peptide **9** was incubated with the adenine and 7-deazaguanine thioesters, initially in the presence of dT_{20} template. After 2 hours, an aliquot was removed for analysis and, as expected, showed predominantly adenine nucleobases anchored to the peptide (Fig. 4D). An excess of dA_{20} and dC_{20} DNA strands were then added to the reaction. We reasoned that, because of the greater length of the DNA strands relative to the peptide, the added dA_{20} would displace any assembled oligomer that was bound to the dT_{20} template, thereby preventing dT_{20} from further templating oligomer assembly. These processes would leave only the dC_{20} strand available in solution to act as a template. Although the recently displaced, predominantly adenine-substituted peptides would not be expected to initially interact with the dC_{20} strand, nucleobase exchange involving the 7-deazaguanine monomers in solution would eventually make possible nucleation of productive interactions between dC_{20} and the oligomer. HPLC analysis of the reaction mixture 4 hours after the addition of the dA_{20} and dC_{20} DNA strands indicated a substantial enrichment of anchored 7-deazaguanine moieties relative to the analysis before the addition of dA_{20} and dC_{20} (Fig. 4D), supporting the suggestion that the oligomers are capable of dynamic response to changing external conditions.

Although we have focused here on peptide backbones, a wide variety of nonpeptidic polythiol backbone architectures could additionally be suitable foundations for anchoring thioester-based recognition units. Furthermore, a number of other reversible covalent bonds, such as acetal (*29*), disulfide, acylhydrazone (*9*, *12*), or imine (*16*, *18*–*20*) linkages, are also compatible with aqueous conditions and therefore could probably be used to engineer dynamic informational oligomers using suitably functionalized backbone and nucleobase derivatives. Although the templating results obtained thus far are encouraging, emerging experimental and theoretical evidence (*30*–*33*) indicates that several factors can limit the degree to which template affinity affects the amplification of library members in dynamic combinatorial libraries such as this one. An important

Table 1. Thermal denaturation data for various peptide backbones. All thermal denaturations were conducted at 260 nm with the use of equimolar adenine-substituted peptide and oligonucleotide (4 μM), unless otherwise noted. See table S1 for concentrations at which nucleobase anchoring reactions were conducted (typically 100 μM) before addition of the oligonucleotide and dilution for UV analysis. "Aba" refers to 4-acetamidobenzoic acid, which was added in some cases to facilitate peptide concentration determination. Underlined letters represent amino acids of the D-chirality. "[βD]" refers to isoaspartic acid (the β^3-amino acid derived from coupling to the Asp side chain); see fig. S4 for structure. "Sar" refers to sarcosine (the *N*-methylated derivative of glycine). A dash indicates that an analysis was conducted, but it did not give a typical sigmoidal melting transition. nd, not determined.

Peptide number	Peptide sequence	T_m (°C)		
		dT_{10}	dT_{20}	rU_{20}
1	Ac-$(EC)_{10}$-$CONH_2$	17	34	22
2	Aba-$(EC)_{10}$-$CONH_2$	15	27	nd
3	Aba-$(\underline{E}C)_{10}$-$CONH_2$	10	15	nd
4	Aba-$(\underline{EC})_{10}$-$CONH_2$	7	15	nd
5	Aba-$(\underline{EC})_{10}$-$CONH_2$	15	28	16
6	Aba-$(DC)_{10}$-$CONH_2$	16	30	17
7	Ac-$(RC)_{10}$-$CONH_2$*	27	43	39
8	Aba-$(RC)_{10}$-$CONH_2$	21	31	nd
9	Aba-$(ECGC)_5$-$CONH_2$	19	32	13
10	Aba-$(GCRC)_5$-$CONH_2$	15	30	–‡
11	Aba-$GCRC(GC)_3RC(GC)_3RC$-$CONH_2$	14	25	nd
12	Aba-$RC(GC)_8RC$-$CONH_2$	12	20	nd
13	Ac-$(EC)_4$-$CONH_2$	<5	11	nd
14	Ac-$(EC)_6$-$CONH_2$	19	26	nd
15	Ac-$(EC)_8$-$CONH_2$	18	30	nd
16	Ac-$(ECGC)_3$-$CONH_2$	18	23	nd
17	Ac-$(GCEC)_3$-$CONH_2$	18	23	nd
18	Ac-$(RC)_4$-$CONH_2$	8	20	nd
19	Ac-$(RC)_6$-$CONH_2$*	19	31	nd
20	Ac-$(RC)_8$-$CONH_2$*	21	34	nd
21	Aba-$(EC)_{16}$-$CONH_2$†	23	39	nd
22	Aba-$(EC)_{20}$-$CONH_2$†	–‡	43	nd
23	Aba-$([\beta D]C)_{10}$-$CONH_2$	9	20	11
24	Ac-$(SarCRC)_5$-$CONH_2$	21	37	nd
–	dA_{10}	35	46	nd

*Before analysis, the sample was annealed by heating to 60°C. †Peptide and oligonucleotide concentrations of 1 μM were used for analysis. ‡The sample did not exhibit a typical sigmoidal melting transition.

limitation for the oligomers described here is that library members assembled from fewer building blocks have an entropic advantage over species assembled from a larger number of building blocks. Although template binding energy can overcome this disadvantage, such a handicap could make the assembly of long oligomers challenging. It remains to be seen whether the sequence integrity of the tPNA oligomers will be sufficient to propagate genetic information through multiple rounds of replication or templated synthesis.

References and Notes

1. G. K. Mittapalli *et al.*, *Angew. Chem. Int. Ed.* **46**, 2478 (2007).
2. S. Karkare, D. Bhatnagar, *Appl. Microbiol. Biotechnol.* **71**, 575 (2006).
3. A. Eschenmoser, *Chimia (Aarau)* **59**, 836 (2005).
4. L. Zhang, A. Peritz, E. Meggers, *J. Am. Chem. Soc.* **127**, 4174 (2005).
5. F. Beck, P. E. Nielsen, in *Artificial DNA*, Y. E. Khudyakov, H. A. Fields, Eds. (CRC Press, Boca Raton, FL, 2003), pp. 91–114.
6. U. Diederichsen, *Angew. Chem. Int. Ed. Engl.* **35**, 445 (1996).
7. R. E. Kleiner, Y. Brudno, M. E. Birnbaum, D. R. Liu, *J. Am. Chem. Soc.* **130**, 4646 (2008).
8. D. A. Fulton, *Org. Lett.* **10**, 3291 (2008).
9. D. T. Hickman, N. Sreenivasachary, J.-M. Lehn, *Helv. Chim. Acta* **91**, 1 (2008).
10. S. Ladame, *Org. Biomol. Chem.* **6**, 219 (2008).
11. P. T. Corbett *et al.*, *Chem. Rev.* **106**, 3652 (2006).
12. N. Sreenivasachary, D. T. Hickman, D. Sarazin, J.-M. Lehn, *Chem. Eur. J.* **12**, 8581 (2006).
13. W. G. Skene, J.-M. P. Lehn, *Proc. Natl. Acad. Sci. U.S.A.* **101**, 8270 (2004).
14. Y. Higaki, H. Otsuka, A. Takahara, *Macromolecules* **37**, 1696 (2004).
15. S. J. Rowan, S. J. Cantrill, G. R. L. Cousins, J. K. M. Sanders, J. F. Stoddart, *Angew. Chem. Int. Ed.* **41**, 899 (2002).
16. X. Li, D. G. Lynn, *Angew. Chem. Int. Ed.* **41**, 4567 (2002).
17. K. Oh, K.-S. Jeong, J. S. Moore, *Nature* **414**, 889 (2001).
18. Z.-Y. J. Zhan, D. G. Lynn, *J. Am. Chem. Soc.* **119**, 12420 (1997).
19. J. T. Goodwin, D. G. Lynn, *J. Am. Chem. Soc.* **114**, 9197 (1992).
20. N. V. Hud, S. S. Jain, X. Li, D. G. Lynn, *Chem. Biodivers.* **4**, 768 (2007).
21. R. Pascal, L. Boiteau, A. Commeyras, *Top. Curr. Chem.* **259**, 69 (2005).
22. J.-P. Biron, A. L. Parkes, R. Pascal, J. D. Sutherland, *Angew. Chem. Int. Ed.* **44**, 6731 (2005).
23. L. E. Orgel, *Crit. Rev. Biochem. Mol. Biol.* **39**, 99 (2004).
24. C. De Duve, in *Molecular Origins of Life*, A. Brack, Ed. (Cambridge Univ. Press, Cambridge, 1998), pp. 219–236.
25. Materials and methods are available as supporting online material on *Science* Online.
26. J. Leclaire, L. Vial, S. Otto, J. K. M. Sanders, *Chem. Commun. (Camb.)* **15**, 1959 (2005).
27. M. G. Woll, S. H. Gellman, *J. Am. Chem. Soc.* **126**, 11172 (2004).
28. R. Larsson, Z. Pei, O. Ramström, *Angew. Chem. Int. Ed.* **43**, 3716 (2004).
29. H. D. Bean, F. A. L. Anet, I. R. Gould, N. V. Hud, *Orig. Life Evol. Biosph.* **36**, 39 (2006).
30. P. T. Corbett, J. K. M. Sanders, S. Otto, *Chem. Eur. J.* **14**, 2153 (2008).
31. P. T. Corbett, S. Otto, J. K. M. Sanders, *Chem. Eur. J.* **10**, 3139 (2004).
32. K. Severin, *Chem. Eur. J.* **10**, 2565 (2004).
33. A. Grote, R. Scopelliti, K. Severin, *Angew. Chem. Int. Ed.* **42**, 3821 (2003).

34. This work is dedicated in memory of our friend and colleague Professor Leslie E. Orgel (1927–2007). We thank R. Krishnamurthy and A. Eschenmoser for helpful discussions. Support was provided in part by the Skaggs Institute for Chemical Biology, the NASA Earth and Space Science Fellowship Program (grant NNX07AR35H to J.M.B.), and the NASA Science Mission Directorate's Planetary Science Division (NRA NNH07ZDA001N).

Supporting Online Material

www.sciencemag.org/cgi/content/full/1174577/DC1
Materials and Methods
SOM Text
Figs. S1 to S7
Table S1
References

6 April 2009; accepted 26 May 2009
Published online 11 June 2009;
10.1126/science.1174577
Include this information when citing this paper.

Impact of Shifting Patterns of Pacific Ocean Warming on North Atlantic Tropical Cyclones

Hye-Mi Kim, Peter J. Webster,* Judith A. Curry

Two distinctly different forms of tropical Pacific Ocean warming are shown to have substantially different impacts on the frequency and tracks of North Atlantic tropical cyclones. The eastern Pacific warming (EPW) is identical to that of the conventional El Niño, whereas the central Pacific warming (CPW) has maximum temperature anomalies located near the dateline. In contrast to EPW events, CPW episodes are associated with a greater-than-average frequency and increasing landfall potential along the Gulf of Mexico coast and Central America. Differences are shown to be associated with the modulation of vertical wind shear in the main development region forced by differential teleconnection patterns emanating from the Pacific. The CPW is more predictable than the EPW, potentially increasing the predictability of cyclones on seasonal time scales.

North Atlantic tropical cyclones (hereafter "cyclones") have a substantial societal impact in the United States, Mesoamerica, and the Caribbean, and much effort has been expended in predicting their number and frequency (*1*–*4*). Over the past 150 years, U.S. landfall frequencies and damages have been smaller during El Niño ($800 million/year) than during La Niña ($1600 million/year) (*5*). The phase of the El Niño Southern Oscillation (ENSO) is a critical predictor used in empirical forecasting of the number of cyclones (*1*, *6*, *7*). Correlations between the phase of ENSO and cyclone activity have been well documented: Activity is reduced in the El Niño phase whereas it is increased in the La Niña phase, which is attributed to alterations in vertical wind shear (*1*) or atmospheric stability (*8*) associated with the different phases of ENSO.

Several recent studies (*9*–*13*) have identified episodes of warming in the central Pacific Ocean (central Pacific warming, CPW), in contrast to the conventional El Niño warming that occurs generally in the cold tongue region of the East Pacific Ocean (eastern Pacific warming, EPW). Warming and cooling events are defined based on the detrended sea-surface temperature (SST) (*14*) anomaly index for August to October, as discussed in the Supporting Online Material (SOM). EPW, CPW, and Eastern Pacific cooling (EPC) events are defined as follows: Niño 3 (fig. S1) warming greater than 1 standard deviation (SD), for EPW; Niño 3 or Niño 3.4 cooler than 1 SD, for EPC; and for CPW, Niño 4 warming exceeding 1 SD, while Niño 3 stays below this range. The results are shown in fig. S2.

With these definitions, a total of 9 EPW years, 5 CPW years, and 12 EPC years were identified. SST anomalies for all warming events since 1950 are shown in fig. S3. Although the frequency of the total number of warm events (i.e., CPW + EPW) has stayed approximately the same, the occurrence of CPW events has been increasing at the expense of EPW events, especially since the early 1990s (fig. S2). The frequency of cold-phase events (EPC) has remained approximately the same.

Figure 1, A to C, displays the composite of SST anomalies during the period August to October for EPW, CPW, and EPC events, respectively. The CPW (Fig. 1B) is confined to the central Pacific with a maximum SST anomaly near the dateline, whereas EPW events (Fig. 1A) are located 60° to 80° to the east, in a location similar to that of the EPC maximum negative anomaly (Fig. 1C). The magnitude of the CPW anomaly is smaller than that associated with EPW but is set against a higher background SST, making it possibly more conducive to the formation of deep convection. Remote climate associations during CPW and EPW have been found to be different (*11*). For example, a CPW event appears to be associated with reduced rainfall in the western United States and increased rainfall in the eastern United States, opposite to that expected during an EPW (*15*).

The monthly variation in the frequency of tropical cyclone formation from June to November is shown in Fig. 1D for EPW, CPW, and EPC, in addition to the climatological average, using the National Hurricane Center Best Track tropical

School of Earth and Atmospheric Science, Georgia Institute of Technology, 311 Ferst Drive, Atlanta, GA 30332, USA.

*To whom correspondence should be addressed. E-mail: pjw@eas.gatech.edu

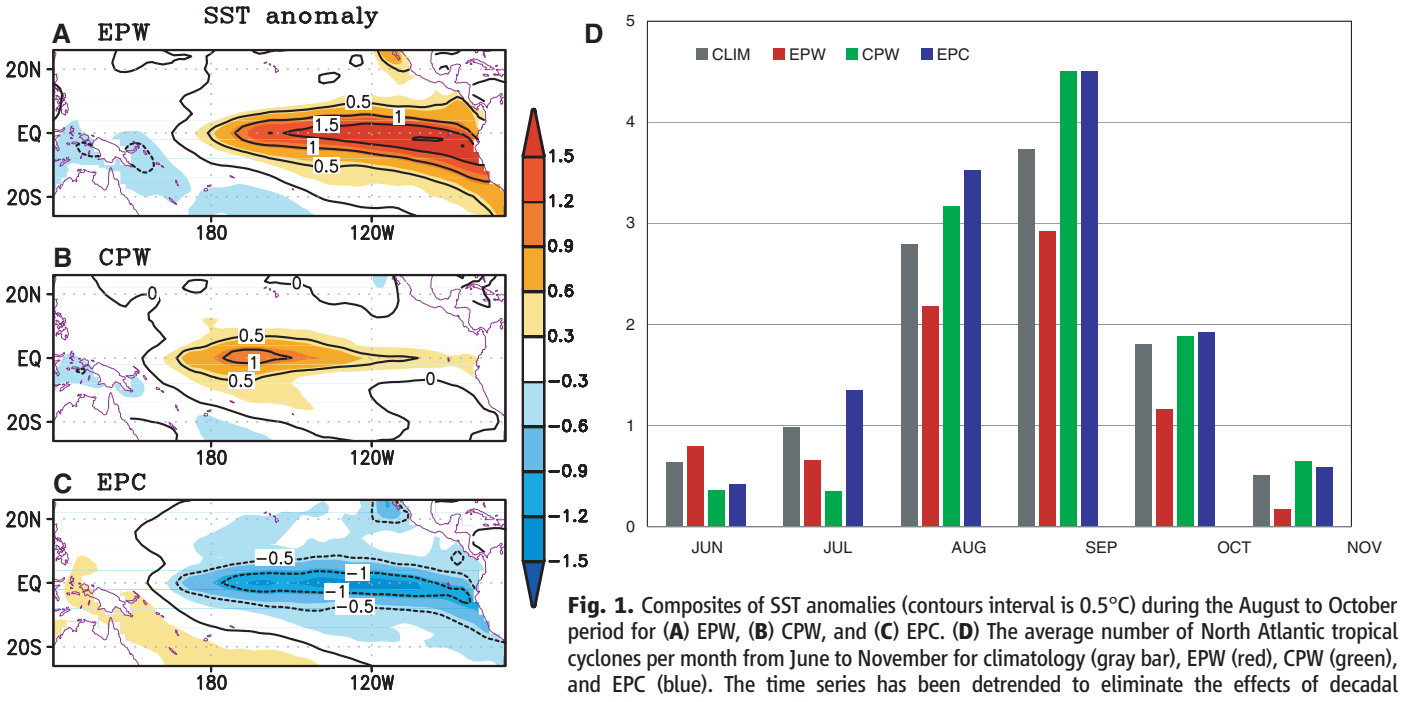

Fig. 1. Composites of SST anomalies (contours interval is 0.5°C) during the August to October period for (**A**) EPW, (**B**) CPW, and (**C**) EPC. (**D**) The average number of North Atlantic tropical cyclones per month from June to November for climatology (gray bar), EPW (red), CPW (green), and EPC (blue). The time series has been detrended to eliminate the effects of decadal variability or climate trends.

cyclone database (*16*) from 1950 to 2006. The database was detrended to avoid the possible statistical influence of a climate trend (*17*–*19*) or decadal variability (*20*, *21*). Climatologically, the greatest number of cyclones occurs during August to October. There is a clear difference between the number of cyclones forming during EPW and EPC events, as noted earlier (*1*), but there is almost as large a difference between the EPW and CPW events. The accumulated cyclone energy (ACE) also shows that the overall cyclone activity is larger in CPW events than in EPW events (table S1).

The location of the Pacific warming also affects the location of cyclogenesis and the tracks of tropical cyclones. Figure 2 shows the composite of mean track density anomalies relative to the 57-year climatology. To calculate the track density, "best track" locations are binned into 5° × 5° grid boxes. Track density for a specific type of Pacific warming or cooling event is defined as the number of cyclones passing through each grid box during the ASO period divided by the total number of years for that type of event. Track density is smoothed by averaging the eight-grid points surrounding the main grid point with 1:8 weighting and the total divided by 2. This technique provides anomaly patterns of the locus of tropical storms (*22*). A bootstrap technique (*23*) is applied to determine statistical significance of the track density. For the EPW events, a composite anomaly is constructed with 9 years chosen at random from among the 57 years of data. The process is repeated 10,000 times to obtain a probability distribution at 90 and 95% levels. The same process is applied for CPW but by choosing 5 years and, for EPC, 12 years. Confidence limits are shown as contours on Fig. 2. During an EPW (Fig. 2A), track density is reduced over most of the North Atlantic, with a concentration in the western and Caribbean regions. The tracks during a CPW event (Fig. 2B) differ markedly from those occurring during an EPW event: Compared to climatology, track density for CPW increases across the Caribbean, the Gulf of Mexico, and the U.S. east coast, but it decreases in the central and western North Atlantic. During an EPC event (Fig. 2C), large increases in track density occur across the entire North Atlantic.

The year 2004 was a CPW year. Seasonal cyclone forecasts predicted lower-than-average activity based on predictions of El Niño by the National Oceanic and Atmospheric Administration Climate Prediction Center (*24*) using the Niño 3.4 index. However, the cyclone activity was unusually high, contrary to normal expectations for an El Niño year. A total of 15 tropical cyclones developed in the North Atlantic, of which 12 were named storms. In 2004, tropical cylones caused a total of $40 billion in damage and led to the loss of 3000 lives. There was a concentration of cyclones in the Caribbean and the Gulf of Mexico. Also, 2002 was a CPW year. The number of landfalling cyclones was again higher than expected in an El Niño year. ACE was below average, but the track density anomaly was close to that shown in Fig. 2B.

The differences in cyclone tracks for EPW, CPW, and EPC are consistent with changes in atmospheric circulation caused by differential heating in the Pacific that forces changes in vertical shear in the main development region of the North Atlantic (5°N to 20°N, 85°W to 15°W). Figure S4 shows that the wind shear (the difference in zonal wind speed between 200 and 850 hPa) is stronger during EPW periods and weaker during EPC periods, whereas during CPW periods the wind shear anomaly is almost neutral. Strengthening or weakening of the vertical wind shear occurs largely through changes in the upper-level westerly flow (fig. S5) and is thought to be a major factor inhibiting or enhancing the formation and intensification of cyclones (*1*).

We have shown that there are statistically significant differences between the frequency and tracks of cyclones during EPW compared to CPW events. For these associations to be useful in seasonal prediction, the location of the anomalous Pacific warming needs to be forecast well in advance of the hurricane season. Prediction of the Niño 3.4 and Niño 3 (e.g., EPW) is hampered by the existence of a "predictability barrier" (*25*–*27*) that limits the prediction of Niño 3.4 or 3 before April or May. To perform an initial assessment of the relative predictability of EPW and CPW, we compare the predictability of Niño 3 (indicative of an EPW event) and Niño 4 index (indicative of a CPW event) using the ECMWF Seasonal Forecasting System (see SOM) (*28*). On the first day of each calendar month in the period 1981 to 2007, 11 7-month ensembles were generated, giving a total of 3564 7-month integrations. The results of this "serial integration" are shown in Fig. 3 as anomaly correlations in ensemble mean as a function of lead time (1 to 7 months) for the entire year. The two bold diagonal lines indicate target months June and November, framing the North Atlantic hurricane season. We define useful predictability occurring when correlations are greater than 0.7. The Niño 3 (or EPW) predictability (Fig. 3A)

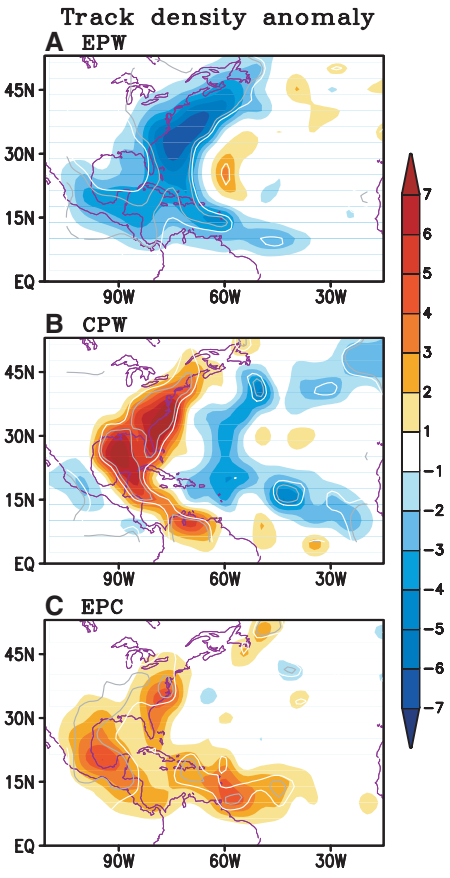

Fig. 2. Composites of track density anomaly (multiplied by 10) during the August to October period for (**A**) EPW, (**B**) CPW, and (**C**) EPC. Light (dark) contours show statistical significance at the 90% (95%) level.

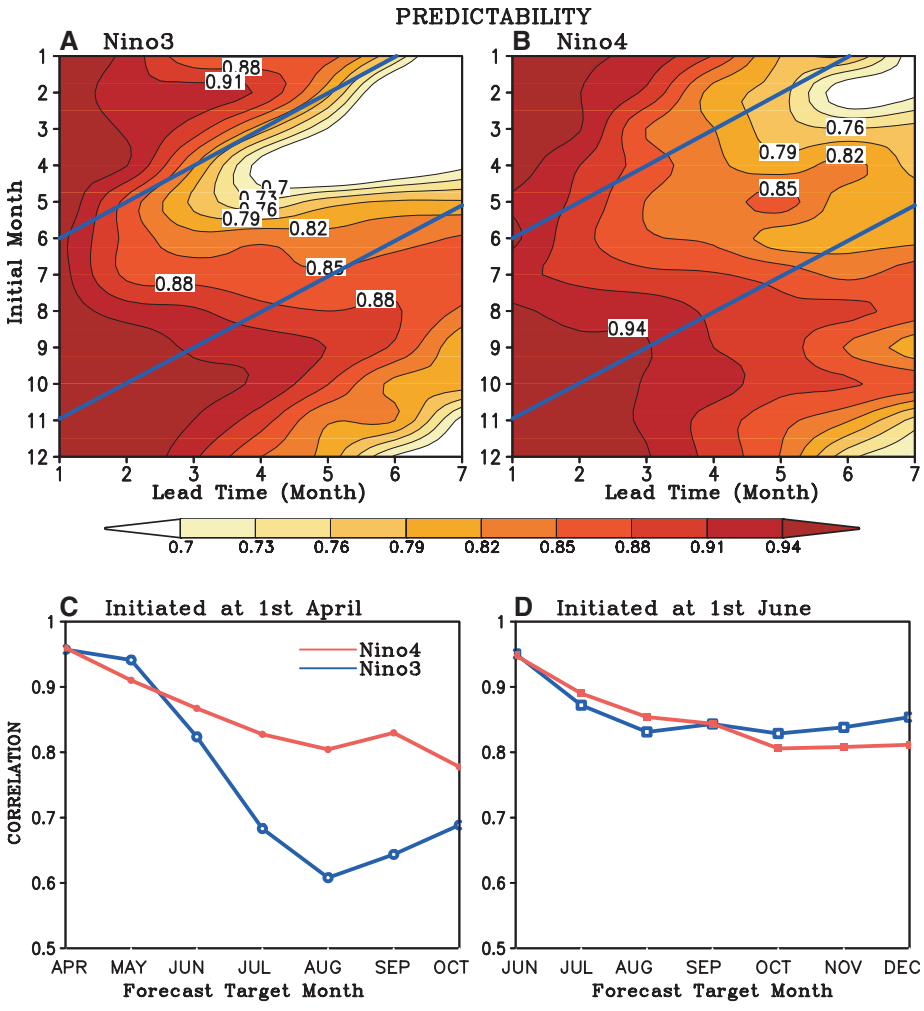

Fig. 3. Estimates of the predictability of EPW and CPW events. Correlations between predicted and observed values of SST anomalies for the (**A**) Niño 3 and (**B**) Niño 4 regions (fig. S1) as a function of initial month and lead-time. The predictability target zone for the period June through November (the North Atlantic tropical cyclone season) lies between the two blue diagonal lines. (**C** and **D**) Correlation of hindcasts initiated on 1 April and 1 June. Niño 4 (or CPW) possesses useful predictability for the target zone 2 to 3 months in advance of Niño 3 (or EPW).

shows clear seasonality, with the spring predictability diminishing rapidly into the hurricane season target months. Hindcasts made earlier than May provide little information about the ensuing hurricane season. By contrast, the Niño 4 (or CPW) predictability (Fig. 3B) has no obvious spring barrier. Figure 3, C and D, showing hindcasts initialized on 1 April and 1 June, indicate extended predictability earlier in the season for CPW than for EPW.

At present, it is difficult to assess why there has been an increased frequency of CPW events during the past few decades while EPW events have declined. Determining whether the CPW is a new mode associated with a general warming of the tropical oceans, or is connected to decadal modes of Pacific variability that have strong SST expressions in the central tropical Pacific such as the North Pacific Gyre Oscillation (*29*), is hampered by both data and model inadequacies. Many of the models used in the Intergovernmental Panel on Climate Change (IPCC) AR-4 constructions (*30*) do not reproduce major elements of interdecadal variability. Furthermore, SST data in the equatorial central and eastern Pacific before the 1920s were sparse, and it is difficult to determine what form of Pacific warming took place during earlier phases of the Pacific Decadal Oscillation. We do know that since 1960, especially since 1990, CPW events have become more prevalent and that there is a greater and earlier predictability of a CPW event than an EPW event. In addition, there is preliminary evidence that the character of Pacific cooling events has also changed during the past few decades. Future work will determine whether these differences result in changes in the characteristics of North Atlantic cyclones.

References and Notes

1. W. M. Gray, *Mon. Weather Rev.* **112**, 1649 (1984).
2. W. M. Gray, C. W. Landsea, P. W. Mielke Jr., K. J. Berry, *Weather Forecast.* **8**, 73 (1993).
3. J. B. Elsner, T. H. Jagger, *J. Clim.* **19**, 2935 (2006).
4. F. Vitart *et al.*, *Geophys. Res. Lett.* **34**, L16815 (2007).
5. R. A. Pielke Jr., C. N. Landsea, *Bull. Am. Meteorol. Soc.* **80**, 2027 (1999).
6. W. M. Gray, *Mon. Weather Rev.* **112**, 1669 (1984).
7. M. A. Saunders, R. E. Chandler, C. J. Merchant, F. P. Robert, *Geophys. Res. Lett.* **27**, 1147 (2000).
8. B. H. Tang, J. D. Neelin, *Geophys. Res. Lett.* **31**, L24204 (2004).
9. N. K. Larkin, D. E. Harrison, *Geophys. Res. Lett.* **32**, L13705 (2005).
10. K. Ashok, S. Behera, A. S. Rao, H. Y. Weng, T. Yamagata, *J. Geophys. Res.* **112**, C11007 (2007).
11. H. Y. Weng, K. Ashok, S. Behera, A. S. Rao, T. Yamagata, *Clim. Dyn.* **29**, 113 (2007).
12. H. Y. Kao, J. Y. Yu, *J. Clim.* **22**, 615 (2009).
13. J. S. Kug, F. F. Jin, S. I. An, *J. Clim.* **22**, 1499 (2009).
14. T. M. Smith, R. W. Reynolds, *J. Clim.* **17**, 2466 (2004).
15. E. M. Rasmusson, T. H. Carpenter, *Mon. Weather Rev.* **110**, 354 (1982).
16. C. W. Landsea *et al.*, in *Hurricanes and Typhoons: Past, Present and Future* (Columbia Univ. Press, New York, 2004), p. 177.
17. P. J. Webster, G. J. Holland, J. A. Curry, H. R. Chang, *Science* **309**, 1844 (2005).
18. K. Emanuel, *Nature* **436**, 686 (2005).
19. G. J. Holland, P. J. Webster, *Philos. Trans. R. Soc. London Ser. A* **365**, 2695 (2007).
20. S. B. Goldenberg, C. W. Landsea, A. M. Mestas-Nunez, W. M. Gray, *Science* **293**, 474 (2001).
21. J. B. Elsner, B. H. Bossak, X. F. Niu, *Geophys. Res. Lett.* **28**, 4123 (2001).
22. C. H. Ho, J. H. Kim, H. S. Kim, C. H. Sui, D. Y. Gong, *J. Geophys. Res.* **110**, D19104 (2005).
23. B. Efron, R. Tibishrani, *Science* **253**, 390 (1991).
24. www.cpc.noaa.gov/products/outlooks/hurricane2004/August/hurricane.html

25. P. J. Webster, S. Yang, *Q. J. R. Meteorol. Soc.* **118**, 877 (1992).
26. P. J. Webster, *Meteorol. Atmos. Phys.* **56**, 33 (1995).
27. C. Torrence, P. J. Webster, *Q. J. R. Meteorol. Soc.* **124**, 1985 (1998).
28. www.ecmwf.int/services/dissemination/3.1/Seasonal_Forecasting_ System_3.html
29. E. Di Lorenzo *et al.*, *Geophys. Res. Lett.* **35**, L08607 (2008).
30. G. A. Meehl *et al.*, *Bull. Am. Meteorol. Soc.* **88**, 1383 (2007).

31. We thank J. S. Kug and C. D. Hoyos for their valuable comments and help. The paper benefited from the constructive suggestions of the two anonymous reviewers. This research has been supported in part by Climate Dynamics Division of the National Sciences Foundation under Award NSF-ATM 0531771 and 0826909 and the Georgia Institute of Technology Foundation. We are indebted to the European Centre for Medium Range Weather Forecasts for access to the System 3 seasonal forecast archives

Supporting Online Material
www.sciencemag.org/cgi/content/full/325/5936/77/DC1
SOM Text
Figs. S1 to S5
Table S1
References

25 March 2009; accepted 28 May 2009
10.1126/science.1174062

Successful Conservation of a Threatened *Maculinea* Butterfly

J. A. Thomas,[1,2]* D. J. Simcox,[2] R. T. Clarke[2,3]

Globally threatened butterflies have prompted research-based approaches to insect conservation. Here, we describe the reversal of the decline of *Maculinea arion* (Large Blue), a charismatic specialist whose larvae parasitize *Myrmica* ant societies. *M. arion* larvae were more specialized than had previously been recognized, being adapted to a single host-ant species that inhabits a narrow niche in grassland. Inconspicuous changes in grazing and vegetation structure caused host ants to be replaced by similar but unsuitable congeners, explaining the extinction of European *Maculinea* populations. Once this problem was identified, UK ecosystems were perturbed appropriately, validating models predicting the recovery and subsequent dynamics of the butterfly and ants at 78 sites. The successful identification and reversal of the problem provide a paradigm for other insect conservation projects.

The conservation of insects poses formidable challenges (*1*). National extinction rates of temperate butterflies and other arthropods have recently exceeded those of terrestrial vertebrates and vascular plants (*2*–*6*), and population extinctions have frequently occurred on nature reserves where species' resources remained abundant (*6*–*8*). Moreover, every early attempt to conserve a declining butterfly failed because of inadequate understanding of the causes of decline (*7*, *8*). In 1974, the International Union for Conservation of Nature therefore selected three butterflies, including the ~six species of *Maculinea* (Large Blues), as global flagships for lepidopteran conservation (*9*), advocating research into their ecology and the maintenance of source habitats (*10*); the longest-running initiative involves *Maculinea arion*.

M. arion is an extreme specialist that switches from feeding on a plant to living as a social parasite inside *Myrmica* ant colonies during a 10-month larval instar and 3-week pupal period (Fig. 1). In the UK, *M. arion*'s population was estimated to include 91 colonies over the period of 1795 to the 1840s, declining to ~25 populations supporting tens of thousands of adults in 1950, and to 2 colonies of ~325 total individuals in 1972 before national extinction in 1979 (Fig. 2A) (*11*, *12*). Nine sites were declared conservation areas from 1930 to 1969, which preserved *M. arion*'s *Thymus*- and *Myrmica*-rich grasslands but failed to slow extinctions (*12*).

To understand *M. arion*'s decline on superficially unchanged sites, annual variation in every factor causing mortality or reduced natality in the life cycle was identified and measured from 1972 to 1978 in its last UK population on Site X, Dartmoor (fig. S1) (*13*). We quantified 18 life-table parameters during 6 years of typical and extreme weather (table S1), including adult dispersal (*14*), oviposition choice and egg distribution (*15*), adult natality, egg and larval mortality on *Thymus* species, cannibalism on *Thymus* (*16*), adoption by *Myrmica* ant species (*17*), host specificity (*18*), queen effect on workers (*19*), and the carrying capacity of ant colonies (*20*). Mortality on *Thymus* (egg-larval instar$_{III}$) was low and had no influence on population dynamics (fig. S2), although the distribution of *Thymus* determined which *Myrmica* ant nests were accessible to larvae (*17*). Post-adoption larval instar$_{IV}$ mortality inside *Myrmica* nests was the key factor determining overall population changes (fig. S2), an analysis supported by phenomenological and spatial automata models (*16*, *21*). We identified four causes of *M. arion* mortality at this stage: (i) availability of the preferred ant host species (*18*), (ii) presence/absence of queen ants (*19*), (iii) larval density within ant nests (*20*), and (iv) drought effects on host food availability (*22*). Factors (i) and (iii) were most variable: Five *Myrmica* species foraged beneath *Thymus* on Dartmoor and adopted instar$_{IV}$ larvae with probabilities proportional to worker abundance (*17*), but survival was 5.3 times higher in colonies of *Myrmica sabuleti* than with those of its congeners (*18*); population-scale survival with *M. sabuleti* decreased with larval density per nest (fig. S3).

Failure by female butterflies to lay their full potential of eggs amplified the population de-

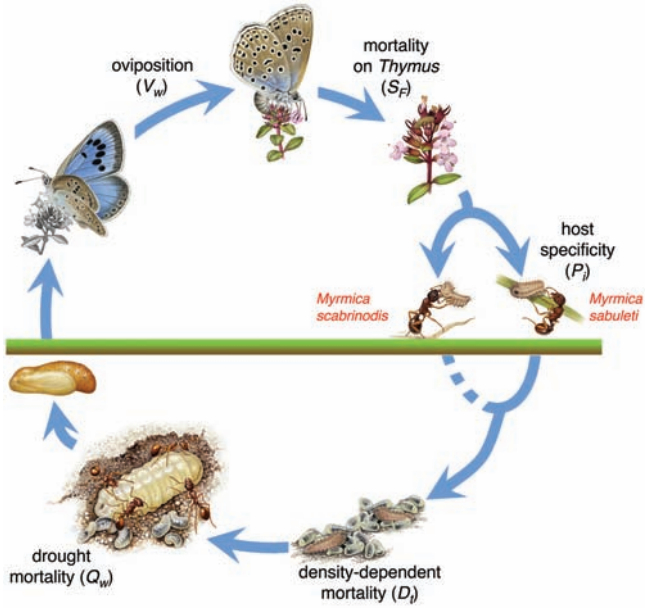

Fig. 1. Life cycle of *M. arion*. Adult butterflies oviposit on *Thymus* species flowers from June through July (model parameter V_w). Larval instars$_{I-III}$ feed on flowerheads for 3 weeks, with (including eggs) survival (S_F) depending on parasites, predation, and cannibalism. The small final instar$_{IV}$ larva abandons *Thymus* and is adopted into the underground nest of the first *Myrmica* ant worker to encounter it, with survival (P_t) depending on its adoption into primary (*M. sabuleti*) or secondary (*M. scabrinodis*) host-species' nests. *M. arion* larvae acquire ~98% of their final biomass eating ant brood and frequently experience density-dependent mortalities ($1 - D_t$) in nests that adopt more than 1 larva; mortalities in ant nests are amplified in drought years (Q_W). After 10 months, the larva pupates in the *Myrmica* nest, emerging as an adult 2 to 3 weeks later. [Illustrations by Richard Lewington]

[1]Department of Zoology, University of Oxford, South Parks Road, Oxford, OX1 3PS, UK. [2]Centre for Ecology and Hydrology, Maclean Building, Benson Lane, Crowmarsh Gifford, Wallingford, Oxfordshire, OX10 8BB, UK. [3]Centre for Conservation Ecology and Environmental Change, School of Conservation Sciences, Bournemouth University, Fern Barrow, Talbot Campus, Poole, Dorset BH12 5BB, UK.

*To whom correspondence should be addressed. E-mail: jeremy.thomas@zoo.ox.ac.uk

cline from 1974 to 1976 (fig. S2). We observed no emigration (*14*) or eggs on sites 260 to 400 m away from primary colonies. Predation by birds and invertebrates was high but stable, reducing the mean female longevity to 3.9 ± SE 0.6 (standard error of 0.6) days and natality to 51 ± 8.9 eggs, which is about 25% of the number laid by caged females. After single inactive days of wet weather, an average female laid 56 ± 14% more eggs on the next suitable day but failed to compensate for prolonged wet periods in 1974 (table S1). In contrast, a drought in 1975 reduced mean female life spans to 2.1 ± 0.3 days and average natality to 20 eggs. On the basis of historical records, there is only an 8% chance of two such extreme summers in a 7-year period, but both were included as model parameters due to the unpredictability of future weather.

We reduced the 18 life-table factors to seven influential parameters in a mechanistic model describing *M. arion*'s population dynamics on its last UK site in the period of 1972 to 1978

$$a_{t+1} = a_t S_F (P_{sab(t)} + cP_{scab(t)}) D_t Q_w V_w \quad (1)$$

where a_t is the predicted egg numbers in year t; S_F is the mean survival of eggs and early larval instars on *Thymus* [estimate = 0.37, see supporting online material (SOM)]; $P_{sab(t)}$ and $P_{scab(t)}$ are the proportion of instar$_{IV}$ larvae adopted respectively by *M. sabuleti* or other secondary-host species in year t (larvae die if no *Myrmica* coincides with *Thymus*); c is the initial density-independent survival within secondary-host ant nests (0.19) (*18*); Q_w is the reduction in larval survival in *Myrmica* nests in drought years (0.56) (table S1); V_w is the number of eggs per adult (table S1) in a typical year (25.5 eggs), a prolonged wet summer (11.5), or an extreme drought summer (8.0); and D_t is the density-dependent survival within *Myrmica* nests, where

$$D_t = \alpha - \beta \log(L_t/R_t) \quad (2)$$

and L_t is the larval density per *Myrmica* nest in year t = (total larvae entering ant nests)/(number of available nests), and R_t is the relative worker size = (mean worker ant weight in year t)/(mean worker ant weight at Site $X_{1972\text{-}77}$). The calibration data fit to Eq. 2 is shown in fig. S3.

We found that Eq. 1 fitted actual egg population numbers [R^2 = 95% (where R is the correlation coefficient), P = 0.005] and annual changes (R^2 = 76%, $P < 0.05$) on Site X from 1972 to 1978 and, thus, was used to estimate the amount of habitat manipulation needed to optimize conditions for host *Myrmica* species in all subsequent conservation projects. Varying the ratio of *M. sabuleti* [$P_{sab(t)}$] to other *Myrmica* species [$P_{scab(t)}$] co-occurring with *Thymus* predicted a butterfly growth rate λ of greater than 1 if more than 68% of larvae are adopted by their primary host, assuming the low butterfly densities and conditions on Site X in the 1970s. In optimum habitat of 100% *Thymus* coexistence with host ants, no extreme weather, and the median ant densities and biomass subsequently recorded on conservation sites, we predicted λ = 5.49, stabilizing after 12 years under density-dependent parameter D_t at a capacity (K) of 910 adults per hectare.

Surveys and habitat analyses (*13*) of every former *M. arion* site in fig. S1 enabled us retrospectively to analyze the cause of its decline. Overexploitation (butterfly collecting) was ruled out as a factor (*11*, *12*), and no relation was observed between *M. arion* population survival time and grassland patch size or isolation over the 50 years before national extinction (Fig. 2B). Instead, we found that the quality of grassland habitat, represented by the availability of *M. sabuleti*, was the driver to extinction. Despite abundant *Thymus* and other *Myrmica* species, only 0 to 38% of food plants coexisted with *M. sabuleti* on former sites (Fig. 3A), well be-

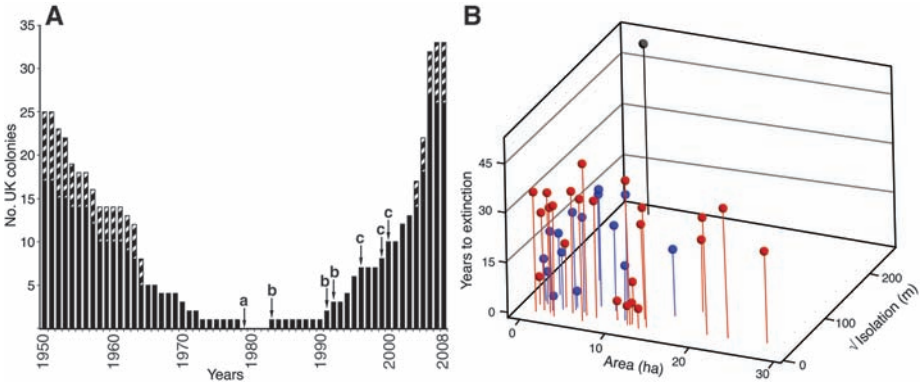

Fig. 2. Populations of *M. arion* in the UK. (**A**) Number of colonies since 1950. Hatched bars indicate temporary colonies. Arrows: "a" represents extinction of native UK populations, "b" indicates reintroduction from Sweden to UK restoration sites, and "c" denotes introductions using UK populations. (**B**) The persistence of 39 UK populations known in 1929 to the extinction of the last in 1979, plotted against each population's site area and the square root of distance from the nearest neighboring occupied habitat patch in 1929. No colonization was observed during this period. Red, Atlantic coast populations; blue, Cotswolds; black, Dartmoor. No relation was found between persistence time and either landscape parameter [area$_{allsites}$: R^2 = 2%, P = 0.39; isolation$_{allsites}$: R^2 = 5%, P = 0.20; area$_{withinlandscape}$: R^2 = 1 to 14%, P = 0.70 to 0.18; isolation$_{withinlandscape}$: R^2 = 5 to 9%, P = 0.46 to 0.16].

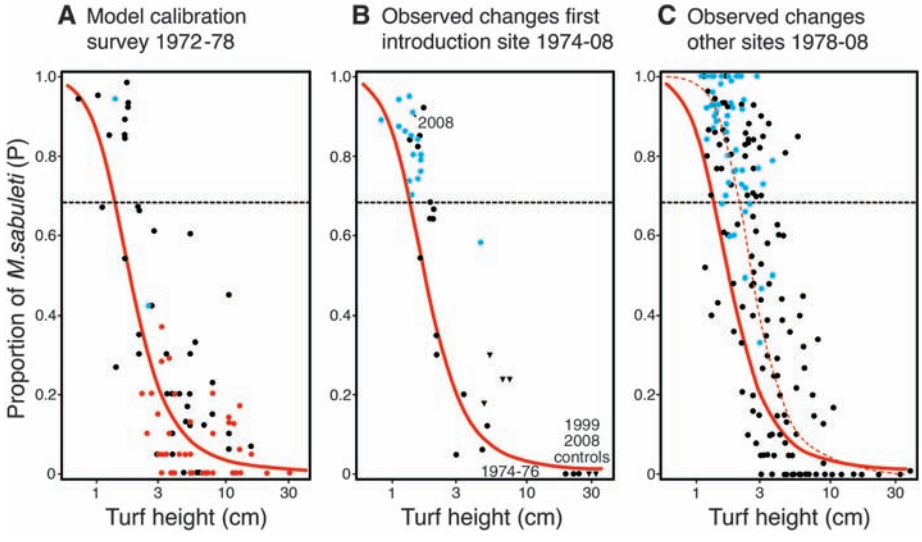

Fig. 3. Relation between the proportional occurrence (P_{sab}) of ant *M. sabuleti* in *Thymus* grasslands and turf height (H). Horizontal dashed lines denote that minimum P_{sab} (68%) was required for *M. arion*'s basic reproductive rate λ > 1. (**A**) Model calibration was calculated on the basis of P_{sab} and H recorded from 1972 to 1978 surveys. Blue, occupied *M. arion* sites (dot at 0.42 denotes the site in year of extinction); red, known extinct sites; black, other sites. Fitted empirical logistic: $\log_e[(P_{sab} + 0.01)/(1 - P_{sab} + 0.01)] = \alpha_H + \beta_H (1/\sqrt{H} + 0.1)$, $\alpha_H = -5.95$ (SE = 0.40), $\beta_H = 8.12$ (SE = 0.74), R^2 = 56%, $P < 0.001$. (**B**) Annual relation after application of grazing regime on site Y from 1974 to 2008. Dots denote experimental grassland [colors as in (A)], and triangles represent unmanaged controls. (**C**) Model application to 77 other restoration sites sampled (N = 334) from 1978 to 2008. The dashed line indicates an empirical logistic fit to restored sites: $\alpha_H = -6.63$ (SE = 0.40), $\beta_H = 11.02$ (SE = 0.64), R^2 = 61%, $P < 0.001$.

low the minimum predicted for $\lambda > 1$. Only on Site X, where the butterfly persisted, did *M. sabuleti* densities exceed the 68% model threshold. *M. sabuleti* presence was closely correlated with vegetation structure; in particular, occurrence decreased with turf height (Fig. 3A and fig. S4B). The fitted relation suggested swards less than 1.4 cm tall were needed to provide the minimum threshold host-ant density for *M. arion*. Turf height, in turn, correlated with soil temperature (fig. S5) during key growth periods for *M. sabuleti* (*23*). When mean swards exceeded ~2 cm, the microclimate in their warmest daytime brood chambers near the soil surface fell more than 2° to 3°C relative to 1-cm tall turf, allowing less thermophilous congeners, especially *M. scabrinodis*, to outcompete *M. sabuleti* (fig. S4C) (*23*). As human mediated grazing declined, the hillsides to which *M. sabuleti* was confined were grazed primarily by rabbits. When the rabbit population declined because of myxomatosis, all but one (farmed) *M. arion* site became too overgrown for the primary host (Fig. 3A).

Unaware of the inconspicuous habitat degradation, early conservationists took inappropriate measures on the basis of false assessments of *M. arion*'s decline. Thus, a fence erected in 1931 to deter butterfly collectors inadvertently excluded the herbivores that maintained its specialized habitat, resulting in rapid extinction of the population (*12*). By the time the cause of the decline was evident, the last UK population was extinct (Fig. 2A). Since then, 52 *Thymus* grasslands have been managed and restored, and at least 50 additional sites are at earlier stages of restoration, with the criteria defined by Eq. 1 (Fig. 3). Although isolation and fragmentation were not implicated in *M. arion*'s decline (Fig. 2B), where possible chains of sites were restored within the butterfly's ~250-m dispersal range (*14*) in four landscapes (fig. S1). Meanwhile, a suitable donor race was identified from Öland, Sweden, with a phenology that synchronized with its resources under observed and predicted UK climates (fig. S6).

Myrmica populations responded rapidly to the changed vegetation structure. On Site Y, Dartmoor (fig. S1), *M. sabuleti* was not detected from 1973 to 1974, yet it coexisted with 84% of *Thymus* within a decade after scrub clearance and the reintroduction of seasonal grazing, while remaining absent from ungrazed controls (Fig. 3B; $R^2 = 81\%$ for fit of niche-model). Similar patterns occurred on 77 other conservation grasslands (Fig. 3C), where host-ant co-occurrence with *Thymus* initially averaged 9% (45% maximum). On many managed sites, *M. sabuleti* now dominates 100% of *Thymus*-grassland, sometimes forming super colonies with 5 to 10 nest-centers per square meter and mean worker (hence brood) weights 13 to 82% higher than on Site X in the 1970s. Compared with early data, the fit with turf height was less precise, although recalibration showed the same strong pattern (Fig. 3C; $R^2 = 37$ and 61%, respectively), with the minimum threshold host-ant density for *M. arion* now occurring in turf less than 2.1 cm tall. This tolerance of taller swards by *M. sabuleti* is largely explained by recent climate warming reducing the vegetation's shading effect (*24*). *Thymus* populations were less dynamic. On average, the density of flowering plants increased by 265 ± 80% but dispersed to encompass previously inaccessible *Myrmica* colonies only at two sites.

Successful releases of *M. arion* (SOM) were made from Öland, Sweden, to three UK sites in 1983 to 1992 (a fourth to the Cotswolds failed, presumably due to an excessive climatic difference relative to Öland). Four later introductions (Fig. 2A) to distant sites or new regions were sourced from established populations in Somerset, UK. By 2008, the butterfly had naturally colonized 25 other conservation sites, albeit establishing peripheral colonies in seven cases (Fig. 2A). The largest populations contained 1000 to 5000 adult butterflies per hectare, an order of magnitude greater than any previous population of *M. arion* recorded worldwide.

Long-term predictions of butterfly population dynamics (Fig. 4A and figs. S7 and S8) were estimated from the initial number of *M. arion* (a_0) introduced in year 0, and thereafter from annual variation in habitat and weather parameters $P_{sab(t)}$, $P_{scab(t)}$, $D_{tw,}$ and V_w, with no adjustment for observed butterfly numbers during its subsequent 16 to 21 generations. Observed *M. arion* populations closely followed model predictions (Fig. 4A and fig. S7), increasing in 5 to 10 generations toward their theoretical carrying capacities, where they stabilized or experienced temporary declines because of drought (e.g., 1996 to 1997) or suboptimal management (Site X, 2000 to 2004). In seven *M. arion* populations that have

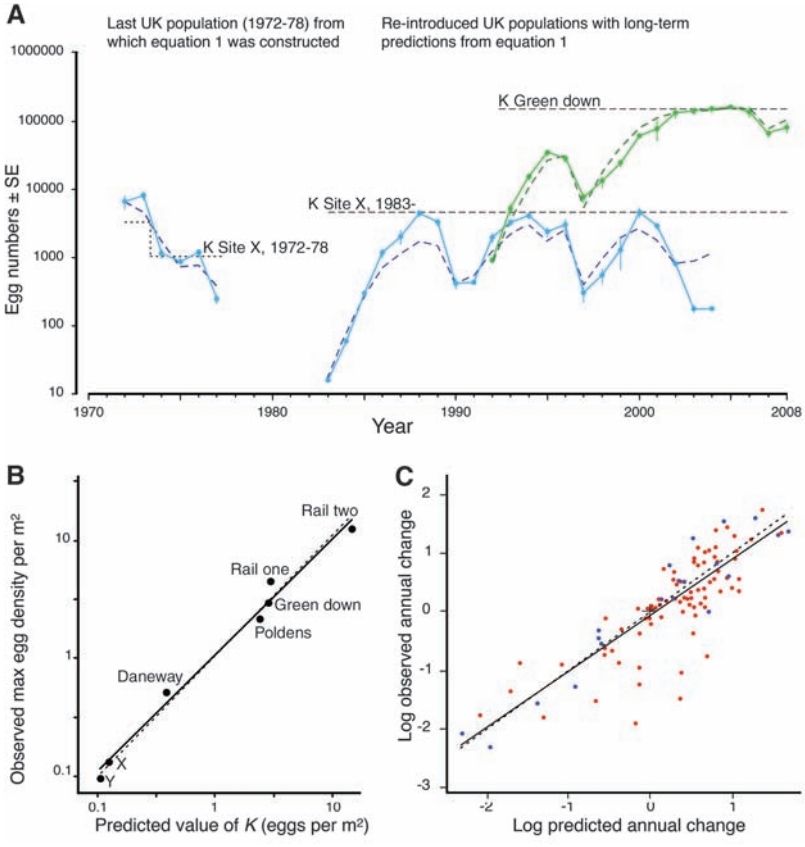

Fig. 4. Prediction of the long-term population dynamics of *M. arion* in the UK. (**A**) Fit of Eq. 1 to recorded changes on Site X (blue lines), from which it was parameterized in the period of 1972 to 1978, and its ability to predict observed numbers after *M. arion* was re-introduced following conservation management to Site X ($R^2_C = 69\%$) (SOM) and Green Down (green lines, $R^2_C = 94\%$). Solid lines indicate observed numbers, dashed lines denote model predictions, and K indicates the site carrying capacity (equilibrium level) for *M. arion* estimated from Eq. 1, where density effects (D_t) negate further growth. (**B**) Estimated and observed values of carrying capacity per square meter. Dotted line, 1:1 ratio; solid line, fitted regression; $R^2 = 98.6\%$; $P < 0.01$ (before conservation management, $K = 0$ except on Site X). (**C**) Prediction of annual changes ($N = 99$) in *M. arion* egg numbers on 19 conservation sites from 1983 to 2008 (red, Site X). The plot shows the log of observed change [$\log(E_{t+1}/E_t)$] versus the log of predicted change [$\log(a^0_{t+1}/E_t)$], where E_t is the observed egg number in year t, and a^0_{t+1} is the predicted egg number in year $t + 1$ from Eq. 1 with a_t replaced by E_t. Dotted line, 1:1 ratio; solid line, fitted regression; $R^2 = 71\%$; $P < 0.001$.

existed long enough for density-dependent mortalities to halt further growth, observed peak densities correlate closely with estimated site carrying capacities per square meter (Fig. 4B): The fact that site values vary by two orders of magnitude is due to differences in the ratio of *M. sabuleti* to other ants, *Myrmica* nest densities, and worker biomass. Because of the parameterization of stabilizing density-dependent larval mortalities within *Myrmica* nests (Eq. 2), model predictions of butterfly numbers 10 to 20 years ahead were as close to observed numbers as in the first decade (fig. S8). On more recently restored UK sites, the direction and size of annual *M. arion* population change was also close to model predictions (Fig. 4C).

M. arion's UK re-establishment is too recent for settled landscape-scale dynamics to emerge. During its natural colonization of 23 Polden Hills' sites, *M. arion* spread by stepping-stone occupation of neighboring habitat patches, taking 14 years to reach the furthest one, 4.4 km from a source introduction. The rate of increase of colonization distance from original sources was 1.9 times greater during years 8 to 14 than in years 0 to 4 ($P < 0.02$), possibly reflecting selection for dispersive adults consistent with shifts in thorax widths measured in UK *M. arion* populations during previous range changes (*25*). Seven sites experienced temporary occupancy in 2003 to 2008 (Fig. 2A): All were smaller than other conservation areas (average of 0.11 and 1.55 ha, respectively, and Mann-Whitney $P = 0.008$) and are regarded as ephemeral satellites of neighboring populations.

Surveys of *M. arion* across Europe have revealed similar declines for similar reasons (SOM). Today, successful but smaller-scale management is being applied in other nations on the basis of UK results, and *M. arion*'s global listing has changed from "vulnerable" to "near-threatened" (*26*). It will shortly downgrade from "endangered" to "vulnerable" in Europe and is one of just three UK butterflies due to meet the Convention of Biological Diversity's target to reverse species' declines by 2010 (*27*). The others inhabit similar-structured grassland: Their successful conservation derived directly from extensions of this research (*7*).

The *Maculinea* project tackled problems typical of many temperate butterflies that were disappearing from apparently suitable sites (*7*, *8*) and provided insights for quicker, cheaper approaches. Having recognized that immature stages (and ant nest sites) typically exploit a narrow subset of their named resource and that the availability of optimum larval habitat alongside adult metapopulation constraints largely determines population sizes and persistence (*7*, *28*), successful conservation was achieved across the genus *Maculinea*. Similarly, the declines of several phytophagous Palaearctic butterflies were reversed by identifying the subsets of food plants preferred by larvae, then perturbing ecosystems to generate them (*7*). Despite these short-cuts, species-conservation is impractical for the vast majority of insects, for which the preservation of primary ecosystems or a community approach are appropriate (*1*). However, because many other threatened species increased on UK sites following targeted management for *M. arion* (*29*), we consider that successful species-based and community conservation for insects represent different routes to the same end.

References and Notes

1. A. J. A. Stewart, T. R. New, O. T. Lewis, *Insect Conservation Biology* (CABI, Wallingford, UK, 2007).
2. J. A. Thomas *et al.*, *Science* **303**, 1879 (2004).
3. J. A. Thomas, R. T. Clarke, *Science* **305**, 1563 (2004).
4. A. Kosior, *Oryx* **41**, 79 (2007).
5. K. F. Conrad *et al.*, *Biol. Conserv.* **132**, 279 (2006).
6. A. Erhardt, *J. Appl. Ecol.* **22**, 849 (1985).
7. J. A. Thomas, in *The Scientific Management of Temperate Communities for Conservation*, I. Spellerberg, B. Goldsmith, M. G. Morris, Eds. (Blackwells, Oxford, 1991), pp. 149–197.
8. T. R. New *et al.*, *Annu. Rev. Entomol.* **40**, 57 (1995).
9. J. A. Thomas, J. Settele, *Nature* **432**, 283 (2004).
10. S. M. Wells, R. M. Pyle, N. M. Collins, *The IUCN Invertebrate Red Data Book* (International Union for Conservation of Nature, Gland, Switzerland, 1983).
11. G. M. Spooner, *Entomology* **96**, 199 (1963).
12. J. A. Thomas, *Oryx* **15**, 243 (1980).
13. Materials and methods, as well as additional information, are available as supporting material on *Science* Online.
14. K. Schönrogge *et al.*, *Ecol. Lett.* **9**, 1032 (2006).
15. J. A. Thomas, G. W. Elmes, *Proc. R. Soc. London Ser. B. Biol. Sci.* **268**, 471 (2001).
16. N. Mouquet *et al.*, *Ecol. Monogr.* **75**, 525 (2005).
17. J. A. Thomas, *Oecologia* **132**, 531 (2002).
18. J. A. Thomas, G. W. Elmes, J. C. Wardlaw, M. Woyciechowski, *Oecologia* **79**, 452 (1989).
19. J. A. Thomas, J. C. Wardlaw, *Oecologia* **85**, 87 (1990).
20. J. A. Thomas, J. C. Wardlaw, *Oecologia* **91**, 101 (1992).
21. R. T. Clarke *et al.*, in *Studies in the Ecology and Conservation of Butterflies in Europe 2*, J. Settele, E. Kuehn, J. A. Thomas, Eds. (Pensoft, Sofia, Bulgaria, 2005), pp. 115–119.
22. G. W. Elmes, J. C. Wardlaw, K. Schönrogge, J. A. Thomas, *Entomol. Exp. Appl.* **110**, 53 (2004).
23. G. W. Elmes *et al.*, *J. Insect Conserv.* **2**, 67 (1998).
24. Z. G. Davies, R. J. Wilson, S. Coles, C. D. Thomas, *J. Anim. Ecol.* **75**, 247 (2006).
25. J. P. Dempster, in *The Conservation of Insects and Their Habitats*, N. M. Collins, J. A. Thomas, Eds. (Academic, London, 1991), pp. 143–153.
26. www.iucnredlist.org/search
27. M. S. Warren, personal communication.
28. P. R. Ehrlich, I. Hanski, *On the Wings of Checkerspots* (Oxford Univ. Press, New York, 2004).
29. G. W. Elmes, J. A. Thomas, *Biodivers. Conserv.* **1**, 155 (1992).

30. We thank R. M. May for comments, R. Lewington for Fig. 1 illustrations, and 140 others for contributions and assistance (see reference S16). Funding, experimental sites and other resources were generously provided by the European Union Macman and Biodiversa (CLIMIT) programs, Natural England, Centre for Ecology and Hydrology, the National Trust, the Somerset Wildlife Trust, Network Rail, J and F Clark Trust, Butterfly Conservation, Gloucester Wildlife Trust, Millfield School, Defra, the World Wildlife Fund, Sir Terence Conran, Holland and Barrett, Hydrex, ICI, and R. Mattoni.

Supporting Online Material

www.sciencemag.org/cgi/content/full/1175726/DC1
Materials and Methods
SOM Text
Figs. S1 to S8
Table S1
References and Notes

1 May 2009; accepted 20 May 2009
Published online 18 June 2009;
10.1126/science.1175726
Include this information when citing this paper.

Meningococcal Type IV Pili Recruit the Polarity Complex to Cross the Brain Endothelium

Mathieu Coureuil,[1]* Guillain Mikaty,[1] Florence Miller,[2,3] Hervé Lécuyer,[1,4] Christine Bernard,[1] Sandrine Bourdoulous,[2,3] Guillaume Duménil,[1]† René-Marc Mège,[5] Babette B. Weksler,[6] Ignacio A. Romero,[7] Pierre-Olivier Couraud,[2,3] Xavier Nassif[1,4]

Type IV pili mediate the initial interaction of many bacterial pathogens with their host cells. In *Neisseria meningitidis*, the causative agent of cerebrospinal meningitis, type IV pili–mediated adhesion to brain endothelial cells is required for bacteria to cross the blood-brain barrier. Here, type IV pili–mediated adhesion of *N. meningitidis* to human brain endothelial cells was found to recruit the Par3/Par6/PKCζ polarity complex that plays a pivotal role in the establishment of eukaryotic cell polarity and the formation of intercellular junctions. This recruitment leads to the formation of ectopic intercellular junctional domains at the site of bacteria–host cell interaction and a subsequent depletion of junctional proteins at the cell-cell interface with opening of the intercellular junctions of the brain-endothelial interface.

Neisseria meningitidis is a commensal bacterium of the human nasopharynx that, after bloodstream invasion, crosses the blood-brain barrier (BBB) (*1*). Few pathogens have a tropism for the brain, indicating that *N. meningitidis* possess specific components to interact with the BBB. Meningeal colonization by invasive capsulated *N. meningitidis* is the consequence of the bacterial adhesion onto brain endothelial cells (*2*, *3*), which is followed by bacterial division onto the apical surface of the cells (movie S1). This process is

mediated by type IV pili (Tfp) (*4*–*9*). In addition, by powering a form of cell locomotion reported as twitching motility (*10*), Tfp lead to the spread of the bacteria on the surface of the cells and the formation of microcolonies. Subsequent to the formation of these microcolonies, Tfp trigger the recruitment of cortical actin and signal transducing proteins, leading to the formation of filopodia-like structures (*2*, *11*–*13*). The crossing of the BBB by *N. meningitidis* implies that, after Tfp-mediated adhesion, the bacteria transcytose through the brain capillaries and/or open the brain endothelium.

To investigate whether adhesion of *N. meningitidis* affects the integrity of adherens junctions (AJs) and/or tight junctions (TJs) of human brain endothelial cells, we analyzed the consequences of infection by *N. meningitidis* on the distribution of junctional proteins by using the human brain microvascular endothelial cell line hCMEC/D3 (*14*). After infection, components of the AJ (VE-cadherin, p120-catenin, and β-catenin) and the TJ (ZO1, ZO2, and claudin-5) were targeted underneath *N. meningitidis* colonies (Fig. 1A). At the site of *N. meningitidis* adhesion, these junctional proteins codistributed with each other and with the actin honeycomb-like network. In noninfected cells, the recruitment of junctional proteins usually occurs at the cell-cell interface and is controlled by several polarity proteins (Par3/Par6/PKCζ) (*15*–*17*). In infected monolayers, Par3 and Par6 were observed underneath *N. meningitidis* colonies (Fig. 1B). Thus, *N. meningitidis* triggers a signal leading to the formation of an ectopic domain containing filopodia-like structures and enriched in junctional proteins, thus resembling spot-like AJs observed during early steps of junctional biogenesis. We refer to this domain as an "ectopic early junction-like domain" (*18*). By using isogenic derivatives, Tfp-induced signaling was shown to be responsible for the formation of these ectopic early junctionlike domains (fig. S1, A and B). However, Tfp retraction through the PilT motor was not required for formation of the ectopic domains (fig. S1, D and E).

The small guanosine triphosphatase Cdc-42 is required for polarization of mammalian cells (*19*, *20*). The role of this component in the recruitment of the polarity complex by *N. meningitidis* was investigated. Transfection of a dominant negative mutant of Cdc42 or knockdown of Cdc42 by RNA interference (RNAi) inhibited the recruitment of Par6, Par3 (Fig. 2A and fig. S2A), VE-cadherin, p120-catenin, and actin (Fig. 2B and figs. S2B and S3). These results link the Cdc42/polarity complex pathway with the formation of the ectopic early junctionlike domains.

The role of the polarity complex in the recruitment of junctional proteins was further explored by studying the inhibition of Par3 and Par6 with either dominant negative mutants or knockdown by RNAi. PKCζ inhibition was assessed by using a PKCζ pseudosubstrate inhibitor (PKCζ-PS) (*21*). Inhibition of Par6 and PKCζ reduced the recruitment of p120-catenin, VE-cadherin, and actin (Fig. 2, B and C, and figs. S2C and S3) and that of Par3 (Fig. 2D and fig. S2E), consistent with the finding that the Par6/PKCζ complex recruits Par3 at intercellular junction domains (*22*). On the other hand, inhibition of Par3 reduced only the recruitment of VE-cadherin (Fig. 2B and figs. S2D and S3), consistent with Par3 being specifically needed for junctional proteins targeting at early cell-cell junctions (*23*). These observations confirmed the role of the polarity complex in the recruitment of the junctional proteins by *N. meningitidis*.

The sequence of events leading to the targeting of AJ proteins at the cell-cell junctions dur-

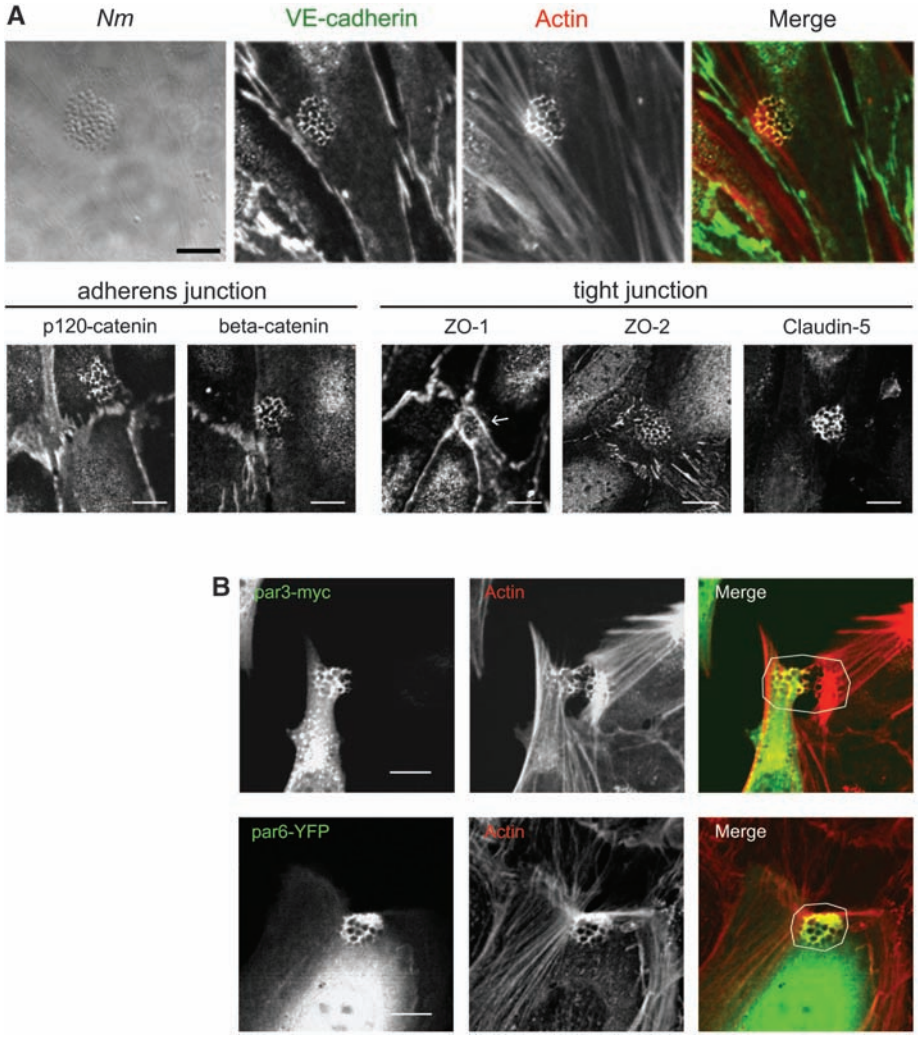

Fig. 1. *N. meningitidis* recruits ectopic junctionlike domains beneath colonies. (**A**) VE-cadherin (green), the main component of the endothelial AJ, colocalized with actin (red) beneath *N. meningitidis* (*Nm*) colonies (top row). Two other AJ components, p120-catenin and β-catenin, and three components of the TJ, ZO-1, ZO-2, and claudin-5, are recruited under *N. meningitidis* colonies (bottom row). Arrow indicates a bacterial colony. Scale bars indicate 10 μm. (**B**) Yellow fluorescent protein (YFP)–tagged Par6 (par6-YFP) or myc-tagged Par3 (par3-myc), both green, are recruited underneath *N. meningitidis* colonies where they colocalize with actin (red). Areas outlined in white indicate the presence of a *N. meningitidis* colony. Scale bars, 10 μm. The formation of these ectopic early junctionlike domains is not found underneath all *N. meningitidis* colonies. Signaling underneath bacterial microcolonies required a minimal number of 20 bacteria per colony to be detected by immunofluorescence, with around 40 to 50% of microcolonies containing 40 to 50 bacteria. The average number of colonies signaling after 2 hours of infection is 40%.

[1]Université Paris Descartes, Faculté de Médecine, INSERM (U-570), 75015 Paris, France. [2]Institut Cochin, Université Paris Descartes, CNRS (UMR 8104), 75015 Paris, France. [3]INSERM, U567, 75014 Paris, France. [4]AP-HP, Hôpital Necker-Enfants Malades, Paris F-75015, France. [5]INSERM UMR-S 839, Université Pierre et Marie Curie-Paris6, Institut du Fer à Moulin, 75005 Paris, France. [6]Weill Cornell Medical College, New York, NY 10021, USA. [7]Department of Life Sciences, The Open University, Walton Hall, Milton Keynes MK7 6AA, UK.

*To whom correspondence should be addressed. E-mail: mathieu.coureuil@inserm.fr

†Present address: INSERM U970, Paris Cardiovascular Research Center, Paris F-75015, France.

ing cellular polarization remains unknown. To get insight into this process, we engineered a VE-cadherin knockdown of hCMEC/D3 cells by stable expression of a VE-cadherin short hairpin RNA (VEC shRNA) (Fig. 3, A and B, and fig. S4A). In this cell line, p120-catenin and actin were still recruited beneath *N. meningitidis* colonies, whereas recruitment of β-catenin was dramatically reduced. On the other hand, down-regulation of p120-catenin using RNAi (Fig. 3C, S4B) resulted in inhibition of VE-cadherin and of actin recruitment. Consistent with a previous report, cortactin and Arp2/3 were not recruited by the bacterial colonies in p120-catenin knockdown cells (*24*) (fig. S4C). Furthermore, inhibition of Src kinase, which phosphorylate cortactin and is activated after the formation of the cortical plaque (*25*), did not modify p120-catenin recruitment but inhibited VE-cadherin and actin recruitment (fig. S4, D and E). Taken together, these results strongly suggest that p120-catenin–mediated recruitment of actin and VE-cadherin requires the recruitment and phosphorylation of cortactin by the Src kinase. In summary, Cdc42, via the polarity complex, organizes this ectopic early junction-like domain, mainly by the initial recruitment of p120-catenin.

We asked whether the signal triggered by Tfp and leading to the formation of these ectopic early junctionlike domains destabilized intercellular junctions, especially by redirecting a recycling pool of junctional proteins to the *N. meningitidis* adhesion site. First, inhibition of protein synthesis did not prevent recruitment of VE-cadherin (fig. S5A). Second, inhibition of clathrin-coated pit formation blocked VE-cadherin recruitment (fig. S5, B and C), suggesting that VE-cadherin internalization is required for its targeting underneath *N. meningitidis* colonies. Third, when monolayers were tagged before infection with a VE-cadherin monoclonal antibody, antibodies were relocalized beneath colonies in infected monolayers (fig. S6). Thus, the VE-cadherin delocalized by the bacteria was coming from the intercellular junctions. This redistribution of the AJ proteins was associated with a reduction of the amount of tagged VE-cadherin at the intercellular junction (fig. S6 and movie S2). Thus, the junctional VE-cadherin is internalized and then mistargeted at the site of bacterial cell interactions.

Depletion of intercellular junction proteins from the cell-cell interface could open a paracellular route for bacterial spread. Indeed, *N. meningitidis* was shown to increase permeability to Lucifer Yellow (LY), a compound that

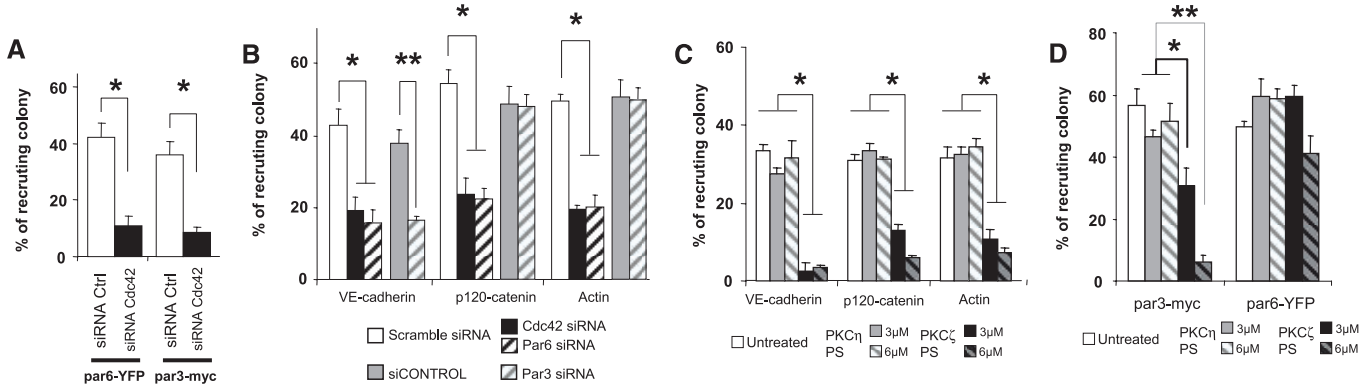

Fig. 2. The Cdc42-Par3/Par6/PKCζ pathway controls the formation of ectopic early junctionlike domains. Data are expressed as mean ± SEM. (**A**) Knockdown of Cdc42 was performed by using specific small interfering RNA duplexes (Cdc42 siRNA). Cells were cotransfected with par6-YFP or par3-myc. Knockdown of Cdc42 by RNAi reduced the recruitment of par6-YFP and par3-myc by fourfold. **t* test ($P < 0.005$). (**B**) Knockdown of Cdc42, Par6 and Par3 were performed as described (*27*) (Cdc42 siRNA, Par6 siRNA, and Par3 siRNA). Scramble siRNA and siCONTROL were used as control for Cdc42/Par6 and Par3 knockdown, respectively. Knockdown of Cdc42 by RNAi reduced the recruitment of VE-cadherin, p120-catenin, and actin by 2.2-fold, 2.3-fold, and 2.5-fold, respectively. See also fig. S3. Knockdown of Par6 by RNAi reduced the recruitment of VE-cadherin, p120-catenin, and actin by 2.7-fold, 2.4-fold, and 2.4-fold, respectively. Knockdown of Par3 by RNAi reduced the recruitment of VE-cadherin by twofold. **t* test ($P < 0.01$), ***t* test ($P < 0.002$). (**C** and **D**) HCMEC/D3 cells were either incubated with 3 μM or 6 μM of PKCζ-PS or PKCη-PS (control) or left untreated. (C). PKCζ-PS (6 μM) reduced VE-cadherin, p120-catenin, and actin recruitment by 8.5-fold, 5-fold, and 4.9-fold, respectively. **t* test ($P < 0.001$). (D) HCMEC/D3 cells were transfected with either par6-YFP or par3-myc. Par3-myc recruitment was reduced 9-fold by 6 μM PKCζ-PS, but par6-YFP recruitment was not affected [**t* test ($P < 0.001$), ***t* test ($P < 0.01$)].

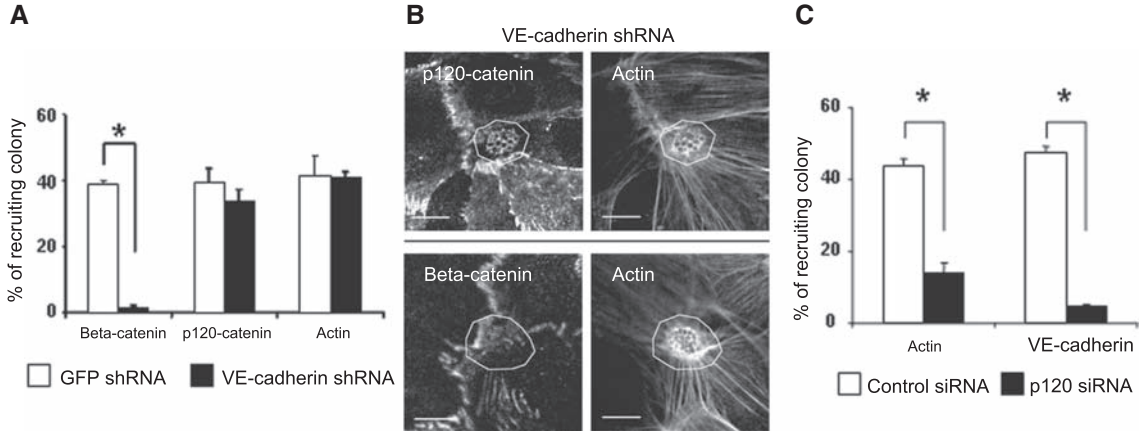

Fig. 3. P120-catenin is key to the recruitment of both actin and AJ proteins. (**A** and **B**) VE-cadherin silencing was performed by stable expression of a VE-cadherin shRNA (VEC shRNA). (A) Recruitment of β-catenin, p120-catenin, and actin was determined by immunofluorescence. Knockdown of VE-cadherin had no effect on the recruitment of p120-catenin and actin but reduced β-catenin recruitment by 20-fold. **t* test ($P < 0.001$). Data are expressed as mean ± SEM. (B) In VEC-shRNA–expressing cells, p120-catenin was still recruited beneath *N. meningitidis* colonies, where it colocalized with actin (top), whereas β-catenin was no longer recruited (bottom). Areas outlined in white indicated the location of a *N. meningitidis* colony. Scale bars, 10 μm. (**C**) Silencing of p120-catenin was performed by using a specific siRNA duplex (p120 siRNA). Recruitment of VE-cadherin and actin was determined by immunofluorescence. Knockdown of p120-catenin reduced VE-cadherin and actin recruitment by 10-fold and 4-fold, respectively. **t* test ($P < 0.001$). Data are expressed as mean ± SEM.

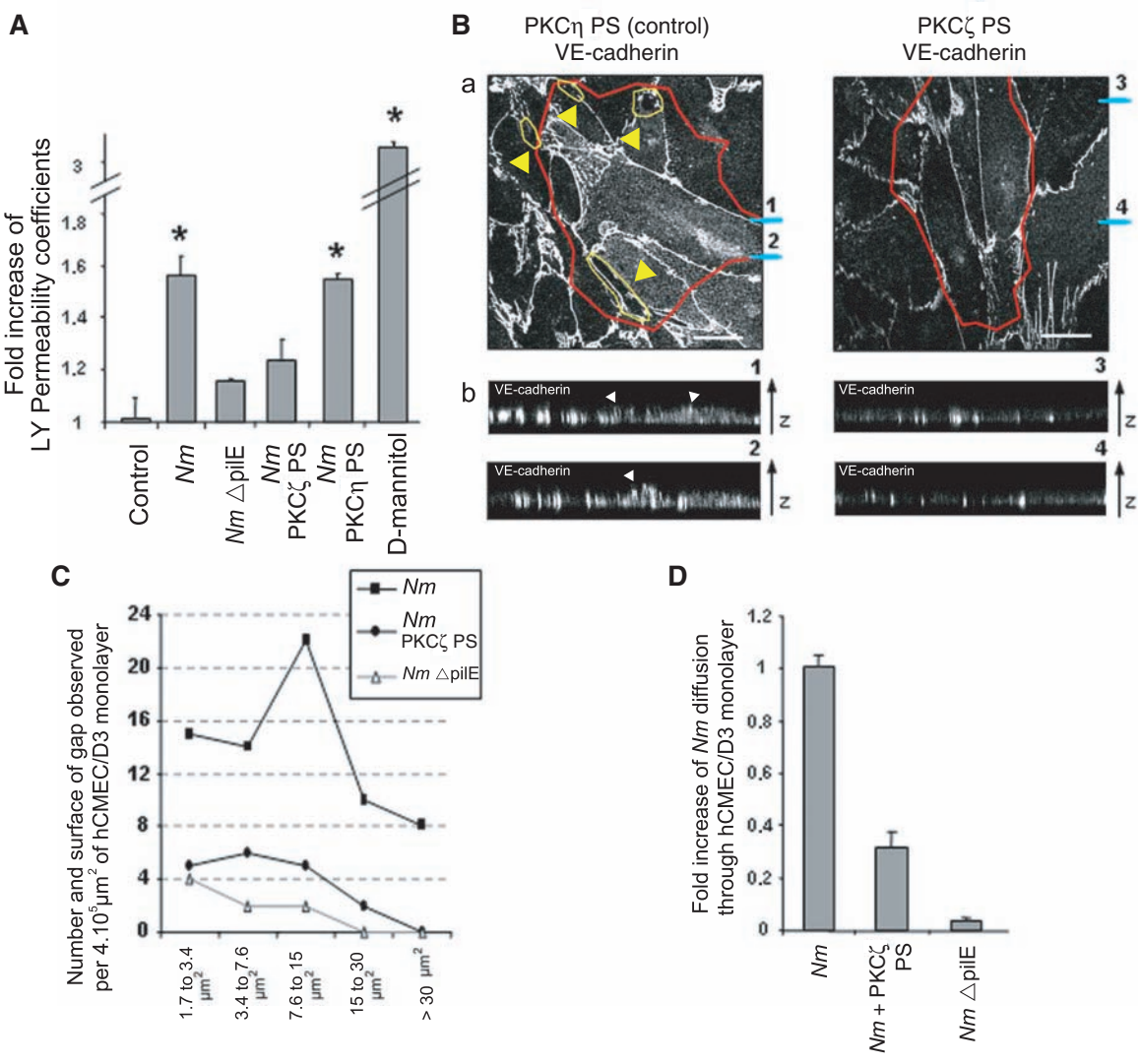

Fig. 4. *N. meningitidis*–induced PKCζ activity facilitates cell-cell junction opening. (**A**) The permeability coefficient of Lucifer Yellow was measured 4 hours postinfection by *N. meningitidis* (*Nm*) or its nonpiliated isogenic strain (*Nm* ΔpilE), or after treatment by PKCζ-PS or PKCη-PS (6 μM). *N. meningitidis* induced a 1.55-fold increase compare with control. D-mannitol, which disrupts all cell-cell junctions, induced a 3.1-fold increase. *t test ($P < 0.001$). (**B**) HCMEC/D3 cells were incubated with 6 μM of PKCζ-PS or of PKCη-PS (control). (a) VE-cadherin localization was analyzed on the basolateral cross section of *N. meningitidis*–infected cells. Yellow arrowheads and areas outlined in yellow indicate gaps between cells. Areas outlined in red indicate the presence of *N. meningitidis* colonies. Blue bars marked 1 to 4 refer to *Z*-axis reconstruction images 1 to 4 in (b). Scale bars, 20 μm. (b) *Z*-axis reconstructions from a stack of 0.12-μm interval images show that VE-cadherin is apically relocalized underneath *N. meningitidis* colonies (white arrows) only in cells treated with PKCη-PS (control). (**C**) HCMEC/D3 cells grown on 3.0-μm pore size inserts were treated or not with PKCζ-PS and incubated with *N. meningitidis* or its nonpiliated isogenic strain (*N.meningitidis* ΔpilE). Size and quantity of gaps observed 4 hours after infection are calculated as described (*27*). (**D**) Diffusion of *N. meningitidis* through an hCMEC/D3 monolayer, 4 hours postinfection, is 3.2-fold higher than diffusion of *N. meningitidis* in the presence of 6 μM PKCζ-PS and 16.5-fold higher than diffusion of its nonpiliated derivative (*Nm* ΔpilE). The rate of *N. meningitidis* internalization, determined by gentamicin protection assay, is very low (1 colony-forming unit in 3.5×10^5), identical to that of a control without cells, thus excluding a possible transcytosis of bacteria. Data are expressed as fold increase of *N. meningitidis* diffusion and calculated as described (*27*). Data from (B) to (D) are one representative experiment of three independent duplicates. Data are expressed as mean ± SEM.

marks passive paracellular diffusion (Fig. 4A) (*26*). Moreover, this increase relied on PKCζ activity and bacterial piliation (Fig. 4A). This modification of permeability was associated with the formation of gaps between infected cells (Fig. 4B). The number of gaps increased over time and was reduced by the PKCζ-PS (Fig. 4, B and C). Gaps did not form when cells were infected with a nonpiliated strain, showing that these gaps are due to Tfp-mediated signaling (Fig. 4C). Indeed, piliated strain cross the monolayer at a rate higher than those of nonpiliated isogenic derivatives or a piliated strain in the presence of PKCζ-PS (Fig. 4D). Thus, the signaling induced by *N. meningitidis* Tfp that leads to the recruitment of the polarity complex is associated with large alterations of the intercellular junctions that are sufficient for the bacteria to cross the brain endothelial cell monolayer.

In summary, *N. meningitidis* microcolonies trigger via type IV pili a signal resembling the one responsible for the formation of AJ at cell-cell junctions. This leads to the formation of ectopic early junctionlike domains (fig. S7), thus disorganizing the cell-cell junctions and opening the paracellular route, which allows *N. meningitidis* to cross the BBB and to invade the meninges.

References and Notes

1. M. van Deuren, P. Brandtzaeg, J. W. van der Meer, *Clin. Microbiol. Rev.* **13**, 144 (2000).
2. B. Pron *et al.*, *J. Infect. Dis.* **176**, 1285 (1997).
3. E. Mairey *et al.*, *J. Exp. Med.* **203**, 1939 (2006).
4. M. Virji *et al.*, *Mol. Microbiol.* **5**, 1831 (1991).
5. X. Nassif *et al.*, *Mol. Microbiol.* **8**, 719 (1993).
6. T. Rudel, I. Scheurerpflug, T. F. Meyer, *Nature* **373**, 357 (1995).
7. H. Kallstrom, M. K. Liszewski, J. P. Atkinson, A. B. Jonsson, *Mol. Microbiol.* **25**, 639 (1997).
8. M. Kirchner, D. Heuer, T. F. Meyer, *Infect. Immun.* **73**, 3072 (2005).
9. A. J. Merz, M. So, M. P. Sheetz, *Nature* **407**, 98 (2000).
10. J. S. Mattick, *Annu. Rev. Microbiol.* **56**, 289 (2002).
11. A. J. Merz, C. A. Enns, M. So, *Mol. Microbiol.* **32**, 1316 (1999).
12. G. Mikaty *et al.*, *PLoS Pathog.* **5**, e1000314 (2009).
13. E. Eugene *et al.*, *J. Cell Sci.* **115**, 1231 (2002).
14. B. B. Weksler *et al.*, *FASEB J.* **19**, 1872 (2005).
15. H. A. Muller, E. Wieschaus, *J. Cell Biol.* **134**, 149 (1996).
16. T. Yamanaka *et al.*, *Genes Cells* **6**, 721 (2001).
17. T. W. Hurd, L. Gao, M. H. Roh, I. G. Macara, B. Margolis, *Nat. Cell Biol.* **5**, 137 (2003).

18. V. Vasioukhin, C. Bauer, M. Yin, E. Fuchs, *Cell* **100**, 209 (2000).
19. G. Joberty, C. Petersen, L. Gao, I. G. Macara, *Nat. Cell Biol.* **2**, 531 (2000).
20. W. Koh, R. D. Mahan, G. E. Davis, *J. Cell Sci.* **121**, 989 (2008).
21. S. Etienne-Manneville, J. B. Manneville, S. Nicholls, M. A. Ferenczi, A. Hall, *J. Cell Biol.* **170**, 895 (2005).
22. A. Suzuki, S. Ohno, *J. Cell Sci.* **119**, 979 (2006).
23. T. Ooshio *et al.*, *J. Cell Sci.* **120**, 2352 (2007).
24. S. Boguslavsky *et al.*, *Proc. Natl. Acad. Sci. U.S.A.* **104**, 10882 (2007).
25. I. Hoffmann, E. Eugene, X. Nassif, P. O. Couraud, S. Bourdoulous, *J. Cell Biol.* **155**, 133 (2001).
26. V. L. Madgula, B. Avula, V. L. N. Reddy, I. A. Khan, S. I. Khan, *Planta Med.* **73**, 330 (2007).
27. Materials and methods are available as supporting material on *Science* Online.
28. The authors thank M. Drab, P. Martin, I. Allemand, and N. Simpson for reviewing the manuscript and M. Garfa-Traore and N. Goudin for technical support. M.C. was funded by la Fondation pour la Recherche Médicale (FRM).

Supporting Online Material
www.sciencemag.org/cgi/content/full/1173196/DC1
Materials and Methods
Figs. S1 to S7
References
Movies S1 and S2

6 March 2009; accepted 18 May 2009
Published online 11 June 2009;
10.1126/science.1173196
Include this information when citing this paper.

Role of Layer 6 of V2 Visual Cortex in Object-Recognition Memory

Manuel F. López-Aranda,[1,2,4] Juan F. López-Téllez,[1,2,4] Irene Navarro-Lobato,[1] Mariam Masmudi-Martín,[1] Antonia Gutiérrez,[3,4] Zafar U. Khan[1,2,4]*

Cellular responses in the V2 secondary visual cortex to simple as well as complex visual stimuli have been well studied. However, the role of area V2 in visual memory remains unexplored. We found that layer 6 neurons of V2 are crucial for the processing of object-recognition memory (ORM). Using the protein regulator of G protein signaling–14 (RGS-14) as a tool, we found that the expression of this protein into layer 6 neurons of rat-brain area V2 promoted the conversion of a normal short-term ORM that normally lasts for 45 minutes into long-term memory detectable even after many months. Furthermore, elimination of the same-layer neurons by means of injection of a selective cytotoxin resulted in the complete loss of normal as well as protein-mediated enhanced ORM.

The current dominant view of visual memory is the multiple-domain approach, under which different components of recognition memory such as perception, storage, familiarity, and recollection are subserved by different modules in the brain (*1*–*5*). Recognition memory, one of the most studied examples of declarative memory, is generally considered to consist of two components, recollection and familiarity, and depends on the medial temporal lobe (MTL), a structure composed of the hippocampus and adjacent perirhinal, entorhinal, and parahippocampal cortices (*6*, *7*). In contrast, perceptual learning is a domain-of-perception module localized outside the MTL, which includes ventral visual-stream structures such as area V2. However, the multiple-domain approach has been contradicted (*7*–*10*). It is argued that the entire ventral visual-to-hippocampal stream is important for visual memory (*9*). This

[1]Laboratory of Neurobiology, Centro de Investigaciones Médico-Sanitarias, University of Malaga, Campus Teatinos s/n, 29071 Malaga, Spain. [2]Department of Medicine, Faculty of Medicine, University of Malaga, Campus Teatinos s/n, 29071 Malaga, Spain. [3]Department of Cell Biology, Faculty of Science, University of Malaga, Campus Teatinos s/n, 29071 Malaga, Spain. [4]Centro de Investigación Biomédica en Red sobre Enfermedades Neurodegenerativas (CIBERNED), Institute of Health Carlos III, Madrid, Spain.

*To whom correspondence should be addressed. E-mail: zkhan@uma.es

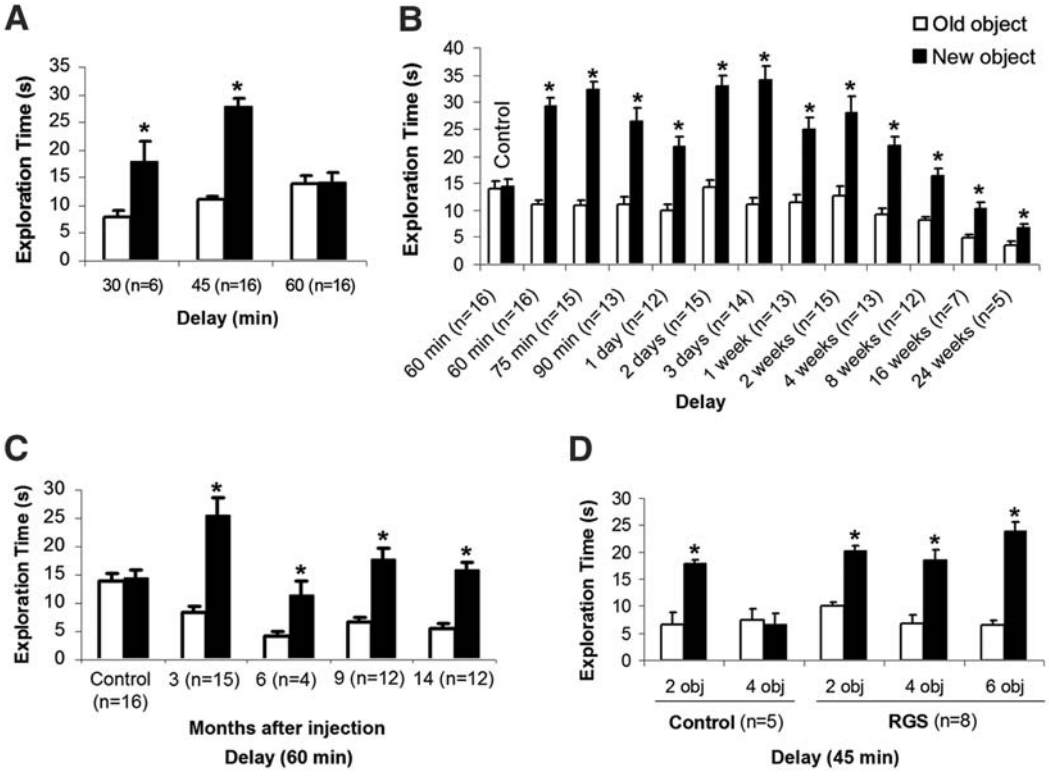

Fig. 1. Animal performance on ORM task. (**A**) When an object was shown for 3 min, normal rats could retain the object information in memory for 30 and 45 min but not for 60 min. (**B**) Injection of lentivirus–RGS-14 into layer 6 of area V2 boosted the animal ORM capacity such that the animal was able to retain the same object information for more than 24 weeks. (**C**) The ability of RGS-14 animals to convert 45-min memory into long-term memory remained even after 14 months when a novel visual stimulus was presented. (**D**) Normal animals could retain information about two different objects (obj) but were unable to remember when four objects were shown. Animals with RGS-14 were able to keep in memory the information about six different objects shown. In all figures, the exploration time is derived from one old object and one new object except in (D), in which values are derived from multiple old objects, as indicated in the figure, and 1 new object. Delay is the interval between exploration trial and memory test trial (*30*). Values are presented as mean ± SEM obtained from number (*n*) of animals indicated beneath the bars. Asterisk indicates a significantly longer exploration time for a new object ($P < 0.05$).

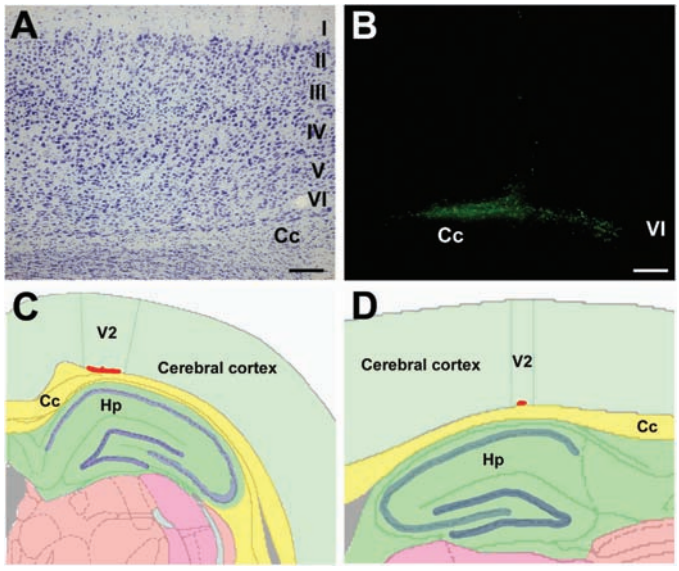

Fig. 2. Localization of RGS-14 protein in lentivirus–RGS-14–injected animals. (**A**) Cresyl violet staining of area V2 in the adjacent section indicates the corresponding layer 6. (**B**) A coronal brain section shows the localization of RGS-14 proteins as green fluorescence in layer 6 of the V2 visual cortex. (**C** to **D**) Drawings show localization of RGS-14 protein (red) at the injection site obtained from the analysis of coronal (n = 5 rat brains) (C) and sagittal (n = 7 rat brains) (D) serial sections. Both sections represent the maximum spread area observed. Area V2 is delimited by thin lines within the cerebral cortex in both (C) and (D). Distribution of cortical layers from layer 1 (I) to layer 6 (VI) is shown in (B). Cc, corpus callosum; Hp, hippocampus; scale bars, 125 μm.

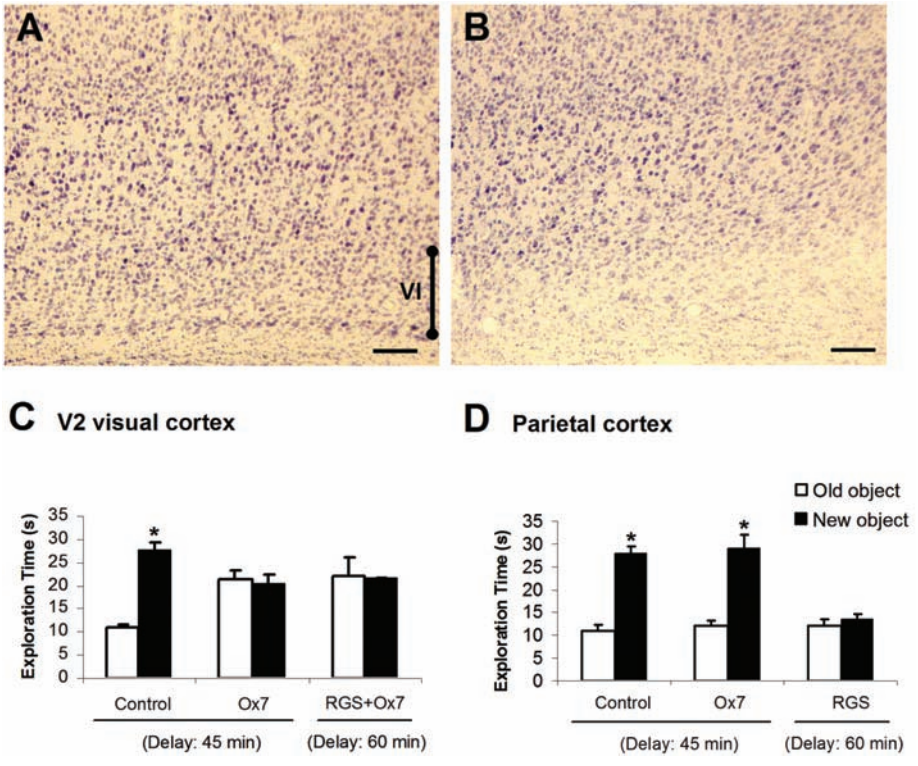

Fig. 3. Ox7-SAP injection in layer 6 and determination of ORM. (**A**) A normal view of layer 6 (VI) of the V2 visual cortex stained with cresyl violet. (**B**) Injection of Ox7-SAP (Ox7) into layer 6 of area V2 resulted in a major loss of neurons in this layer. (**C**) The behavioral performance of animals injected with Ox7-SAP (B) on the ORM task showed a complete loss of normal visual memory after 45 min. Similarly, when RGS-14 animals with confirmed enhanced ORM, as shown in Fig. 1, were treated with Ox7-SAP, the RGS-14–mediated effect on ORM was also abolished. (**D**) Injection of Ox7-SAP into the same layer of parietal cortex, an area just adjacent to V2, produced no effect on normal memory. Furthermore, in contrast to area V2, RGS-14–mediated effect on ORM was also absent in this area. Values are presented as mean ± SEM obtained from 5 to 8 animals in each case. Asterisk shows significantly higher exploration time for a new object (P < 0.05).

theory, unlike the dominant one, predicts that object-recognition memory (ORM) alterations could result from the manipulation in V2, an area that is highly interconnected within the ventral stream of visual cortices. In the monkey brain, this area receives strong feedforward connections from the primary visual cortex (V1) and sends strong projections to other secondary visual cortices (V3, V4, and V5) (*11*, *12*). Most of the neurons of this area are tuned to simple visual characteristics such as orientation, spatial frequency, size, color, and shape (*13*–*15*). V2 cells also respond to various complex shape characteristics, such as the orientation of illusory contours (*15*) and whether the stimulus is part of the figure or the ground (*16*). Anatomical studies implicate layer 3 of area V2 in visual-information processing. In contrast to layer 3, layer 6 of the visual cortex is composed of many types of neurons, and their response to visual stimuli is more complex. But the importance of layer 6 in visual-information processing remains an enigma.

We used a multidomain protein known as regulator of G protein signaling–14 (RGS-14) to dissect out the role of area V2 in visual memory. This protein contains a conserved RGS domain, which binds active Gi/o α–guanosine triphosphate (α-GTP) to confer GTPase activating protein activity (*17*, *18*), a GoLoco/GPR motif that binds to inactive Gi α-GDP and Gi α1/3 (*19*–*21*), a tandem Rap1/2–binding domain (RBD) (*22*), and other regions with unknown functions (*23*, *24*). RGS-14 protein is associated with microtubules and is an important factor in mitosis (*25*). Although the expression of RGS-14 protein was observed in monkey and rat brain (*26*), very little is known about its role in brain functions.

We used animal performance on ORM tests to evaluate visual memory. Rats were exposed to two identical objects for 3 min in an open field, and then they were analyzed for the length of time that object information was retained in their memory. During the ORM test session, one of the two identical objects was replaced with a new object, and the exploration time for both objects was recorded. After the memory test with delay periods of 30, 45, and 60 min, normal animals were able to retain object information for 30 and 45 min but not for 60 min (Fig. 1A). We called this limited visual memory of normal animals short-term ORM or normal ORM, and surpassing the normal ORM time limit was considered to be an increase in memory. Normal animals injected with lentivirus of RGS-14 into layer 6 of area V2 of rat brain 3 weeks before the test were subjected to the evaluation of ORM status. The overexpression of RGS-14 protein into layer 6 produced a large increase in the normal ORM (Fig. 1B). In contrast to normal animals, in which ORM lasted for 45 min, a visual stimulus of the same length of time to RGS animals led to the formation of long-term ORM, lasting for many months (Fig. 1B). Injection of lentivirus of RGS-12 (a protein that belongs to the same family as

RGS-14), saline solution, or vehicle lentivirus into the same area showed no such change in the ORM level. The performance of rats was similar to that of normal noninjected animals (fig. S1). The average exploration time during the initial 3-min exploration session of two identical objects was not significantly different between the vehicle-control (16.09 ± 0.81 s; n = 16 rats) and animals injected with RGS-14 (18.62 ± 1.47 s; n = 15 rats) (fig. S2). This finding excludes other factors than RGS-14 protein being involved into the memory boost. The injection of lentivirus of RGS-14 into the 2/3 layer of the V2 visual cortex, an area dorsal to the target site, and into CA1 and the dentate gyrus of hippocampus, areas ventral to the target site, did not produce an effect similar to that seen with the injection into layer 6 of the V2 visual cortex (fig. S3). Overexpression of RGS-14 protein in this layer not only boosted ORM but also maintained this characteristic for more than 14 months toward novel visual stimuli (Fig. 1C). In addition, the capacity to retain information on multiple objects was also higher in RGS animals. Normal animals could retain the information about two different objects but were unable for four objects. However, in contrast to normal animals, RGS animals could retain information about six objects (Fig. 1D).

After the behavioral experiments, brains of animals injected with lentivirus–RGS-14 were processed for immunocytochemistry to localize the area and/or site of protein expression in order to uncover the anatomical correlate of the memory enhancement observed in these animals. Brain sections were incubated with specific antibodies to RGS-14 (*26*) coupled with green fluorescence to visualize the protein. The expression of RGS-14 protein in area V2 was mainly localized in layer 6 (Fig. 2B). The analysis of injection site in sequential coronal (n = 5 rat brains) (Fig. 2C) as well as sagittal (n = 7 rat brains) (Fig. 2D) brain sections further confirmed the RGS-14 protein localization in layer 6 of area V2. Fig. 2, C and D, provides a 360° view of the RGS-14 protein localization area observed in the brain.

Next, we tested the importance of layer 6 neurons of area V2 in the formation of ORM by means of selective elimination of the neurons of this layer. Would the elimination of neurons in this layer abolish the both normal (short-term) and long-term memory mediated by the RGS-14 protein? We injected Ox7-SAP, a saporin-based immunotoxin that selectively eliminates neurons (*27*, *28*), into layer 6 of area V2 and evaluated the visual memory of animals. Injection of the immunotoxin resulted in the loss of almost all the neurons of this area while leaving other cells and structure intact (Fig. 3B). However, no damage to the hippocampus was observed (fig. S4). Behavioral performance of the Ox7-SAP–injected animals on an ORM task showed a complete loss of normal ORM [delay of 45 min (Fig. 3C)], suggesting a major role of layer 6 neurons in visual memory. In addition to the facilitation in long-term ORM formation, layer 6 neurons are crucial for normal ORM. Furthermore, injection of Ox7-SAP in RGS animals abolished the protein-mediated enhancement in ORM [delay of 60 min (Fig. 3C)]. This result further confirmed the association of layer 6 neurons in the formation of long-term ORM. In contrast to area V2, injection of Ox7-SAP in layer 6 of parietal cortex, an area adjacent to area V2, did not produce any effect on normal ORM [delay of 45 min (Fig. 3D)]. Similarly, overexpression of RGS-14 protein in other areas, such as layers 2/3 of area V2, dentate gyrus and CA1 of the hippocampus (fig. S3), and layer 6 of the parietal cortex (Fig. 3D), also had no effect on long-term ORM (delay of 60 min).

The loss of both normal and RGS-mediated enhanced ORM after elimination of area V2 layer 6 neurons led us to question whether this layer of neurons serves as an ORM storage site. In RGS animals, after encoding information on novel objects, layer 6 neurons of area V2 were eliminated by Ox7-SAP treatment, and stored ORM was traced. Despite the absence of layer 6 neurons, these animals were able to recall information on objects shown before the Ox7-SAP treatment (fig. S5). However, their normal as well as RGS-mediated enhanced ORM were lost for novel visual stimuli (fig. S6). Thus, our results show that layer 6 of area V2 is implicated in ORM formation but not in its storage.

After passing through area V2, visual information continues ventrally through other visual areas to the MTL, a domain where ORM is thought to be processed (*6*, *7*). Our findings of the role of layer 6 neurons in the formation of both normal (short-term) and long-term ORM provide a new dimension to our understanding and emphasize the importance of V2, an area localized outside of MTL. It is proposed that layer 6 neurons of area V2 modulate the processing of visual information flow by either direct or indirect intrinsic connections within this area from layer 6 to other layers. In accordance with our results, a magnetic resonance imaging study designed to map the functional activation of the visual cortices in response to visual stimulus (*29*) showed the activation of area V2 during both visual perception and recall. In conclusion, our results show that layer 6 of area V2, an area which previously was thought to be involved in perception and perceptual learning, not only plays a critical role in the formation of short- and long-term visual memory but also contradicts the multiple domain theory and supports the view that the entire stream of ventral visual-to-hippocampus, and not the MTL alone, is important for visual memory processing. Additionally, the role of RGS-14 protein in the enhancement of visual memory makes this protein an important pharmaceutical target for the treatment of ORM defects as well as for boosting the memory capacity.

References and Notes

1. E. Tulving, D. L. Schacter, *Science* **247**, 301 (1990).
2. H. Eichenbaum, A. P. Yonelinas, C. Ranganath, *Annu. Rev. Neurosci.* **30**, 123 (2007).
3. M. W. Brown, J. P. Aggleton, *Nat. Rev. Neurosci.* **2**, 51 (2001).
4. L. R. Squire, S. Zola-Morgan, *Science* **253**, 1380 (1991).
5. Y. Miyashita, *Annu. Rev. Neurosci.* **16**, 245 (1993).
6. L. R. Squire, C. E. Stark, R. E. Clark, *Annu. Rev. Neurosci.* **27**, 279 (2004).
7. L. R. Squire, J. T. Wixted, R. E. Clark, *Nat. Rev. Neurosci.* **8**, 872 (2007).
8. E. A. Murray, T. J. Bussey, L. M. Saksida, *Annu. Rev. Neurosci.* **30**, 99 (2007).
9. T. J. Bussey, L. M. Saksida, *Hippocampus* **17**, 898 (2007).
10. T. J. Bussey, L. M. Saksida, *Curr. Opin. Neurobiol.* **15**, 730 (2005).
11. I. Stepniewska, J. H. Kaas, *J. Comp. Neurol.* **371**, 129 (1996).
12. R. Gattas, A. P. Sousa, M. Mishkin, L. G. Ungerleider, *Cereb. Cortex* **7**, 110 (1997).
13. J. Hegde, D. C. Van Essen, *J. Neurosci.* **20**, RC61 (2000).
14. J. Hegde, D. C. Van Essen, *J. Neurophysiol.* **92**, 3030 (2004).
15. A. Anzai, X. Peng, D. C. Van Essen, *Nat. Neurosci.* **10**, 1313 (2007).
16. I. Maruko *et al.*, *J. Neurophysiol.* **100**, 2486 (2008).
17. H. Cho, T. Kozasa, K. Takekoshi, J. De Gunzburg, J. H. Kehrl, *Mol. Pharmacol.* **58**, 569 (2000).
18. S. Hollinger, J. B. Taylor, E. H. Goldman, J. R. Hepler, *J. Neurochem.* **79**, 941 (2001).
19. R. J. Kimple *et al.*, *J. Biol. Chem.* **276**, 29275 (2001).
20. R. J. Kimple, M. E. Kimple, L. Betts, J. Sondek, D. P. Siderovski, *Nature* **416**, 878 (2002).
21. F. S. Willard *et al.*, *J. Biol. Chem.* **283**, 36698 (2008).
22. S. Traver *et al.*, *Biochem. J.* **350**, 19 (2000).
23. R. R. Neubig, D. P. Siderovski, *Nat. Rev. Drug Discov.* **1**, 187 (2002).
24. M. Abramow-Newerly, A. A. Roy, C. Nunn, P. Chidiac, *Cell. Signal.* **18**, 579 (2006).
25. L. Martin-McCaffrey *et al.*, *Cell Cycle* **4**, 953 (2005).
26. M. F. Lopez-Aranda, M. J. Acevedo, F. J. Carballo, A. Gutierrez, Z. U. Khan, *Eur. J. Neurosci.* **23**, 2971 (2006).
27. N. Traissard *et al.*, *Neuropsychopharmacology* **32**, 851 (2007).
28. B. C. Nolan, J. H. Freeman Jr., *Behav. Neurosci.* **119**, 190 (2005).
29. D. Le Bihan *et al.*, *Proc. Natl. Acad. Sci. U.S.A.* **90**, 11802 (1993).
30. Materials and methods are available as supporting material on *Science* Online.

31. We thank E. C. Muly and P. Koulen for advice and review of the manuscript. This work was supported financially by Ministerio de Ciencia e Innovacion grant BFU 06-0306 and Junta de Andalucia grant CTS 586/07 to Z.U.K. and FIS PI060556 grant to A.G. M.F.L. is the recipient of a CIBERNED contract. Application for the patent on RGS-14 protein has already been filed, and issue of patent is pending.

Supporting Online Material

www.sciencemag.org/cgi/content/full/325/5936/87/DC1
Materials and Methods
Figs. S1 to S6
References

13 January 2009; accepted 22 May 2009
10.1126/science.1170869

Jmjd6 Catalyses Lysyl-Hydroxylation of U2AF65, a Protein Associated with RNA Splicing

Celia J. Webby,[1]* Alexander Wolf,[2]* Natalia Gromak,[3]* Mathias Dreger,[4] Holger Kramer,[5] Benedikt Kessler,[5] Michael L. Nielsen,[6]† Corinna Schmitz,[2] Danica S. Butler,[1] John R. Yates III,[7] Claire M. Delahunty,[7] Phillip Hahn,[8] Andreas Lengeling,[8,9] Matthias Mann,[6] Nicholas J. Proudfoot,[3] Christopher J. Schofield,[1]‡§ Angelika Böttger[2]‡§

The finding that the metazoan hypoxic response is regulated by oxygen-dependent posttranslational hydroxylations, which regulate the activity and lifetime of hypoxia-inducible factor (HIF), has raised the question of whether other hydroxylases are involved in the regulation of gene expression. We reveal that the splicing factor U2 small nuclear ribonucleoprotein auxiliary factor 65-kilodalton subunit (U2AF65) undergoes posttranslational lysyl-5-hydroxylation catalyzed by the Fe(II) and 2-oxoglutarate–dependent dioxygenase Jumonji domain-6 protein (Jmjd6). Jmjd6 is a nuclear protein that has an important role in vertebrate development and is a human homolog of the HIF asparaginyl-hydroxylase. Jmjd6 is shown to change alternative RNA splicing of some, but not all, of the endogenous and reporter genes, supporting a specific role for Jmjd6 in the regulation of RNA splicing.

Metazoan cells respond to limiting oxygen by activation of the hypoxia-inducible factor (HIF) system (*1*). The HIFα subunits are regulated by Fe(II)– and 2-oxoglutarate (2OG)–dependent oxygenase catalysis; prolyl-hydroxylation promotes HIFα degradation via the ubiquitin-proteasome system, and asparaginyl hydroxylation reduces the HIF transcriptional activity by blocking its interaction with p300 (*2*). Sequence analyses suggest that Jumonji domain-6 protein (Jmjd6) (*3*–*9*) is a homolog of the HIF asparaginyl hydroxylase (factor-inhibiting HIF) (*1*).

To investigate the function of Jmjd6, we assayed for proteins interacting with Jmjd6 in cells using tandem-affinity purification coupled with mass spectrometry (MS) analyses (*10*, *11*). A substantial proportion (22 of 39) of the potential Jmjd6-interacting proteins are connected to RNA metabolism, processing, and splicing (table S1) with ~25% being nuclear proteins possessing Arg-Ser (RS) domains (12 of 39). We confirmed the interaction of Jmjd6 with the splicing factor U2 small nuclear ribonucleoprotein auxiliary factor 65-kDa subunit (U2AF65) (*12*) and cisplatin resistance–associated overexpressed protein (CROP)

[1]Chemistry Research Laboratory and Oxford Centre for Integrative Systems Biology, University of Oxford, 12 Mansfield Road, Oxford, Oxon OX1 3TA, UK. [2]Department of Biology II, Ludwig-Maximilians-University, Munich, Großhaderner Strasse 2, D-82152 Planegg-Martinsried, Germany. [3]Sir William Dunn School of Pathology, University of Oxford, South Parks Road, Oxford, Oxon OX1 3RE, UK. [4]Department of Physiology, Anatomy, and Genetics, University of Oxford, Parks Road, Oxford, Oxon OX1 3PT, UK. [5]Henry Wellcome Building for Molecular Physiology, University of Oxford, Oxford, OX3 7BN, UK. [6]Department of Proteomics and Signal Transduction, Max-Planck-Institute of Biochemistry, Am Klopferspitz 18, D-82152 Martinsried, Germany. [7]Department of Chemical Physiology, The Scripps Research Institute, La Jolla, CA 92037, USA. [8]Research Group Infection Genetics, Helmholtz Centre for Infection Research, Inhoffenstrasse 7, D-38124 Braunschweig, Germany. [9]Roslin Institute and Royal (Dick) School of Veterinary Studies, University of Edinburgh, EBVC, Roslin, EH25 9RG, UK.

*These authors contributed equally to the work.
†Present address: Department of Proteomics, Novo Nordisk Foundation Center for Protein Research, University of Copenhagen, DK-2200 Copenhagen, Denmark.
‡These authors contributed equally to the work.
§To whom correspondence should be addressed. E-mail: christopher.schofield@chem.ox.ac.uk (C.J.S.); boettger@zi.biologie.uni-muenchen.de (A.B.).

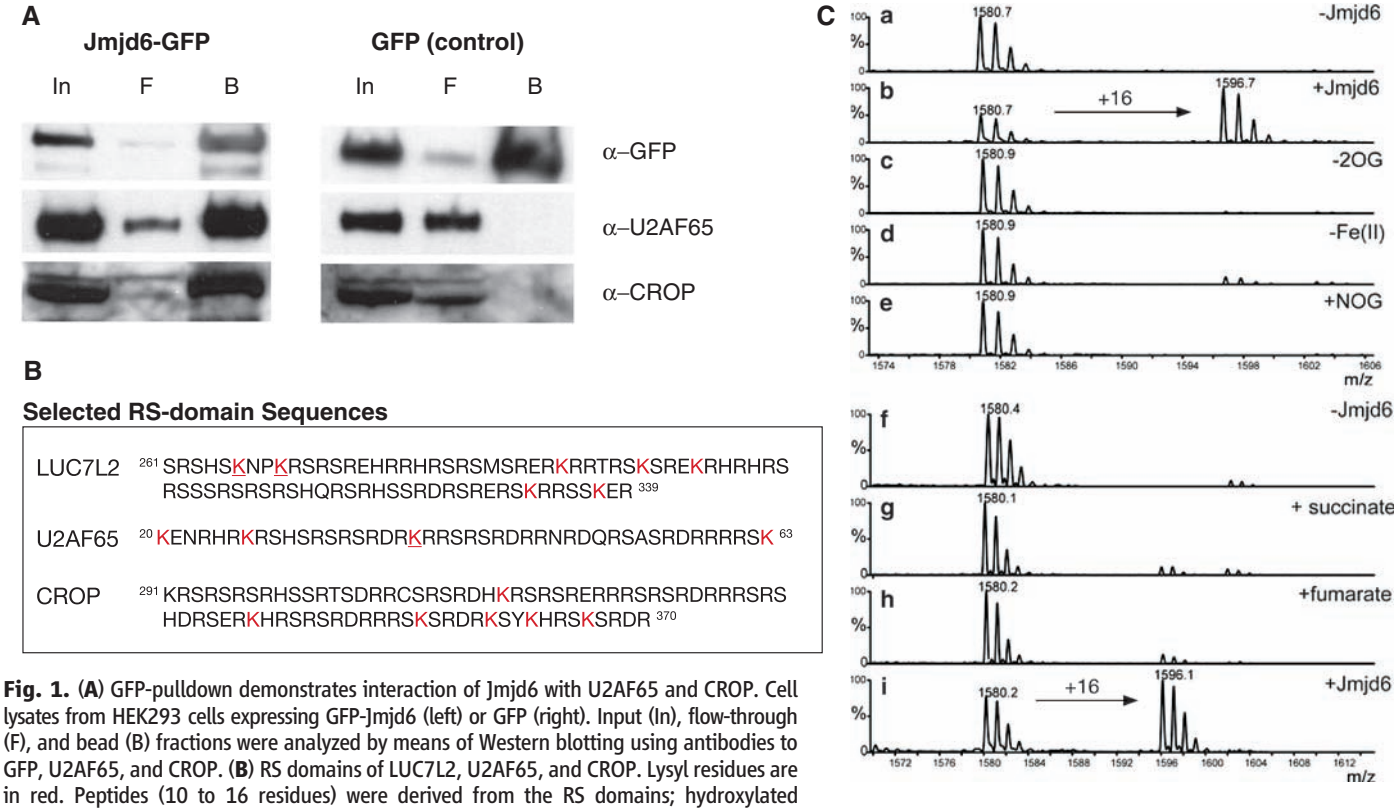

Fig. 1. (**A**) GFP-pulldown demonstrates interaction of Jmjd6 with U2AF65 and CROP. Cell lysates from HEK293 cells expressing GFP-Jmjd6 (left) or GFP (right). Input (In), flow-through (F), and bead (B) fractions were analyzed by means of Western blotting using antibodies to GFP, U2AF65, and CROP. (**B**) RS domains of LUC7L2, U2AF65, and CROP. Lysyl residues are in red. Peptides (10 to 16 residues) were derived from the RS domains; hydroxylated residues are underlined. (**C**) MALDI–time-of-flight analysis of $LUC7L2_{267\text{-}278}$ with Jmjd6. Assays included $LUC7L2_{267\text{-}278}$ (100 μM), ascorbate (100 μM), Fe(II) (100 μM), 2OG (500 μM), Tris (50 mM, pH 7.5), and Jmjd6 [(b) and (i)]. (a) and (f) are controls without Jmjd6. (c) to (h) include all components except 2OG (c), Fe(II) (d), and with NOG (12 mM) (e), succinate (1 mM) (g), and fumarate (1 mM) (h).

(*13*) using pull-down assays (Fig. 1A and fig. S1A) (*14*) in human embryonic kidney (HEK) 293T (HEK293T) cells. Endogenous U2AF65 and Jmjd6 coimmunoprecipitate in HeLa cells with antibody to U2AF65 (fig. S1B), and the interaction is disrupted by means of ribonuclease (Rnase) treatment (fig. S2).

Jmjd6 has recently been reported to be a histone arginine demethylase (*7*). However, we considered the possibility that arginine-rich sequences present in RS domains (Fig. 1B) of many of the Jmjd6-interacting proteins (table S1) may be Jmjd6 substrates. RS domain sequences from U2AF65, CROP, and LUC7-like2 (LUC7L2) were synthesized with dimethylated arginine residues and incubated with Jmjd6 in the presence of oxygen, Fe(II), and 2OG and analyzed by means of matrix-assisted laser desorption/ionization (MALDI) MS. Peptides $U2AF65_{28\text{-}43}(R35Me_{2sym})$, $U2AF65_{28\text{-}43}(R33Me_{2sym})$, and $LUC7L2_{267\text{-}282}(R274Me_{2sym})$ did not show dimethyl arginine-demethylation (–14 shift in mass). Recombinant Jmjd6 also did not produce demethylated arginine histone H4 and H3 fragment peptides. Instead, a clear +16-dalton or +32-dalton mass shift relative to unreacted peptide was observed for RS-rich and histone peptides (figs. S3 and S4). This observation indicates the incorporation of one or two oxygen atom(s) into the peptide, as observed by Chang *et al*. (*7*). No hydroxylation was observed in the absence of oxygen. The $CROP_{321\text{-}336}$ peptide did not contain any lysine residues and was not hydroxylated. The +16-dalton mass shift observed with $LUC7L2_{267\text{-}278}$ was 2OG- and Fe(II)–dependent and was inhibited by the known oxygenase inhibitor *N*-oxalylglycine (NOG) (*1*) and the Krebs cycle intermediates succinate and fumarate (1 mM) (Fig. 1C). Substitution of the proposed Fe(II)–binding residues (*9*) with nonchelating residues (H187A and H187A-D189A) inactivated Jmjd6, implying an intact Fe(II)–binding center is required for catalysis. Incubation under $^{18}O_2$ reveals the origin of introduced hydroxyl group as from dioxygen (fig. S5). MS/MS analyses of $LUC7L2_{267\text{-}278}$ indicated oxidation of Lys-3, corresponding to Lys-269 in LUC7L2 (fig. S6); nuclear magnetic resonance (NMR) analyses demonstrated oxidation to occur at C-5 on the side chain (fig. S7).

The shortest U2AF65 and LUC7L2 peptide (Fig. IB) substrate observed to undergo hydroxylation possesses 12 residues ($LUC7L2_{267\text{-}278}$). Shorter peptides were not (<5%) hydroxylated under standard conditions. When $LUC7L2_{263\text{-}278}$ was tested, both +16 and +32 mass shifts were observed. When either of the two target lysines in $LUC7L2_{263\text{-}278}$ was individually substituted for an arginine, only a single hydroxylation occurred. The simultaneous substitution of both of the lysines to arginines ablated hydroxylation (fig. S8), as did substitution with a tri-, di-, or monomethylated lysine residue (fig. S9).

Liquid chromatography–mass spectrometry (LC-MS)/MS analyses of full-length recombinant U2AF65 after incubation with Jmjd6, 2OG, and iron (ascorbate is not required for Jmjd6 activity) indicates that U2AF65 is a Jmjd6 substrate (figs. S10 and S11). LC-MS/MS analysis of endogenous U2AF65 from HeLa cells revealed hydroxylation at Lys-15 and Lys-276 at ratios of ~1:100 and 1:250 hydroxylated:unhydroxylated residues (Fig. 2, A and B), respectively. Overexpression of Jmjd6 in HeLa cells resulted in the increased hydroxylation of U2AF65 (fivefold at Lys-15) (fig. S12).

The available data suggest that factors in addition to the local sequence determine Jmjd6 selectivity. For example, Lys-15 and Lys-276 in intact proteins appear to be substrates of Jmjd6, whereas the peptides $U2AF65_{12\text{-}26}$ and $U2AF65_{274\text{-}287}$ are not. All the synthetic peptides found to be hydroxylated in vitro are very basic and carry a predicted overall charge of at least +4. Precedent for structural factors other than local sequence selectivity comes from work on the HIF hydroxylases (*1*).

U2AF65 is required for mRNA splicing (*15*). Modulation of splice-site recognition by U2AF65 influences alternative splicing (*16*). Jmjd6 knockdown (but not knockdown of a nonspecific DNA-binding

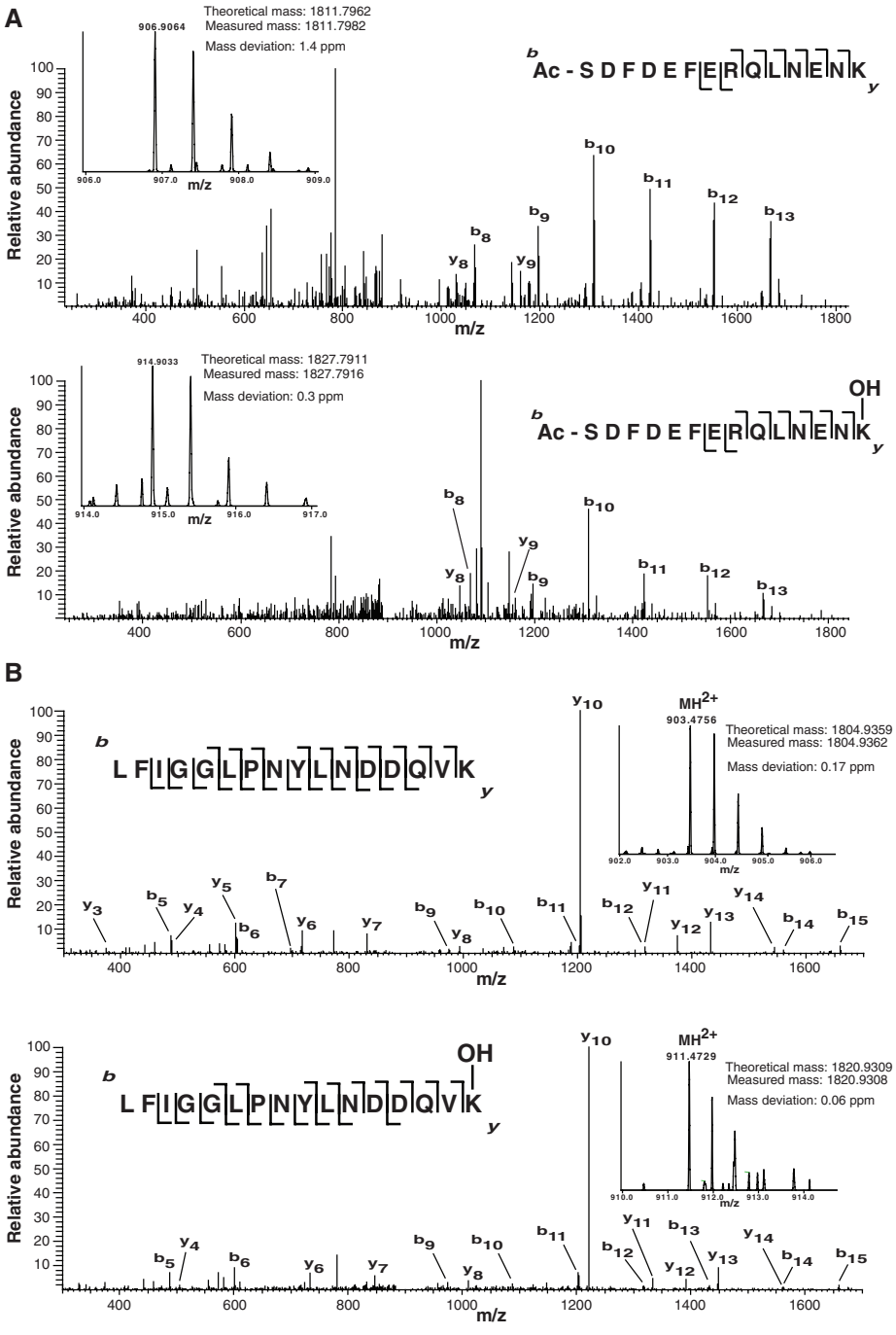

Fig. 2. MS/MS analysis of endogenous U2AF65 reveals hydroxylation of Lys-15 (**A**) and Lys-276 (**B**). U2AF65 was immunoprecipitated from HeLa cells, digested with protease, then analyzed. Data for the unmodified (top) and hydroxylated peptides (bottom) are shown. Inserts show the MH^{2+} peptide precursor ions that were fragmented; the b and y fragment ions are not indicated.

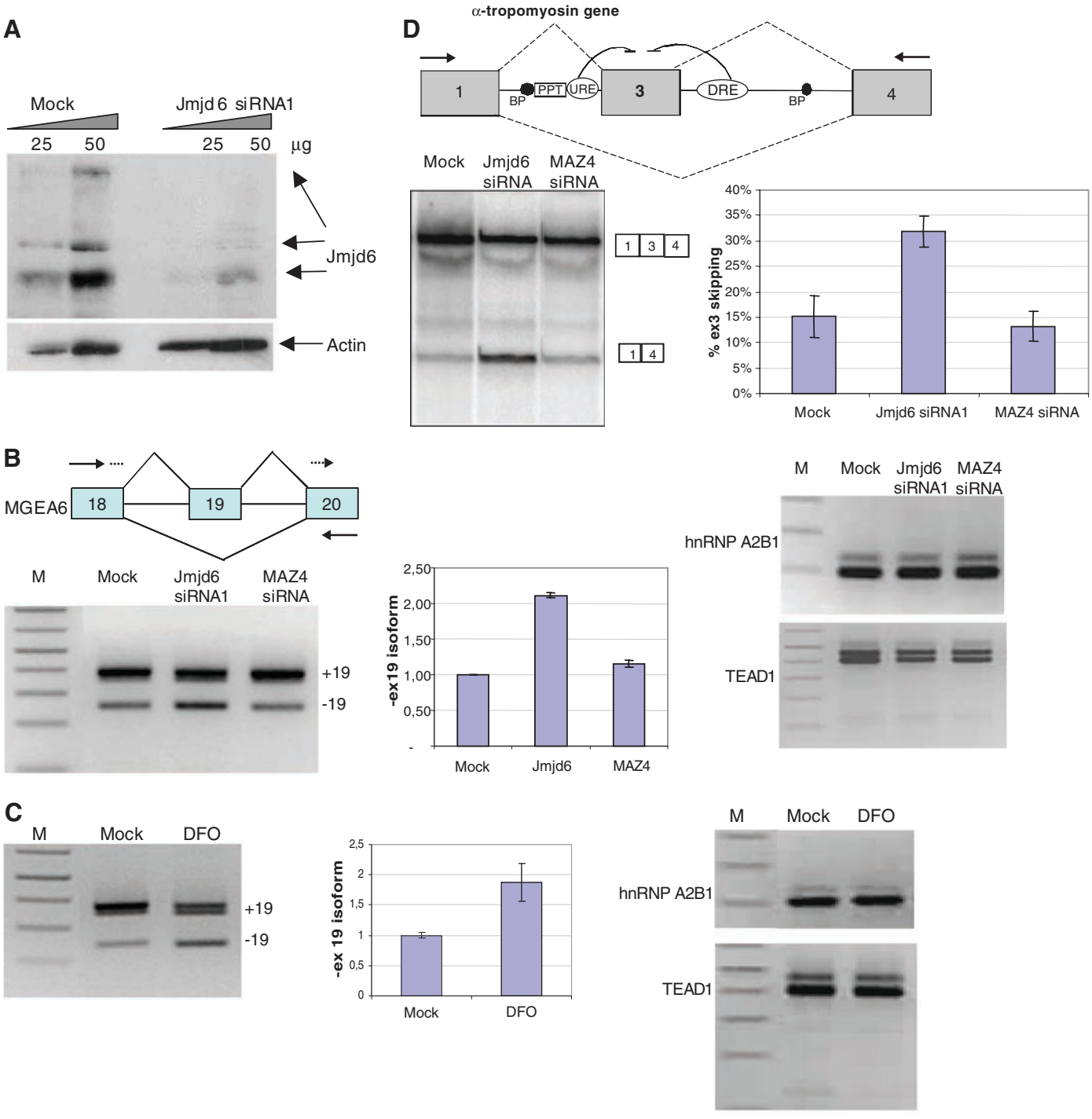

Fig. 3. Jmjd6 regulates alternative splicing. (**A**) RNA interference–mediated depletion of human Jmjd6 in HeLa cells. Western blot analyses of protein from mock and Jmjd6 siRNA-treated HeLa cells with antibodies to Jmjd6 and actin. (**B**) (Top left) Exon structure of MGEA6 gene showing exons (18 to 20) in boxes, introns as horizontal lines, and splicing patterns as diagonal lines. Arrows indicate the location of primers for reverse transcription polymerase chain reaction (RT-PCR) analyses. The forward primer used for quantitative PCR of –ex19-spliced isoform (spanning exon 18- exon 20 splice junction) is shown as a dashed line. (Bottom left and middle) RT-PCR analyses detecting endogenous MGEA6 RNA from mock cells, cells treated with Jmjd6 siRNA1, or siRNA targeting MAZ4. Histogram on the right shows the mean amount of –ex19-spliced isoform (±SD) compared with that in mock-treated cells analyzed by means of quantitative PCR from three independent experiments. (Right) Alternative splicing of human endogenous hnRNPA2B1 and TEAD1 genes is not affected in cells treated with Jmjd6 siRNA1 or MAZ4 siRNA. (**C**) (Left and middle) RT-PCR analysis detecting MGEA6 RNA from HeLa cells treated with DFO (100 µM over 24 hours). The splicing products +ex19 and –ex19 are indicated. The histogram shows the mean amount of –ex19-spliced isoform (±SD) compared with that in mock-treated cells analyzed by means of quantitative PCR from three independent experiments. (Right) Alternative splicing of human endogenous hnRNPA2B1 and TEAD1 genes is not affected in HeLa cells treated with DFO. (**D**) (Top) The α-TM minigene construct, with exons 1, 3, and 4 shown as boxes and introns as lines. Splicing patterns are shown as diagonal dashed lines. Arrows indicate the location of primers used in RT-PCR analysis. (Bottom) RT-PCR analyses of α-TM minigene construct transfected in mock-treated HeLa cells, cells treated with Jmjd6 siRNA1, or siRNA targeting MAZ4. The histogram shows the mean percentage of α-TM exon 3 skipping (±SD) from three independent experiments.

protein, MAZ4) altered the alternative splicing pattern of the endogenous tumor antigen gene *MGEA6*, which is regulated by the splicing regulatory protein SF2/ASF (*17*) with an increase in the amount of exon 19 skipping (–19) of the MGEA6 gene (Fig. 3, A and B, and figs. S13 and S14). A similar splicing pattern was also observed when HeLa cells were treated with the hypoxia mimic desferrioxamine (DFO) (*1*), a 2OG oxygenase inhibitor (Fig. 3C). In contrast, alternative splicing of the hnRNPA2B1 and TEAD1 genes was not affected by Jmjd6 knockdown or DFO (Fig. 3, B and C).

The α-tropomyosin (α-TM) minigene construct (Fig. 3D) (*18*) recapitulates splicing regulation of the α-TM gene and contains exons 1, 3, and 4 surrounded by their intronic regulatory sequences (*18*). Splicing the α-TM minigene construct generates two mRNA isoforms: 1-3-4 and 1-4. We overexpressed the α-TM construct both in mock-treated cells and cells treated with small interfering RNA (siRNA) targeting Jmjd6 and MAZ4 (Fig. 3D). The Jmjd6 knockdown cells, but not mock-treated cells or cells treated with siRNA targeting the MAZ4 protein, produced a clear increase in the amount of 1-4 spliced isoform (Fig. 3D). A second siRNA duplex (siRNA2) targeting another region of Jmjd6 mRNA had a similar though smaller effect on α-TM alternative splicing (fig. S13). Treatment of the Jmjd6 KD cells with cycloheximide did not affect α-TM splicing (fig. S13). Together these results imply a role for Jmjd6 in the regulation of alternative splicing.

Lysyl hydroxylation is the dominant oxidative catalytic activity of Jmjd6. Jmjd6-catalyzed arginine demethylation cannot be ruled out but would have to occur at a level below our current levels of detection. Although histone peptides were found to be Jmjd6 substrates, our subcellular localization and interaction analyses imply that histones, if interacting with Jmjd6 at all, are not a focus of Jmjd6 activity. Furthermore, in extensive MS-based analysis on endogenous histones we have accrued no evidence for hydroxylation of lysine residues (histones H2A, H2B, H3, and H4). Instead, we have shown that U2AF65, a protein important for pre-mRNA splicing, is an endogenous Jmjd6 substrate. Jmjd6 has a selective effect on splicing, even though U2AF65 is a ubiquitous splicing factor. This may reflect different intron 3′ splice site strengths, which in turn may have altered affinity for the hydroxylated form or forms of U2AF65 and possibly other splicing factors.

Our results on lysyl-hydroxylation of nuclear proteins support proposals (*19*) that post-translational hydroxylation in both the cytoplasm and the nucleoplasm is ubiquitous and that changes in oxygen tension elicit systems-wide effects on proteins and protein biosynthesis, and may provide a regulatory mechanism for alternative splicing.

References and Notes

1. G. L. Semenza, *Genes Dev.* **14**, 1983 (2000).
2. C. J. Schofield, P. J. Ratcliffe, *Nat. Rev. Mol. Cell Biol.* **5**, 343 (2004).
3. J. Bose *et al.*, *J. Biol.* **3**, 15 (2004).
4. V. A. Fadok *et al.*, *Nature* **405**, 85 (2000).
5. Y. Kunisaki *et al.*, *Blood* **103**, 3362 (2004).
6. M. O. Li, M. R. Sarkisian, W. Z. Mehal, P. Rakic, R. A. Flavell, *Science* **302**, 1560 (2003).
7. B. Chang, Y. Chen, Y. Zhao, R. K. Bruick, *Science* **318**, 444 (2007).
8. M. Cikala *et al.*, *BMC Cell Biol.* **5**, 26 (2004).
9. A. Wolf, C. Schmitz, A. Bottger, *EMBO Rep.* **8**, 465 (2007).
10. M. P. Washburn, D. Wolters, J. R. Yates 3rd, *Nat. Biotechnol.* **19**, 242 (2001).
11. Materials and methods are available as supporting material on *Science* Online.
12. P. D. Zamore, J. G. Patton, M. R. Green, *Nature* **355**, 609 (1992).
13. Y. Nishii *et al.*, *FEBS Lett.* **465**, 153 (2000).
14. U. Rothbauer *et al.*, *Mol. Cell. Proteomics* **7**, 282 (2008).
15. E. A. Sickmier *et al.*, *Mol. Cell* **23**, 49 (2006).
16. M. L. Hastings, E. Allemand, D. M. Duelli, M. P. Myers, A. R. Krainer, *PLoS One* **2**, e538 (2007).
17. R. Karni *et al.*, *Nat. Struct. Mol. Biol.* **14**, 185 (2007).
18. N. Gromak, C. W. Smith, *Nucleic Acids Res.* **30**, 3548 (2002).
19. M. E. Cockman *et al.*, *Proc. Natl. Acad. Sci. U.S.A.* **103**, 14767 (2006).

20. We thank A. Lamond, Y. W. Lam, and H. Hermeking for discussions and reagents; U. Rothbauer for the green fluorescent protein (GFP) nanotrap; H. Koenig for the pGEX-2T-U2AF65 plasmids; T. Claridge and R. Hamed for NMR analyses; and J. McCullagh and F. Sobott for MS analyses. This work was funded by the Glasstone Fellowship (to C.W.), Deutsche Forschungsgemeinschaft grants BO1748-3 awarded to A.B. and LE2130/2-1 awarded to A.L., the UK Biotechnology and Biological Sciences Research Council, the European Union, and the Wellcome Trust (to N.P.R.). C.J.S is a cofounder of ReOx.

Supporting Online Material

www.sciencemag.org/cgi/content/full/325/5936/90/DC1
Materials and Methods
Figs. S1 to S15
Table S1
References

5 May 2009; accepted 22 May 2009
10.1126/science.1175865

Essential Role of the Glycosyltransferase Sxc/Ogt in Polycomb Repression

Maria Cristina Gambetta, Katarzyna Oktaba, Jürg Müller*

Polycomb group proteins are conserved transcriptional repressors that control animal and plant development. Here, we found that the *Drosophila* Polycomb group gene *super sex combs* (*sxc*) encodes Ogt, the highly conserved glycosyltransferase that catalyzes the addition of *N*-acetylglucosamine (GlcNAc) to proteins in animals and plants. Genome-wide profiling in *Drosophila* revealed that GlcNAc-modified proteins are highly enriched at Polycomb response elements. Among different Polycomb group proteins, Polyhomeotic is glycosylated by Sxc/Ogt in vivo. *sxc/Ogt*–null mutants lacked O-linked GlcNAcylation and failed to maintain Polycomb transcriptional repression even though Polycomb group protein complexes were bound at their target sites. Polycomb repression appears to be a critical function of Sxc/Ogt in *Drosophila* and may be mediated by the glycosylation of Polyhomeotic.

The *Drosophila* gene *super sex combs* (*sxc*) was originally identified because mutations in this gene caused lethality at the pupal stage and homeotic transformations of multiple body segments into segments normally present in more posterior body regions (*1*). This phenotype suggested that multiple homeotic (HOX) genes were expressed outside of their normal expression domains, and the HOX gene *Ultrabithorax* (*Ubx*) was indeed misexpressed in *sxc* mutant larvae (*2*). Consequently, *sxc* was classified as a Polycomb group (PcG) gene. To explore the role of *sxc* in PcG repression, we stained larvae that were transheterozygous for two different *sxc*-null mutations with antibodies against the protein products of the PcG target genes *Ubx*, *Abdominal-B* (*Abd-B*), *Sex combs reduced* (*Scr*), *engrailed* (*en*), *Distal-less* (*Dll*), and *teashirt* (*tsh*). Each of these genes was expressed outside of its normal expression domain (fig. S1). *sxc* is thus needed for repression of multiple PcG target genes in *Drosophila* larvae.

We fine-mapped the *sxc* gene to a 160-kb genomic interval (*3*). Sequencing candidate open reading frames in genomic DNA from *sxc* mutants (*3*) revealed that sxc^{1}, sxc^{4}, sxc^{5}, and sxc^{7} each had individual base changes in the open reading frame of CG10392 that changed an amino-acid codon into a premature termination codon or a codon for a different amino acid (Fig. 1A). In sxc^{6}, a point mutation destroys the splice acceptor site in the fourth intron of CG10392 (Fig. 1A). CG10392 encodes O-linked *N*-acetylglucosamine (O-GlcNAc) transferase (Ogt), the enzyme that catalyzes addition of GlcNAc to serine or threonine residues of a broad range of nuclear and cytosolic proteins in animals and plants (*4*, *5*). The molecular lesions in five different *sxc* alleles therefore identified *sxc* as the gene that encodes Ogt, and in the following we call this gene *sxc/Ogt*. We next analyzed the Ogt protein in extracts from *sxc*

Gene Expression Programme, European Molecular Biology Laboratory (EMBL), Meyerhofstrasse 1, 69117 Heidelberg, Germany.

*To whom correspondence should be addressed. E-mail: juerg.mueller@embl.de

mutant larvae with an antibody to Ogt. No Ogt protein was detected in *sxc*^{3}, *sxc*^{6}, or *sxc*^{7} mutants, suggesting that these are protein-null mutations (Fig. 1B). Ogt^{N948I} (the mutant Ogt protein encoded by *sxc*^{4}) and Ogt$^{\Delta 1031\text{-}1059}$ (the C-terminally truncated Ogt protein encoded by *sxc*^{5}) were both expressed as stable polypeptides in mutant larvae (Fig. 1B). The phenotype of *sxc*^{4} and *sxc*^{5} mutants is as severe as that of the protein null mutants *sxc*^{3}, *sxc*^{6}, or *sxc*^{7} (*1*–*3*). The expressed Ogt$^{\Delta 1031\text{-}1059}$ and Ogt^{N948I} proteins, containing lesions predicted to affect the fold of the glycosyltransferase domain (*6*, *7*), therefore seem to be completely nonfunctional. An intact glycosyltransferase domain in Ogt is thus critical for Polycomb repression.

More than 100 different proteins have been reported to bear the O-GlcNAc modification in mammalian cells, including RNA polymerase II and several transcription factors and coregulators (*4*, *5*). Labeling of *Drosophila* polytene chromosomes with wheat germ agglutinin (WGA), a lectin that binds with high affinity to GlcNAc residues (*8*, *9*), suggested that GlcNAcylated proteins are also present on *Drosophila* chromosomes (*10*). We determined the genome-wide distribution of GlcNAc-modified proteins in the chromatin of imaginal disc cells from *Drosophila* larvae by performing chromatin immunoprecipitation (ChIP) assays with an antibody that recognizes the O-GlcNAc modification (*11*) and with a WGA-affinity resin (*3*). We hybridized the precipitated material to high-density whole-genome tiling arrays and analyzed them using TileMap (*12*) using a stringent cutoff. Only genomic regions significantly enriched by both antibody to O-GlcNAc and WGA-affinity resin were considered, resulting in a high-confidence set of 1138 genomic sites bound by GlcNAc-modified proteins (Fig. 2A) (*3*). We next compared the GlcNAc profile with the genome-wide binding profile of the PcG protein Ph that we had generated in parallel (*3*) and with that of the PcG protein complex PhoRC (*13*). 490 of the 1138 GlcNAc sites overlapped with Polycomb response elements (PREs) bound by Ph and/or PhoRC (Fig. 2A, left). Moreover, among the 1% top-ranked GlcNAc sites nearly all (111 of 114) overlapped with Ph- and/or PhoRC-bound regions (Fig. 2A, right). In PcG target genes misexpressed in sxc mutants (fig. S1), GlcNAc-modified proteins were specifically localized at PREs (Fig. 2B and fig. S2). To validate these findings, we performed ChIP assays with the antibody to O-GlcNAc in imaginal discs from wild-type or *sxc* mutant larvae and analyzed immunoprecipitates for enrichment of selected DNA sequences of the PcG target genes *Ubx*, *Abd-B*, *Scr*, *en*, *Dll*, *tsh*, and *pannier* (*pnr*) (Fig. 3A). GlcNAc ChIP signals were present at PREs in wild-type but not in *sxc* mutant larvae, demonstrating that the antibody to O-GlcNAc indeed specifically immunoprecipitated GlcNAc-modified proteins bound at these PREs (Fig. 3A). We also compared the GlcNAc profile at the *Ubx* gene in wing (*Ubx* repressed) and haltere/third leg–disc cells (*Ubx* active). GlcNAcylated proteins were bound at *Ubx* PREs both in cells in which the gene is repressed and in cells in which it is active (Fig. 3A), much like the PcG protein complexes PhoRC, Polycomb repressive complex 1 (PRC1), or PRC2 (*14*).

We next performed ChIP assays with antibodies against the PhoRC subunit Pho, the PRC1 subunit Ph, and the PRC2 subunit E(z) to test whether binding of any of these protein complexes might be affected in *sxc* mutants. Comparison of the ChIP profiles in wild-type and *sxc* mutant wing discs showed that binding of Pho and E(z) at PREs was largely unaffected in *sxc* mutants (Fig. 3B). Ph was also bound at high levels at all PREs in *sxc* mutant discs, but Ph ChIP signals were 1.5- to twofold reduced at most PREs as compared with those in wild-type discs (Fig. 3B), even though nuclear localization of Ph appeared comparable in wild-type and *sxc* mutant cells (fig. S3). However, not only Pho and E(z) but also Ph were all bound at wild-type levels at the *Scr* and *tsh* PREs in *sxc* mutant discs (Fig. 3B), and yet Polycomb repression at these two genes was lost in the mutant discs (fig. S1). These results suggest that loss of target gene repression is not solely due to reduction of PcG protein complex binding, although it is possible that binding of other PcG proteins is more severely affected in *sxc* mutants. Lastly, we performed ChIP analyses with antibodies against trimethylated lysine 27 of histone H3 (H3-K27me3), the PcG-specific chromatin modification generated by PRC2 (*15*). H3-K27me3 levels in target-gene chromatin were comparable in wild-type and *sxc* mutant larvae, and so were bulk H3-K27me3 levels (fig. S4). Sxc/Ogt is therefore apparently not critical for recruitment of PRC2 or for its ability to trimethylate H3-K27 in target gene chromatin.

The similarity between the GlcNAc and PcG protein ChIP profiles prompted us to test whether any of the PcG proteins themselves may carry the O-GlcNAc modification. We used WGA-agarose to affinity-purify GlcNAc-modified proteins from wild-type or *sxc* mutant larval extracts and probed the purified material with antibodies against the PhoRC subunits dSfmbt and Pho; the PRC1 subunits Ph, Pc, Ring, and Scm; and the PRC2 subunits Su(z)12 and Nurf55. Ph, but none of the other proteins tested, was strongly enriched after WGA-affinity purification from wild-type but not from *sxc* mutant larvae (Fig. 4). This enrichment of Ph was also observed under denaturing conditions (Fig. 4). This suggests that Ph itself is GlcNAcylated by Sxc/Ogt. PRC1 components Ring, Pc, or Scm did not copurify with GlcNAc-modified Ph in these WGA pull-down assays from larval extracts (Fig. 4), although Ring and Pc were readily detected together with Ph in such purifications from embryonic nuclear extracts (fig. S4). This finding could be explained by differential association of Ph with PRC1 components and/or different accessibility of GlcNAc moieties on Ph during embryonic and larval development. WGA-purifications failed to provide evidence for GlcNAcylation of the large subunit of RNA polymerase II (Fig. 4) Rpb1, which was previously proposed to be a mechanism by which Ogt might mediate transcriptional repression in mammalian cells (*16*).

The work reported here shows that GlcNAcylation by Sxc/Ogt plays an essential role in PcG repression. Ogt is a single-copy gene in mice, flies, and worms, and the only known glycosyltransferase that adds GlcNAc moieties to nuclear and cytosolic proteins (*4*, *5*). Ogt is essential in

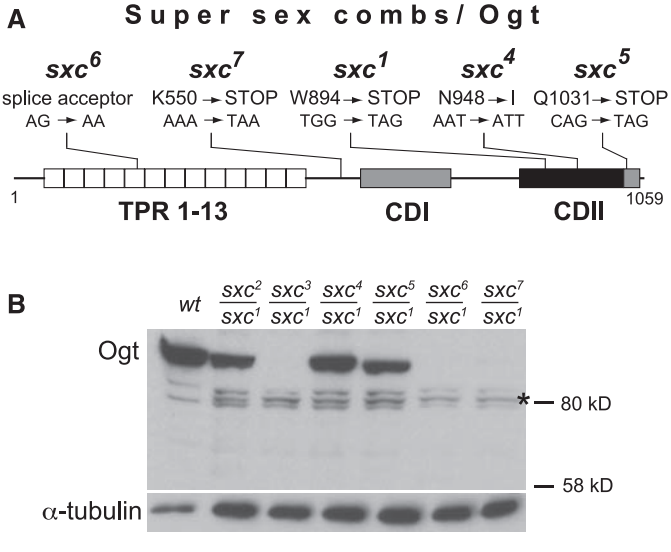

Fig. 1. Molecular characterization of the *Drosophila* PcG gene *sxc/Ogt*. (**A**) Structure of the Sxc/Ogt protein and lesions in *sxc* mutant alleles. The 13 tetratrico peptide repeats and the bipartite glycosyltransferase domain composed of CDI and CDII, also called N- and C-terminal GT-B subdomains (*6*, *7*), are shown as white, gray, and black boxes, respectively. Base substitutions in *sxc* mutant alleles are indicated. Ogt$^{\Delta 1031\text{-}1059}$, encoded by *sxc*^{5}, lacks the C-terminal helix (gray box) that forms part of the CDI domain. Asn948, mutated in *sxc*^{4}, is conserved in fly, worm, mouse, and human Ogt. (**B**) Detection of Sxc/Ogt protein in wild-type (*wt*) and *sxc* mutant larvae. Immunoblot of imaginal disc extracts from third instar larvae of the indicated genotype, probed with antibodies to human Ogt (top) and α-tubulin (bottom) is shown. The 80-kD protein (asterisk) is a truncated protein encoded by *sxc*^{1}. The viable allele *sxc*^{2} expresses a full-length protein (*3*). Lack of functional Ogt in *sxc*^{7}/*sxc*^{1} mutants is further supported by the loss of O-GlcNAcylation on nucleoporins (fig. S6).

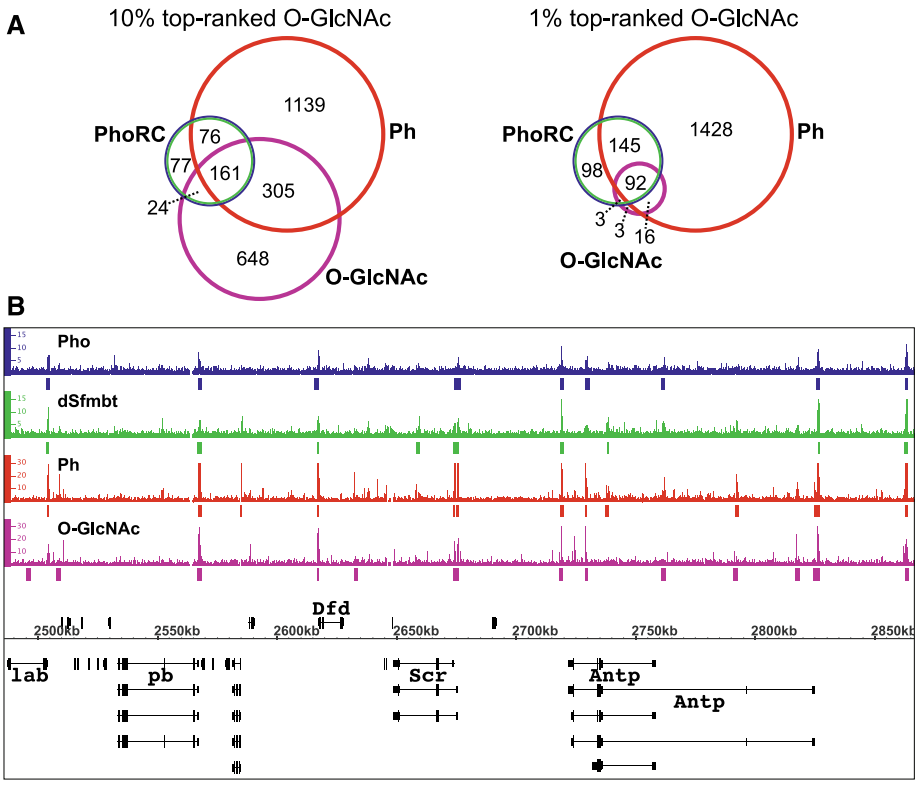

Fig. 2. O-GlcNAc–modified proteins are localized at PREs in *Drosophila*. (**A**) Venn diagrams showing the overlap of 1138 10% top-ranked O-GlcNAc sites (left) or 114 1% top-ranked O-GlcNAc sites (right) with 1689 Ph and 338 PhoRC-bound regions in larval imaginal discs (tables S1 and S2) (*3*). (**B**) ChIP profiles of O-GlcNAc, Ph, and PhoRC subunits Pho and dSfmbt at the Antennapedia complex in imaginal disc cells. Hybridization intensities for oligonucleotide probes are plotted as color bars above the genomic map (release 5, kilobase coordinates) of *Drosophila melanogaster*; significantly enriched regions are marked below plots (*3*). The HOX genes *labial* (*lab*), *proboscipedia* (*pb*), *Deformed* (*Dfd*), *Scr*, and *Antennapedia* (*Antp*) on the plus (above) and minus (below) strand are represented with exons (black boxes) and introns (thin black lines).

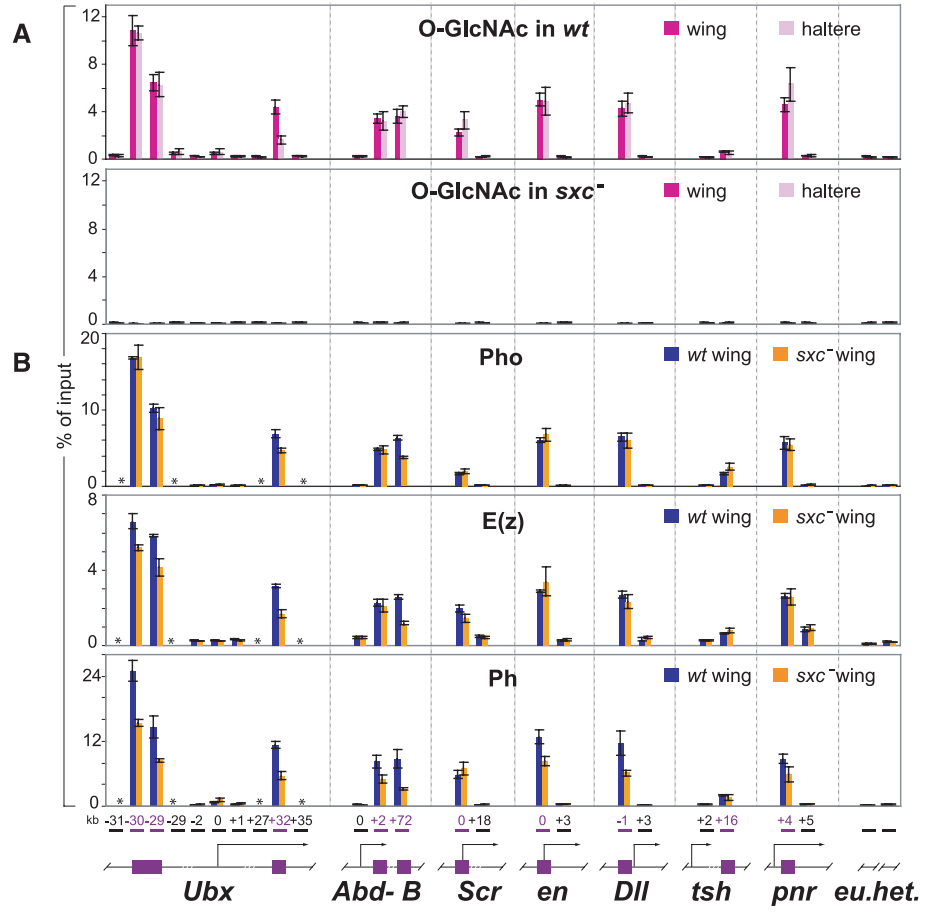

Fig. 3. O-GlcNAc modification and PcG protein binding in wild-type and *sxc* mutant chromatin. (**A**) ChIP analysis monitoring O-GlcNAc modification in wing (magenta) and haltere/third leg (pink) imaginal discs from *wt* and sxc^{7}/sxc^{1} mutant (sxc^{-}) larvae. Graphs show results from independent immunoprecipitation reactions (n = 3 immunoprecipitation reactions) with antibody to O-GlcNAc. ChIP signals, quantified by means of quantitative polymerase chain reaction, are presented as mean percentage of input chromatin precipitated at each region; error bars indicate ±SD (*3*). Locations of PREs (purple boxes) and other regions relative to transcription start sites are indicated in kilobases; euchromatic (*eu.*) and heterochromatic (*het.*) control regions were mapped outside of these genes. In *wt* larvae, GlcNAc ChIP signals at the –30 kb *Ubx* PRE were comparable in wing and haltere/third leg chromatin, but at the +32kb PRE the signal in haltere/third-leg chromatin was two- to threefold lower than in wing chromatin, paralleling PRC1 and PRC2 binding (*14*). (**B**) ChIP signals in WT (blue bars) and sxc^{-} wing discs (orange bars) representing Pho, E(z), and Ph binding.

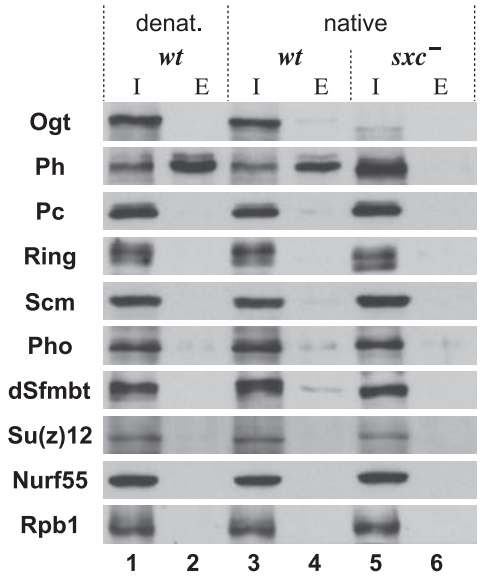

Fig. 4. Sxc/Ogt glycosylates Ph in *Drosophila*. Extracts of wild-type (WT) or sxc^{1}/sxc^{7} (sxc^{-}) mutant larvae were subjected to affinity-purification with WGA-agarose under native or denaturing (denat.) conditions (*3*) and probed with antibodies to PRC1 subunits Ph, Pc, Ring, and Scm; PhoRC subunits dSfmbt and Pho; PRC2 subunits Su(z)12 and Nurf55; the large RNA polymerase II subunit Rpb1; and Ogt. "I" indicates 0.5% of input extract and "E" indicates 10% of affinity-purified material. Ph, but none of the other proteins, is strongly enriched in WGA affinity–purified material (lanes 2 and 4); no enrichment of any protein is seen in material purified from *sxc* mutant larvae (lane 6). Weak enrichment of dSfmbt under native (lane 4) but not denaturing conditions (lane 2) probably reflects association with GlcNAc-modified Ph. Levels of Ph are increased in *sxc* mutant larvae as compared with those in WT larvae (compare lane 5 with lanes 1 and 3), possibly reflecting a failure to downregulate Ph expression by the PcG system through PREs in the Ph gene (*23*).

mice, in which it is required for the viability of embryonic stem cells (*17*, *18*), but dispensable for the normal development of *Caenorhabditis elegans* (*19*). In contrast, *Drosophila* mutants lacking Sxc/Ogt and O-GlcNAcylation display a specific phenotype: loss of Polycomb repression. *sxc* mutants show no other obvious developmental defects, suggesting that PcG repression is the main process that critically depends on O-GlcNAcylation in *Drosophila*. We provide evidence that Ph is GlcNAcylated. Although it remains to be determined whether Ph is indeed the relevant Sxc/Ogt substrate in PcG repression, it is tempting to speculate that the function of Sxc/Ogt in gene silencing may be to GlcNAcylate Ph. The *sxc* null phenotype is not as severe as that of other PcG mutants, notably that of *ph* [(*1*, *20*, *21*) and this study]. Thus, if GlcNAcylation of Ph contributes to its function, Ph still retains partial repressor activity in the absence of this modification. One possibility would be that GlcNAcylation of Ph is needed for efficient anchoring of Ph to PREs and/or for the capacity of PRE-tethered Ph to maintain a repressed chromatin state at target genes.

All *Drosophila* PcG proteins are conserved in vertebrates, and the PcG system represses a large set of orthologous developmental regulator genes both during *Drosophila* development and in mammalian embryonic stem cells (*13*, *22*). Thus, GlcNAcylation of Polyhomeotic homologs, or perhaps other PcG proteins, may also be an evolutionary ancient and essential function of Ogt in vertebrates.

References and Notes

1. P. W. Ingham, *Cell* **37**, 815 (1984).
2. P. W. Ingham, *Cold Spring Harb. Symp. Quant. Biol.* **50**, 201 (1985).
3. Materials and methods are available as supporting material on *Science* Online.
4. D. C. Love, J. A. Hanover, *Sci. STKE* **312**, re13 (2005).
5. G. W. Hart, M. P. Housley, C. Slawson, *Nature* **446**, 1017 (2007).
6. C. Martinez-Fleites, *Nat. Struct. Mol. Biol.* **15**, 764 (2008).
7. A. J. Clarke *et al.*, *EMBO J.* **27**, 2780 (2008).
8. L. I. Davis, G. Blobel, *Cell* **45**, 699 (1986).
9. G. D. Holt, G. W. Hart, *J. Biol. Chem.* **261**, 8049 (1986).
10. W. G. Kelly, G. W. Hart, *Cell* **57**, 243 (1989).
11. J. R. Turner, A. M. Tartakoff, N. S. Greenspan, *Proc. Natl. Acad. Sci. U.S.A.* **87**, 5608 (1990).
12. H. Ji, W. H. Wong, *Bioinformatics* **21**, 3629 (2005).
13. K. Oktaba *et al.*, *Dev. Cell* **15**, 877 (2008).
14. B. Papp, J. Müller, *Genes Dev.* **20**, 2041 (2006).
15. J. Müller, C. P. Verrijzer, *Curr. Opin. Genet. Dev.* **19**, 150 (2009).
16. W. G. Kelly, M. H. Dahmus, G. W. Hart, *J. Biol. Chem.* **268**, 10416 (1993).
17. R. Shafi *et al.*, *Proc. Natl. Acad. Sci. U.S.A.* **97**, 5735 (2000).
18. N. O'Donnell *et al.*, *Mol. Cell. Biol.* **24**, 1680 (2004).
19. J. A. Hanover *et al.*, *Proc. Natl. Acad. Sci. U.S.A.* **102**, 11266 (2005).
20. J.-M. Dura *et al.*, *Cell* **51**, 829 (1987).
21. D. Beuchle, G. Struhl, J. Müller, *Development* **128**, 993 (2001).
22. L. A. Boyer *et al.*, *Nature* **441**, 349 (2006).
23. M. O. Fauvarque, V. Zuber, J. M. Dura, *Mech. Dev.* **52**, 343 (1995).

24. We thank C. Fritsch and B. Papp for initial efforts to map *sxc*; M. Nekrasov, A. Nowak, and N. Ly-Hartig for raising E(z), Nurf55, and Scm antibodies, respectively; R. Matos and A. Gaytan for reagents; J. deGraaf and V. Benes (of the EMBL Genomics Core Facility) for technical support; and J. Gagneur, C. Girardot, B. Honda, P. Ingham, and K. Osborne for discussions. Comments from E. Conti helped to improve the manuscript. The authors are supported by EMBL and by grants from the Deutsche Forschungsgemeinschaft. The microarray data have been deposited in the ArrayExpress database under the accession number E-TABM-697.

Supporting Online Material

www.sciencemag.org/cgi/content/full/1169727/DC1
Materials and Methods
Figs. S1 to S6
Tables S1 and S2
References

12 December 2008; accepted 19 May 2009
Published online 28 May 2009;
10.1126/science.1169727
Include this information when citing this paper.

Ligand-Gated Chloride Channels Are Receptors for Biogenic Amines in *C. elegans*

Niels Ringstad,* Namiko Abe,*† H. Robert Horvitz‡

Biogenic amines such as serotonin and dopamine are intercellular signaling molecules that function widely as neurotransmitters and neuromodulators. We have identified in the nematode *Caenorhabditis elegans* three ligand-gated chloride channels that are receptors for biogenic amines: LGC-53 is a high-affinity dopamine receptor, LGC-55 is a high-affinity tyramine receptor, and LGC-40 is a low-affinity serotonin receptor that is also gated by choline and acetylcholine. *lgc-55* mutants are defective in a behavior that requires endogenous tyramine, which indicates that this ionotropic tyramine receptor functions in tyramine signaling in vivo. Our studies suggest that direct activation of membrane chloride conductances is a general mechanism of action for biogenic amines in the modulation of *C. elegans* behavior.

Biogenic amines function in diverse neuronal circuits as neurotransmitters and neuromodulators. Therapeutics for many psychiatric disorders, including major depression, schizophrenia, and bipolar affective disorder, target signaling pathways of such biogenic amines as serotonin, dopamine, and noradrenaline (*1*). Biogenic amine signaling pathways are also targets of drugs of abuse (*1*). Almost all known biogenic amine receptors are G protein–coupled receptors (GPCRs) that signal though the activation of heterotrimeric guanine nucleotide–binding proteins (G proteins), which activate second-messenger signaling pathways. However, there exists a second type of biogenic amine receptor:

Howard Hughes Medical Institute, Department of Biology, and McGovern Institute for Brain Research, MIT, Cambridge, MA 02139, USA.

*These authors contributed equally to this work.
†Present address: Department of Anatomy and Neurobiology, Washington University School of Medicine, St. Louis, MO 63110, USA.
‡To whom correspondence should be addressed. E-mail: horvitz@mit.edu

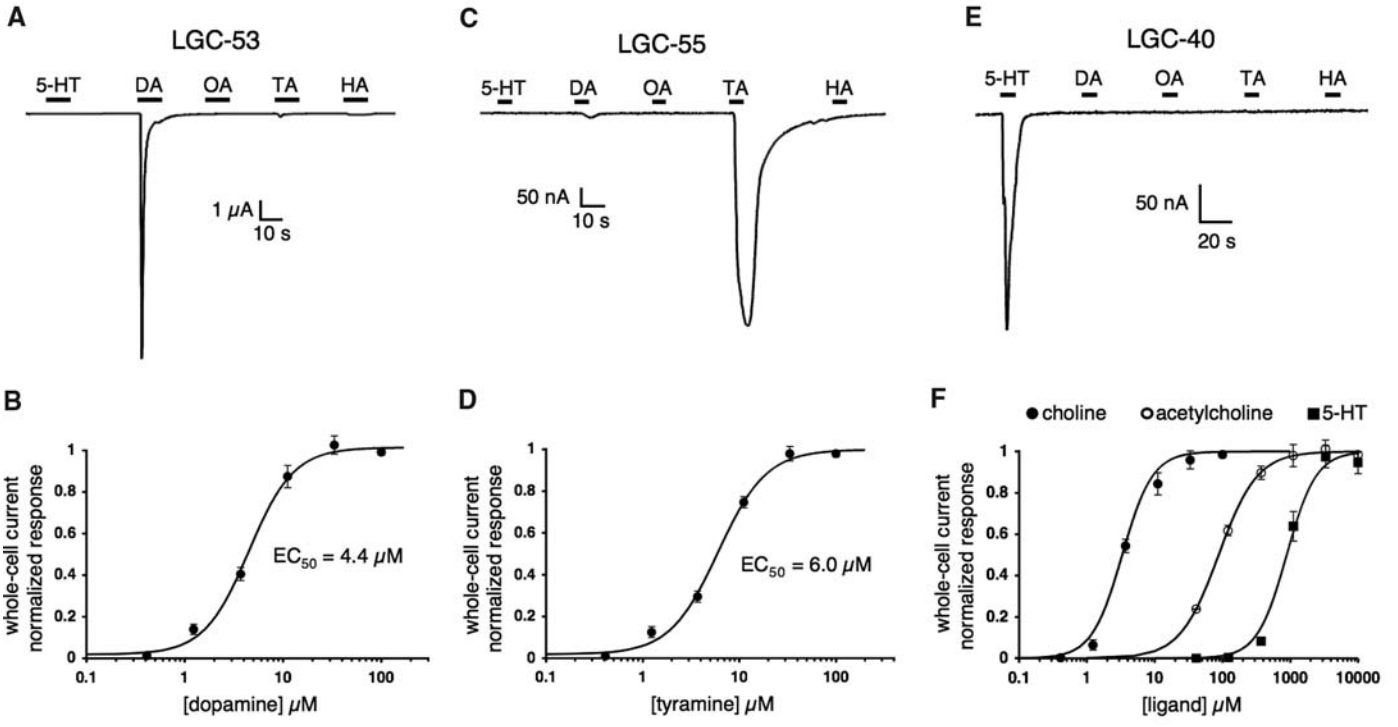

Fig. 1. Biogenic amines evoke currents in *Xenopus* oocytes expressing LGC-53, LGC-55, or LGC-40. (**A**, **C**, and **E**) Whole-cell currents recorded from *Xenopus* oocytes expressing LGC-53, LGC-55, or LGC-40 during application of serotonin (5-HT), dopamine (DA), octopamine (OA), tyramine (TA), and histamine (HA). The concentrations of applied neurotransmitters were 10 μM in (A) and (B) and 100 μM in (C). (**B** and **D**) Dose-response curves for dopamine- and tyramine-evoked currents in *Xenopus* oocytes expressing LGC-53 and LGC-55, respectively. Each point (± SEM) represents the average of three to five recordings. Dose-response data were fitted to the Hill equation and normalized to the maximum amplitude of the current (I_{max}). The EC_{50} of dopamine for LGC-53 was 4.4 μM, and the estimated Hill coefficient was 1.9. The EC_{50} of tyramine for LGC-55 was 6.0 μM, and the estimated Hill coefficient was 1.8. (**F**) Dose-response curves for serotonin-, acetylcholine-, and choline-evoked currents in *Xenopus* oocytes expressing LGC-40. Dose-response data were fitted to the Hill equation and normalized to I_{max}. $n \geq 5$. The EC_{50} of serotonin for LGC-40 was 905 μM, and the estimated Hill coefficient was 2.7. The EC_{50} values of acetylcholine and choline for LGC-40 were 87 μM and 3.4 μM, respectively, and the estimated Hill coefficients were 1.5 and 1.9, respectively.

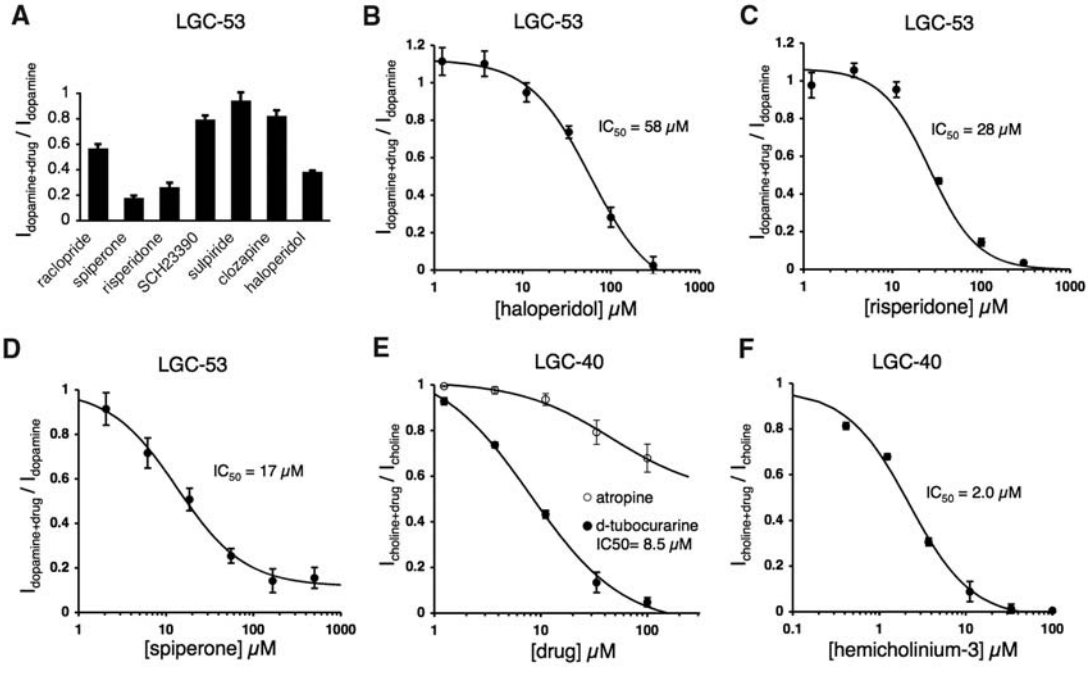

Fig. 2. Pharmacological characterizations of the ionotropic dopamine receptor LGC-53 and the ionotropic choline receptor LGC-40. (**A**) Inhibition of LGC-53 currents by dopamine-receptor antagonists. The mean ratios (± SEM) of the peak currents evoked in the presence and absence of the indicated dopamine receptor antagonist are shown. $n \geq 5$. Drugs were tested at a concentration of 100 μM, and 5 μM dopamine was used to evoke LGC-53 currents. (**B** to **D**) Dose-response curves for the inhibition by haloperidol, risperidone, and spiperone of LGC-53 currents. Dopamine (5 μM) was used to evoke currents in oocytes expressing LGC-53 in the presence of different concentrations of dopamine receptor antagonists. Currents were normalized to the current evoked by 5 μM dopamine in the absence of receptor antagonists. $n \geq 5$. (**E** and **F**) Dose-response curves for the inhibition by atropine, *d*-tubocurarine, and hemicholinium-3 of LGC-40 currents. Currents were evoked by 2 μM choline in oocytes expressing LGC-40 in the presence of different concentrations of compounds. Currents were normalized to the current evoked by 2 μM choline in the absence of any compounds. $n \geq 5$.

biogenic amine-gated ion channels. The vertebrate 5-hydroxytryptamine (serotonin) receptor 3A (5-HT_3 receptor) is a serotonin-gated cation channel (*2*, *3*). Two arthropod histamine receptors and the *Caenorhabditis elegans* MOD-1 serotonin receptor are biogenic amine–gated chloride channels (*4*–*8*). These biogenic amine–gated channels from diverse phyla suggest a mechanism of action for their cognate ligands: fast excitation or inhibition analogous to the response to the activation of nicotinic acetylcholine receptors or to the activation of γ-aminobutyric acid type A ($GABA_A$) receptors, respectively. We report that such a mechanism of action for biogenic amines is more general: a single species, *C. elegans*, expresses multiple ion channels gated by biogenic amines.

The known biogenic amine–gated ion channels are members of the Cys-loop family of ion channels. Using database searches of proteins encoded by the *C. elegans* genome, we identified 26 presumptive Cys-loop family ion channels that are highly similar to the MOD-1 serotonin-gated chloride channel (*9*) [E values reported by the BLAST algorithm range from 10^{-35} to 10^{-94} (table S1)]; 23 have sequences in their pore-forming M2 transmembrane domains, predicted to confer chloride selectivity (*10*). We expressed these 26 receptors individually in *Xenopus laevis* oocytes and tested them for receptor activity using a two-electrode voltage clamp to monitor whole-cell currents evoked by application of a panel of agonists, including the biogenic amines serotonin, dopamine, octopamine, tyramine, and histamine (*11*). We identified three genes that encode ion channels activated by biogenic amines: *lgc-40*, *lgc-53*, and *lgc-55*. LGC-53 was activated with the highest efficacy by dopamine (Fig. 1A), with a median effective concentration (EC_{50}) of 4.4 μM (Fig. 1B). LGC-55 was activated with the highest efficacy by tyramine with an EC_{50} of 6.0 μM (Fig. 1, C and D). LGC-40 was activated only by high concentrations of serotonin (EC_{50} = 905 μM) (Fig. 1, E and F). We tested whether other potential ligands could be more effective and found that choline and acetylcholine gated LGC-40 at lower concentrations (choline EC_{50} = 3.4 μM, acetylcholine EC_{50} = 87 μM) (Fig. 1F) (*12*). Compounds that block ion channels endogenous to *Xenopus* oocytes failed to block agonist-evoked whole-cell currents in oocytes expressing LGC-40, LGC-53, and LGC-55, which indicates that such endogenous channels do not mediate the agonist-evoked currents (fig. S1).

Ligand binding by Cys-loop family ion channels is mediated by the amino-terminal extracellular domains of channel subunits (*13*). We aligned the extracellular domain sequences of LGC-40, LGC-53, and LGC-55 with those of MOD-1 and 5-HT_3 receptor subunits and of other Cys-loop family receptors, but did not identify any amino acids that were conserved specifically among amine-gated channels (fig. S2).

All previously characterized dopamine receptors are GPCRs (*1*). We tested whether antagonists of G protein–coupled dopamine receptors can inhibit the LGC-53 dopamine-gated ion channel. Of seven antagonists tested (Fig. 2A), three acted with a median inhibitory concentration (IC_{50}) of less than 100 μM: risperidone (IC_{50} = 40 μM), haloperidol (IC_{50} = 32 μM), and spiperone (IC_{50} = 38 μM) (Fig. 2, B to D) (*11*). Risperidone, haloperidol, and spiperone all are in clinical use as antipsychotics (*1*). Because these drugs also block LGC-53, we suggest that some of their actions as therapeutics might be through inhibition of a yet-to-be-identified human dopamine receptor that, like LGC-53, is composed of Cys-loop family channel subunits.

We tested *d*-tubocurarine and atropine, antagonists of ionotropic and G protein–coupled acetylcholine receptors, respectively (*1*), and hemicholinium-3, a blocker of the high-affinity choline transporter (*14*), for effects on choline-evoked currents in oocytes expressing LGC-40

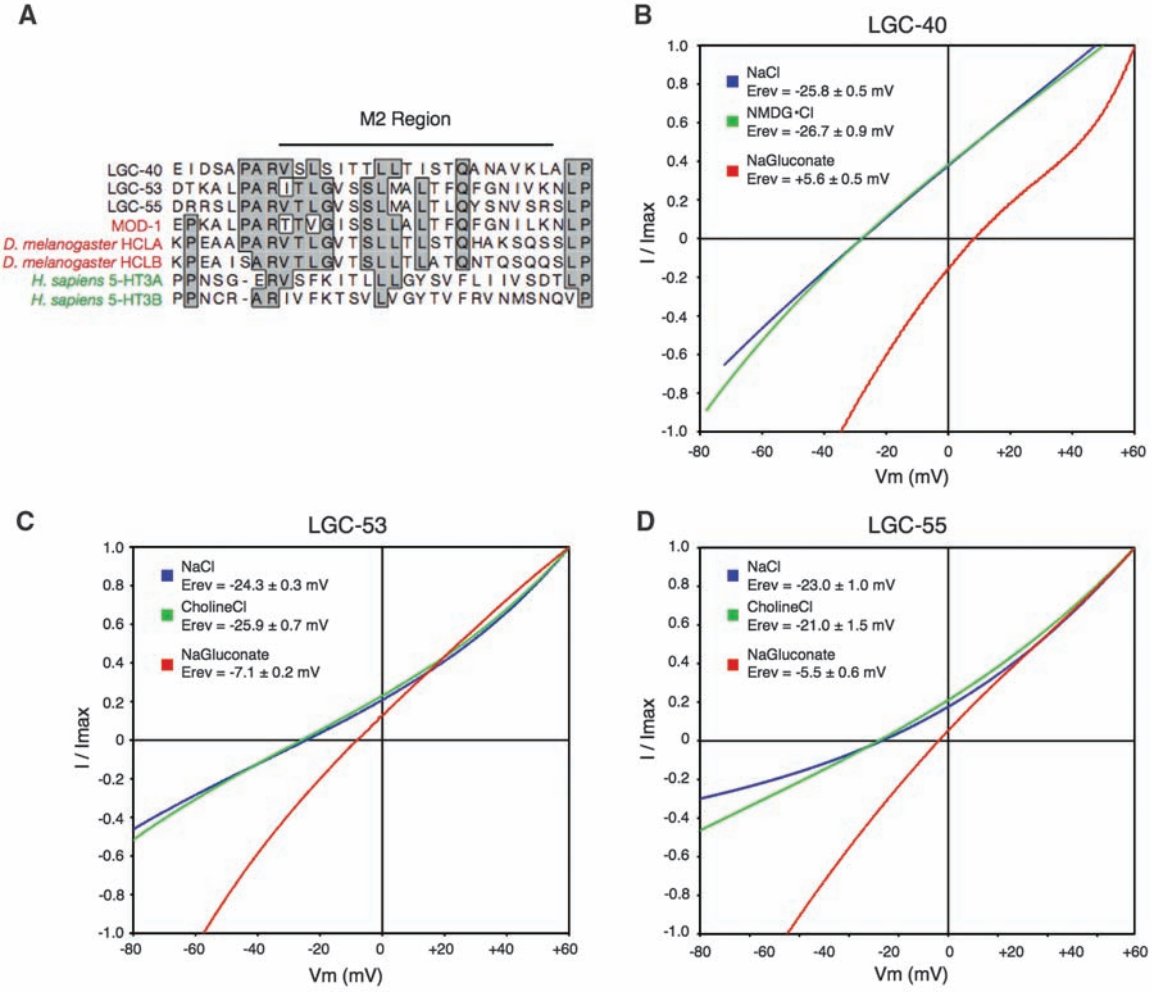

Fig. 3. LGC-40, LGC-53, and LGC-55 are chloride channels. (**A**) Alignment of sequences from the presumptive M2 region of amine-gated ion channels, which determines ion selectivity of Cys-loop family ion channels (*10*, *13*, *29*). Cation-selective 5-HT_3 receptor subunits are labeled in green, and anion-selective MOD-1, HCLA, and HCLB subunits are labeled in red. (**B** to **D**) Current-voltage relations (*I-V* curves) of LGC-40, LGC-53, and LGC-55 in ND96 medium (which contains 96 mM sodium and 104 mM chloride), sodium-free medium (0 mM sodium and 104 mM chloride), or low-chloride medium (96 mM sodium and 8 mM chloride). The mean reversal potential ± SEM from four to five experiments under each condition is shown.

(Fig. 2, F and G). LGC-40 currents were blocked by low concentrations of *d*-tubocurarine (IC_{50} = 8.3 μM) but were relatively insensitive to atropine (Fig. 2F). Hemicholinium-3 was the most effective antagonist of the LGC-40 channel, with an IC_{50} of 2.0 μM (Fig. 2G). Thus, LGC-40 is sensitive to both a canonical antagonist of acetylcholine-gated ion channels and an inhibitor of the high-affinity choline transporter.

The presumptive M2 regions, which are predicted to determine the ion selectivity of Cys-loop family ion channels, of LGC-40, LGC-53, and LGC-55 are more similar to the M2 regions of known chloride channels than to those of known cation channels (Fig. 3A) (*10*, *13*). To test whether these receptors are chloride channels, we measured the reversal potentials of agonist-evoked currents in *Xenopus* oocytes expressing LGC-40, LGC-53, and LGC-55 (Fig. 3, B through D). In solutions containing 96 mM Na^+ and 104 mM Cl^-, ligand-evoked currents reversed at –23 to –26 mV, close to the reversal potential for chloride in *Xenopus* oocytes (*15*). Replacement of sodium ions with *N*-methyl-D-gluconate (NMDG) or choline did not alter the reversal potentials of the evoked currents. Replacement of chloride ions with gluconate shifted the reversal potentials positively by 17 to 31 mV (Fig. 3, B to D) (*16*). These data indicate that LGC-40, LGC-53, and LGC-55 are chloride channels. The observed shift in reversal potential was less than predicted for channels that are perfectly selective for chloride over other anions (our unpublished observations); perhaps these channels might also pass the anions we used to replace chloride.

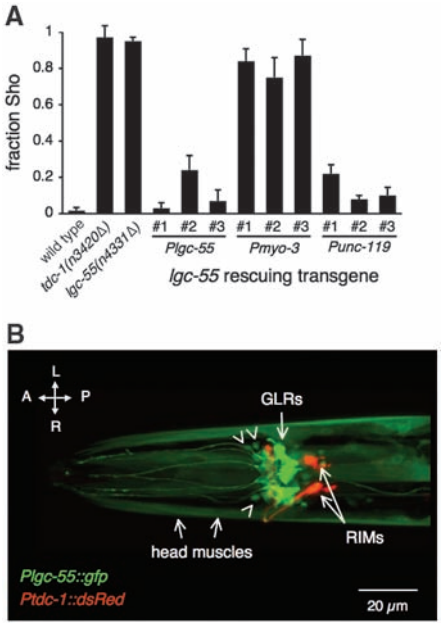

Fig. 4. LGC-55 is required for the tyraminergic modulation of head movements by *C. elegans* and is expressed in the GLR glia-like cells and head muscles. (**A**) The fractions of animals that have the Sho phenotype and cannot suppress head oscillations are plotted for the wild type, *tdc-1* and *lgc-55* mutants, and *lgc-55* mutants carrying rescuing transgenes that express the *lgc-55* cDNA using its own promoter, the pan-neuronal *unc-119* promoter, or the pan-muscle *myo-3* promoter. In each experiment, we tested 20 individuals of each genotype for the Sho phenotype. The mean fraction of animals with the Sho phenotype ± SEM is plotted, $n \geq 3$. Three independent lines (labeled #1 to 3) carrying each transgene were assayed. (**B**) Expression of *lgc-55*. An *lgc-55::gfp* reporter transgene is expressed in the GLR glia-like cells and head muscles (*17*). Arrowheads indicate some of the unidentified head neurons that express the reporter transgene. The tyraminergic RIM neurons, which provide the tyramine that inhibits head movements during reversals, are labeled with a *tdc-1::dsRed* reporter transgene.

To identify biological functions of these amine-gated chloride channels, we isolated *lgc-40*, *lgc-53*, and *lgc-55* deletion mutants (fig. S3). *lgc-55* mutants, which lack the tyramine-gated chloride channel, had a behavioral defect that indicates an in vivo function for this receptor in tyraminergic signaling. Tyramine from the RIM motor neurons suppresses small rapid head movements during touch-evoked locomotory reversals (*17*). (RIM neurons are a pair of inter–motor neurons that innervate muscles in the head via neuromuscular junctions in the nerve ring.) Animals lacking endogenous tyramine fail to suppress these head oscillations and exhibit the Sho phenotype (suppression of head oscillations–defective), as do animals lacking the tyraminergic RIM motor neurons (*17*) (Fig. 4A). Similarly, *lgc-55* mutants continued to execute head movements during touch-evoked reversals (Fig. 4A). The Sho phenotype of *lgc-55* mutants was rescued by transgenes containing the *lgc-55* cDNA fused to *lgc-55* promoter sequences and by transgenes containing the *lgc-55* cDNA fused to the *unc-119* promoter, which drives expression broadly in the nervous system (*18*). To identify cells that express LGC-55, we created transgenic animals expressing green fluorescent protein under the control of the *lgc-55* promoter (*18*). We observed expression of this reporter transgene in head muscles and in the glia-like GLR cells, which are connected to the head muscles by gap junctions (*19*), and weaker expression in many unidentified head neurons (Fig. 4B). We also observed strong expression in the ALM and AVM mechanosensory neurons (not shown). Expression of *lgc-55* in muscles, including head muscles, did not rescue the Sho phenotype of *lgc-55* mutants (Fig. 4A). Our findings suggest that LGC-55 can act in the GLR cells or neurons to control head movements and establish that the LGC-55 tyramine receptor functions in vivo in the tyraminergic control of head movements. No behavioral abnormalities were detected in mutants that carry deletions in *lgc-40* and *lgc-53* (*20*).

We conclude that, including MOD-1, there exist in *C. elegans* at least four ligand-gated chloride channels that can be activated by biogenic amines. Our results indicate that ligand-gated chloride channels constitute a class of receptor for biogenic amines and that direct activation of membrane chloride conductances is a general mechanism of biogenic amine action in *C. elegans*. Biogenic amine–gated chloride channels might exist in the nervous systems of animals other than *C. elegans* and arthropods. In mollusks, synaptic dopamine rapidly activates a chloride conductance that is blocked by picrotoxin, an antagonist of ligand-gated chloride channels (*21*–*24*). In the mammalian brain, histaminergic neurons project to the hypothalamus and use rapid inhibitory synaptic signals that (i) are not mediated by G protein signaling, (ii) are picrotoxin-sensitive, and (iii) are mediated by chloride conductances (*25*). The molecular identity of the histamine receptor in this synapse is not known, but the recent demonstration that $GABA_A$ receptor subunits can form histamine-gated chloride channels in vitro suggests that an ionotropic histamine receptor might contain known ligand-gated chloride channel subunits (*26*). If direct activation of ligand-gated chloride channels is a mechanism of biogenic amine action in the mammalian brain, such receptors might be therapeutic targets, given the many links between aminergic signaling and psychiatric disorders (*1*, *27*).

References and Notes

1. J. R. Cooper, F. E. Bloom, R. H. Roth, *The Biochemical Basis of Neuropharmacology* (Oxford Univ. Press, New York, ed. 8, 2003).
2. V. Derkach, A. Suprenant, R. A. North, *Nature* **339**, 706 (1989).
3. A. V. Maricq, A. S. Peterson, A. J. Brake, D. Julius, *Science* **254**, 432 (1991).
4. R. C. Hardie, *Nature* **339**, 704 (1989).
5. G. Gisselmann, H. Pusch, B. T. Hovemann, H. Hatt, *Nat. Neurosci.* **5**, 11 (2002).
6. Y. Zheng *et al.*, *J. Biol. Chem.* **277**, 2000 (2002).
7. C. Gengs *et al.*, *J. Biol. Chem.* **277**, 42113 (2002).
8. R. Ranganathan, S. Cannon, H. R. Horvitz, *Nature* **408**, 470 (2000).
9. Materials and methods are available as supporting material on *Science* Online.
10. M. J. Gunthorpe, S. C. Lumis, *J. Biol. Chem.* **276**, 10977 (2001).
11. Descriptions of how we expressed *lgc-40, lgc-53*, and *lgc-55* in *Xenopus laevis* oocytes are in (*9*). We recorded whole-cell currents using a two-electrode voltage clamp (Warner Instruments). The ground electrode was connected to the recording chamber (Warner Instruments model RC-3Z) using an agar bridge. Data were acquired with Clampex 8.0 (Molecular Devices) and analyzed offline with Clampfit (Molecular Devices). Oocyte membrane potential was held at –60 mV for all experiments. To identify new Cys-loop family biogenic amine receptors, oocytes expressing candidate channels were sequentially superfused with ND96 (96 mM NaCl, 2.5 mM KCl, 1 mM $MgCl_2$, 1.8 mM $CaCl_2$, and 5 mM Hepes, pH 7.6) containing GABA (100 μM), glycine (100 μM), glutamate (100 μM), histamine (100 μM), serotonin (1 mM), dopamine (100 μM), octopamine (100 μM), or tyramine (100 μM). Candidate receptors not activated by these ligands were also tested with ivermectin (10 μM), which can activate many ligand-gated chloride channels (*28*).
12. The following compounds were tested for LGC-40 agonist activity: *N*-acetyl 5-hydroxytryptamine, adenosine, adenosine triphosphate, carnosine, epinephrine, FLRFamide (FLFR is Phe-Leu-Arg-Phe-NH_2) (*29*), FMRFamide, 5-hydroxytryptophan, homocarnosine, melatonin, methoxytyramine, norepinephrine, *O*-methyl

5-hydroxytryptamine, *o*-methoxylphenylethylamine, phenylethylamine, tryptamine. All chemicals were purchased from Sigma and tested at 1 mM concentrations, except for the FLRFamide and FMRFamide peptides, which were tested at 10 μM.
13. C. N. Connolly, K. A. Wafford, *Biochem. Soc. Trans.* **32**, 529 (2004).
14. T. Okuda *et al*., *Nat. Neurosci.* **3**, 120 (2000).
15. K. Kusano, R. Miledi, J. Stinnakre, *J. Physiol.* **328**, 143 (1982).
16. For ion replacement experiments, oocytes expressing LGC-40, LGC-53, or LGC-55 were held at a resting potential of −90 mV. LGC-40, LGC-53, or LGC-55 currents were evoked with 2 μM choline, 5 μM dopamine, and 5 μM tyramine, respectively, in ND96 medium, sodium-free medium (96 mM cholineCl or NMDG-Cl replacing NaCl) or low-chloride medium (96 mM NaGluconate replacing NaCl). After 5 s, a voltage ramp of 20 mV/s from −90 mV to +60 mV was applied. Currents from voltage ramps recorded in the absence of ligands were subtracted from these current traces.
17. M. J. Alkema, M. Hunter-Ensor, N. Ringstad, H. R. Horvitz, *Neuron* **46**, 247 (2005).
18. Descriptions of *lgc-55* rescuing transgenes and the *lgc-55* reporter transgene are in (*9*).
19. J. White, E. Southgate, J. N. Thompson, S. Brenner, *Philos. Trans. R. Soc. London B Biol. Sci.* **314**, 1 (1986).
20. *lgc-40* and *lgc-53* mutants were grossly normal in locomotion, egg laying, defecation, and pharyngeal pumping. We also tested *lgc-53* mutants for defects in slowing in response to detection of a bacterial food source and for resistance to exogenous dopamine in locomotion and egg-laying assays. For experimental details, see (*9*).
21. K. A. Green, G. A. Cottrell, *Pfluegers Arch.* **434**, 313 (1997).
22. N. S. Magoski, A. G. M. Bulloch, *J. Neurophysiol.* **81**, 1330 (1999).
23. T. I. Webb, J. W. Lynch, *Curr. Pharm. Des.* **13**, 2350 (2007).
24. And references in ref. (*27*).
25. G. I. Hatton, Q. Z. Yang, *J. Neurosci.* **21**, 2974 (2001).
26. A. Saras *et al*., *J. Biol. Chem.* **283**, 10470 (2008).
27. L. H. Tecott, S. L. Smart, in *Comprehensive Textbook of Psychiatry*, B. J. Sadock, V. A. Sadock, Eds. (Lippincott, Williams & Wilkins, New York, ed. 8, 2003), pp. 49–60.
28. Q. Shan, J. L. Haddrill, J. W. Lynch, *J. Biol. Chem.* **276**, 12556 (2001).
29. Single-letter abbreviations for the amino acid residues are as follows: A, Ala; C, Cys; D, Asp; E, Glu; F, Phe; G, Gly; H, His; I, Ile; K, Lys; L, Leu; M, Met; N, Asn; P, Pro; Q, Gln; R, Arg; S, Ser; T, Thr; V, Val; W, Trp; and Y, Tyr.
30. We thank Y. Kohara for *lgc-40*, *lgc-53*, and *lgc-55* cDNA clones, A. Fire for expression vectors, R. O'Hagan for help with electrophysiology, A. Hellman for deletion screening, M. Alkema for discussions, J. Kehoe for bringing to our attention reports of dopamine-activated chloride conductances in mollusks, and D. Denning and B. Galvin for suggestions concerning the manuscript. This work was supported by NIH grant GM24663. N.R. received support from the Howard Hughes Medical Institute, the Life Sciences Research Foundation and The Medical Foundation. H.R.H. is an Investigator of the Howard Hughes Medical Institute.

Supporting Online Material

www.sciencemag.org/cgi/content/full/325/5936/96/DC1
Materials and Methods
Figs. S1 to S3
Table S1
References

2 December 2008; accepted 20 April 2009
10.1126/science.1169243

LXR Regulates Cholesterol Uptake Through Idol-Dependent Ubiquitination of the LDL Receptor

Noam Zelcer,* Cynthia Hong, Rima Boyadjian, Peter Tontonoz†

Cellular cholesterol levels reflect a balance between uptake, efflux, and endogenous synthesis. Here we show that the sterol-responsive nuclear liver X receptor (LXR) helps maintain cholesterol homeostasis, not only through promotion of cholesterol efflux but also through suppression of low-density lipoprotein (LDL) uptake. LXR inhibits the LDL receptor (LDLR) pathway through transcriptional induction of Idol (inducible degrader of the LDLR), an E3 ubiquitin ligase that triggers ubiquitination of the LDLR on its cytoplasmic domain, thereby targeting it for degradation. LXR ligand reduces, whereas LXR knockout increases, LDLR protein levels in vivo in a tissue-selective manner. Idol knockdown in hepatocytes increases LDLR protein levels and promotes LDL uptake. Conversely, adenovirus-mediated expression of Idol in mouse liver promotes LDLR degradation and elevates plasma LDL levels. The LXR-Idol-LDLR axis defines a complementary pathway to sterol response element–binding proteins for sterol regulation of cholesterol uptake.

The low-density lipoprotein (LDL) receptor (LDLR) is central to the maintenance of plasma cholesterol levels (*1*). Mutations in this receptor are the leading cause of autosomal dominant hypercholesterolemia, characterized by elevated plasma cholesterol levels, and increased risk of cardiovascular disease (*2*, *3*). In line with its pivotal role in cholesterol homeostasis, expression of the LDLR is tightly regulated. Transcription of the *LDLR* gene is coupled to cellular cholesterol levels through the action of the sterol response element–binding protein (SREBP) transcription factors (*4*, *5*). Enhanced processing of SREBPs to their mature forms when cellular sterol levels decline leads to increased *LDLR* transcription (*6*). Posttranscriptional regulation of LDLR expression is also a major determinant of lipoprotein metabolism. Genetic studies have identified mutations in the genes encoding the LDLR adaptor protein 1 (*LDLRAP1/ARH*) (*7*, *8*) and the SREBP target gene proprotein convertase subtilisin/kexin 9 (*PCSK9*) that result in altered stability, endocytosis, or trafficking of the LDLR (*9*–*13*).

The liver X receptors (LXRs) are also important transcriptional regulators of cholesterol metabolism. LXRα (NR1H3) and LXRβ (NR1H2) are sterol-dependent nuclear receptors activated in response to cellular cholesterol excess (*14*). LXR target genes such as *ABCA1* and *ABCG1* promote the efflux of cellular cholesterol and help to maintain whole-body sterol homeostasis (*15*, *16*). Mice lacking LXRs accumulate sterols in their tissues and manifest accelerated atherosclerosis, whereas synthetic LXR agonists promote reverse cholesterol transport and protect mice against atherosclerosis (*17*–*19*). The coordinated regulation of intracellular sterol levels by the LXR and SREBP signaling pathways led us to investigate whether LXRs control the uptake as well as efflux of cholesterol.

We initially tested the ability of LXRs to modulate LDL uptake in HepG2 human liver cells and primary mouse macrophages (*20*). Treatment with synthetic LXR ligand (GW3965 or T1317) decreased binding and uptake of boron-dipyrromethene (BODIPY)-labeled LDL (Fig. 1A). The LXR ligands modestly induced changes in LDLR mRNA expression (fig. S1A); however, they decreased LDLR protein levels rapidly and in a dose-dependent manner, and this effect was independent of cellular sterol levels (Fig. 1, B to D). Levels of ABCA1 protein, an established target of LXR, were reciprocally increased by LXR ligands (Fig. 1, B to D). LXR ligands had no effect on LDLR levels in macrophages or mouse embryonic fibroblasts (MEFs) lacking LXRα and LXRβ (Fig. 1E and fig. S1B). LXR activation also decreased LDLR protein but not mRNA levels in human SV589 fibroblasts (fig. S1, C and D) (*21*).

To investigate the link between endogenous LXR ligands and LDLR expression, we used an adenovirus vector encoding oxysterol sulfotransferase (Sult2b1) (*22*, *23*). Depletion of oxysterol agonists by Sult2b1 in SV589 cells led to increased LDLR protein, and this effect was reversed by synthetic ligand (fig. S1E). We further tested the effect of LXR agonists on LDLR produced from a transfected vector (i.e., not subject to endogenous SREBP regulation). In HepG2 cells stably expressing an LDLR–green fluorescent protein (GFP) fusion protein, LDLR-GFP expression was localized primarily on the plasma membrane (Fig. 1F). Ligand activation of LXR decreased LDLR-GFP

Howard Hughes Medical Institute and Department of Pathology and Laboratory Medicine, University of California, Los Angeles (UCLA), Los Angeles, CA 90095, USA.

*Present address: Division of Biopharmaceutics, Leiden/Amsterdam Center for Drug Research, Gorlaeus Laboratories, Leiden University, P.O. Box 9502, 2300RA Leiden, Netherlands.
†To whom correspondence should be addressed. E-mail: ptontonoz@mednet.ucla.edu

levels and redistributed the protein from the plasma membrane to intracellular compartments.

To investigate the mechanism by which LXR affects the LDLR, we examined LXR target genes by transcriptional profiling. We identified a potential mediator, denoted on our array as 9430057C20Rik (table S1), that corresponds to a protein originally identified on the basis of its interaction with myosin regulatory light chain (*24*). We propose that this protein, which has been variably referred to as Mir and Mylip, be renamed Idol (for inducible degrader of the LDLR) to reflect its biologic function. Idol contains a band 4.1 and Ezrin/Radixin/Moesin homology (FERM) domain that mediates interactions with cytoplasmic domains of transmembrane proteins (*25*, *26*). Unique among FERM domain-containing proteins, Idol also contains a C-terminal RING domain and has been proposed to act as an E3 ubiquitin ligase, although its biological substrate(s) have not been identified (*24*, *27*). *Idol* mRNA is widely expressed in mice in vivo (fig. S2A). Exposure of cells to increasing concentrations of LDL induced the expression of both *Idol* and *Abca1* mRNA, indicating that their expression is responsive to extracellular cholesterol levels (fig. S2B). Furthermore, LXR agonists induced *Idol* expression in multiple cells in an LXR-dependent manner, including primary hepatocytes, primary macrophages, MEFs, and HepG2 cells (Fig. 2A and fig. S2, C to E). Treatment of mice with GW3965 induced expression of *Idol* in multiple tissues, including the spleen, intestine, and adrenals (Fig. 2B). Only modest regulation of Idol by LXR agonist was observed in liver, consistent with the degree of *Abca1* regulation (fig. S2F). Idol mRNA levels were also substantially decreased in the spleen and liver of *Lxr*$\alpha\beta^{-/-}$ mice compared with those of wild-type (WT) controls (fig. S2G).

LXR regulation of *Idol* was not sensitive to cycloheximide, suggesting that it was a direct transcriptional effect (fig. S3A). It was not secondary to induction of SREBP-1c, because oxysterols that block SREBP processing still induced *Idol* expression (fig. S3B). LXRs activate target genes by binding to consensus elements (LXREs) in their promoters. We identified an LXRE ~2.5 kilobases upstream of the mouse *Idol* translation start site (fig. S3C) and generated a reporter construct encompassing this region. Activation by LXRα and GW3965 resulted in a roughly fourfold increase in reporter activity that was largely abolished in the absence of a functional LXRE (fig. S3D). Electromobility shift analysis showed that LXR/RXR bound to WT but not mutant versions of the Idol LXRE (fig. S3E).

Given that Idol is a putative E3 ubiquitin ligase, we hypothesized that Idol induction might underlie the ability of LXRs to regulate LDLR abundance. Using a cotransfection system in human embryonic kidney (HEK) 293T cells, we found that Idol expression redistributed LDLR-GFP from the plasma membrane to an intracellular compartment (Fig. 2C) and reduced the level of LDLR-GFP protein in a dose-dependent manner (Fig. 2D). Even levels of Idol protein too low to be detected by our antibody were effective. In contrast, Idol carrying a point mutation [$Cys^{387} \rightarrow Ala^{387}$ (C387A)] in the catalytic RING domain (*27*) had no effect on the LDLR (Fig. 2C and fig. S4A). Idol levels are very low, even when driven from an exogenous vector, suggesting that Idol is an unstable protein. In support of this idea, Idol levels were greatly enhanced when the RING domain was mutated, raising the possibility that Idol might catalyze its own degradation (fig. S4A).

The effect of Idol on membrane proteins appears to be selective for the LDLR. Levels of transfected LRP1-GFP or β-amyloid precursor protein–GFP proteins, both of which undergo regulated endocytosis similar to the LDLR, were unaffected by Idol expression (fig. S4A). Similarly, Idol did not influence protein levels of ABCA1-GFP, endogenous transferrin receptor, endogenous myosin regulatory light chain, or the LDLR family members Lrp4 and SorLA (fig. S4, A and B). The very closely related family member ApoER2 was marginally affected by Idol. Adenovirus-mediated expression of Idol reduced LDLR protein levels in primary hepatocytes, HepG2 cells, and McR-H7777 rat hepatocytes (Fig. 2E) and also reduced LDL uptake in MEFs and McR-H7777 cells (Fig. 2F).

To explore the role of endogenous Idol in LDLR regulation, we developed short hairpin RNAs (shRNAs) targeting Idol (fig. S5). Idol-specific shRNAs increased LDLR protein levels in MEFs (Fig. 3A) and McR-H7777 cells (Fig. 3B) without affecting *LDLR* or LXR or SREBP2 target mRNAs (Fig. 3C and fig. S5), suggesting that Idol activity is a physiological mechanism for reg-

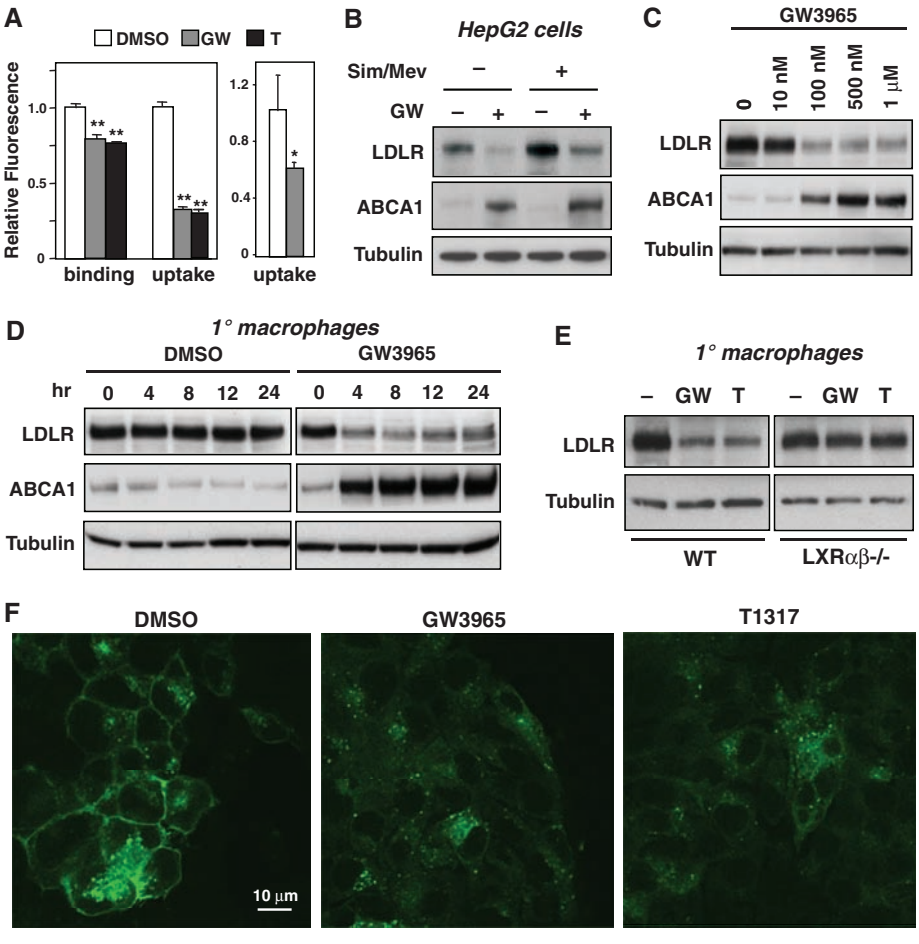

Fig. 1. Activation of LXR inhibits LDL uptake through reduction in LDLR protein expression. (**A**) BODIPY-LDL binding and uptake in HepG2 cells (left) and mouse peritoneal macrophages (right) treated with dimethyl sulfoxide (DMSO) or the synthetic LXR ligands GW3965 (GW) and T0901317 (T) ($n = 6$ animals per group). $^*P < 0.05$; $^{**}P < 0.01$. Error bars in this and all subsequent figures represent the mean ± SD. (**B**) HepG2 cells were pretreated with DMSO or GW (1 μM) for 8 hours and subsequently grown in lipoprotein-deficient serum (LPDS) or in sterol-depletion medium (LPDS supplemented with 5 μM simvastatin and 100 μM mevalonic acid) containing either DMSO or GW for an additional 18 hours. (**C**) Primary mouse peritoneal macrophages were cultured in sterol-depletion medium and treated with indicated doses of GW for 8 hours. (**D**) Peritoneal macrophages were cultured in sterol-depletion medium and treated with GW (1 μM) for the indicated time. (**E**) Peritoneal macrophages from WT or *Lxr*$\alpha\beta^{-/-}$ mice were cultured in sterol-depletion medium and treated with LXR ligands. (**F**) Immunofluorescence images of HepG2 cells stably expressing LDLR-GFP treated with DMSO, GW, or T (1 μM) for 72 hours. All blots are representative of at least three independent experiments.

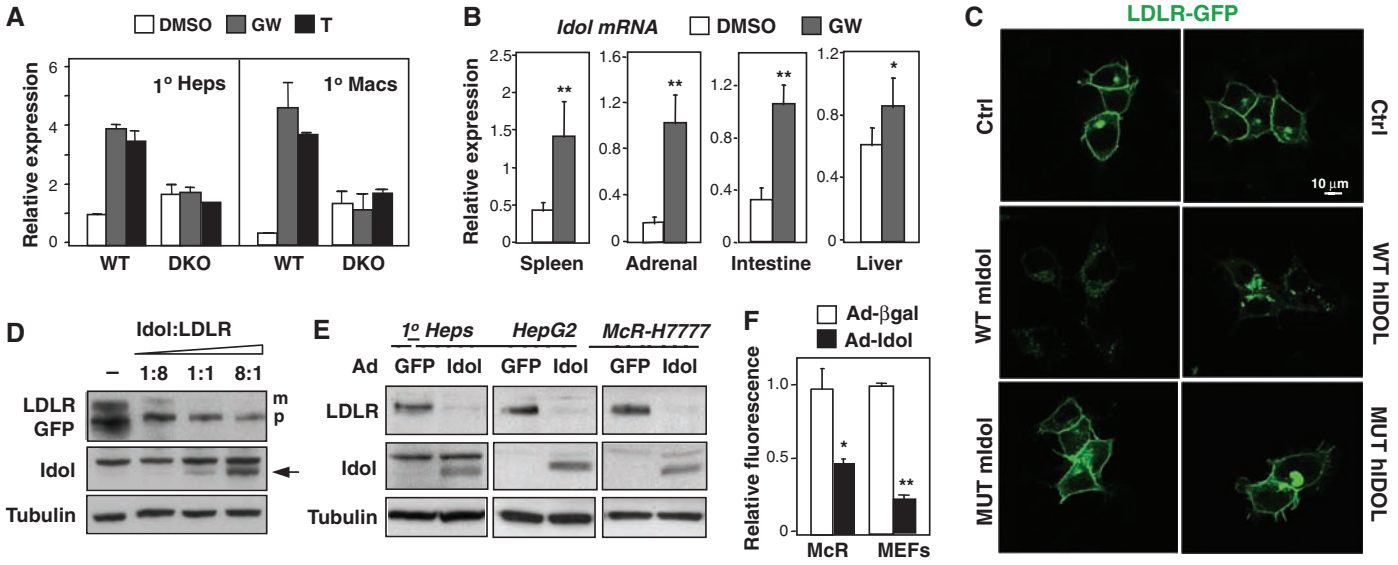

Fig. 2. The LXR target gene Idol is a regulator of LDLR protein levels. (**A**) LXR-dependent regulation of Idol in primary mouse hepatocytes and peritoneal macrophages after treatment with GW or T (1 μM). DKO, LXR double knockout. (**B**) Induction of Idol mRNA expression in tissues of mice treated with 40 mg/kg GW3956 by oral gavage for 3 days (n = 6 per group). Gene expression was measured by real-time PCR. (**C**) Immunofluorescence images of HEK293 cells cotransfected with LDLR-GFP and either WT or RING domain mutant human and mouse Idol. (**D**) Dose-dependent reduction of LDLR-GFP protein in HEK293 cells cotransfected with mIdol and LDLR-GFP expression plasmids. Total cell lysates were analyzed by immunoblotting. Arrow indicates the Idol protein. (**E**) Primary hepatocytes, HepG2 cells, or McR-H7777 cells were cultured in sterol-depletion medium and infected with Ad-GFP or Ad-Idol. Total cell lysates were analyzed by immunoblotting. (**F**) BODIPY-LDL uptake in McR-H777 (McR) cells and LXRα MEFs after infection with Ad-βgal or Ad-Idol (n = 3). All blots are representative of at least three independent experiments. *P < 0.05; **P < 0.01.

ulating LDLR abundance. In support of this idea, Idol-specific shRNAs increased LDL uptake in both fibroblasts (Fig. 3D) and McR-H7777 cells (Fig. 3E). Finally, the ability of an LXR ligand to reduce LDLR protein levels was diminished by Idol shRNA, implicating Idol in LXR-dependent regulation of the LDLR (Fig. 3F).

Pulse-chase labeling studies showed that Idol did not block *LDLR* mRNA translation or appearance of the immature protein, but it completely prevented appearance of the mature glycosylated form (Fig. 4A). Given that mutation of the RING domain inactivates Idol, the most parsimonious explanation for our data is that Idol acts as an E3 ligase to trigger ubiquitination of the LDLR itself, thereby marking it for degradation. We found that ubiquitination of transfected LDLR in 293T cells was dramatically enhanced by expression of active but not mutant Idol (Fig. 4B). Analysis of a series of LDLR receptor mutants that become trapped at various stages of the maturation or recycling pathway revealed that Idol is capable of acting in the endoplasmic reticulum (ER). LDLR [Gly^{546} → Asp^{546} (G546D)], which is unable to exit the ER (*28*), could still be degraded by Idol (Fig. 4C). Treatment of cells with brefeldin A, which blocks protein trafficking out of the ER, did not inhibit ubiquitination of the WT LDLR (fig. S6A) or the G546D mutant (fig. S6B). Treatment with ammonium chloride, a disruptor of lysosomal pH, inhibited LXR-induced endogenous LDLR degradation (fig. S6C). These data suggest that Idol can ubiquitinate the precursor LDLR in the ER and that subsequent trafficking to the lysosome is required for degradation. We also observed LXR ligand-dependent ubiquitination of endogenous LDLR in primary macrophages (Fig. 4D) and Idol-dependent ubiquitination of endogenous LDLR in primary hepatocytes (Fig. 4E). GW3965 triggered LDLR ubiquitination within 4 hours, consistent with the time course of LDLR degradation (Figs. 1D and 4D).

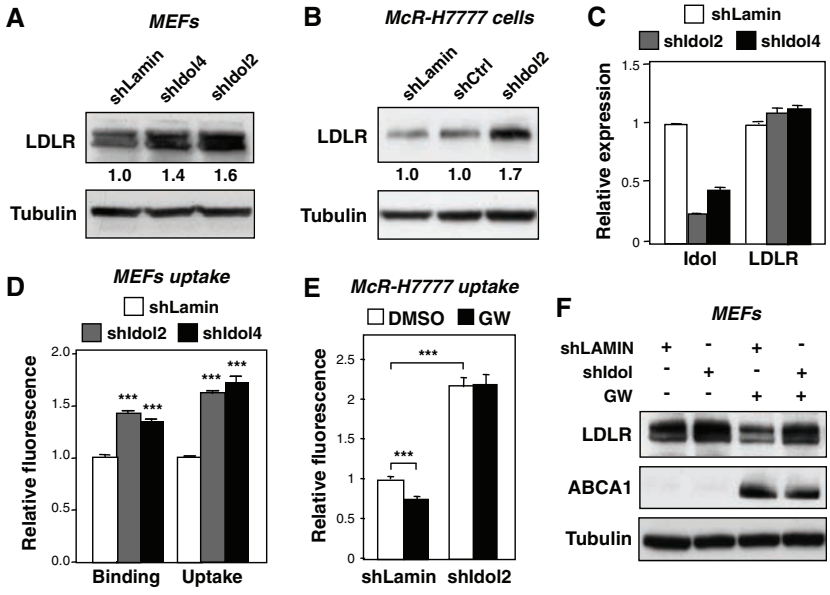

Fig. 3. Idol knockdown induces LDLR protein expression and promotes LDL uptake. (**A**) LXRα MEFs were infected with control (shLamin) or two independent adenoviral Idol shRNA constructs and cultured in sterol-depletion medium. Cell lysates were analyzed by immunoblotting. (**B**) Immunoblot analysis of lysates from McR-H7777 cells treated as in (A). (**C**) Gene expression was analyzed by real-time PCR in LXRα MEFs treated as in (A). (n = 3). (**D**) BODIPY-LDL binding and uptake was determined for LXRα MEFs after infection with Ad-shLAMIN, Ad-shIdol2, or Ad-shIdol4 (n = 3). (**E**) BODIPY-LDL uptake was determined for McR-H7777 cells after infection with Ad-shLAMIN or Ad-shIdol2 followed by treatment with DMSO or GW (1 μM) as indicated (n = 4). (**F**) LXRα MEFs were infected with Ad-shLAMIN or Ad-shIdol2 for 24 hours. Subsequently, cells were treated with DMSO or GW followed by culture in sterol-depletion medium. All blots are representative of at least three independent experiments. ***P < 0.001.

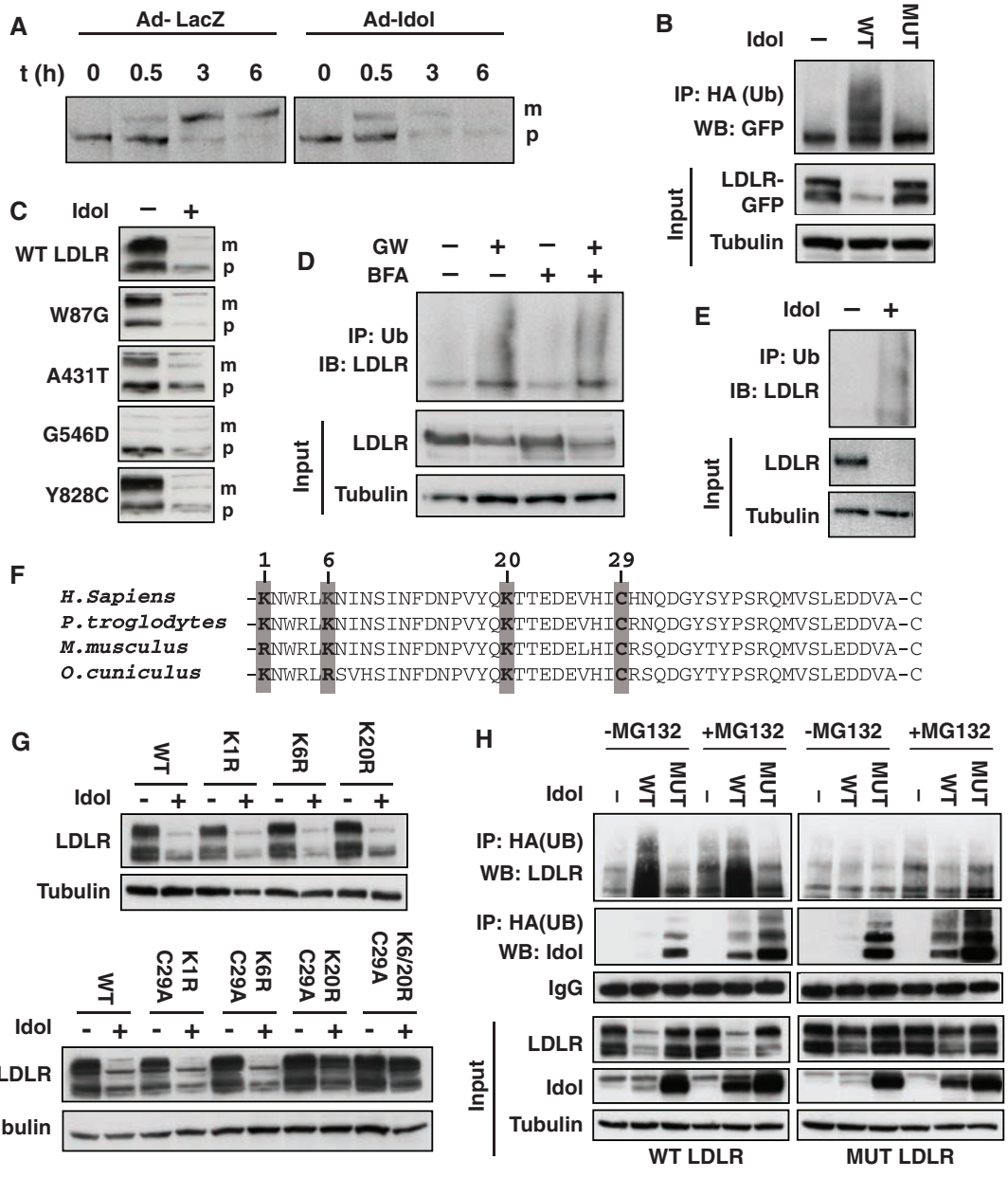

Fig. 4. Idol reduces LDLR protein expression through ubiquitination of conserved residues in its cytoplasmic domain. (**A**) 24 hours after infection with Ad-LacZ or Ad-Idol HepG2-LDLR-GFP, cells were pulsed with [^{35}S]methionine and [^{35}S]cysteine for 15 min and chased as indicated. Samples were immunoprecipitated at the indicated time points after labeling. (**B**) HEK293 cells were cotransfected with LDLR-GFP, Idol, and HA-ubiquitin expression plasmids. After 36 hours, lysates were subjected to immunoprecipitation (IP) and immunoblotting. HA, hemagglutinin; Ub, ubiquitin; WB, Western blot. (**C**) Total HEK293 cell lysates were analyzed by immunoblotting 48 hours after cotransfection with Idol and WT or mutant LDLR expression plasmids. p, immature protein; m, mature glycosylated form. (**D**) Peritoneal macrophages were cultured in sterol-depletion medium and treated with 1 μM GW3965 for 4 hours. Total lysates were immunoprecipitated with anti-ubiquitin, then immunoblotted (IB) for LDLR. (**E**) Primary mouse hepatocytes were infected with Ad-GFP or Ad-Idol and cultured in sterol-depletion medium. After 24 hours, lysates were immunoprecipitated with anti-ubiquitin antibody and then immunoblotted for LDLR. (**F**) Evolutionary conservation of the LDLR intracellular domain. Potential ubiquitination sites are indicated. (**G**) Immunoblot analysis of HEK293 total cell lysates cotransfected with control or Idol expression plasmids along with the indicated mutated LDLR constructs. Numbering in the LDLR constructs refers to Fig. 1F. (**H**) HEK293 cells were cotransfected with LDLR, mutant LDLR (K6R/K20R/C29A), Idol, and HA-ubiquitin expression plasmids as indicated. Subsequently, cells were treated with vehicle or 25 μM MG132 for 6 hours. Blots are representative of at least two independent experiments. IgG, immunoglobulin G.

We determined the structural requirements for Idol-dependent LDLR degradation with the use of mutational analysis. Idol had no effect on an LDLR lacking the entire 50–amino acid intracellular domain (fig. S6D). The LDLR intracellular domain contains three highly conserved lysine residues and one cysteine that could be potential sites for ubiquitination (Fig. 4F) (*29*). Single mutations of any of these residues, or combined mutation of all three lysine residues, did not prevent Idol from degrading the LDLR (Fig. 4G and fig. S6E). However, superimposing a cysteine mutation on constructs containing two or three mutated lysines rendered the LDLR insensitive to degradation. Additional mutagenesis revealed that either an intact Lys^{20} (K20) or an intact Cys^{29} (C29) was required for Idol-mediated degradation (Fig. 4G and fig. S6E). Finally, not only did combined mutation of the K20 and C29 residues block LDLR degradation by Idol, it also blocked ubiquitination (Fig. 4H). The proteasome blocker MG132, despite stabilizing Idol protein, did not stabilize the LDLR, consistent with previous reports that degradation of the LDLR occurs in the lysosome (Fig. 4H) (*30*, *31*).

To investigate whether activation of the LXR-Idol pathway affects LDLR expression in vivo, we treated mice with GW3965. LXR agonist reduced LDLR protein levels in a tissue-selective manner, concordant with the degree of Idol induction (Figs. 2B and 5A). Whereas prominent effects were observed in intestine and peritoneal macrophages, LXR ligand had minimal effect on Idol mRNA and LDLR protein levels in the liver. Notably, we observed a reciprocal effect on LDLR protein levels in resident macrophages and intestine when we analyzed mice in which the LXR-Idol pathway is inactive (Fig. 5B). LDLR protein levels were substantially higher in macrophages and intestine of LXRαβ$^{-/-}$ mice as compared with WT controls. LDLR levels were also slightly higher in the liver. Thus, gain or loss of LXR-Idol activity affects LDLR expression in vivo.

Because Idol was not subject to strong LXR regulation in the liver, we employed an alternative strategy to test its function in this tissue. We infected mice with adenoviral vectors encoding β-galactosidase or mouse Idol. Idol expression

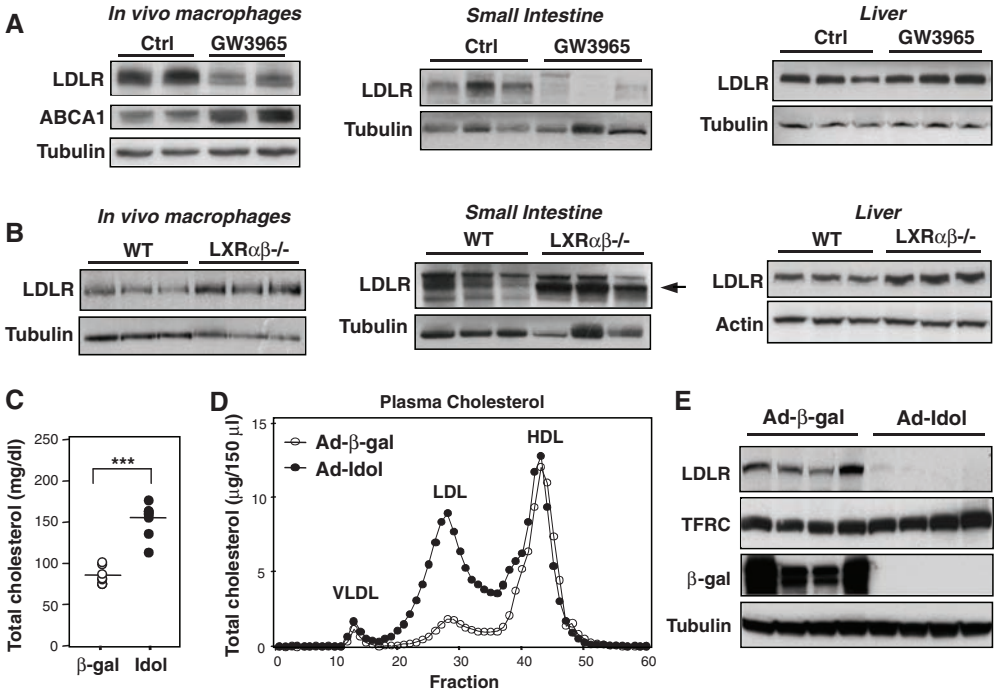

Fig. 5. Idol expression regulates LDLR expression and affects plasma cholesterol and LDL levels in vivo. (**A**) C57BL/6 mice were treated for 3 days with 40 mg/kg per day GW3965 by oral gavage. Total lysates from resident peritoneal macrophages, small intestine (ileum), and liver were analyzed for protein levels by immunoblotting. Macrophages were isolated from the peritoneal cavity and processed without in vitro culture. (**B**) Total lysates from macrophages, small intestine (ileum), and liver from WT and Lxr$\alpha\beta^{-/-}$ mice were analyzed by immunoblotting. Macrophages were isolated from the peritoneal cavity and processed without in vitro culture. (**C**) Analysis of plasma cholesterol 6 days after transduction of C57BL/6 mice with Ad-β-gal or Ad-Idol. (n = 8 mice per group) ***$P < 0.001$. (**D**) Cholesterol content of size-fractionated lipoproteins from mice infected with Ad-β-gal or Ad-Idol. (**E**) Immunoblot analysis of total liver lysates. Data are representative of at least two independent experiments.

increased plasma levels of total and unesterified cholesterol, whereas levels of triglycerides, free fatty acids, and glucose were not significantly altered (Fig. 5C and fig. S7A). Fractionation of plasma lipoproteins revealed that Idol expression caused a phenotype reminiscent of that exhibited by *Ldlr*$^{(-/-)}$ mice, with the appearance of a prominent LDL peak not present in the control mice (Fig. 5D and fig. S7B). Plasma apoB protein levels were increased by approximately threefold in Idol-transduced mice, and there was no difference in PCSK9 levels (fig. S7, C and D). Consistent with our in vitro results, hepatic expression of LXR and SREBP-2 target genes was not affected by Idol expression (fig. S7E), but LDLR protein levels were markedly reduced (Fig. 5E). In contrast, transferrin receptor levels were not altered by Idol. Finally, Idol adenovirus had no effect on plasma cholesterol levels (fig. S8A) or lipoprotein profiles (fig. S8B) in *Ldlr*$^{(-/-)}$ mice, demonstrating that Idol requires LDLR expression for these effects.

In summary, we have shown that the sterol-sensitive nuclear receptor LXR regulates LDLR-dependent cholesterol uptake through a pathway independent of the SREBPs. LXR induces the expression of Idol, which in turn catalyzes the ubiquitination of the LDLR, thereby targeting it for degradation. These results provide a potential explanation for an earlier observation that an ectopically expressed LDLR could still be regulated by sterols (*32*). Identification of the Idol-LDLR pathway fills a gap in our understanding of how LXRs control cholesterol homeostasis. The ability of LXRs to respond to excess cellular cholesterol by promoting efflux through ABC transporters has been extensively documented (*14*). The LXR-Idol-LDLR pathway provides a mechanism to simultaneously limit LDL cholesterol uptake. Idol and ABCA1 are coordinately regulated by LXR in a cell-type selective manner, consistent with this functional link.

The LXR-Idol pathway appears to be most active in peripheral cells such as macrophages, adrenals, and intestine. At the same time, however, Idol is constitutively expressed in the liver, and gain or loss of Idol function in cultured hepatocytes regulates LDLR protein levels and affects LDL uptake. Forced expression of Idol in liver in vivo profoundly reduces LDLR levels, further indicating that Idol is capable of degrading LDLR in this tissue.

Whether Idol expression is required for LDLR degradation in vivo is a critical question that remains to be addressed. If it is required, then conceivably the Idol pathway could be targeted pharmacologically so as to increase LDLR levels and enhance LDL clearance.

References and Notes

1. D. W. Russell *et al.*, *Cell* **37**, 577 (1984).
2. H. Tolleshaug, K. K. Hobgood, M. S. Brown, J. L. Goldstein, *Cell* **32**, 941 (1983).
3. M. S. Brown, J. L. Goldstein, *Science* **232**, 34 (1986).
4. C. Yokoyama *et al.*, *Cell* **75**, 187 (1993).
5. X. Hua *et al.*, *Proc. Natl. Acad. Sci. U.S.A.* **90**, 11603 (1993).
6. J. L. Goldstein, R. A. DeBose-Boyd, M. S. Brown, *Cell* **124**, 35 (2006).
7. C. K. Garcia *et al.*, *Science* **292**, 1394 (2001); published online 26 April 2001 (10.1126/science.1060458).
8. J. C. Cohen, M. Kimmel, A. Polanski, H. H. Hobbs, *Curr. Opin. Lipidol.* **14**, 121 (2003).
9. M. Abifadel *et al.*, *Nat. Genet.* **34**, 154 (2003).
10. J. Cohen *et al.*, *Nat. Genet.* **37**, 161 (2005).
11. N. G. Seidah *et al.*, *Proc. Natl. Acad. Sci. U.S.A.* **100**, 928 (2003).
12. K. N. Maxwell, J. L. Breslow, *Proc. Natl. Acad. Sci. U.S.A.* **101**, 7100 (2004).
13. S. W. Park, Y. A. Moon, J. D. Horton, *J. Biol. Chem.* **279**, 50630 (2004).
14. N. Zelcer, P. Tontonoz, *J. Clin. Invest.* **116**, 607 (2006).
15. J. J. Repa *et al.*, *Science* **289**, 1524 (2000).
16. M. A. Kennedy *et al.*, *Cell Metab.* **1**, 121 (2005).
17. D. J. Peet *et al.*, *Cell* **93**, 693 (1998).
18. R. K. Tangirala *et al.*, *Proc. Natl. Acad. Sci. U.S.A.* **99**, 11896 (2002).
19. S. B. Joseph *et al.*, *Proc. Natl. Acad. Sci. U.S.A.* **99**, 7604 (2002).
20. Materials and methods are available as supporting material on *Science* Online.
21. C. M. Adams *et al.*, *J. Biol. Chem.* **279**, 52772 (2004).
22. W. Chen, G. Chen, D. L. Head, D. J. Mangelsdorf, D. W. Russell, *Cell Metab.* **5**, 73 (2007).
23. S. J. Bensinger *et al.*, *Cell* **134**, 97 (2008).
24. P. A. Olsson, L. Korhonen, E. A. Mercer, D. Lindholm, *J. Biol. Chem.* **274**, 36288 (1999).
25. R. A. Anderson, R. E. Lovrien, *Nature* **307**, 655 (1984).
26. A. Bretscher, K. Edwards, R. G. Fehon, *Nat. Rev. Mol. Cell Biol.* **3**, 586 (2002).
27. B. C. Bornhauser, C. Johansson, D. Lindholm, *FEBS Lett.* **553**, 195 (2003).
28. H. H. Hobbs, D. W. Russell, M. S. Brown, J. L. Goldstein, *Annu. Rev. Genet.* **24**, 133 (1990).
29. K. Cadwell, L. Coscoy, *Science* **309**, 127 (2005).
30. K. N. Maxwell, E. A. Fisher, J. L. Breslow, *Proc. Natl. Acad. Sci. U.S.A.* **102**, 2069 (2005).
31. D. W. Zhang *et al.*, *J. Biol. Chem.* **282**, 18602 (2007).
32. M. F. Sharkey, A. Miyanohara, R. L. Elam, T. Friedmann, J. L. Witztum, *J. Lipid Res.* **31**, 2167 (1990).

33. We thank members of the Tontonoz and Edwards laboratories and J. Wohlschlegel, P. Edwards, and S. G. Young for fruitful discussions. We thank P. Tarr for assistance with confocal microscopy, K. Matter and A. Gonzalez for LDLR plasmids, and I. Koster for critically reading the manuscript. N.Z. was supported by a long-term postdoctoral fellowship from the Human Frontier Science Program Organization. P.T. is an investigator of the Howard Hughes Medical Institute. This work was also supported by NIH grants HL066088, HL090553, and HL030568. UCLA and two of the authors (N.Z. and P.T.) have filed a patent related to this work.

Supporting Online Material

www.sciencemag.org/cgi/content/full/1168974/DC1
Materials and Methods
Figs. S1 to S8
Table S1
References

25 November 2008; accepted 22 May 2009
Published online 11 June 2009;
10.1126/science.1168974
Include this information when citing this paper.

Wellplate-Transfer Robot

The Wellplate-Transfer Robot System is an automated platform designed to handle multiwell microplates. At the center of the system is a mountable three-axis robot that automatically transfers standard wellplates from 11 slot hotels to an Applied Scientific Instruments (ASI) automated XY stage. The ASI stage provides high resolution and high repeatability and can be mounted onto any common research-grade inverted microscope. The focus can also be automated with one of ASI's DC servomotor Z-drives, which can be retrofitted to the fine-focus shaft of most microscopes or with one of ASI's patented piezo-Z top-plate stages for nanometer-scale focusing. The robot can be controlled through its Teaching Pendant or through RS-232 serial communication.

ASI/Applied Scientific Instrumentation
For information 800-706-2284
www.ASIimaging.com

TLC Plate Readers

The Chromascan and Chromascan Lite thin-layer chromatography (TLC) plate readers provide rapid, accurate documentation and analysis of nonradioactive TLC plates. Both lines feature a high-resolution 16-bit, color charge–coupled device camera inside a darkroom. It takes just a few simple mouse clicks and a few seconds for the instrument to provide accurate results as TLC plate images and chromatograms. These good-laboratory-practices compliant systems are compact enough to fit inside a fume hood and can be supplied with a computer or connected to one in the laboratory. The darkrooms are designed with overhead ultraviolet (254 nm and 365 nm) and white lighting to provide the flexibility to automatically image all fluorescent or visible TLC plates. The Chromascan darkroom is computer controlled and its camera has a motorized zoom lens with feedback, for full-process automation.

Syngene
For information 800-686-4407
www.syngene.com

Microplate Mover

The Orbiter RS is a high-speed microplate mover offering reliable performance with flexible plate handling. Extensive vertical reach allows multiple stacked or high-density instruments to be loaded in a small footprint, and a bidirectional telescoping arm provides superior reach, improved user safety, and unlimited base rotations within a 360° workspace. It accommodates plate formats from shallow to deep well, in addition to tip boxes and lids, tubes, and racks. This flexibility is further supported by random or sequential plate access, and the ability to mix modes of storage as assay requirements change. For safety, the robotic arm is able to pass through the base and remain inside the rotating base while turning. It features closed-loop motion control, collision detection, and position recovery.

Thermo Fisher Scientific
For information 905-332-2000
www.thermofisher.com

Microplate Handler

The BenchCel R-Series microplate handlers feature a high-speed robot that can access integrated microplate stacks and peripheral instruments. This customizable, modular design provides the flexibility and scalability required to meet the needs of the most diverse laboratory applications. They are available in two-rack, four-rack, and six-rack configurations, with options for rack capacity and style. Even the smallest instrument in the series can support three peripheral instruments, allowing customers to create highly configurable workstations that combine a broad range of functionality, including barcode labeling, microplate sealing, plate reading, centrifugation, and sophisticated liquid handling using Agilent or third-party peripherals. The series offers the convenience of being able to store and handle most types of microplates, lidded plates, tip boxes, and tube racks. A novel delidding function removes and replaces lids as needed.

Agilent Automation Solutions (formerly Velocity11)
For information +44-1763-269110
www.velocity11.com

Homogenizing System

The DPS-20 from Pro Scientific is a compact, dual-processing homogenizing system that combines the functions of mechanical and ultrasonic homogenizing for faster sample preparation. It features an innovative, three-in-one design and offers users the choice of a fully automated ultrasonic homogenizing configuration, fully automated mechanical homogenizing, or both. This advanced system offers optimum control and flexibility and can support a wide range of processing needs. The instrument can save time by merging the advantages of each homogenizing method for faster and more efficient sample breakdown. Its automation capacity allows for repeat processing and consistent results.

Scientific Laboratory Supplies
For information +44-(0)-1159-821-111
www.scientific-labs.com

Electronically submit your new product description or product literature information! Go to **www.sciencemag.org/products/newproducts.dtl** for more information.

Newly offered instrumentation, apparatus, and laboratory materials of interest to researchers in all disciplines in academic, industrial, and governmental organizations are featured in this space. Emphasis is given to purpose, chief characteristics, and availabilty of products and materials. Endorsement by *Science* or AAAS of any products or materials mentioned is not implied. Additional information may be obtained from the manufacturer or supplier.

POSITIONS OPEN

UNIVERSITY OF NOTRE DAME

MANAGING DIRECTOR
Energy Frontier Research Center

The University of Notre Dame (**website: http://www.nd.edu**) is seeking a Managing Director for the Energy Frontier Research Center (EFRC) Materials Science of Actinides within the College of Engineering. The EFRC partners five universities and three national laboratories. The Managing Director will maintain continuous communication with the technical leads at each of these institutions to ensure that the program remains consistent with the proposed research plan. The Managing Director will facilitate communications between technical leads concerning new research findings and synergisms between the individual groups, and will be instrumental in strategic planning. Ph.D. required.

Please apply online at **website: http://ND.jobs** to **Job #09204.** For additional information about working at the University of Notre Dame and various benefits available to employees, please visit **website: http://hr.nd.edu/employment/working_at_nd.shtml.**

The University of Notre Dame is an Equal Employment Opportunity/Affirmative Action Employer.

FACULTY POSITION, PHARMACOLOGY

The Division of Basic Pharmaceutical Sciences (DBPS) at Xavier University of Louisiana, College of Pharmacy invites applications for one 12-month, tenure-track position at the rank of **ASSISTANT** or **ASSOCIATE PROFESSOR.** Candidates for this position must have a Ph.D. degree in pharmacology or a closely related field. Preference will be given to candidates with previous teaching and ongoing research experience. The successful candidate will also be expected to establish a funded research program in his or her area of interest. Applicants should submit (i) a letter of intent; (ii) curriculum vitae; (iii) a statement of research interests; and (iv) the names and addresses (e-mail address and telephone number) of at least three references to: **Tarun K. Mandal, Ph.D., Chair, DBPS Faculty Search Committee, Xavier University College of Pharmacy, 1 Drexel Drive, New Orleans, LA 70125. E-mail: dbpsjob@xula.edu; telephone: 504-520-7650; fax: 504-520-7954.**

Xavier University of Louisiana is an Equal Opportunity Employer. Women, minorities, and persons with disabilities are encouraged to apply.

CAREER OPPORTUNITY

Doctor of Optometry (O.D.) degree in 27 months for Ph.D.s in science and M.D.s. Excellent career opportunities for O.D./Ph.D.s and O.D./M.D.s in research, education, industry, and clinical practice. This unique program starts in March 2009, and features small classes and 12 months devoted to clinical care.

Contact the **Admissions Office, telephone: 800-824-5526** at the **New England College of Optometry, 424 Beacon Street, Boston, MA 02115.** Additional information at **website: http://www.neco.edu, e-mail: admissions@neco.edu.**

SHANTOU UNIVERSITY MEDICAL COLLEGE in Shantou, China, is launching nationally and internationally competitive research and teaching programs and has many openings for leading and up-and-coming scientists working at different disciplines and Pearl River Scholar in key disciplines. Selected candidates will be sufficiently supported with startup fund, relocation expenses, housing, and competitive salary packages. Please visit the **website: http://www.med.stu.edu.cn/zj.htm** for more information. Interested candidates should send curriculum vitae to **e-mail: lqchen@stu.edu.cn.**

POSITIONS OPEN

TEXAS TECH UNIVERSITY Health Sciences Center

ASSISTANT OR ASSOCIATE PROFESSOR
Center of Excellence for Infectious Diseases

The newly created Center of Excellence for Infectious Diseases at the Paul L. Foster School of Medicine, Texas Tech University Health Sciences Center, El Paso, Texas, is seeking candidates for tenure-track faculty positions at Assistant or Associate Professor level. This is part of a state-funded initiative to enhance research in infectious diseases. The Center is primarily interested in investigators with research interests in molecular immunology, host-pathogen interactions, vaccine development, and animal models for translational studies.

Successful candidates are expected to develop and maintain independently funded research programs in infectious diseases or a related field. The position reports to the co-directors of the Center of Excellence for Infectious Diseases.

Minimum qualifications: M.D. or Ph.D. degree in a related field and at least three years of postdoctoral experience with a strong publication record.

Preferred qualifications: Candidates with funded grant support and experience in emerging infectious diseases and cutting edge technologies are particularly encouraged to apply.

The Center offers competitive salary and startup packages, newly constructed laboratory space, BSL-2 and BSL-3 laboratories, and a supportive interactive environment. Interested candidates must apply online at **website: http://jobs.texastech.edu, requisition #77147** by submitting curriculum vitae, a short write-up of research interests, and three letters of recommendation. For further information, please e-mail or contact:

Manjunath Swamy, M.D.
E-mail: manjunath.swamy@ttuhsc.edu or
Premlata Shankar, M.D.
E-mail: premlata.shankar@ttuhsc.edu
Co-Directors of the Center of Excellence for Infectious Diseases

The positions are open until filled. Application review will begin immediately.

Texas Tech University Health Sciences Center is an Equal Opportunity/Affirmative Action Employer.

POSTDOCTORAL FELLOWS, M.D., Ph.D., D.D.S., OR M.D.-Ph.D.

The University of Alabama at Birmingham Center for Metabolic Bone Disease has three openings for Postdoctoral Fellows interested in hard tissue, bone biology, and related diseases. Fellows will be funded by an NIH T32 Institutional Training Grant which *requires recipients to be either U.S. citizens or permanent residents.* The UAB Comprehensive Bone Research Program has one of only six NIH P30 Research Core Centers focused on hard tissues and has a core research faculty of more than 50.

These full-time positions are available for up to three years with the current NIH stipend amount based on the awardees' experience and are available for training in basic, translational, or clinical investigations.

Submit an application to **Dr. Jay McDonald** consisting of: (1) a copy of your current curriculum vitae; (2) a one- to two-page statement of your research interests; and (3) the names of three references.

Applications will be accepted until all three positions are filled.

Jay M. McDonald, M.D.
Professor, Department of Pathology
Director, Center for Metabolic Bone Disease
The University of Alabama at Birmingham
LHRB 509, 701 19th Street South
Birmingham, AL 35294-0007
Telephone: 205-934-6666
Fax: 205-975-9927
E-mail: mcdonald@uab.edu

WWW.NIH.GOV
Positions NIH
THE NATIONAL INSTITUTES OF HEALTH

National Institute of Neurological Disorders and Stroke
Health Science Policy Analyst

The National Institute of Neurological Disorders and Stroke (NINDS), located in Bethesda, Maryland, part of the National Institutes of Health, Department of Health and Human Services, is seeking applications for a Health Science Policy Analyst vacancy in its Office of Science Policy and Planning (OSPP) in the Office of the Director. The incumbent is responsible for analyzing and monitoring developments in neuroscience as they affect NINDS programs; for furnishing policy and programmatic guidance and assistance as required to Institute scientific program staff; and for consulting with the appropriate institute staff regarding the many policy issues relevant to NINDS, NIH, and DHHS. The ability to both function independently in a staff capacity and to develop collaborative relationships is essential. In conjunction with OSPP staff members or other Institute staff, the applicant will prepare reports and analyses of research findings; prepare written testimony and related briefing materials for Congressional hearings; coordinate strategic planning efforts; attend, plan, and coordinate meetings for the NINDS; and scientific initiatives.

This is a civil service position that will be filled at the GS-12 or GS-13 grade level. The salary range is $73,100 - $113,007. Applicants are strongly encouraged to apply on-line through USA Jobs. For information on how to apply for the Health Science Policy Analyst vacancy, and for the full vacancy announcement, please go to: (http://jobsearch.usajobs.opm.gov/getjob.asp?JobID=31797224). When applying for this vacancy, please make sure to reference vacancy announcement number NINDS-2009-349682-DE. Supporting documents (i.e., curriculum vitae, copy of all transcripts) may be faxed to 301-402-2232, Attn: Erin Bandak or sent via e-mail to bandake@mail.nih.gov Please be aware that if all the requested supporting documents are not submitted before the closing date, it will result in non consideration of your application.

National Institute of Neurological Disorders and Stroke

Staff Scientist
Microscopic and Image Analysis

The Division of Intramural Research of the National Institute of Neurological Disorders and Stroke is recruiting a Staff Scientist. The individual will work under the guidance of Drs. Chris McBain, John Isaac and Jeffrey Diamond and is expected to work on collaborative research efforts between the three labs as well as maintain existing equipment. The successful candidate will be well versed in a variety of microscopic and image analysis techniques including digital fluorescence, confocal and two-photon microscopy. The ability to operate and maintain light, confocal and two-photon imaging systems is essential. In addition, having a working knowledge of commercially available software environments for image analysis and image processing and digital data presentation would be advantageous. The successful candidate will possess a Ph.D. in the neurosciences or a closely related field. Applicants should have at least 3-4 years postdoctoral experience and an established track-record in the physiology of neural circuits. Candidates will be required to communicate the results of their research clearly and effectively both orally and in writing and must have good interpersonal skills. Salary and benefits will be commensurate with experience. Interested candidates should send a statement of research interests and goals, CV, bibliography and three letters of recommendation to: Chris J. McBain, Ph.D., Porter Neuroscience Center, Bldg. 35, Room 3C903, 35 Convent Drive, Bethesda, MD 20892 or by email to mcbainc@mail.nih.gov. Evaluation of applications will begin July 20, 2009.

NATIONAL CANCER INSTITUTE

Staff Scientist
Experimental Transplantation and Immunology

A Staff Scientist position is available in the Experimental Transplantation and Immunology section of the National Cancer Institute in the laboratory of Dr. Dennis Hickstein to develop zebrafish zebrafish models of human cancer.

Experience in molecular genetic techniques is recommended. Previous experience with the zebrafish model is desirable. The laboratory is located on the main campus in the new Clinical Research Center, This position is ideally suited for an individual who has recently completed post-doctoral training in a laboratory working in the zebrafish system. The laboratory is part of a highly interactive group emphasizing basic approaches to human malignancy.

The NCI offers competitive salaries along with an excellent work environment. The DHHS and NIH are Equal Opportunity Employers that value and foster diversity throughout the entire organization.

Interested applicants should send a CV, brief description of research interests and experience, and contact information for three references to:

Dennis D. Hickstein, M.D., Senior Investigator,Experimental Transplantation and Immunology, Center for Cancer Research, National Cancer Institute, Bldg. 10/CRC, Room 3-3142, Bethesda, MD 20892,
Email: hicksted@mail.nih.gov.

The NIH Director's Wednesday Afternoon Lecture Series

Biomedical scientists around the world are invited to join us online to hear leading investigators present their latest results to the NIH Intramural Research community. Lectures may be viewed live at 3:00 p.m., EDT (20:00 GMT) on Wednesdays, from September through June. Live webcasts can be viewed under "Today's Events" at: <http://videocast.nih.gov/>

The lecture series session has ended and will resume on September 16, 2009. The schedule of lectures will be available at: <http://www1.od.nih.gov/wals/schedule.htm.

Center for iPS Cell Research and Application
Institute for Integrated Cell-Material Sciences
Kyoto University

Director: Shinya Yamanaka

Professor (2 - as Principal Investigator) at CiRA, iCeMS
Kyoto University, Japan (**http://www.icems.kyoto-u.ac.jp/cira/**)

Workplace: Center for iPS Cell Research and Application (CiRA), Institute for Integrated Cell-Material Sciences, Kyoto University (Kawara-cho 53, Shogoin, Sakyo-ku, Kyoto 606-8507, Japan) OR another research facility in the city

Job Description:
(1) Research on regulation of cellular conditions utilizing nuclear reprogramming techniques.
(2) Development of differentiation induction techniques according to various characteristics of iPS cell clones.
(3) Establishment of various disease-specific iPS cells and development techniques for their clinical application.
(4) Pre-clinical study for cell transplantation therapy utilizing small- or medium-sized mammals.
(5) Other researches utilizing advantages of iPS cells

Starting Date: October 2009 or after (Negotiable)

Pay: To be determined in accordance with Kyoto University Regulations

Application Docs:
(1) Curriculum vitae
(2) Lists of acquired research funds, publications, presentations, and patents
(3) A brief summary of scientific achievements (3-10 pages)
(4) Research plan (3-10 pages). Please state your research policy and targets at CiRA for the period of 5 years
*Please be advised that your application documents will NOT be returned to you.

Application Deadline: August 31, 2009

Screening Process: Candidates will be screened based on application documents submitted and by an interview (or a series of interviews) as needed. Candidates will be notified of the results in writing.

If hired: You will be a professor in accordance with Kyoto University Regulations. Whereas you may be appointed as an associate professor according to your experience and achievement, you are surely an individual principal investigator, and there is a possibility to be promoted to professor after hired as an associate professor. Your work will be assessed in 2014 by the internal and external evaluation committees, and you may then receive some advice on your research policy and targets. In case of poor achievement by then, you are possibly to be transferred to a different department in the center.

You are expected to read the "Message from the Director" posted on the homepage of CiRA's website carefully prior to submitting your application documents. The above "(4) Research plan" should be prepared taking that into account.

Postal Address: Shogoin Kawara-cho 53, Sakyo-ku, Kyoto 606-8501, Japan, CiRA Support Office, iCeMS, Kyoto University

Please be sure to clearly state **"Application for CiRA Professor"** on the envelope, enclosing the above 4 application documents in it, and mail it to the above postal address by **August 31, 2009**. Please keep in mind that applying by Email is not acceptable.

Contact: Tetsuya ISHII
Head of research management office
CiRA, iCeMS, Kyoto University
Phone: 81-75-751-4057
Email: collaboration@cira.kyoto-u.ac.jp

TEXAS A&M UNIVERSITY

Faculty Positions in Prokaryotic Biology

The Department of Biology at Texas A&M University (TAMU) invites applications for tenure-track **Assistant Professor** positions in microbiology. Exceptional applicants at other levels may also be considered.

Candidates pursuing innovative research in all areas of prokaryotic biology will be considered, including but not limited to biotechnology, cell, developmental, environmental, or evolutionary microbiology, genetic mechanisms and genomics, host-pathogen interactions, and synthetic biology. The primary criteria for selection will be excellence and creativity in research and scholarship. We strongly encourage applications from candidates who will increase the exposure of our students to a diverse culture.

The successful candidates will be expected to maintain a vigorous, externally funded research program and to contribute to the teaching of undergraduate and graduate students. We offer a highly interactive and collegial research environment, a strong modern infrastructure, and a competitive startup package. More information about our department can be found at **www.bio.tamu.edu**. For full consideration, applicants should send a letter of intent, *curriculum vitae*, statement of research and teaching interests, and three letters of recommendation by **September 1, 2009** to:

Microbiology Faculty Search Committee
Department of Biology
Texas A&M University
3258 TAMU
College Station, TX 77843-3258

If you have questions about this search, please direct e-mails to **Dr. Michael Benedik**, Chair of the Search Committee, at **microsearch@mail.bio.tamu.edu**

Texas A&M University is an Equal Opportunity Employer and has a policy of being responsive to the needs of dual-career couples.

McLaughlin Research Institute

Assistant Professor in Mammalian Neuroscience

McLaughlin Research Institute seeks an innovative scientist who can take advantage of the Institute's strengths in mouse genetics to address important problems in neurobiology, neurological or psychiatric diseases, or related areas. Low animal care costs and transgenic services facilitate mouse-intensive projects that would be cost-prohibitive at many other facilities. Applicants with interests in animal models for human neurological disease, stem cell models or stem cell therapy, novel strategies for genome modification or dissection of cellular function, electrophysiology, or behavior, are particularly encouraged to apply. Candidates should possess a doctoral degree and a record of research excellence as a postdoctoral fellow. Applicants should be capable of developing productive research programs that can compete successfully for grant funding. The willingness and ability to establish both intramural and extramural collaborations is essential. The successful applicant will move into newly renovated laboratory space available in March 2010.

The Institute is a small, non-profit organization located near Montana's Rocky Mountain front that offers a non-bureaucratic, interactive research environment in a spacious modern research building. Faculty members also benefit from the active involvement of MRI's Scientific Advisory Committee (**Irv Weissman, David Baltimore, David Cameron, Neal Copeland, Jeff Frelinger, Leroy Hood, Nancy Jenkins, and James Spudich**). For additional information see **www.montana.edu/wwwmri**. For specific questions about the Institute, contact **George Carlson, John Mercer, John Bermingham, Teresa Gunn**, or **Deb Cabin** at **MRI**.

Applications, including names and contact information for three to five individuals who may serve as references, should be sent to:

Search Committee
1520 23rd Street South
Great Falls, MT 59405
search@mri.montana.edu

An Equal Opportunity/Affirmative Action Employer.

USC
UNIVERSITY OF SOUTHERN CALIFORNIA

Keck School of Medicine of the University of Southern California

W. M. Keck Endowed Professorship

The University of Southern California is seeking an internationally recognized leader in biomedical research to hold the W. M. Keck endowed Professorship within the Department of Biochemistry and Molecular Biology. This recruitment is part of a major expansion of the basic research programs in the Keck School of Medicine, which includes the areas of stem cell biology, neuroscience, the molecular and genetic bases for human diseases, and cancer biology and therapy. The appointment will be made at the level of Associate or Full Professor.

Please send Curriculum Vitae, preferably by email (**cmmunoz@usc.edu**), to:

Michael R. Stallcup, Ph.D.
Chair, Department of Biochemistry and Molecular Biology
University of Southern California
1441 Eastlake Avenue, NOR 6316
Los Angeles, CA 90089-9176

The University of Southern California is an Equal Opportunity Affirmative Action Employer. Women and individuals belonging to minority groups are particularly encouraged to apply.

The **Faculty of Natural Sciences** invites applications for a tenured

W3 Professorship for Inorganic and Analytical Chemistry (Chair)

(in succession of Prof. Dr. Dr. h. c. mult. Rudi van Eldik)

The successful candidate is expected to represent the field of Inorganic Chemistry in research and teaching at the university. The research interests of the applicant should strengthen current and ongoing activities of the Department of Chemistry & Pharmacy in the area of inorganic molecular synthesis with potential applications in catalysis and/or molecular materials. Based on innovative synthesis concepts, the design, development and application of novel, functional and complex systems are envisioned.

The future chair of Inorganic and Analytical Chemistry will be joining a strongly interdisciplinary environment. The diversity of research currently undertaken by the chemistry faculty is characterized by programs like the Excellence Cluster "Engineering of Advanced Materials", the Graduate School of "Molecular Science" and the DFG Research Initiative 583 "Redox Active Metal Complexes". Active participation in these programs and corresponding follow-up initiatives will be appreciated.

Qualifications of interested candidates include a university doctoral degree, an established record of teaching at the university level and a habilitation or equivalent qualification that may have been gained outside the university or during an Assistant/Associate Professorship.

Candidates for this position should be aged 52 years or under at the time of appointment. Exceptions may be considered in certain cases as determined by the Ministry for Science, Research and Art, subject to approval by the Ministry of Finance.

The University of Erlangen-Nuremberg actively encourages applications from female candidates as part of our ongoing commitment to increase female representation in research and teaching. Disabled candidates are given preference if equally qualified.

Application documents (curriculum vitae, photograph, list of publications and teaching activities, certified copies of degree documents but no publications) and a brief statement of research interests are due on **September 25, 2009**, the latest and should be mailed to: Dekan der Naturwissenschaftlichen Fakultät, Friedrich-Alexander-Universität Erlangen-Nürnberg, Universitätsstraße 40, 91054 Erlangen, Germany.

Friedrich-Alexander-Universität Erlangen-Nürnberg

Grundzertifikat audit familiengerechte hochschule

www.uni-erlangen.de

Chromatin, Inc.

Chromatin Inc. is a rapidly growing biotech company that is unlocking the potential of plants to produce greater value and meaningful products for consumer, grower, seed producer, processor, and bio-energy markets. With facilities in Chicago and Champaign, Illinois, Chromatin is leveraging its proprietary mini-chromosome technology to introduce multiple genes ("gene stacks") simultaneously into plant cells. The company has formed multiple partnerships with leading agricultural companies to advance mini-chromosome applications in traditional crops such as corn. Chromatin is now expanding its technology to bio-energy feedstocks, developing gene stacks that improve yields and reduce the costs of feedstock conversion to fermentable sugars.

Chromatin is recruiting a number of highly motivated, results-oriented individuals. Successful candidates will join a talented team of researchers to advance the company's goals. All candidates are expected to work independently as well as in a team-based environment with a high level of organization, attention to detail, and ability to complete tasks. Good written and oral communication skills are essential. Full-time positions include health, vision, dental and 401 (k) benefits. Positions are located in Chicago and Champaign, IL. Please see **www.chromatininc.com** for more details.

Chromatin, Inc. is currently recruiting for the following positions:

Director of Bio-energy Crop or Project Manager (Job number 0609-01) to lead the company's mini-chromosome technology in bio-energy crop genetics, transformation and molecular biology. The successful candidate will manage a talented team of scientists and represent Chromatin in its partnership with a leading agbiotech company. The candidate must have a broad understanding of plant molecular biology, demonstrated leadership of research teams and an excellent track record in molecular biology, genetics, and/or cell culture. Applicants should exhibit strong management skills and have 5+ years of supervisory experience in an industry setting or a goal-oriented collaborative research program.

Director of Bioinformatics (Job number 0609-02) to develop the analysis pipeline for several projects targeted at crop improvement and technology development. Successful candidates will have experience in life sciences and computational approaches, specifically with state of the art high-throughput sequence data analysis, database design and management, genetic mapping (QTL and association mapping) and strong statistical skills. Applicants should have a PhD in Biology or Computer Science or a related field, and 5+ years of post-degree experience, including 2+ years of supervisory experience. The ability to work with a team and communicate well with management, biologists and programmers as well as external scientists is essential.

Director of Carbohydrate Research (Job number 0609-03) with expertise in carbohydrate biochemistry and biosynthetic pathways to build and manage a program focused on improving bioenergy feedstocks. Key responsibilities include directing research on carbohydrate pathway optimization and developing and managing collaborations with external partners. The successful candidate will have a Ph.D., a broad background in plant biology and metabolic engineering, a proven track record in starch and/or sugar pathway engineering, demonstrated leadership in building and managing a successful and innovative research program and 5+ years of supervisory experience, preferably in an industry setting.

Plant Transformation Lead (Job number 0609-04) to manage mini-chromosome transformation efforts. Ideal candidates will have extensive cell culture skills with a variety of plant species, with specific emphasis on monocots and experience in transgenic plant production including the design and execution of experiments using new technologies. Knowledge of commercial transgenic plant production and tracking is a plus. Successful candidates must have a Masters, Ph.D., or the equivalent experience in an industrial setting as well as supervisory experience.

Plant Tissue Culture Scientist (Job number 0609-05) and **Molecular Biology Scientists and Research Associates (Job number 0609-07)** positions are also available. Please see **www.chromatininc.com** for more details.

Application Process: Submit CV and cover letter referencing the job for which you are applying to: **careers@chromatininc.com**.

Chromatin is an Equal Opportunity Employer.

GRADUATE PROGRAM

International Max Planck Research School

PhD Program in
Structure and Function of Biological Membranes

Max Planck Institute of Biophysics
Max Planck Institute of Brain Research
Goethe University

Frankfurt am Main, Germany

Several PhD fellowships are available in the International Max Planck Research School in Frankfurt. The two Max Planck Institutes and research groups at Frankfurt University offer a unique environment for the study of biological membranes and membrane proteins. PhD opportunities exist in internationally leading laboratories in the areas of membrane protein structure determination, membrane biochemistry, molecular biology, and functional studies by electrophysiological and spectroscopic methods, computational biophysics and structural bioinformatics, as well as studies of whole membranes, cells and organelles.

Highly qualified candidates with degrees in biochemistry, chemistry, physics, biology, medicine or related subjects are invited to apply for the next round of admission. Selection interviews will take place in Frankfurt on 17 and 18 November 2009. Application forms can be downloaded from the website of the Research School at *www.biophys.mpg.de/research-school*. Completed application forms and two letters of reference should arrive no later than **16 August 2009**.

For further details please contact:

Dr. Janet Vonck
MPI of Biophysics
Max-von-Laue-Str. 3
D-60438 Frankfurt am Main
Germany
E-mail: **research.school@biophys.mpg.de**
Tel: +49+69-6303-3004/3001
Fax: +49+69-6303-3002

SYMPOSIUMS

Weill Cornell Medical College

EXPERIMENTAL PATHOLOGY FACULTY POSITIONS

The Department of Pathology and Laboratory Medicine of the Weill Cornell Medical College invites applications for faculty positions in experimental pathology. Candidates are expected to develop and maintain productive, independent, externally funded research programs in basic mechanisms of human disease which fall within the broad areas of molecular oncology and cancer genetics.

Candidates may hold an MD, a PhD, or combined MD and PhD degrees but must possess a sufficient amount of post-doctoral research training to develop an independent research program. Teaching responsibilities will include graduate and medical students.

The Department offers a supportive intellectual environment in which several mid-level and senior scientists direct well-funded independent research programs in molecular oncology, immunobiology, and vascular biology. Modern research laboratory facilities, excellent core facilities, and competitive start-up packages are available.

Interested applicants should submit a curriculum vitae, representative recent publications, and a brief description of past scientific accomplishments, future research plans, and career objectives, as well as the names of three individuals familiar with the applicant and the applicant's research program. Applications will be accepted until all positions are filled. Please submit via email to **rubinma@med.cornell.edu** or to:

Dr. Mark A. Rubin
Vice Chairman for Experimental Pathology
Department of Pathology and Laboratory Medicine
Weill Cornell Medical College
1300 York Avenue, Box #69
New York, New York 10065

Weill Cornell Medical College is an Equal Opportunity/Affirmative Action Employer. Women and minority candidates are encouraged to apply.

Full time Associate/Full Professor Positions

Reproductive Medicine and Reproductive Biology

Nanjing Medical University Nanjing, China

Nanjing Medical University is currently seeking Senior Scientists for the lab of Reproductive Medicine. This lab was constructed with the great support from Nanjing Medical University and the Government of Jiangsu Province in 1997 and focused on the research of gametogenesis and the related human reproduction disease. With 12 years booming development, this lab now becomes the candidate of Key State lab of Reproductive Medicine in China. In order to elevate the scientific research levels of Nanjing Medical University, especially in the field of Reproductive Medicine and to serve Chinese people better in Reproduction Health, we warmly invite you to join us. The university will offer a dynamic and stimulating research environment which involves multidisciplinary interactions. We provide a highly competitive benefit and compensation package for the positions including the independent lab room and start-up research funds.

Keyword: Reproductive Medicine, Nanjing,

Minimum requirements:

- Amazing passion for the research of Reproductive Medicine and Reproductive Biology and potential to transfer the research into clinical application
- Has been working as an Assistant Professor in a University abroad or has completed post-doctoral training with outstanding academic records
- Ability to work in a team and be flexible to manage the research team well

Contact: Mr. Hanzhan Gu, Department of Human Resouce, Nanjing Medical University, 140 Hanzhong Road, Nanjing, Jiangsu Province, 210029, The People's Republic of China; Tel/Fax: 86-25-86862642; Email: ghz@njmu.edu.cn.

POSITIONS OPEN

POSTDOCTORAL POSITION (100 percent, multiyear) in mouse genetics and neurodegenerative disease available immediately at University of California, Davis to use mouse models to study the genetic, cellular, molecular, and mitochondrial mechanisms of neurodegenerative disease. Expertise in cloning, conditional knockouts, and overexpression of genes required. Salary depends upon experience (NIH scale). Send curriculum vitae to **e-mail: gcortopassi@ucdavis.edu. Website: http://cortopassilab.ucdavis.edu.**

UCD is an Affirmative Action/Equal Opportunity Employer.

POSTDOCTORAL RESEARCH OPPORTUNITY, AQUATIC INVASIVE SPECIES

The University of Michigan Cooperative Institute for Limnology and Ecosystems Research (CILER) announces a two-year Postdoctoral invasive species research opportunity in support of National Oceanic and Atmospheric Administration's (NOAA) Aquatic Invasive Species Program (AISP). This is a cooperative venture of AISP/National Center for Research on Aquatic Invasive Species (NCRAIS) and CILER. The position will be filled competitively based on recommendation of an advisory panel after review of submitted proposals. There are six potential NOAA host sites in the United States. Funding is available for one position. The University of Michigan/CILER must receive proposals by e-mail or on a CD by surface mail by 5 p.m. Eastern Time on August 10, 2009. For more information and application guidance, visit our **website: http://www.ciler.snre.umich.edu/.**

POSITIONS OPEN

Two **POSTDOCTORAL POSITIONS** are available immediately in the Center for Cardiovascular Sciences at Albany Medical College, New York, in the laboratory of **Dr. Mohamed Trebak.** The successful candidate will have a Ph.D. degree and proven research ability as demonstrated by publications in peer-reviewed journals and letters of recommendation. She/he will also possess a strong knowledge base in biochemistry, cell biology, signal transduction, molecular biology, and physiology. We are especially interested in candidates with strong hands-on experience in patch clamp electrophysiology and/or molecular biology.

Topics of research focus on calcium signaling in vascular smooth muscle and endothelial cells. Specifically, the role of TRPC and STIM/Orai ion channels in native calcium entry pathways and vascular function. This laboratory uses mouse and rat animal models of cardiovascular diseases and a wide range of in vitro technologies including patch clamp electrophysiology, calcium imaging, molecular and cellular biology, and biochemical techniques.

Interested individuals should send a cover letter and curriculum vitae and provide contact information of three references, preferably electronically, to: **Dr. Mohamed Trebak, e-mail: trebakm@mail.amc.edu.**

STAFF SCIENTIST. Experienced basic scientist at the level of **ASSOCIATE PROFESSOR** or higher, with a past record of extramural funding procurement. Areas of research desired include intestinal or hepatic immunology or non-alcoholic fatty liver diseases (NAFLD). Candidates should have an M.D. and/or Ph.D. degree or equivalent. Send curriculum vitae and references to: **M. Michael Wolfe, M.D., Chief, Section of Gastroenterology, Boston Medical Center and Boston University School of Medicine, 650 Albany Street, X 504, Boston, MA, 02118.**

An Equal Opportunity Employer.

MARKETPLACE

Part of IBC's
Drug Discovery & Development Week

August 4-6, 2009
World Trade Center Boston/Seaport Hotel
Boston, MA USA

New Frontiers in Cancer Drug Development

Innovations in Discovery Science, Translational Research and Cancer Clinical Trials

focus on

- Exploiting Cancer Stem Cells
- Combining Molecular Targeted Therapies
- Epigenetics and Emerging Targets
- Companion Diagnostics and Biomarkers
- Regulatory Pathways and Perspectives

Conference Keynote

From Empiric to Specific: How Can We Translate Science into Cancer Treatments and Get it Right More Reliably?

George D. Demetri, M.D.
Director, **Ludwig Center at Dana-Farber/ Harvard Cancer Center**
Center for Sarcoma and Bone Oncology
Dana-Farber Cancer Institute

Featured Presentation

The Evolving Treatment Paradigm in Multiple Myeloma

Kenneth C. Anderson, M.D.
Chief, Division of Hematologic Neoplasia,
Dana-Farber Cancer Institute
and Kraft Family Professor of Medicine,
Harvard Medical School

Debate and Discussion:

Point:
The current approach to first-in-class innovation in oncology isn't working

Counterpoint:
Novel target discovery platforms are feeding innovation in oncology

Plenary Keynote

Global Pharma Innovator: Daiichi Sankyo's Challenge to Build a Competitive Pharmaceutical Company in the Global Market

Takashi Shoda
President and CEO,
Daiichi Sankyo Co., Ltd.,
Japan

Register Today
Use Priority Code
D9201CSA

www.drugdisc.com/Cancer

Organized by
ibc Life Sciences
an informa business

What makes you happy? How about Western blots in 55 minutes without equipment?

Put a smile on your face and your research with the chemiluminescent Thermo Scientific Pierce Fast Western Blot Kit 55-minute Western blot procedure.

- Fast – all the sensitivity you need in a fraction of the time; save 3-4 hours per blot over traditional blotting methods
- Convenient – no expensive hardware or extra bench space needed; eliminates membrane clogging issues
- Economical – costs about the same as a classical Western blot
- Easy – optimized kit includes all reagents except primary antibody
- Versatile – kits work with both rabbit and mouse primary antibodies

Visit *www.thermo.com/fastwest*

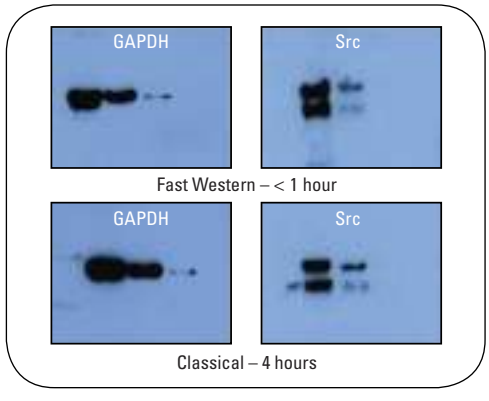

The sensitivity you need in less time with no expensive hardware.
Target proteins were probed using a classical Western blot procedure (3-4 hours) and the Fast Western Blot Kit procedure (55 minutes).

Moving science forward

Thermo SCIENTIFIC
Part of Thermo Fisher Scientific